



University of
**Southern
Queensland**

**THROUGH-THICKNESS DIELECTRIC SENSING FOR
THERMOSET COMPOSITE CURE ANALYSIS AND
PROCESS VALIDATION**

A Thesis submitted by

Molly Hall

BSc Materials Science & Engineering

For the award of

Doctor of Philosophy

2023

ABSTRACT

Thermoset composites are an attractive material choice for high performance applications due to their superior properties and high level of tailorability compared with traditional homogeneous materials. However, implementation of these materials is challenging due to their high level of uncertainty within the manufacturing process. Sources of variation include slight differences between material batches and the natural temperature variation in manufacturing equipment causing a range of expected final part properties. Much research has been conducted on quantifying the expected variation and methods of monitoring the cure reaction to explicitly identify how the part cure progresses. The research presented in this thesis focuses on the use of dielectric sensors as a method for live-monitoring of the thermoset cure reaction, as a strategy for capturing and validating material cure state information. Dielectric sensors are an appealing option for in-situ monitoring of the thermoset cure reaction because they provide qualitative and quantitative information on the cure reaction progression. However, to date, there is no clear consensus on which dielectric parameter should be used for performing these analyses, or how they should be executed. In this research, a systematic approach to material cure state determination was completed and a new, comprehensive set of parameter-independent dielectric analysis techniques are presented. The results are compared with numerical simulations and analytical testing, demonstrating high accuracy and part-to-part repeatability. The newly proposed methods are comparable or better than existing techniques and allow for more analysis flexibility. The methods were further validated during a study on a novel dielectric sensor which is designed to monitor through the thickness of parts up to 20 mm. While the design of the prototype sensor influenced the signal reading, a correction factor was determined which allowed for successful implementation of the newly proposed dielectric analysis methods. The methods showed high accuracy and part-to-part repeatability for composite laminates of thicknesses between 2 and 20 mm. The culmination of this thesis is an exploration of the cure kinetics modelling variability that is expected for this material system. A stochastic approach with Monte Carlo methods was used to characterise the influence of cure kinetics modelling and oven temperature uncertainty on the polymer viscosity and cure reaction. A novel approach for quantifying cure kinetics uncertainty is provided and the results of the subsequent convergence analyses were validated with experimental trials. Results indicate that the time to fully cured has high amount of variability (upwards of 10%), and suggestions for ensuring process robustness are provided.

CERTIFICATION OF THESIS

I *Molly Hall* declare that the PhD Thesis entitled *Through-Thickness Dielectric Sensing for Thermoset Composite Cure Analysis and Process Validation* is not more than 100,000 words in length including quotes and exclusive of tables, figures, appendices, bibliography, references, and footnotes.

This Thesis is the work of *Molly Hall* except where otherwise acknowledged, with the majority of the contribution to the papers presented as a Thesis by Publication undertaken by the student. The work is original and has not previously been submitted for any other award, except where acknowledged.

Signed: *Molly Hall*

Date: 28 November 2023

Endorsed by:

Professor Xuesen Zeng

Principal Supervisor

Doctor Tristan Shelley

Associate Supervisor

Professor Peter Schubel

Associate Supervisor

Student and supervisors' signatures of endorsement are held at the University.

STATEMENT OF CONTRIBUTION

The articles produced from this study were a joint contribution of the authors. The details of the scientific contribution of each author are provided below:

Literature Review: Hall, M., Zeng, X., Shelley, T., & Schubel, P. (2022). In Situ Thermoset Cure Sensing: A Review of Correlation Methods. *Polymers (Basel)*, 14(15), 2978.

DOI: <https://doi.org/10.3390/polym14152978>

The overall contribution of Molly Hall was 80% related to the conceptualisation, methodology, data collection and interpretation, critical review of related literature, analysis, writing the original draft, and revising the final submission. Xuesen Zeng, Tristan Shelly, and Peter Schubel contributed to the structuring of the manuscript, reviewing, editing, and providing technical advice.

Paper 1: Hall, M., Zeng, X., Shelley, T., & Schubel, P. (2023). Dielectric Parameter Independent Curing Analysis of Out-Of-Autoclave Carbon Fibre/Epoxy Composites. *Composites Part A: Applied Science and Manufacturing*, 107755.

DOI: <https://doi.org/https://doi.org/10.1016/j.compositesa.2023.107755>

The overall contribution of Molly Hall was 85% related to the conceptualisation, methodology, design of experiments, experimental works, data collection, analysis, and interpretation of data, writing the original draft and revising the final submission. Xuesen Zeng, Tristan Shelly, and Peter Schubel contributed to the concept development, design of experiments, reviewing, editing, and providing important technical advice.

Paper 2: Hall, M., Zeng, X., Shelley, T., & Schubel, P. (2023). Impact of Through-Thickness Dielectric Sensor Effects on Carbon Fibre/Epoxy Cure Monitoring.

Submitted to *Composites Part A: Applied Science and Manufacturing* (accepted pending minor revisions).

The overall contribution of Molly Hall was 85% related to the conceptualisation, methodology, design of experiments, experimental works, data collection, analysis, and interpretation of data, writing the original draft and revising the final submission. Xuesen Zeng, Tristan Shelly, and Peter Schubel contributed to the concept development, design of experiments, reviewing, editing, and providing important technical advice.

Paper 3: Hall, M., Zeng, X., Shelley, T., & Schubel, P. (2023). Stochastic Modelling of Out-Of-Autoclave Epoxy Composite Cure Cycles Under Uncertainty.

Submitted to Composites Part A: Applied Science and Manufacturing (accepted pending minor revisions).

The overall contribution of Molly Hall was 85% related to the conceptualisation, methodology, design of experiments, software and coding, experimental works, data collection, analysis and interpretation of data, writing the original draft and revising the final submission. Xuesen Zeng, Tristan Shelly, and Peter Schubel contributed to the concept development, design of experiments, reviewing, editing, and providing important technical advice.

ACKNOWLEDGEMENTS

Firstly and especially, I would like to thank my supervisors: Professor Xuesen Zeng, Dr Tristan Shelley, and Professor Peter Schubel. I would not have started on this journey, nor would I be looking at it from the other end if it weren't for your unwavering support and patience. Thank you for keeping me going.

Another big thank you goes to my partners at Boeing (Chris Howe, David Reynolds, and Alexey Makhnutin) and Netzsch (Dr Alexander Chaloupka and Andrew Gillen). Thank you for your guidance, support, and mentorship through this entire process.

I also couldn't have done this without the support from my friends, both those who I see regularly and those who I haven't seen since pre-COVID. Josh, looking at you here! Thanks for being my faraway best friend and supporter, even when we're terrible at keeping in touch. Thanks also to Peter for helping me acclimate to living in Australia, and especially for making sure I know which aisles of Bunnings are important. A major thanks goes to Tom for all of the Taco Wednesdays that we've spent talking about beer rankings, literary theories, and stochastic modelling approaches.

A major thank you to my family for supporting me when I decided to move to pretty much the opposite side of the world to start a PhD at the beginning of a pandemic. Great appreciation goes to my father who inspired me from a very early age to do a PhD, specifically in something that is not biology. And another goes to my mother, who made sure that I know that being an engineer is not a good excuse for dressing like one.

My final thank you goes to Matt. Thank you for supporting me, for Friday date nights and Saturday adventures, for pouring all the wine, for letting me get all the cats, and for generally keeping me sane. I couldn't have finished this without you.

TABLE OF CONTENTS

ABSTRACT.....	i
CERTIFICATION OF THESIS.....	ii
STATEMENT OF CONTRIBUTION.....	iii
ACKNOWLEDGEMENTS.....	v
TABLE OF CONTENTS.....	vi
LIST OF FIGURES	viii
ABBREVIATIONS	x
CHAPTER 1: INTRODUCTION	1
1.1 Background & motivation	1
1.2 Problem statement	3
1.3 Research objectives	5
1.4 Scope and limitations.....	6
1.5 Thesis structure.....	7
CHAPTER 2: (LITERATURE REVIEW) IN SITU THERMOSET CURE SENSING: A REVIEW OF CORRELATION METHODS	9
2.1 Introduction	9
2.2 Links and implications.....	9
2.3 Published paper.....	9
CHAPTER 3: (PAPER 1) DIELECTRIC PARAMETER INDEPENDENT CURING ANALYSIS OF OUT-OF-AUTOCCLAVE CARBON FIBRE/EPOXY COMPOSITES	38
3.1 Introduction	38
3.2 Links and implications.....	38
3.3 Published paper.....	38
CHAPTER 4: (PAPER 2) IMPACT OF THROUGH-THICKNESS DIELECTRIC SENSOR EFFECTS ON CARBON FIBRE/EPOXY CURE MONITORING	52
4.1 Introduction	52

4.2	Links and implications.....	52
4.3	Paper manuscript	52
CHAPTER 5: (PAPER 3) STOCHASTIC MODELLING OF OUT-OF-AUTOCLAVE EPOXY COMPOSITE CURE CYCLES UNDER UNCERTAINTY		88
5.1	Introduction	88
5.2	Links and implications.....	88
5.3	Paper manuscript	88
CHAPTER 6: DISCUSSION AND CONCLUSION		118
6.1	Conclusions	118
6.2	Suggestions for future work	120
REFERENCES		122
APPENDIX A: MANUFACTURING PROCEDURE.....		131
A1.	IDEX Sensor Definition	131
A2.	NETZSCH DEA 288 Ionic.....	132
A3.	Thermocouples	132
A4.	Analytical Testing (DMA and DSC).....	134
APPENDIX B: DEA SIGNAL EVALUATION		135
B1.	Dielectric Smoothing Procedure and Frequency Selection	135
B2.	TMM Sensor Correction Factor	140
B3.	TMM Fully Cured Prepreg Test	140
APPENDIX C: STOCHASTIC MODELLING CODE (MATLAB)		142

LIST OF FIGURES

Figure 1 - Depiction of the major steps in the aerospace development and manufacturing cycle, as they pertain to thermoset composite cure methods. The development stages are broadly adapted from the Building Block approach [11].....	4
Figure 2 - Description of NETZSCH dielectric sensors, from NETZSCH brochure [162]. The IDEX sensors used in this study are the IDEX filtered type.....	131
Figure 3 - Description of the NETZSCH DEA 288 Ionic, from NETZSCH brochure [162].	132
Figure 4 - Thermocouple definition, with type K 7/0.2 mm dimensions being used for this research [163].....	133
Figure 5 - Thermocouple connector definition, with Type K plugs being used for this research [164].....	133
Figure 6 - Image of TMM analytical panels cut into DMA coupons via waterjet.....	134
Figure 7 - Smoothing to a Level 8, which successfully retains the graph features while still simplifying the signal.....	135
Figure 8 - An unsuccessful smoothing practice to Level 9, which is performed on the same signal as shown in Figure 7. Smoothing to a 9 in this case causes the graph to distort away from the original signal.....	136
Figure 9 - Signal from Figure 7 shown with the first derivative of the signal (left) unsmoothed and (right) smoothed. In both cases the original signal (the loss factor) was smoothed, and the derivative was calculated from the smoothed signal.	136
Figure 10 - Signal comparison for 1 Hz, 10 Hz, 100 Hz, and 1 kHz measurements which are (left) unsmoothed and (right) smoothed. The red arrow indicates the maximum area of noise on the 1 kHz measurement, and how the area is more consistent after smoothing.	137
Figure 11 - Complete set of frequency measurements for the loss factor in IDEX5 showing (left) the time-dependent response for each frequency and (right) the frequency-dependent response for the duration of cure (40 minutes to 250 minutes).	138
Figure 12 - Dissipation factor for IDEX5 at frequencies of 1 Hz, 10 Hz, and 100 Hz showing that the single peak behaviour is present in the 100 Hz signal.	139
Figure 13 - Cure event correlations for IDEX3 performed on 1 Hz, 10 Hz, 100 Hz, and 1 kHz frequencies.	140
Figure 14 - RAVEN simulation of TMM20-2 post cure, demonstrating full conversion.	141

Figure 15 - An example output from the above MATLAB code, which varies the cure kinetics by 3% and temperature by 5%. 147

ABBREVIATIONS

CF	Carbon fibre
CFRP	Carbon fibre reinforced polymer
COV	Coefficient of variation
DEA	Dielectric analysis
DMA	Dynamic mechanical analysis
DoC	Degree of cure
DSC	Dynamic scanning calorimetry
FBG	Fibre Bragg grating
FRP	Fibre reinforced polymer
LIC	Log of the ionic conductivity
MWS	Maxwell/Wagner/Sillar (polarisation)
OFI	Optical fibre interferometer
OFR	Optical fibre refractometer
PEEK	Polyether ether ketone
Prepreg	Pre-impregnated (in reference to a composite raw material form in which the fibres are pre-impregnated with the uncured resin system prior to layup and cure)
TC	Thermocouple
T_g	Glass transition temperature
TMM	Tool mounted monotrode

CHAPTER 1: INTRODUCTION

1.1 Background & motivation

Flying vehicle technology has advanced immensely from the first hot air balloons in 1782 [1] to current trends such as hypersonic flight vehicles [2]. As vehicle technology gets more complex, the demand for advanced and high-capability materials has also increased [3]. Materials capable of strength retention at high temperatures [4], complex manufacturing methods using advanced materials [5], and nanotechnology [6] have all shown to be popular aerospace sector research topics within recent years. However, polymer composite materials have remained one of the highest impact research areas due to their high strength-to-weight ratio [7], flexible manufacturing techniques [8], and applicability to very large-acreage components [9]. Composites such as fibre reinforced polymers (FRP) are extremely appealing for aerospace applications due to the tailorability of part properties. Further, their low density contributes to major design objectives such as range extension, reduced fuel consumption, and overall flight efficiency. However, composite parts are also susceptible to quality issues such as fibre damage and displacements, voids and porosity, part deformations, and incomplete or degraded cure reactions [10]. Many of these items are challenging to inspect, resulting in the implementation of composites structures to be challenging, complex, and time-consuming.

Compared with traditional metallic components, which have easily end-item-inspectable features, the certification process for composite structures can be burdensome. The overall process is commonly described as a building block approach [11] (Chapter 4) and progresses from small scale development up to full systems testing. Each step of the design and validation process progresses a technology through the Technology Readiness Levels (TRL) until the system is prepared for production at TRL10 [12-15]. With respect to composite materials this commonly includes certification by test, meaning fabrication and testing of physical hardware, or certification by analysis, meaning using simulated or predicted data based on numerical models [16]. Most commonly, certification involves a mixture of both testing and analysis [11] (Chapter 4). Implementation of thermoset composites entails validation of the cure process, typically by analytical testing and cure simulations, to ensure completeness of the cure reaction. The cure reaction is directly related to the mechanical performance of the components [17, 18], and validation of the cure process is critical in ensuring that the quality requirements are met. For this reason, there is much emphasis on how simulation or modelling techniques are used and how quality requirement are verified in production.

Numerical methods and modelling techniques are extremely prevalent within composites manufacturing during product development, certification, and during general optimisation activities. They are used for predicting part defects [19], evaluating resin flow during infusion processes [20, 21], and designing [22] and evaluating cure cycles [23, 24]. Cure simulations use a kinetic model for a thermoset resin system [25, 26] and predict the outcome of the cure reaction for a given temperature profile. Common output metrics include the degree of cure and glass transition temperature (T_g) and can also include information on resin viscosity and the cure reaction rate. Simulation tools which incorporate finite element analysis can provide insight on how the through-thickness or 3-dimensional complexity impacts the cure progression [23, 27, 28]. A key desired outcome of a cure simulation exercise is to determine the optimal cure profile to be used in production. Once a cure cycle is verified, the regulatory requirements necessitate that it be verified for the subsequent production components [29]. Production verification can occur by validating the equipment parameters or by monitoring the response of the material to the process cycle.

Process monitoring is a well-researched topic for thermoset composites. Off-line methods such as dynamic scanning calorimetry (DSC) [30] and dynamic mechanical analysis (DMA) [31] are analytical methods which are used to determine the degree of cure and T_g of a composite material after it has been fabricated. However, these are destructive techniques, and are therefore more applicable to the development process rather than to serial production. There is currently much interest in on-line sensing methods which monitor the cure reaction as it progresses, with multiple sensing types being explored. Thermocouples, fibre optic systems, ultrasonic sensors, and dielectric sensors have all demonstrated the ability to monitor the thermoset cure reaction [32, 33], however challenges remain. Sensors such as thermocouples [34] and optical fibres [35, 36] are challenging to integrate into flight structures, as they must be embedded into the part and are therefore considered a foreign object that could lead to premature failure. Ultrasonic sensors [37-39] can capture material phase transitions during cure, however, are not able to produce quantitative degree of cure information. Dielectric sensors show much promise for cure monitoring, as they can identify material phase transitions and degree of cure [36, 40, 41]. They also come in multiple configurations including parallel plate [42] and tool-mounted sensors [43] which can monitor the cure in a non-invasive manner. However, there are multiple published methods for using dielectric analysis for thermoset cure monitoring and no consensus to date on how the methods should be implemented. Despite these challenges, current efforts to evaluate robustness of in-line sensing techniques show much promise for live cure monitoring of aerospace structures.

Numerical modelling and process monitoring are critical technologies for verification of composite structures. Composite parts can be time-intensive to manufacture which has resulted in much research on optimisation methods. The objective of these activities is commonly to accelerate the process conditions while still fabricating parts which meet the quality objectives. There are many methods for optimisation such as exhaustive testing matrices [44] and numerical methods [22, 45-48]. The aim of cure optimisation typically targets a specific feature such as the total process time [22], temperature gradient [49], exotherm temperature [50] or part quality and performance [20, 51]. Single-objective optimisations can address one of these, whereas multiple objective functions can address multiple features, even when they have conflicting solutions [50-52]. A key component of numerical optimisation is having an accurate model which can predict the optimised parameters. Regardless of the feature being optimised, the actual part in production must still meet strict quality requirements. Live process monitoring methods can ensure these requirements are met and protect the integrity and safety of the structure.

1.2 Problem statement

From a high level, a key problem within thermoset composites manufacturing is that there are many sources of uncertainty which are not accounted for in the current certification scheme [53]. Rather, factors of safety are applied to account for the probability of failure. However, as manufacturing trends continue towards process optimisation there comes a very real risk of composite structures being manufactured which may not meet the stringent quality requirements [54, 55]. A simplistic depiction of the current certification process, which is depicted in Figure 1, conveys the major steps in certification and verification as they relate to composites parts [11]. Initially, a cure cycle is developed which complies with the requirements listed in aerospace standards. This step typically involves cure simulations to predict how specific geometries will respond to a given cure cycle. Once a cure cycle is selected, a process validation activity commences. During this stage, hardware is manufactured according to the proposed cure cycle and engineering requirements. Destructive testing is typically involved, usually by embedding thermocouples to check internal temperatures or completing off-line analytical testing on sections of the component to verify the degree of cure. Once a component makes its way into production with an approved cure cycle, the manufacturing requirements must be validated. Since embedded sensors are typically treated as foreign objects and are therefore not acceptable for flight hardware, all process monitoring methods must be indirect.

During production it is common to monitor the equipment parameters, such as temperature, for compliance with the approved cure profile.

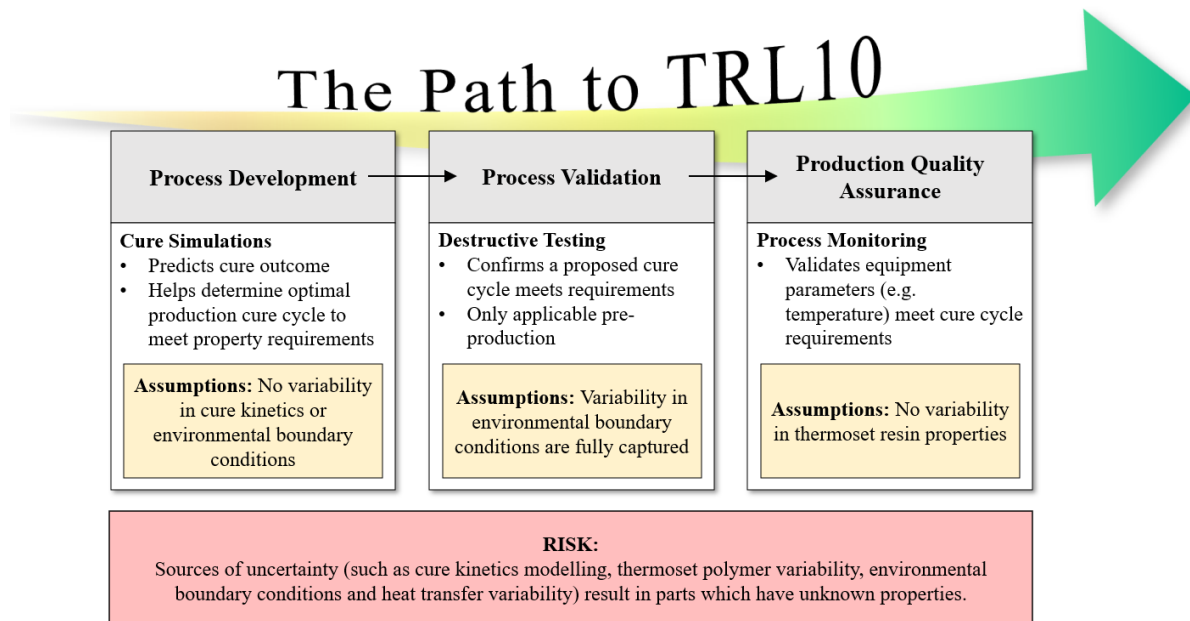


Figure 1 - Depiction of the major steps in the aerospace development and manufacturing cycle, as they pertain to thermoset composite cure methods. The development stages are broadly adapted from the Building Block approach [11].

This system relies on assumptions of material and process exactness and assumes that the extent of variation is fully understood. For example, commercially offered cure simulation programs are deterministic, meaning they accept a single input variable and produce a single resulting output variable. This paradigm neglects that cure kinetics parameters can vary due to the slight resin composition changes which can occur between batches [56]. The slight material variations can impact the accuracy of cure simulations, and potentially have an unanticipated response to natural temperature fluctuations. Process monitoring of actual parts during the development process is a great way of capturing expected variation in environmental boundary conditions such as temperature and heat transfer over time and over spatial areas. However, this testing is not a guarantee of how every individual material batch will behave and does not necessarily provide a complete picture for future production.

Neglecting these sources of variation can result in a very real risk that the cure progression of a given part is unknown. By implementing direct cure monitoring methods, such as using cure sensing technology, the extent of cure for a given part can be verified to meet the requirements. Unfortunately, to-date there are few robust and non-invasive cure sensors. The methods reported in literature are varied, with no clear consensus of which methods are the most

accurate and repeatable. Further, most commercialised sensors provide contact-measurements and neglect the cure gradient which occurs through the thickness of a component [57]. The issues presented here can be addressed by quantifying the expected process variation and using a high-fidelity sensing network to monitor where a given part fits within this variation. The research presented in this thesis aims to close this gap by investigating the robustness of through-thickness dielectric sensing, and characterising the variability expected from curing an out-of-autoclave epoxy prepreg.

1.3 Research objectives

This research focuses on the integration dielectric analysis techniques into thermoset composites cure monitoring. Also within the scope of this thesis is an exploration into the influence of uncertainty on the output of thermoset cure, with the aim of demonstrating that directly monitoring the cure progression with a high-quality sensing system is necessary to guarantee part quality. These topics will be satisfied by fulfilling the following objectives:

1. Identification of a comprehensive set of dielectric cure analysis methods, inclusive of existing methods and newly proposed methods. Further, this includes establishment of a standard set of definitions and guidelines for implementing dielectric analysis techniques.
2. Evaluation of a novel through-thickness dielectric sensor for sensor functionality and applicability for through-thickness dielectric cure monitoring. This includes evaluation for:
 - a. Multiple laminate thicknesses
 - b. Influence of temperature
 - c. Influence of polarisation effects
 - d. Influence of sensor design
3. Development of a method for quantifying cure kinetics uncertainty which can be applied to any characterised thermoset system. The method aims to be computation-only and require no additional testing or material characterisation.
4. Identification of expected cure variation under sources of uncertainty using numerical modelling and a stochastic approach for an out-of-autoclave prepreg system, including experimental validation of the results.

5. Recommendations for process considerations for guaranteeing satisfactory part quality for an out-of-autoclave prepreg system.

These objectives will support the understanding of dielectric capabilities for monitoring thermoset cure and assess their suitability in capturing the expected variation in cure as predicted by numerical modelling.

1.4 Scope and limitations

This research has been conducted with a specific focus on the implementation and execution of specific dielectric analysis methodologies, and the ability of dielectrics to reliably detect variance in thermoset cure. This will be accomplished using a combination of experimental studies using dielectric analysis and stochastic cure modelling to establish the extent of expected cure variability. The use of experimental data to validate the modelling approach is expected to enable development of manufacturing guidelines for robust cure processes. These topics are expected to also provide valuable guidelines for the implementation of dielectric sensing and their capability of capturing variation due to uncertainty. With respect to this scope, the following limitations should be considered:

1. The literature review presented in Chapter 2 includes an overview of thermocouples, ultrasonic sensors, and fibre optic sensors in addition to the review on dielectric sensing. These technologies are included for completeness, and it should be noted that this study only explores the use of dielectric sensing techniques for thermoset cure. Thermocouples are used for temperature monitoring as a method for validating the dielectric sensing information and are not specifically investigated here for cure monitoring.
2. This study specifically focuses on the CYCOM® 5320-1 out-of-autoclave carbon fibre/epoxy prepreg material system. Application of dielectric analysis on alternate resin systems are out of scope of this research.
3. It is acknowledged that dielectric sensors show much promise for use in flow monitoring of resin infusion and resin transfer moulding processes. As the material system under investigation in this research is a prepreg, meaning there is no large-scale flow of resin through a preform, investigation into flow detection is not included.
4. The stochastic modelling methodology presented includes a novel method for assessing sources of uncertainty due to cure modelling variability. A 0-dimensional cure simulation was used for the purposes of assessing the effectiveness of this method in

contrast with existing methods. Higher dimensional cure simulations, such as those which require finite element modelling, are deemed out of scope as they are not necessary for the validation of the proposed method.

5. The stochastic modelling approach focuses specifically on cure kinetics and temperature uncertainty and their impacts on cure progression and resin viscosity. There are many additional sources of uncertainty in composites cure which will not be considered here.

Despite these limitations it is expected that this research will provide valuable insight into the use of a novel sensing methodology for capturing variability in thermoset cure.

1.5 Thesis structure

This research is presented as a thesis by publication. This thesis consists of six chapters including this introduction which provides the background and problem statement, research objectives, and scope. The body of this thesis is organised as follows:

- Chapter 2 contains the published manuscript of a literature review of four sensor types which can be used for thermoset cure monitoring, titled *In Situ Thermoset Cure Sensing: A Review of Correlation Methods*. It critically reviews the correlation methods used for analysing cure data from thermocouple, dielectric, fibre optic, and ultrasonic sensors. It should be noted that the remainder of this thesis is focused on dielectric sensing.
- Chapter 3 contains the published manuscript for Paper 1, titled *Dielectric Parameter Independent Curing Analysis of Out-Of-Autoclave Carbon Fibre/Epoxy Composites*. This contains the initial investigation into dielectric cure sensing techniques and presents a new comprehensive set of analysis methodologies.
- Chapter 4 contains the submitted manuscript for Paper 2, titled *Impact of Through-Thickness Dielectric Sensor Effects on Carbon Fibre/Epoxy Cure Monitoring*. This paper implements the methods proposed in Paper 1 on a novel through-thickness dielectric sensor. The focus of this paper is evaluating the prototype sensor, which is designed for monitoring cure through parts up to 20 mm in thickness. Specific emphasis is on assessing the sensor signal quality and implementing the signal to through-thickness cure monitoring.
- Chapter 5 contains the submitted manuscript for Paper 3, titled *Stochastic Modelling of Out-Of-Autoclave Epoxy Composite Cure Cycles Under Uncertainty*. This paper

explores the influence of cure kinetics modelling and environmental temperature uncertainty on the cure process for an out-of-autoclave resin system. It presents a novel methodology for characterising uncertainty for complex cure kinetic models and includes validation of the stochastic outputs using experimental results.

- Chapter 6 summarises the conclusions of this research and provides suggestions for future work.

This thesis also contains three appendices, which provide additional detail on manufacturing, analysis, and methods used throughout this thesis. It is recommended to use these appendices as supplements to the chapters as specified below:

- Appendix A contains procedure details related to materials manufacturing and analysis conducted in Chapters 3 and 4. This includes sensor details, data collection and analysis techniques, further details on analytical testing procedures, and test coupon measurements.
- Appendix B contains dielectric analysis methods for signal evaluation, and supplements the methods provided in Chapters 3 and 4. These methods include further detail on the signal smoothing process and selection of test frequencies. Additionally provided is further detail on the through-thickness sensor correction factor rationale, and the method used to evaluate the signal in the presence of a fully cured test sample.
- Appendix C provides the MATLAB code used for the stochastic modelling process detailed in Chapter 5. This includes an example of the code for one of the test sets, and an explanation for how the code can be adapted for the other analysis sets.

CHAPTER 2: (LITERATURE REVIEW) IN SITU THERMOSET CURE SENSING: A REVIEW OF CORRELATION METHODS

2.1 Introduction

This chapter presents a comprehensive literature review of key technologies and methods for in-situ thermoset cure monitoring. It focuses on the fundamental data collection and analysis techniques which are employed for thermocouple, dielectric, ultrasonic, and fibre optic sensors. This article critically reviews the methods of correlating sensor parameter values to material cure state information. Specific focus is paid to how the governing equations for the sensing technique are used for the available configurations for each sensor type. While many of the sensor varieties are not yet commercialised, there is much research into their implementation for cure monitoring of thermoset polymers and thermoset composites.

2.2 Links and implications

This review evaluates the expansive literature available on common in-situ thermoset cure monitoring techniques. However, it has identified some clear research gaps. For example, there are a wide range of qualitative and quantitative techniques which are documented in the literature, however, there is little consistency from method to method. One major research gap identified for dielectric sensors, which is the focus of this thesis, is the lack of understanding of how the various methods compare with one another. A systematic comparison of the existing dielectric analysis methods is presented for multiple dielectric sensor types in Chapters 2 and 3, which includes a presentation of a new set of parameter-independent analysis methodologies.

2.3 Published paper

Review

In Situ Thermoset Cure Sensing: A Review of Correlation Methods

Molly Hall , Xuesen Zeng ^{*}, Tristan Shelley  and Peter Schubel

Centre for Future Materials, University of Southern Queensland, Toowoomba, QLD 4350, Australia; molly.hall@usq.edu.au (M.H.); tristan.shelley@usq.edu.au (T.S.); peter.schubel@usq.edu.au (P.S.)

* Correspondence: xuesen.zeng@usq.edu.au

Abstract: Thermoset polymer composites have increased in use across multiple industries, with recent applications consisting of high-complexity and large-scale parts. As applications expand, the emphasis on accurate process-monitoring techniques has increased, with a variety of in situ cure-monitoring sensors being investigated by various research teams. To date, a wide range of data analysis techniques have been used to correlate data collected from thermocouple, dielectric, ultrasonic, and fibre-optic sensors to information on the material cure state. The methods used in existing publications have not been explicitly differentiated between, nor have they been directly compared. This paper provides a critical review of the different data collection and cure state correlation methods for these sensor types. The review includes details of the relevant sensor configurations and governing equations, material combinations, data verification techniques, identified potential research gaps, and areas of improvement. A wide range of both qualitative and quantitative analysis methods are discussed for each sensing technology. Critical analysis is provided on the capability and limitations of these methods to directly identify cure state information for the materials under investigation. This paper aims to provide the reader with sufficient background on available analysis techniques to assist in selecting the most appropriate method for the application.

Keywords: composite manufacturing; thermosetting polymers; cure behaviour; process monitoring; in situ cure monitoring; sensors



Citation: Hall, M.; Zeng, X.; Shelley, T.; Schubel, P. In Situ Thermoset Cure Sensing: A Review of Correlation Methods. *Polymers* **2022**, *14*, 2978. <https://doi.org/10.3390/polym14152978>

Academic Editor: Andrea Sorrentino

Received: 8 June 2022

Accepted: 18 July 2022

Published: 22 July 2022

Publisher's Note: MDPI stays neutral with regard to jurisdictional claims in published maps and institutional affiliations.



Copyright: © 2022 by the authors. Licensee MDPI, Basel, Switzerland. This article is an open access article distributed under the terms and conditions of the Creative Commons Attribution (CC BY) license (<https://creativecommons.org/licenses/by/4.0/>).

1. Introduction

Advanced thermoset polymer composites are implemented in a variety of industries, such as in civil [1,2] and energy [3–5] and in recreational and naval marine applications [6–10] as well as in performance automobiles [11,12] and in aerospace applications [13–15]. The adoption of thermoset materials has increased in recent years due to the tailorability of part properties and wide variety of manufacturing techniques and achievable geometries. Thermosets can be formed as unreinforced plastics or reinforced composites via injection and compression moulding [16] and resin infusion [17] or using automated laydown techniques [18]. The parts must then go through a cure cycle, commonly under elevated temperature and/or pressure conditions, such as in an autoclave or oven [19,20]. Recently, research on fibre-reinforced polymer (FRP) composites has trended towards the development of high-quality parts that are up to tens of metres long [21] and more than 2 cm thick [22], with emphasis on optimising the processing conditions when making these complex parts [23].

Composite parts are susceptible to a variety of quality issues, such as fibre displacements, voids and porosity, geometric deformations, and inconsistent chemical reactions or polymerisations [24]. These final-part variations are frequently a result of manufacturing uncertainty stemming from either variation in the raw materials or in the processing conditions and environment [25]. In advanced composite applications, it is a critical quality objective to achieve a specified resin cure state, as the completion of the polymer conversion

process is directly linked to the mechanical performance of the final product [26]. To capture the effects of this variability, it becomes necessary to monitor the cure process for each individual part.

The final cure state of a thermoset part is typically evaluated using either a quantifiable degree of cure, specified as a percentage of the chemical reaction that has been completed, or by reaching a threshold value for the glass transition temperature (T_g) [27,28]. The degree of reaction or polymerisation can be analysed off-line, where testing is conducted externally to the manufacturing process, or in-line, where a sensor is integrated directly into the manufacturing process and captures live data [29]. The advantages of the in-line or in situ monitoring of composite processing are the ability to monitor the process in real time [30] and the potential to actively control the process as it occurs [31,32]. Further, some major limitations of off-line cure evaluation are that it may require destructive testing, cannot perfectly replicate the process conditions during part of the cure, and cannot be used to update the process conditions in real time.

This paper will briefly review the established off-line cure-monitoring techniques such as Dynamic Scanning Calorimetry (DSC), Dynamic Mechanical Analysis (DMA), and Dynamic Rheometry. A deeper evaluation of direct sensing technologies for in-line curing is then presented, specifically of thermocouple, dielectric, ultrasonic, and fibre-optic sensors. Extensive reviews have been completed regarding the capabilities and limitations of these sensors for composite process and cure monitoring [33,34]; however, a critical review of the correlation methods of these techniques has not been carried out to date. Each type of sensor monitors different parameters, and data analysis must be conducted to convert these parameters into information pertaining to the material cure state, with an example of the data flow and analysis procedure being shown in Figure 1. In this paper, a critical review of correlation processes for four in-line sensing technologies is presented. Special focus has been placed on the specific sensor type and material configuration, the results of the correlation analysis, and how the analysis has been verified for accuracy. The technologies are then evaluated for how effectively they monitor composite cure processes and how appropriate they may be for high-performance applications.

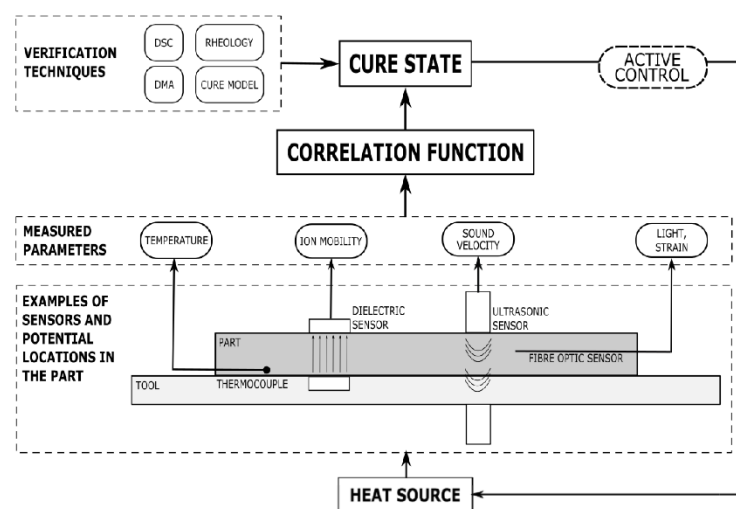


Figure 1. An overview of types of cure sensors, their placement, measured parameters, and verification techniques. The data flow process for an active control system is also proposed, with the sensors being correlated to cure state information during live processing, which can subsequently be used to actively alter the processing conditions.

2. Off-Line Cure Analysis

Off-line cure analysis techniques are frequently used to characterise new material systems or as a quality control evaluation of an existing cured part. Material characterisation enables researchers to build a model of the material that can then be used in process simulations. For example, a research team characterised Hexcel RTM6 using DSC [35] and rheometric [36] analysis to develop a kinetic and a chemoviscosity model of the tested epoxy. Three common off-line analysis techniques are discussed here, including their governing equations and identification principles for cure state information. Other analysis techniques, such as Fourier Transform Infrared (FTIR) [37] and Raman spectroscopy [38], are used for polymer analysis; these will not be discussed further.

2.1. Dynamic Scanning Calorimetry (DSC)

DSC measures heat flow in a sample when it is subjected to isothermal or non-isothermal temperature conditions. By integrating the peak of the heat flow (H) versus the time curve and dividing it by the total heat of reaction (H_R), we can calculate the degree of cure (α), as shown in Equation (1).

$$\alpha = \frac{\int_0^t H dt}{H_R} \quad (1)$$

There is an extensive amount of literature on the use of DSC to characterise cure reactions [39–42], and the procedure for kinetic parameter determination is detailed in standards such as ASTM E 2070, which contains methods for kinetic parameters by differential scanning calorimetry using isothermal methods [43]. DSC can also be used to measure thermoset cure reactions [44] and to calculate the degree of cure of an existing cured part. The residual heat of reaction can be measured for a cured sample, which allows for the calculation of the actual degree of cure of the part based on a known total heat of reaction for the material. DSC analysis is used to validate the results of new sensing technologies and will be mentioned throughout this paper as one of the main verification techniques.

2.2. Dynamic Mechanical Analysis (DMA)

The DMA of composite parts utilises a dual cantilever beam configuration in which a sample is oscillated at a set frequency through a set temperature range. The elastic modulus is evaluated throughout the test; specifically, the storage modulus (E') component, the loss modulus component (E''), and the $\tan\delta$, which is calculated as the ratio of the loss to the storage moduli, are considered. The main output of a DMA test is the T_g , which is calculated as the midpoint of the drop in the storage modulus. ASTM D 7028, which provides methods for T_g determination in Polymer Matrix Composites via DMA [45] details the process for the calculation of T_g by identifying the intersection of the tangent lines around the drop in E' , as shown in Figure 2.

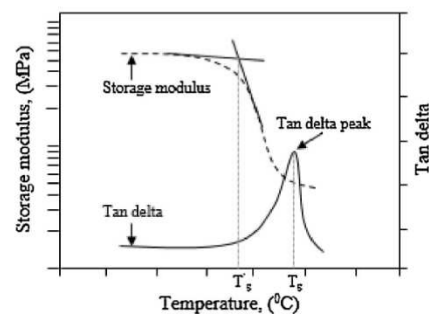


Figure 2. Graphic of the calculation of T_g using an E' modulus curve (left-hand axis) and $\tan\delta$ curve (right-hand axis) from a DMA test. Reprinted with permission from Ref. [46]. 2016, Elsevier.

DMA has been used to identify the cure state of many materials, such as phenolics [47] and epoxies [48]. Such as with DSC, DMA testing is used throughout this paper to verify the T_g calculations of the in-line sensing techniques.

2.3. Dynamic Rheometry

The dynamic rheometry of thermoset composites typically occurs in a parallel-plate oscillating configuration, with the purposes of monitoring the change in the shear modulus under a set temperature range. Like DMA, rheometric testing evaluates the shear storage modulus (G'), the loss modulus (G''), and $\tan\delta$, which is once again the ratio of loss to the storage moduli. From these values, the complex viscosity (η^*) can be calculated by Equation (2) using the complex modulus (G^*) and oscillating frequency (ω):

$$\eta^* = \frac{G^*}{\omega} \quad (2)$$

While this does not specifically relate to the final cure state of a thermoset polymer, resin viscosity can be a critical parameter during processing.

Regarding the cure state, the gel point can be defined in multiple ways in accordance with the rules of ASTM D 7750, which contains methods for evaluating cure behaviour of thermosetting resins [49], an example of which is displayed in Figure 3. Depending on the interactions of fibre and resin, the gel point can be defined as the intersection of G' and G'' , the peak of G'' , the peak of $\tan\delta$, a sudden rapid increase in G' , or a sudden drop in $\tan\delta$.

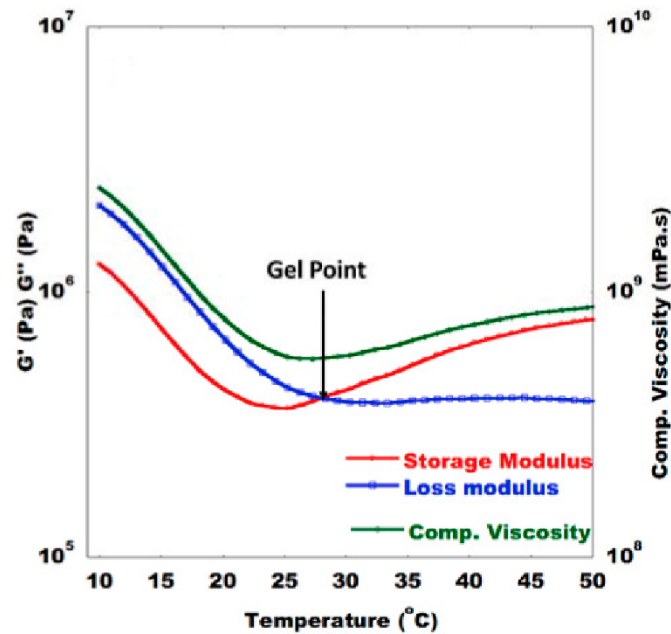


Figure 3. Example of how gel time can be determined by identifying where G' and G'' cross. Reprinted with permission from Ref. [50]. 2019, Elsevier.

The main challenge of rheometric cure monitoring is that during the crosslinking and solidification process, the viscosity trends towards infinite, so later step cure stages cannot be monitored. Despite this, rheometry has been used to evaluate viscosity and

cure progression for several thermoset polymers [42,51] and is also used as a verification technique for the sensors discussed in this paper.

3. In-Line Cure Monitoring Sensor Correlations

3.1. Thermocouple Sensors

3.1.1. Sensor Background and Governing Equations

There are a variety of sensors that are capable of monitoring the thermal properties of composite cure processing, including thermocouples (TCs), infrared thermographers (IRT) [52], heat flux sensors [22], and resistance temperature detectors (RTDs) [53]. While this paper specifically focuses on thermocouples, alternative temperature sensors have been reviewed [29], including details on their functionality, capabilities, and limitations.

Temperature is one of the most common parameters to measure during composite processing, as the time–temperature–transformation relationship of thermosetting polymers is well established [54], and most thermoset resins are cured under the application of a specific heating cycle [55]. Temperature monitoring of both the environmental conditions, for example, the oven or autoclave air temperature, and the material of choice is extremely important. Most composite processes include an air TC to account for environmental uncertainty, such as the natural fluctuations in the equipment over time. Additionally, the actual temperature experienced by the part is critical for cure monitoring, as many thermoset polymers tend to experience exothermic events, or a temperature increases due to the release of heat energy during the chemical reaction. Material uncertainties such as slight variations in the raw material; the initial degree of cure; and the material age, storage conditions, and resin content can all impact the likelihood and peak temperature of an exotherm [25]. For this reason, simply monitoring the equipment temperature may not be sufficient to identify and predict the exact temperature profile that the part is experiencing. Thermocouples are commonly placed in one or more representative locations: in the part, on or in the tool, and in the air, to monitor the environmental conditions. These locations and an overview of the parameter’s monitoring process is shown in Figure 4.

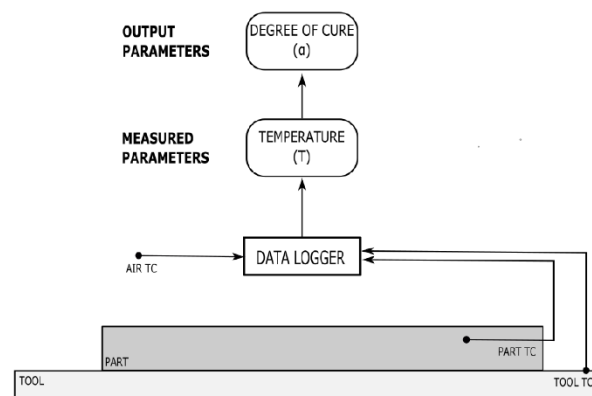


Figure 4. An overview of thermocouple placements and the data collection process flow.

Thermocouples comprise two different metal wires with known Seebeck voltages, which are welded or twisted into a junction at one end and separated at the other. The monitoring temperature (T_m) at the welded junction can be calculated using Equation (3) using the Seebeck coefficient (S), measured voltage (V), and reference temperature at the open junction (T_r).

$$T_m = \frac{V}{S} + T_r \quad (3)$$

This equation is used to reliably calculate the temperature being experienced by the material in question. Using this temperature profile, the material properties can then be predicted according to the methods detailed in the following section.

3.1.2. Correlation Functions

An overwhelming amount of literature exists on the use of thermocouples and temperature devices to monitor the progression of thermoset cure. For example, TCs and IRTs have been used to monitor temperature distributions and exotherms of carbon fibre–epoxy composites and other polymers [56,57] and to monitor part cure as a method to validate simulation results [22]. Thermocouples are used to monitor processing and part temperatures in most composite cure studies, including in almost every paper mentioned in this review, due to their fundamental nature.

The most reliable method of directly correlating the measured temperature to the material degree of cure (α) is by evaluating the thermo-kinetic model of the material, which roughly follows the formula in Equation (4):

$$\frac{d\alpha}{dt} = K(T)f(\alpha) \quad (4)$$

in which $\frac{d\alpha}{dt}$ indicates the change in the degree of cure with respect to time, the component $K(T)$ represents the temperature dependency component, and $f(\alpha)$ represents the reaction model component. $K(T)$ follows an Arrhenius dependence and can be calculated using Equation (5) using the pre-exponential factor (A), activation energy (E), universal gas constant (R), and the temperature:

$$K(T) = Ae^{-\frac{E}{RT}} \quad (5)$$

The reaction model component, $f(\alpha)$, is specific to the material in question. Many reaction models have been proposed, with a comprehensive overview published by Yousefi et al. [44]. Examples include a simple n th-order rate equation [58], the autocatalytic model [59], or model-free kinetic analysis [60]. While some models can be broadly applied to material classes such as epoxies or polyesters, it is also best to conduct a kinetic analysis of each specific material component to increase the accuracy of the results.

In practice, the temperature profile of a composite part can be verified against the kinetic model or against a simulation that incorporates the kinetic model [61]. Once the temperature profile is verified to produce an acceptable degree of cure, it is typical to simply verify that the temperature parameters are met for each process cycle. For applications that may not have the capacity, need, or interest in completing such a process verification, it is common to follow the manufacturers' recommended cure cycle as found in the technical data sheet for most commercial thermosets or for composite materials, such as for Solvay Cycom[®] 5320-1 Prepreg [62]. The material manufacturer typically specifies one or more recommended cure cycles that will ensure that the part reaches a fully cured state. In this case, a temperature reading is taken from a representative location that is either in or on the part, on the tool, or elsewhere in the oven. The main verification method for quality control is to check the temperature as a function of time compared to the recommended cure cycle requirements, as shown in Figure 5, rather than to calculate a specific degree of cure for each individual part. This quality control step ensures that the cured material meets the minimum threshold for mechanical performance, as the required engineering properties can only be met in fully cured parts [63]. It should be noted that the definition of "fully cured" varies based on the specific material and application.

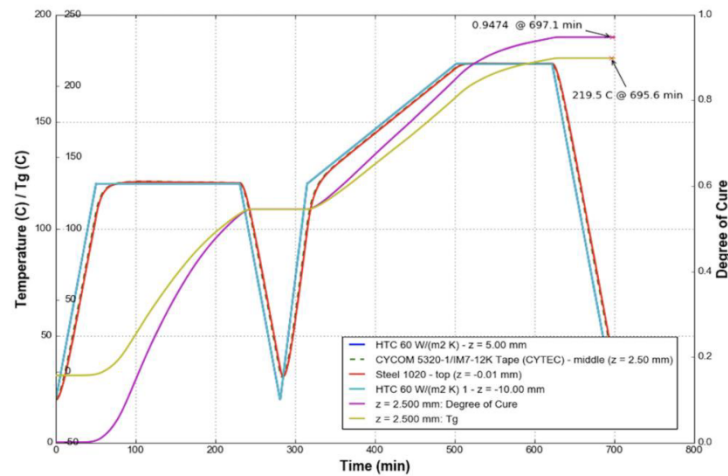


Figure 5. An example of the manufacturer's recommended cure cycle for Cycom[®] 5320-1 Prepreg and its resultant predicted final properties (degree of cure and T_g).

3.1.3. Summary and Future Work

Thermocouples are the most common and widely used sensing technology for composite curing and process monitoring. They monitor not only the cure state, which is measured as the degree of cure, but are also able to monitor other critical process events such as temperature overshoots caused by exothermic events. Additionally, they are frequently required to be used in coordination with other sensing devices, such as those detailed in the below sections, to normalise for temperature effects [64,65] or as a supplemental monitoring technique for data collection. Thermocouples have also been used to monitor resin filling for infusion processes [66] and are commonly used to monitor temperature applications during process optimisation activities [23,67,68]. A major challenge of thermocouples is that to directly measure the material state, they must be embedded into the part, and some applications (such as those which require specific surface finishes) are unable to accept embedded sensors.

3.2. Dielectric Sensors

3.2.1. Sensor Background and Governing Equations

In recent decades, dielectric sensors have been investigated as a new method of in situ cure monitoring for thermoset composite materials due to their versatility and range of available configurations, both when purchased off the shelf and when custom-designed. The three most common types of dielectric sensors are parallel-plate, interdigital, and tool-mounted. Each of these has benefits and limitations, which have been discussed in depth elsewhere [33,34]. For example, parallel-plate dielectrics can detect through-thickness measurements that would otherwise require interdigital sensors to be embedded throughout the thickness of a part. Interdigital and tool-mounted sensors only take measurements of the surface that they are directly in contact with; however, interdigital sensors are commonly used invasively, making them less optimal for industries with stringent quality requirements.

Dielectric sensors work on the principle of monitoring dipole and ion movement within a material under a time-varying electric field (E). The alignment and relaxation of the charged particles within the sample are monitored by the sensor in the form of a capacitive (C) and resistive (R) response [69]. These values are used to calculate the dielectric parameters to be referenced throughout this paper. Thermoset curing can be

evaluated using these parameters due to the time-, temperature-, and frequency-dependent response of the dielectric sensor. The dielectric sensor captures the change in ion mobility, which directly relates to the cure state of the material as it crosslinks. It should be noted that some of the variable representations in this paper may differ from the cited sources to maintain the consistency of the variable meanings used in the following governing equations and correlations.

Permittivity (ϵ') is calculated in Equation (6) using capacitance, electrode spacing (L), the electrode area (A), and the permittivity of free space ($\epsilon_0 = 8.854 \times 10^{-12}$ F/m), as derived from [70]:

$$\epsilon' = \frac{CL}{\epsilon_0 A} \quad (6)$$

Dielectric loss (ϵ'') is calculated in Equation (7) using resistance, the electrical excitation frequency (ω), electrode spacing and area, and the permittivity of free space, as derived from [70]:

$$\epsilon'' = \frac{L}{R\omega A\epsilon_0} \quad (7)$$

Impedance (Z) is calculated in Equation (8) with the resistance, excitation frequency, and conductance, with j as the imaginary component [71]:

$$Z = \frac{1}{\frac{1}{R} + j\omega C} \quad (8)$$

Ion conductivity (σ), which is related to the inverse relationship of ion viscosity and frequency-independent resistivity (ρ), is calculated in Equation (9) using resistance, electrode spacing, and electrode area [71]:

$$\rho = \frac{1}{\sigma} = \frac{RA}{L} \quad (9)$$

The dissipation factor (D), also known as $\tan\delta$, can be calculated in Equation (10) using the permittivity and dielectric loss or the resistance, capacitance, and excitation frequency [72]:

$$D = \tan\delta = \frac{\epsilon''}{\epsilon'} = \frac{1}{\omega RC} \quad (10)$$

While the dielectric response provides a great deal of information, it does not directly relate to information about the cure state of a thermoset polymer. A correlation function is needed to relate the dielectric properties to the state of the chemical reaction, specifically the degree of cure and glass transition temperature. The data may be interpreted qualitatively by evaluating artefacts from a graph or quantitatively by deriving equations. The data must also be corroborated using techniques that are currently known to provide insight into the cure state of a thermoset polymer: typically thermochemical or rheometric testing. Examples of these methods are provided in the following section, with an overview shown in Figure 6.

3.2.2. Correlation Functions

There are many methods for correlating dielectric signals with the degree of chemical reaction that has occurred in the resin or composite. Common methods and their variants will be discussed in this section, including the correlation functions and the supplemental testing techniques.

Dielectric Loss Correlation

Fournier et al. [73] used a dielectric loss correlation through their work evaluating neat epoxy resin using parallel-plate dielectric sensors. The dielectric loss factor (ϵ''), which can be calculated from Equation (7), was used to predict vitrification by identifying the time of maximum loss for each experimental frequency. Dielectric loss correlations have

also been used to identify the gel point and have been verified through comparison to rheology data [74]. Using neat RTM6 epoxy monitored by a tool-mounted dielectric sensor, the glass transition temperature was determined as the local maximum of the dielectric loss graph. Additionally, the crossover point between the permittivity and dielectric loss data can be demonstrated to indicate the gel point. This has been correlated to rheology test data and specifically to the crossover point of the storage modulus and the loss modulus, G' and G'' , as seen in Figure 7.

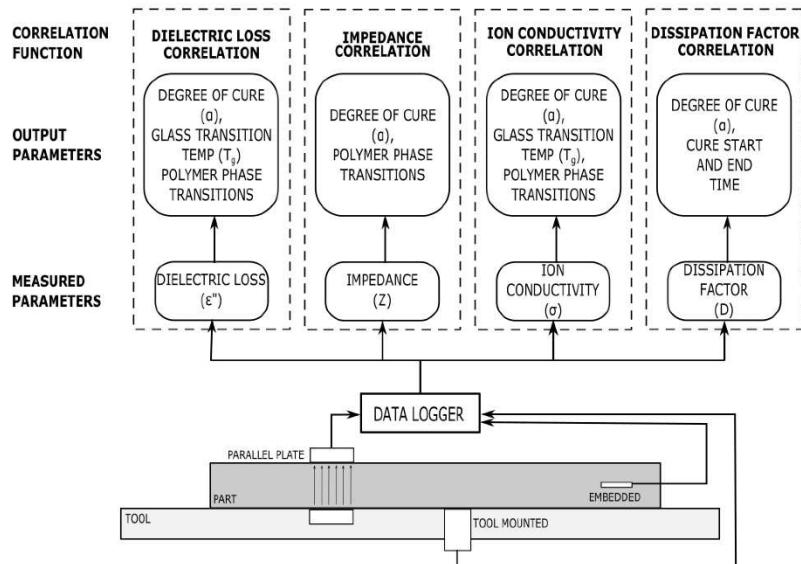


Figure 6. An overview of dielectric sensor correlation methods, including a visual depiction of the types of dielectric sensor, the parameters they measure, and how the parameters are converted into cure information.

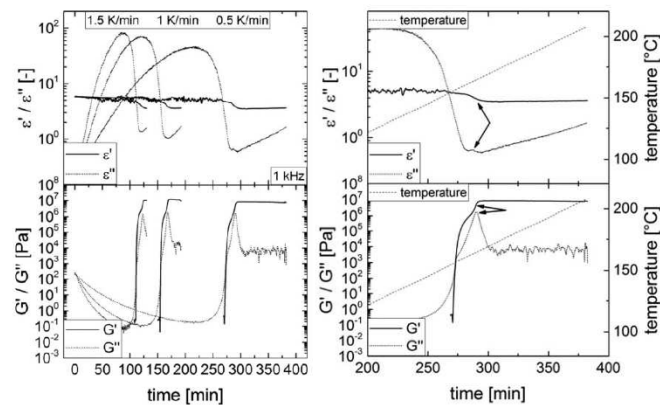


Figure 7. Comparison of dielectric loss to rheological storage and loss as a method to identify T_g (as identified by arrows in the right-hand image). Reprinted with permission from Ref. [74] 2018, John Wiley and Sons.

From a quantitative perspective, Hardis et al. proposed an equation for the degree of cure based on the progression of dielectric loss during the cure of an epoxy monitored with parallel-plate dielectrics [75]. The equation for degree of cure (α) with respect to time is stated in Equation (11):

$$\alpha(t) = \frac{\log \epsilon_0'' - \log \epsilon_t''}{\log \epsilon_0'' - \log \epsilon_\infty''} \quad (11)$$

where the subscripts ϵ'' represent the dielectric loss at start of cure (ϵ_0''), at time t (ϵ_t''), and at cure completion (ϵ_∞''). The degree of cure generated from this equation aligned well with degree of cure measurements determined from DSC and Raman spectroscopy.

Impedance Correlation

Mijovic et al. used an impedance correlation to calculate the resistivity of a sample based on the monitored impedance signal (Z) calculated in Equation (8). Impedance was used to calculate resistivity (ρ), and then boundary conditions were evaluated to derive Equation (12) for the degree of cure [71,76]:

$$\frac{\alpha}{\alpha_m} = \frac{\log \rho - \log \rho_0}{\log \rho_m - \log \rho_0} \quad (12)$$

in which α_m represents the maximum degree of cure, and ρ_0 and ρ_∞ represent the initial and maximum values of resistivity. The cure progression of neat epoxies was evaluated using this function, and graphs of the degree of cure versus time were compared successfully to those produced by HPLC and FTIR analysis, as shown in Figure 8. Further, the vitrification point was identified at the onset of the second step on the graph showing imaginary impedance (Z'') versus time, and this point was successfully correlated to the storage modulus (G'') peak from the corresponding rheological data.

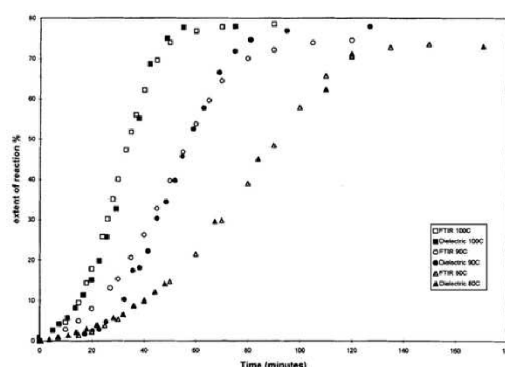


Figure 8. Comparison of degree of cure between dielectric and FTIR analysis represented as the extent of reaction (%) versus time (minutes), with curves indicated at various temperatures. Reprinted with permission from Ref. [76] 2003, John Wiley and Sons.

This method has recently been used for determining the vitrification point of an RTM6 epoxy reinforced with carbon fibre [77,78]. In this method, the imaginary impedance (Z''), a component of Equation (8), is evaluated across multiple frequencies to eliminate the impact of the constant phase element, the second term of Equation (13):

$$Z'' = \frac{\omega CR^2}{1 + \omega^2 C^2 R^2} + \frac{2}{(A_e \omega)^n} \quad (13)$$

in which A_e and n are coefficients of the constant phase element. The first term of Equation (13) provides Z_m'' , or the material impedance, and a plot such as the one in Figure 9 has been overlaid on a graph of degree of cure derived from the material cure model. This qualitative comparison shows similar trends between the term Z_m'' and the degree of cure. Furthermore, the second step or shoulder region on the graph of Z_m'' versus time indicates the vitrification point. Studies by this research group were conducted using both a customized woven sensor for the cure monitoring and a lineal sensor for the flow monitoring of the resin infusion process. Interestingly, the lineal sensor configuration was also able to produce a cure signal that was reasonably similar to that produced by the cure sensor [78].

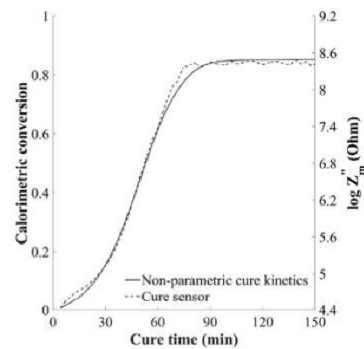


Figure 9. Comparison between Z_m'' and degree of cure generated from cure kinetics model [77].

Similarly, evaluating the frequency spectra of the imaginary impedance has been used to draw a direct correlation to the degree of cure [79]. By applying linear regression to the graph of degree of cure versus $\log(Z''_{max})$ at temperature T , the c coefficients in Equation (14) can be determined:

$$\log Z''_{max} = (c_{11} + c_{12}T)\alpha + c_2 \quad (14)$$

This equation was used to successfully model an isothermal cure cycle of RTM6 epoxy using an interdigitated dielectric sensor and a degree of cure prediction from the cure kinetics model. Figure 10 shows a comparison of this model to the experimental data of Z'' . Furthermore, a non-isothermal cure was shown to fit the model quite closely, although with slightly more errors in the progression of the model.

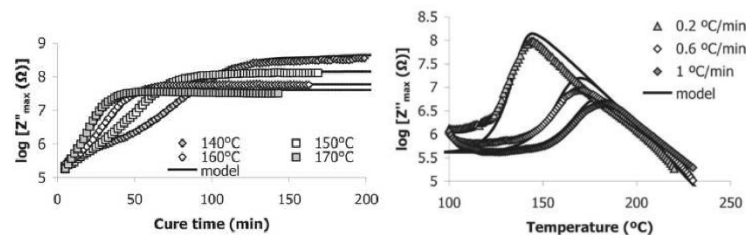


Figure 10. Comparison of experimental values of Z'' with the proposed model for Z'' for an isothermal cure (left) and a non-isothermal cure (right). Reprinted with permission from Ref. [79] 2005, Elsevier.

Ion Conductivity Correlation

Ion conductivity correlations have been used the most frequently due to the connection of ion conductivity, and therefore ion viscosity, to the bulk polymer viscosity. In this section,

various approaches are used based on whether the ion conductivity or ion viscosity, which is also known as the polymer resistivity (ρ), are being monitored.

Starting with ion conductivity, McIlhagger et al. determined the T_g of an epoxy matrix reinforced by both glass and carbon fibres using signals generated from parallel-plate dielectric sensors [53,80]. The derivative of the log of the ionic conductivity, known as the DLIC, approaches zero as the sample approaches full cure. This cure point has been compared to DMA and DSC results in addition to being verified by tension and flexure mechanical performance tests to identify the peak of material performance, which occurs at full cure [80]. Additional critical points have been determined using a plot of the ionic conductivity. The maximum conductivity occurs at the point of minimum resin viscosity, which can be a critical point for out-of-autoclave and resin infusion processing, and as seen in Figure 11, the minimum point of DLIC indicates the onset of gelation [53]. McIlhagger et al. determined the minimum viscosity, gel point, and point of full cure with the data corroborated using DMA and DSC testing [53].

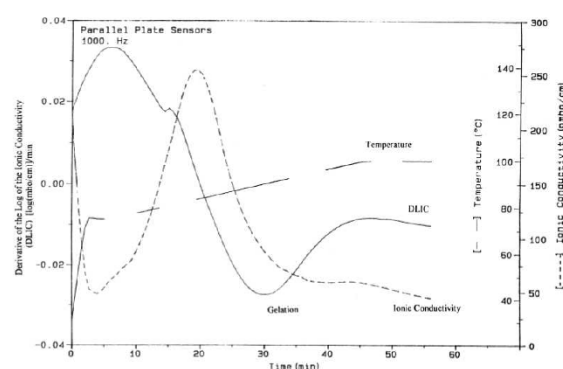


Figure 11. Gel point indicated on a DLIC curve. Reprinted with permission from Ref. [53] 2000, Elsevier.

This correlation method has also been employed elsewhere, specifically in assigning the maximum value of ionic conductivity to the point of minimum polymer viscosity, the inflection point of the LIC after the peak viscosity relating to the onset of gel, and the maximum of dielectric loss corresponding to the onset of vitrification [56,81,82].

Yang et al. proposed Equation (15) as a method to calculate the T_g of an epoxy resin using a miniature interdigital sensor to monitor ionic conductivity:

$$T_g = \frac{\log G_0(T) - \log G(t)}{\log G_0(T) - \log G_\infty(T)} T_{g\infty}(T) \quad (15)$$

where $G_0(T)$ and $G_\infty(T)$ are the temperature-dependent initial and final conductance, $G(t)$ is the time-dependent conductance, and $T_{g\infty}(T)$ is the T_g calculation based on a cure kinetics model [83]. Through this in situ calculation of T_g and use of the DiBenedetto equation, the degree of cure can be calculated as in Equation (16):

$$\alpha = \frac{T_g - T_{g0}}{T_g - \lambda T_g - T_{g0} + \lambda T_{g\infty}} \quad (16)$$

which uses the T_g values calculated from Equation (15) and λ , which is a ratio of the heat capacities as calculated during cure kinetics characterisation. This prediction has indicated a consistent trend, however an error of approximately 5–10% exists when compared with DSC.

Ion viscosity correlations are related to ion conductivity through the inverse relationship $\rho = 1/\sigma$ and is then correlated to polymer viscosity values through Equation (17):

$$\rho = \frac{6\pi\eta r}{q^2 n} \quad (17)$$

which uses polymer viscosity (η), ion particle size (r), ion charge (q), and ion concentration (n) [84]. As the ion viscosity thus has a direct relationship to polymer matrix viscosity, it is possible to understand key information regarding thermoset cure based on our knowledge of viscosity progression.

Boll et al. evaluated a carbon fibre/epoxy composite using a miniature embedded dielectric sensor by estimating that cure completion occurs when ρ reaches a plateau [84]. The cure state was then verified by completing a DSC evaluation of the cured part and by determining the degree of cure from the residual enthalpy. This method was also used by Moghaddam et al. when evaluating the effectiveness of their micro interdigitated sensor compared to current commercial sensors [85].

For a glass-epoxy prepreg monitored with a surface-mounted interdigitated electrode, Park established that the log of the ion viscosity had a linear relation to the cure temperature [86]. This enabled the calculation of Equation (18) for the degree of cure through a derivation of the DiBenedetto equation:

$$\frac{\log \rho - \log \rho_0}{\log \rho_\infty - \log \rho_0} = \frac{T_g - T_{g0}}{T_{g\infty} - T_{g0}} = \frac{\lambda \alpha}{1 - (1 - \lambda)\alpha} \quad (18)$$

in which the subscript 0 indicates the initial condition, and ∞ indicates the fully cured condition. A comparison of the degree of cure calculated from Equation (18) to that derived from DSC and FTIR analysis is shown in Figure 12, with the DEA results being comparable to those of the other methods.

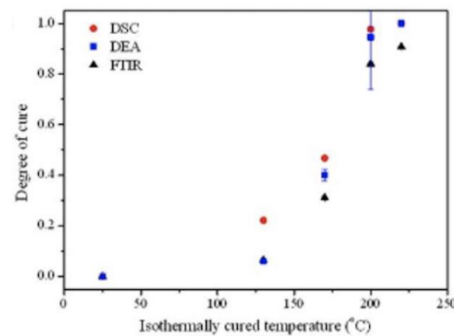


Figure 12. Comparison of degree of cure calculated from dielectric-monitored ion viscosity compared to DSC and FTIR analysis. Reprinted with permission from Ref. [86] 2017, John Wiley and Sons.

A similar equation for degree of cure was calculated from the ion viscosities in accordance with Equation (19):

$$\alpha = \frac{\log \rho - \log \rho_{min}}{\log \rho_{max} - \log \rho_{min}} \quad (19)$$

in which the subscripts indicate the minimum and maximum ion viscosities measured during the cure. Franiecek et al. evaluated Equation (19) for a silica-filled epoxy in which cure was monitored using a tool-mounted monotrode dielectric sensor [87]. The results from this analysis were compared to the degree of cure calculated from DSC, with limited success. While the DEA and DSC graphs follow similar trends, the DEA results are limited by the onset of vitrification, where the DSC results appear to better capture conversion

during the diffusion-controlled period of cure. Figure 13 shows the differences in the results, with the DEA-calculated cure index operating on a shorter time scale than the DSC results.

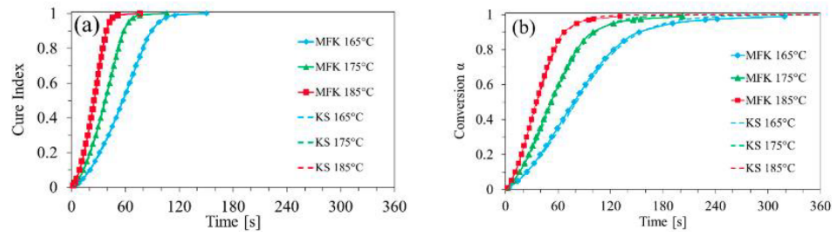


Figure 13. Comparison between cure index derived from DEA (a) and conversion derived from DSC (b) [87].

Interestingly, Franiecek et al. did not limit their investigation into dielectric cure monitoring and instead used the dielectric results to develop a kinetic model. The focus of this paper was to compare both the model-free and model-based kinetic equations derived from dielectric analysis with those derived from DSC results. In this they determined that the dielectric kinetic model aligned with the experimental data; however, as stated previously, the dielectric model and DSC model showed differences around the vitrification point.

Dissipation Factor Correlation

Kim and Lee used a dissipation factor correlation, in which the dissipation factor was normalised for temperature effects, and an equation for the degree of cure was derived [64,88]. An interdigital dielectric sensor was used to monitor the resistance (R) and capacitance (C) of polyester–fibreglass and epoxy–fibreglass composites. The resistance and capacitance were used to calculate the dissipation factor following Equation (10). As the dissipation factor is a function of both the temperature and degree of cure of the matrix, the elimination of the temperature component will allow for the degree of cure to be calculated. The degree of cure determined from D was compared to that of DSC and demonstrated fair accuracy up to a cure level of approximately 70%, as seen in Figure 14.

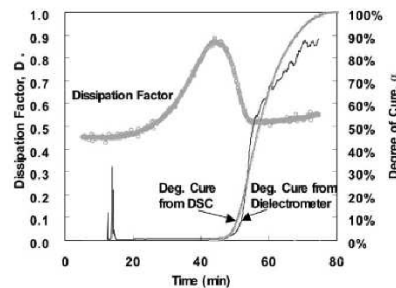


Figure 14. Comparison of degree of cure between dielectric testing and DSC. Reprinted with permission from Ref. [64] 2002, Elsevier.

Using the same method of eliminating the temperature effects, Equation (20) was derived to determine the degree of cure:

$$\alpha = -\frac{1}{s} \log \left[\left(\frac{\log D - \log D_0}{q(T - T_0)} \right) - \frac{p}{q} \right] \quad (20)$$

in which the material parameters D_o , T_o , p , q , and s can be determined experimentally by following the procedure stated in [88].

Another method for evaluating the dissipation factor was calculated from an interdigital dielectric sensor reading and then used to determine the start and end points of cure for a carbon–epoxy composite [89]. The derivative of the dissipation factor was taken with respect to time, enabling the cure start time to be identified as the maximum of dD/dt , and the cure end time to be identified as $dD/dt = 0$.

3.2.3. Summary and Future Work

Dielectric analysis shows much promise for the in-line cure monitoring of thermoset composites. There are many methods of correlating dielectric data to material transitions, such as the gel and vitrification points, and physical properties, such as T_g and the degree of cure. Currently, a major gap in our understanding of dielectric cure analysis is which of these methods is the most accurate, and whether these methods are consistent with one another. The implementation of each technique may be dependent on the fidelity and specificity of data needed for the application, but up until now, the methods have not been compared to ensure if they can be used agonistically or not.

Aside from the capability of the technology to successfully monitor cure, there is other work to be carried out to successfully implement the technology into a production environment. For example, embedded sensors must not impact the integrity of the surrounding part [56]. One strategy is to use extremely small sensors to minimise the performance impact [84,85]. It has also been noted that a tool-mounted sensor can impact the heat transfer through a composite part depending on the tool's material, which can potentially cause a gradient in the degree of cure [90]. Finally, there are a number of opportunities for dielectric sensors to be used for the flow monitoring of resin-infused composite parts in addition to cure monitoring. A great deal of research has been carried out to show that dielectrics can successfully capture resin arrival during an infusion process [77,78,91]. This suggests that a dielectric sensor could be used to characterise multiple process steps with a single device.

3.3. Ultrasonic Sensors

3.3.1. Sensor Background and Governing Equations

Ultrasonic sensor technology is commonly used for the non-destructive inspection of composite part quality and has only recently been viewed as a potential method of monitoring the cure reaction of a thermoset polymer. The main principle of ultrasonic sensor cure monitoring is that as ultrasonic waves are transmitted through the material, the propagation behaviour of these waves is impacted by the progression of the chemical reaction [92,93]. As the polymer continues to react, the density and elastic behaviour change and thus impact the velocity and attenuation of the sound waves. Multiple wave propagation models have been proposed to understand the polymer cure state [94]. All ultrasonic devices function under these principles; however, there are multiple types of transducer and receiver configurations, which are depicted in Figure 15.

The different sensor types each produce an ultrasonic wave with a measured velocity (v) and attenuation (\hat{a}) characteristics, the governing equations for which are provided below. It should be noted that in literature, attenuation is commonly represented as alpha (α); however, here, it will be indicated by (\hat{a}) to differentiate it from the definition of the degree of cure being used throughout this paper.

Longitudinal velocity (c_L) is calculated in Equation (21) using the elastic modulus (E), velocity, and density (ρ) [33]:

$$c_L = \sqrt{\frac{E(1 - \nu)}{\rho(1 + \nu)(1 - 2\nu)}} \quad (21)$$

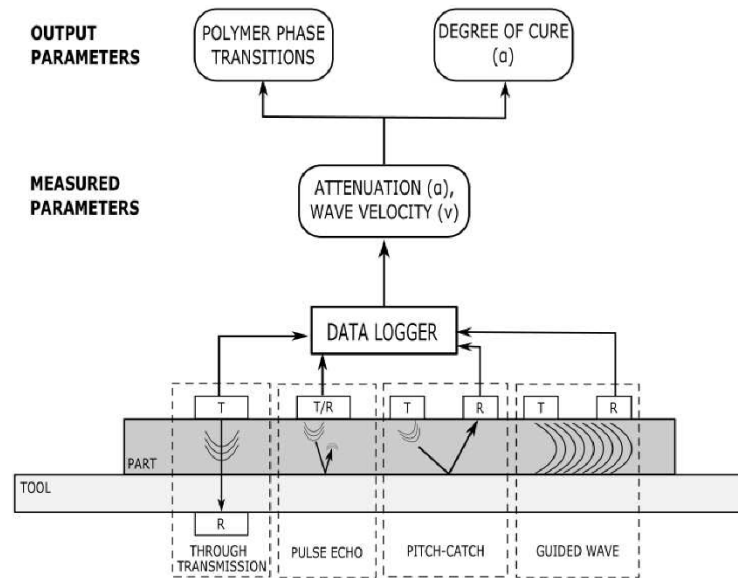


Figure 15. Types of ultrasonic sensors indicating how the ultrasonic waves propagate with the transmitters and receivers. The measurable parameters are linked with the cure parameters.

The shear velocity (c_s) is calculated in Equation (22) using the elastic modulus, density, and velocity [33]:

$$c_s = \sqrt{\frac{E}{2\rho(1 + \nu)}} \quad (22)$$

Attenuation is calculated in Equation (23) using the ratio of the amplitude of the incident wave (A) to the change of amplitude from the incident (ΔA) [33]:

$$a = -\frac{A}{\pi\Delta A} \quad (23)$$

The longitudinal storage modulus (L') is calculated in Equation (24) using the density, longitudinal velocity, attenuation, and wavelength (λ) [95]:

$$L' = \frac{\rho c_L^2 \left(1 - \left(\frac{a\lambda}{2\pi}\right)^2\right)}{\left(1 + \left(\frac{a\lambda}{2\pi}\right)^2\right)^2} \quad (24)$$

The longitudinal bulk modulus (L'') is calculated in Equation (25) using density, longitudinal velocity, attenuation, and wavelength [95]:

$$L'' = \frac{\rho c_L^2 \left(\frac{a\lambda}{2\pi}\right)}{\left(1 + \left(\frac{a\lambda}{2\pi}\right)^2\right)^2} \quad (25)$$

The loss factor, or $\tan\delta$, is calculated as the ratio of the longitudinal storage and bulk moduli in Equation (26) [96]:

$$\tan\delta = \frac{L'}{L''} \quad (26)$$

Like dielectric cure monitoring, the parameters listed in the governing equations in this section do not correlate directly to information on material state or properties. The following section provides an overview of the correlation functions and analysis techniques that have been demonstrated in the literature to date.

3.3.2. Correlation Functions

Data taken from ultrasonic sensors are commonly interpreted qualitatively, with graphic artefacts indicating polymer phase transitions that appear very similar to a DMA curve. Some varieties of ultrasonic monitoring have been referred to as ultrasonic dynamic mechanical analysis [97]. The sound waves cause molecular movement, which becomes restricted as the material becomes cross-linked. The following section is a summary of the methods that have been used in literature and includes information on the type of ultrasonic transducers and what parameters can be monitored with them.

One of the more comprehensive methods for isolating phase transitions was suggested by Lionetto et al. [97] and has been used to evaluate a polyester resin with through transmission ultrasonic monitoring. In this method, the features of the velocity versus time curve are separated into three segments:

1. Velocity is constant when the resin is liquid, but the reaction is still slow;
2. At the gel point, the velocity begins to increase, and the reaction progresses rapidly;
3. The velocity reaches a plateau at the vitrification point, indicating the slowdown of the reaction.

The distinction between these phases is shown in Figure 16, with the vertical lines indicating the approximate gel point and vitrification point.

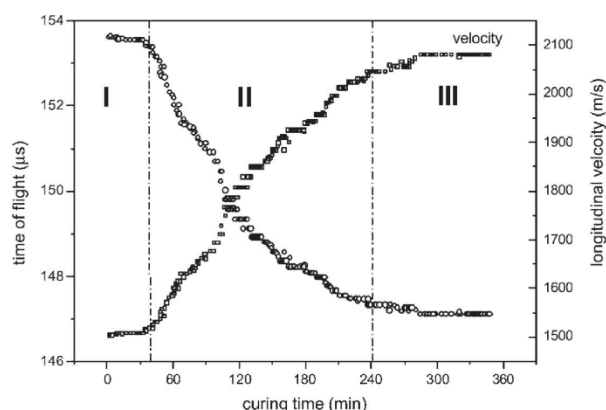


Figure 16. Representation of the three phases of thermoset cure based on the changes in sound velocity. Reprinted with permission from Ref. [98] 2007, John Wiley and Sons.

This method of evaluating cure was also applied to the one-sided air-coupled ultrasound monitoring of polyesters [98,99] and was verified by rheological testing. This viscoelastic interpretation of phase change has also been used for the cure monitoring of epoxies using fibre-optic ultrasound sensors [100].

Ghodhmani et al. [101] used a similar method to identify the different stages of the reaction; however, this was achieved by identifying the key features of the evolution of

the complex's c_{33} viscoelastic coefficient throughout the curing process, with c_{33} being calculated by the following equation, Equation (27):

$$c_{33} = \rho c_L^2 \left(1 + j \frac{2a_L v_L}{\omega}\right) \quad (27)$$

in which ρ is the density, and a_L and v_L are the longitudinal attenuation and velocity. Once c_{33} can be plotted with time, the tangent method can be applied to isolate the three phases of cure:

1. The liquid viscous stage;
2. The glass transition stage;
3. The saturation solid stage.

The transition points of t_{gel} and $t_{saturation}$ are indicated in Figure 17. It should be further noted that the vitrification point can be assigned to the peak of the mechanical loss (δ_m), which also roughly correlates to the inflection point of c_{33} .

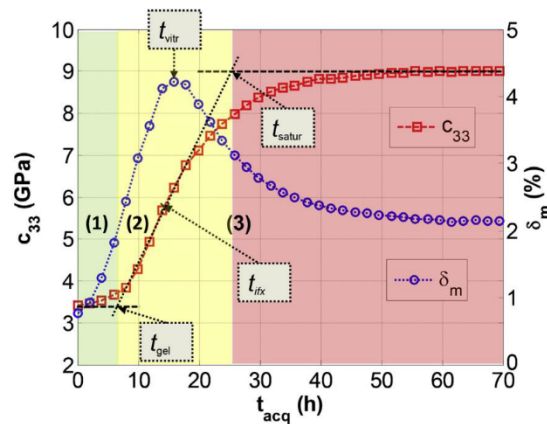


Figure 17. Different stages of the cure reaction based on a tangent evaluation of the complex viscoelastic coefficient, c_{33} . Reprinted with permission from Ref. [101] 2016, Elsevier.

Furthermore, Ghodhmani et al. proposed a degree-of-cure model based on a Weibull distribution model of c_{33} . The equation for the degree of cure is indicated by Equation (28):

$$\alpha(t) = \frac{c_{33}(t) - c_{33,0}}{c_{33,\infty} - c_{33,0}} \quad (28)$$

in which the 0 and ∞ subscripts for c_{33} indicate the initial and maximum values. This model compared to the Kamal chemical reaction model well.

Schmachtenberg et al. measured the sound velocity during the infusion and cure of epoxy-reinforced fibreglass and compared it to the degree of cure calculated off-line using the DSC measurements [102]. The inflection point of the sound velocity curve was correlated to approximately 65% conversion, as shown in Figure 18.

Hudson and Yuan [103] evaluated the cure of epoxy-reinforced carbon fibres using guided-wave ultrasonic monitoring. Specifically, the group velocity of the guided waves was evaluated to determine the correlation to the cure points identified by the Convergent Raven cure simulation program.

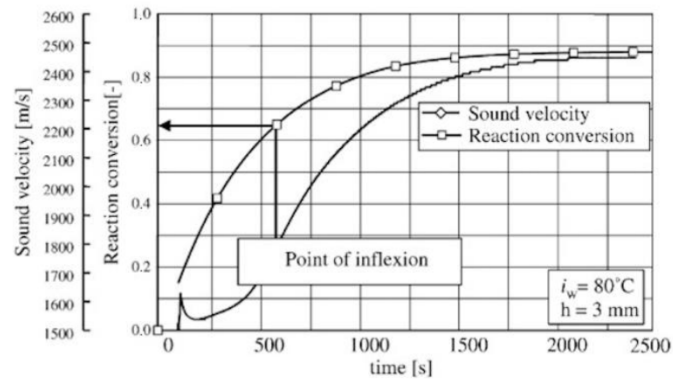


Figure 18. Comparison of degree of cure to the sound velocity of an epoxy-reinforced composite. Reprinted with permission from Ref. [102] 2005, Elsevier.

Samet et al. [104] used attenuation to correlate to material viscosity, which was demonstrated for silicone oils. While the pulse echo configuration was not used with thermoset polymers, the equation for attenuation was shown to correlate to material viscosity, which could be used to monitor the viscosity state of a curing polymer in the future. Finding the peak attenuation has also been used to correlate to the point of vitrification for the through-transmission ultrasonic evaluation of epoxies [105] and polyesters [106].

Maffezzoli et al. [96] used a pulse echo ultrasonic transducer for the process monitoring of a thin sheet of epoxy using the longitudinal velocity and attenuation to calculate the storage and bulk moduli. The loss factor, or $\tan\delta$, calculated from Equation (26) was then graphed, with the peak value indicating the glass transition.

3.3.3. Summary and Future Work

Ultrasonic cure monitoring may have the potential to identify cure transitions; however, this may not be sufficient for high-performance composite applications. Quality assurance requirements in the aerospace industry, for example, commonly depend on reaching a specific threshold of the degree of cure or T_g , and a statement on phase transitions may be insufficient for implementation. However, ultrasonics have also been demonstrated to potentially be capable of evaluating lingering chemical reactions where dielectrics cannot [107]. In a study comparing ultrasonics, dielectrics, and nuclear magnetic resonance, the ultrasonic sensor continued to detect a response after the vitrification point of the resin where dielectric monitoring showed no activity. This could potentially indicate that ultrasonics are more sensitive, particularly in late-stage chemical reactions.

For non-destructive inspection, ultrasonics have also been demonstrated to be useful in other areas of in-process composite inspection. Scholle and Sinapius [108] demonstrated the use of ultrasonics for the cure monitoring of pultrusion processing. Multiple research groups have demonstrated that ultrasonics can successfully detect the flow front and impregnation [102,109] in addition to monitoring the thickness changes [110,111] that occur during resin infusion processing. Ultrasonics have been embedded directly into rheometric plates to collect simultaneous rheology and ultrasonic data [112]. Finally, evaluations have been conducted to capture the mechanical performance impact of embedded sensors [113]. While many ultrasonic sensors are external to the part, it is critical to understand their functional impact when they are used internally.

3.4. Fibre-Optic Sensors

3.4.1. Sensor Background and Governing Equations

Fibre-optic sensors have gained attention for their use in monitoring residual strain during the thermoset cure process [89,114] and for their capabilities for structural health-monitoring in marine [115,116] and energy (wind turbine) [117] applications. The strain-monitoring capability of fibre-optic sensors has been shown to indicate phase changes during cure [81], and its potential for in situ cure monitoring has been reviewed in [117]. The two main types of optical fibres, those that detect optical properties and those that detect mechanical properties, have been reviewed in [33,34]. An overview of the types of sensing technology and their correlation techniques is shown in Figure 19.

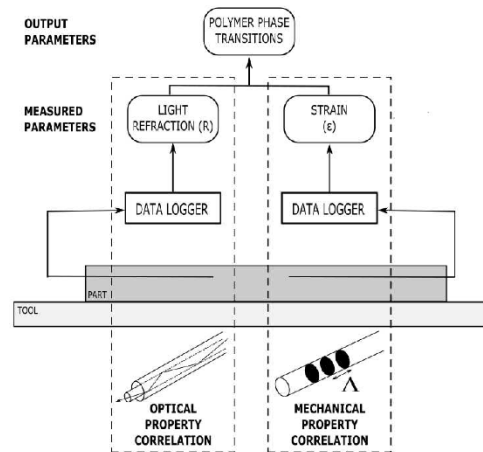


Figure 19. An overview of optical fibre sensing technologies, including their correlation techniques.

Optical fibre refractometers (OFR) utilise a cladded core fibre, in which an open portion of the core is in contact with the composite matrix material. The loss of the incident light signal is monitored based on the reflection coefficient (R_0) calculated using Fresnel's Law in Equation (29), in which n_1 and n_2 , which are the refractive indices of the core and cladding, respectively:

$$R_0 = \left(\frac{n_1 - n_2}{n_1 + n_2} \right)^2 \quad (29)$$

The refractive index (n) of the material under inspection can then be related to its density (ρ) using the Lorentz–Lorenz Law in Equation (30), in which R_M is the molar refractivity, and M is the molar mass of the material:

$$\frac{n^2 - 1}{n^2 + 1} = \frac{R_M}{M} \rho \quad (30)$$

Optical fibre interferometers (OFI), most commonly Fabry–Pérot fibres, monitor the strain imparted to the fibre by identifying the shift in the light wavelength along a series of reflective microspheres on the core of the fibre. The most common type of Fabry–Pérot OFI is a fibre Bragg grating (FBG) optical fibre. Under applied strain, the distance (Λ) between these grating changes, which then causes a shift in the Bragg wavelength (λ_B). The initial Bragg wavelength is calculated via Equation (31) using the grating distance and the effective index of the fibre (n_0) [81]:

$$\lambda_B = 2n_0\Lambda \quad (31)$$

The shift in the Bragg wavelength ($\Delta\lambda_B$) can then be calculated by Equation (32) using the initial Bragg wavelength, the strain-optic coefficient (p_e), the change in strain ($\Delta\epsilon$), the coefficient of thermal expansion (α_{CTE}), the thermo-optic coefficient (ξ), and the change in temperature (ΔT) [118]:

$$\Delta\lambda_B = \lambda_B(1 - p_e)\Delta\epsilon + \lambda_B(\alpha_{CTE} + \xi)\Delta T \quad (32)$$

Equation (32) is divided into a strain-induced component of the Bragg wavelength shift and a thermal component. The decoupling of these components is an important part of interpreting the wavelength shift, as detailed in the following section, which discusses the correlation techniques for both optical property monitoring and strain monitoring.

3.4.2. Correlation Functions

Optical Property Correlations

Fibres that monitor optical properties such as light intensity or output have been correlated to key cure events. An optical fibre with a section of cladding removed was used to monitor the cure of a bismaleimide (BMI)–carbon fibre prepreg by monitoring the attenuation of the change in light intensity [119]. In this study, the minimum attenuation was attributed to the minimum resin viscosity, the increase was attributed to the crosslinking process, and the final plateau was correlated to the end of the cure reaction, each step of which has been correlated to a numerical model.

A second study [66] used this method to evaluate the reflected light intensity of optical fibre sensors during the cure of a resin-infused carbon fibre–epoxy composite. During the infusion process, it was noted that a sharp drop in the sensor signal corresponded to resin arrival. Regarding cure, the rapid increase in the light intensity was attributed to a solidification and density increase during crosslinking, and the subsequent plateau was correlated to the end of the reaction.

A third study [120] also used this method to evaluate the refractive index of a tilted fibre Bragg grating (TFBG) optical fibre to monitor a UV-cured epoxy. In this case, an initial dip in the refractive index was attributed to the temperature response due to the exothermic reaction of the epoxy. The signal increase and plateau were then attributed to the onset of the reaction and cure completion, respectively. Similarly, an optical fibre was used to monitor the power output due to light signal changes during the cure of an epoxy resin, with the plateau of the power signal indicating the gel point [121]. The gel point was confirmed with rheology measurements.

An alternate method was used to evaluate the reflected light intensity of an FBG sensor during the cure of a graphite–epoxy prepreg [122]. In this study, the rapid increase in the reflected light intensity was also attributed to the viscosity increase due to gel and the solidification of the matrix around the fibre. However, it was noted that as the material continued to crosslink, the increase in peak intensity slows down. It was further suggested that the T_g can be identified as the point where the slope of the best-fit lines for peak intensity changes. In this case, the T_g determination of 95 °C agreed with the material specifications.

Mechanical Property Correlations

Optical fibres can also be used to monitor strain measurements using a variety of methods. The most common interpretation of the cure events follows a similar trend to the interpretation of light signals:

1. An initial dip is observed in the signal due to an increase in temperature, as the resin is still liquid and not transmitting strain to the fibre;
2. An increase in the strain measurement is observed due to the crosslinking reaction;
3. The measurement plateaus at cure completion once the matrix has frozen the fibre into place.

Multiple research groups have identified that the strain signal plateaus once the resin forms a solid matrix. An extrinsic Fabry–Pérot interferometer (EFPI) and a FBG sensor were used to identify that the strain signals level off during the vitrification phase when monitoring cure in a carbon fibre–epoxy laminate [123]. Additionally, FBG has been used to monitor a 3D braided preform infused with epoxy in which the Bragg wavelength shift was observed to plateau as the epoxy solidified [124].

An evaluation of epoxy cure with two varieties of optical fibres, a Fresnel optical fibre and an FBG, correlated with the results of both light and strain monitoring strategies, with a comparison of the results in Figure 20 [125]. The signal of the optical fibre was evaluated using the three-phase evaluation detailed in the previous section, whereas the Bragg wavelength identified the peak value as the onset of gel and the plateau of the signal, indicating cure completion.

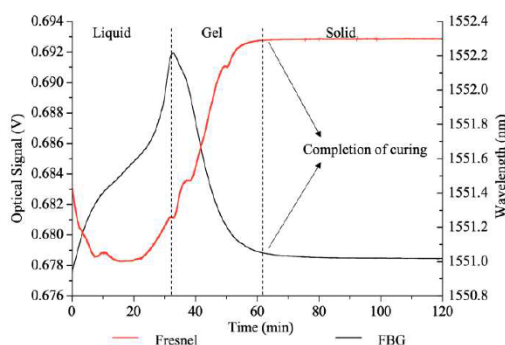


Figure 20. Comparison of cure behaviour for a Fresnel optical fibre sensor signal and the Bragg wavelength from an FBG signal [125].

A dual-period fibre Bragg grating and long-period grating (LPG) were used to monitor RTM6 epoxy cure by isolating the thermal and strain components of the Bragg wavelength shift [65]. By using two sets of gratings superimposed on the same fibre, it becomes possible to decouple the temperature and strain components. During a composite cure, there are two phases: an initial temperature ramp, at which point the resin is liquid and there is no measurable strain, and an isothermal hold, during which there is no temperature change. Using such a fibre can identify the Bragg wavelength shift as being dependent solely on the temperature component during the ramp and solely on the strain component during the dwell. Using this rationale, a $100 \mu\epsilon$ drop in strain was observed during an isothermal cure hold. The onset of this strain drop was identified as the onset of gel, and the end point of the strain drop was correlated to the end of cure. This was compared to dielectric sensor measurements collected on the same sample, which were analysed using the ion viscosity correlation, similar to the methodology used in [56] but using ion viscosity measurements.

3.4.3. Summary and Future Work

Like ultrasonic sensors, at this time, fibre optics may not have the necessary quantitative output required for high-performance composite applications. While the signals can identify phase transitions in the matrix, a specific evaluation of the degree of cure is lacking. Further, it has been established that fibre-optic sensors are quite delicate and that both the embedding and the cure process have the potential to cause bending and constriction, which may negatively impact signal quality [126].

Aside from this, optical fibres show promise for residual stress measurement [122] and structural health monitoring compared to strain gauge measurement and are sensitive to changes in resin flow and mould closing during infusion processes [124]. Optical fibres can also be used to identify resin arrival and flow events during infusion processing [66,127],

commonly by monitoring changes in the light signals as the length of the fibre becomes wetted by the resin [121].

Finally, it is possible to monitor the crystallisation process of thermoplastic polymer by evaluating the residual strain. The processing mechanism for thermoplastic polymers is fundamentally different from the cure processing of thermosetting polymers, as they do not undergo a chemical reaction. For these materials, the sensor monitors the progression of crystallization rather than the progression of cure reaction. The Bragg wavelength shift of an FBG sensor was used to evaluate the crystallisation process for a fibreglass–polypropylene composite and successfully identified the key crystallisation points shown in Figure 21. These results were successfully compared to DSC.

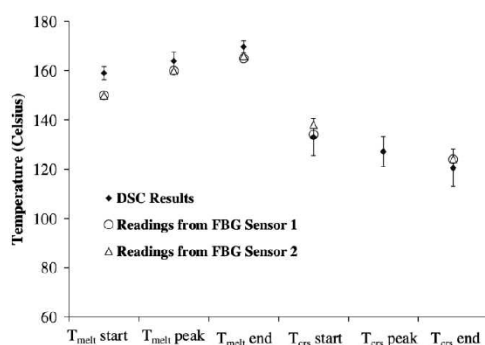


Figure 21. Identification of crystallisation features of a polypropylene composite using an FBG sensor compared to DSC results. Reprinted with permission from Ref. [128] 2005, Elsevier.

4. Conclusions

A critical review of the correlation methods for different in-line composite cure-sensing technologies has been presented. Thermocouple cure monitoring can be reliably correlated to a degree of cure using DSC evaluation or kinetic modelling. Dielectric analysis can produce a wide variety of cure state information, as there are many correlation methods that can be applied to the different monitored parameters. Ultrasonics and fibre optics are commonly used to correlate to the specific phase transitions of the polymer rather than a quantitative measurement of cure state. While the benefits and drawbacks of implementing each type of sensor have been evaluated elsewhere, this paper asserts that it is critical to select a sensor and correlation method to achieve the required fidelity during cure monitoring for the specific application. Providing a qualitative determination of cure ending, such as fibre-optic sensors, may be appropriate for some applications. Whereas an application which requires a degree of cure or T_g with a specific value may benefit from thermocouple or dielectric sensing.

There are multiple areas of potential improvement for in situ cure-sensing technology. The availability of non-invasive sensors and sensors that do not require a permanent installation would increase the ease of implementation. The development of a quantitative measure of cure for sensors, such as ultrasonics, would enable their use in a wider range of applications. A comparison of the different correlation methods for each sensor type would identify the most accurate method for evaluating cure progress, including whether the methods are applicable across multiple materials and multiple cure cycles. Finally, a robust evaluation of the correlation methods across repeated process cycles would indicate if the precision was sufficient to capture manufacturing variations. Future work in these areas would improve the fidelity of data collection and enable new sensing technologies to be readily and confidently adopted.

Author Contributions: M.H.: conceptualization, investigation, writing—original draft, visualization; X.Z.: writing—review and editing, supervision, funding acquisition; T.S.: writing—review and editing, supervision; P.S.: writing—review and editing, supervision, funding acquisition. All authors have read and agreed to the published version of the manuscript.

Funding: This research received no external funding.

Institutional Review Board Statement: Not applicable.

Informed Consent Statement: Not applicable.

Data Availability Statement: The data presented in this study are available on request from the corresponding author.

Conflicts of Interest: The authors declare no conflict of interest.

References

- Alajarmeh, O.; Zeng, X.; Aravinthan, T.; Shelley, T.; Alhawamdeh, M.; Mohammed, A.; Nicol, L.; Vedemikov, A.; Safonov, A.; Schubel, P. Compressive behaviour of hollow box pultruded FRP columns with continuous-wound fibres. *Thin-Walled Struct.* **2021**, *168*, 108300. [CrossRef]
- Alhawamdeh, M.; Alajarmeh, O.; Aravinthan, T.; Shelley, T.; Schubel, P.; Mohammed, A.; Zeng, X. Review on local buckling of hollow box FRP profiles in civil structural applications. *Polymers* **2021**, *13*, 4159. [CrossRef] [PubMed]
- Brøndsted, P.; Lilholt, H.; Lystrup, A. Composite materials for wind power turbine blades. *Annu. Rev. Mater. Res.* **2005**, *35*, 505–538. [CrossRef]
- Marsh, G. Composites—Prime enabler for wind energy. *Reinf. Plast.* **2003**, *74*, 29–45.
- Mishnaevsky, L.; Branner, K.; Petersen, H.N.; Beauson, J.; McGugan, M.; Sørensen, B.F. Materials for wind turbine blades: An overview. *Materials* **2017**, *10*, 1285. [CrossRef]
- Weaver, A. Composites drive VT diversification. *Reinf. Plast.* **1997**, *41*, 28–31.
- Kim, S.-Y.; Shim, C.S.; Sturtevant, C.; Kim, D.; Song, H.C. Mechanical properties and production quality of hand-layup and vacuum infusion processed hybrid composite materials for GFRP marine structures. *Int. J. Nav. Archit. Ocean Eng.* **2014**, *6*, 723–736. [CrossRef]
- Mouritz, A.P.; Gellert, E.; Burchill, P.; Challis, K. Review of advanced composite structures for naval ships and submarines. *Compos. Struct.* **2001**, *53*, 21–42. [CrossRef]
- Hayman, B.; Echtermeyer, A.; McGeorge, D. Use of Fibre Composites in Naval Ships. 2001. Available online: https://www.researchgate.net/profile/Brian-Hayman/publication/242181832_USE_OF_FIBRE_COMPOSITES_IN_NAVAL_SHIPS/links/02c7e52a0c9c912c31000000/USE-OF-FIBRE-COMPOSITES-IN-NAVAL-SHIPS.pdf (accessed on 1 June 2022).
- Kim, D.D.-W.; Hennigan, D.J.; Beavers, K.D. Effect of fabrication processes on mechanical properties of glass fiber reinforced polymer composites for 49 meter (160 foot) recreational yachts. *Int. J. Nav. Archit. Ocean Eng.* **2010**, *2*, 45–56. [CrossRef]
- Feraboli, P.; Masini, A. Development of carbon/epoxy structural components for a high performance vehicle. *Compos. Part B Eng.* **2004**, *35*, 323–330. [CrossRef]
- Feraboli, P.; Masini, A.; Taraborrelli, L.; Pivetti, A. Integrated development of CFRP structures for a topless high performance vehicle. *Compos. Struct.* **2007**, *78*, 495–506. [CrossRef]
- Barile, C.; Casavola, C. Mechanical characterization of carbon fiber reinforced plastics specimens for aerospace applications. *Polym. Compos.* **2018**, *40*, 716–722. [CrossRef]
- Rocha, H.; Semprinoschnig, C.; Nunes, J.P. Sensors for process and structural health monitoring of aerospace composites: A review. *Eng. Struct.* **2021**, *237*, 112231. [CrossRef]
- Mouton, S.; Teissandier, D.; Sébastien, P.; Nadeau, J.P. Manufacturing requirements in design: The RTM process in aeronautics. *Compos. Part A Appl. Sci. Manuf.* **2010**, *41*, 125–130. [CrossRef]
- Rajak, D.K.; Pagar, D.D.; Menezes, P.L.; Linul, E. Fiber-reinforced polymer composites: Manufacturing, properties, and applications. *Polymers* **2019**, *11*, 1667. [CrossRef] [PubMed]
- Hindersmann, A. Confusion about infusion: An overview of infusion processes. *Compos. Part A Appl. Sci. Manuf.* **2019**, *126*, 105583. [CrossRef]
- Frketic, J.; Dickens, T.; Ramakrishnan, S. Automated manufacturing and processing of fiber-reinforced polymer (FRP) composites: An additive review of contemporary and modern techniques for advanced materials manufacturing. *Addit. Manuf.* **2017**, *14*, 69–86. [CrossRef]
- Park, S.Y.; Choi, C.I.I.; Choi, W.J.; Iiwang, S.S. A comparison of the properties of carbon fiber epoxy composites produced by non-autoclave with vacuum bag only prepreg and autoclave process. *Appl. Compos. Mater.* **2018**, *26*, 187–204. [CrossRef]
- Nele, L.; Caggiano, A.; Teti, R. Autoclave cycle optimization for high performance composite parts manufacturing. *Procedia CIRP* **2016**, *57*, 241–246. [CrossRef]
- Summerscales, J.; Searle, T. Low-pressure (vacuum infusion) techniques for moulding large composite structures. *Proc. Inst. Mech. Eng. Part L J. Mater. Des. Appl.* **2005**, *219*, 45–58. [CrossRef]

22. Michaud, D.J.; Beris, A.N.; Dhurjati, P.S. Thick-sectioned RTM composite manufacturing: Part I—In situ cure model parameter identification and sensing. *J. Compos. Mater.* **2002**, *36*, 1175–1200. [[CrossRef](#)]
23. Tifkitsis, K.I.; Skordos, A.A. Stochastic multi-objective optimisation of composites manufacturing process. In Proceedings of the Thematic Conference on Uncertainty Quantification in Computational Sciences and Engineering, Rhodes Island, Greece, 15–17 June 2017; pp. 690–705.
24. Konstantopoulos, S.; Hueber, C.; Antoniadis, I.; Summerscales, J.; Schledjewski, R. Liquid composite molding reproducibility in real-world production of fiber reinforced polymeric composites: A review of challenges and solutions. *Adv. Manuf. Polym. Compos. Sci.* **2019**, *5*, 85–99. [[CrossRef](#)]
25. Mcsogitis, T.S.; Skordos, A.A.; Long, A.C. Uncertainty in the manufacturing of fibrous thermosetting composites: A review. *Compos. Part A Appl. Sci. Manuf.* **2014**, *57*, 67–75. [[CrossRef](#)]
26. Ersoy, N.; Garstka, T.; Potter, K.; Wisnom, M.R.; Porter, D.; Clegg, M.; Stringer, G. Development of the properties of a carbon fibre reinforced thermosetting composite through cure. *Compos. Part A Appl. Sci. Manuf.* **2010**, *41*, 401–409. [[CrossRef](#)]
27. Ogale, A.; Potluri, P.; Rittenschober, B.; Beier, U.; Schlimbach, J. Out-of-autoclave curing of composites for high temperature aerospace applications. In Proceedings of the SAMPE, Seattle, WA, USA, 2–5 June 2014.
28. Boey, F.Y.C.; Lee, T.H.; Sullivan, P.L. High-pressure autoclave curing for a thermoset composite: Effect on the glass transition temperature. *J. Mater. Sci.* **1994**, *29*, 5985–5989. [[CrossRef](#)]
29. Fonseca, G.E.; Dubé, M.A.; Penlidis, A. A critical overview of sensors for monitoring polymerizations. *Macromol. React. Eng.* **2009**, *3*, 327–373. [[CrossRef](#)]
30. Tifkitsis, K.I.; Skordos, A.A. Integration of stochastic process simulation and real time process monitoring of LCM. In Proceedings of the SAMPE, Southampton, UK, 11–13 September 2018.
31. Buczek, M.B. Self-directed process control system for epoxy matrix composites. In Proceedings of the SAMPE, Anaheim, CA, USA, 8–11 May 1995.
32. Dunkersa, J.P.; Flynna, K.M.; Parnasa, R.S.; Sourlas, D.D. Model-assisted feedback control for liquid composite molding. *Compos. Part A Appl. Sci. Manuf.* **2002**, *33*, 841–854. [[CrossRef](#)]
33. Konstantopoulos, S.; Fauster, E.; Schledjewski, R. Monitoring the production of FRP composites: A review of in-line sensing methods. *Express Polym. Lett.* **2014**, *8*, 823–840. [[CrossRef](#)]
34. Torres, M. Parameters' monitoring and in-situ instrumentation for resin transfer moulding: A review. *Compos. Part A Appl. Sci. Manuf.* **2019**, *124*, 105500. [[CrossRef](#)]
35. Karkanas, P.I.; Partridge, I.K. Cure modeling and monitoring of epoxy/amine resin systems. I. Cure kinetics modeling. *J. Appl. Polym. Sci.* **2000**, *77*, 1419–1431. [[CrossRef](#)]
36. Karkanas, P.I.; Partridge, I.K. Cure modeling and monitoring of epoxy/amine resin systems. II. Network formation and chemoviscosity modeling. *J. Appl. Polym. Sci.* **2000**, *77*, 2178–2188. [[CrossRef](#)]
37. Nikolic, G.; Zlatkovic, S.; Cakic, M.; Cakic, S.; Lacnjevac, C.; Rajic, Z. Fast Fourier transform IR characterization of epoxy GY systems crosslinked with aliphatic and cycloaliphatic EH polyamine adducts. *Sensors* **2010**, *10*, 684–696. [[CrossRef](#)] [[PubMed](#)]
38. Merad, L.; Cochez, M.; Margueron, S.; Jauchem, F.; Ferriol, M.; Benyoucef, B.; Bourson, P. In-situ monitoring of the curing of epoxy resins by Raman spectroscopy. *Polym. Test.* **2009**, *28*, 42–45. [[CrossRef](#)]
39. Kamal, M.R.; Sourour, S. Kinetics and thermal characterization of thermoset cure. *Polym. Eng. Sci.* **1973**, *13*, 59–64. [[CrossRef](#)]
40. Kissinger, I.E. Reaction kinetics in differential thermal analysis. *Anal. Chem.* **1957**, *29*, 1702–1706. [[CrossRef](#)]
41. Sbirrazzuoli, N.; Vyazovkin, S. Learning about epoxy cure mechanisms from isoconversional analysis of DSC data. *Thermochim. Acta* **2002**, *388*, 289–298. [[CrossRef](#)]
42. Sbirrazzuoli, N.; Vyazovkin, S.; Mititelu, A.; Sladic, C.; Vincent, L. A study of epoxy-amine cure kinetics by combining isoconversional analysis with temperature modulated dsc and dynamic rheometry. *Macromol. Chem. Phys.* **2003**, *204*, 1815–1821. [[CrossRef](#)]
43. ASTM E2070-13(2018); Standard Test Methods for Kinetic Parameters by Differential Scanning Calorimetry Using Isothermal Methods. ASTM International: West Conshohocken, PA, USA, 2018.
44. Yousefi, A.; Lafleur, P.G.; Gauvin, R. Kinetic studies of thermoset cure reactions: A review. *Polym. Compos.* **1997**, *18*, 157–168. [[CrossRef](#)]
45. ASTM D7028-07(2015); Standard Test Method for Glass Transition Temperature (DMA Tg) of Polymer Matrix Composites by Dynamic Mechanical Analysis (DMA). ASTM International: West Conshohocken, PA, USA, 2015.
46. Ferdous, W.; Manalo, A.; Aravinthan, T.; Van Erp, G. Properties of epoxy polymer concrete matrix: Effect of resin-to-filler ratio and determination of optimal mix for composite railway sleepers. *Constr. Build. Mater.* **2016**, *124*, 287–300. [[CrossRef](#)]
47. Stark, W.; Goering, H.; Michel, U.; Bayerl, H. Online monitoring of thermoset post-curing by dynamic mechanical thermal analysis DMTA. *Polym. Test.* **2009**, *28*, 561–566. [[CrossRef](#)]
48. Kister, G.; Dossi, E. Cure monitoring of CFRP composites by dynamic mechanical analyser. *Polym. Test.* **2015**, *47*, 71–78. [[CrossRef](#)]
49. ASTM D7750-12(2017); Standard Test Method for Cure Behavior of Thermosetting Resins by Dynamic Mechanical Procedures using an Encapsulated Specimen Rheometer. ASTM International: West Conshohocken, PA, USA, 2017.
50. Mphahlele, K.; Ray, S.S.; Kolesnikov, A. Cure kinetics, morphology development, and rheology of a high-performance carbon-fiber-reinforced epoxy composite. *Compos. Part B Eng.* **2019**, *176*, 107300. [[CrossRef](#)]

51. Strobel, M.E.; Kracalik, M.; Hild, S. In-situ monitoring of the curing of a Bisphenol-A epoxy resin by raman-spectroscopy and rheology. *Mater. Sci. Forum* **2019**, *955*, 92–97. [[CrossRef](#)]
52. Pineda, U.; Montés, N.; Domenech, L.; Sánchez, F. On-line measurement of the resin infusion flow variables using artificial vision technologies. *Int. J. Mater. Form.* **2010**, *3*, 711–714. [[CrossRef](#)]
53. McIlhagger, A.; Brown, D.; Hill, B. The development of a dielectric system for the on-line cure monitoring of the resin transfer moulding process. *Compos. Part A Appl. Sci. Manuf.* **2000**, *31*, 1373–1381. [[CrossRef](#)]
54. Aronhime, M.T.; Gillham, J.K. Time-temperature-transformation (TTT) cure diagram of thermosetting polymeric systems. In *Epoxy Resins and Composites III*; Springer: Berlin/Heidelberg, Germany, 1986; Volume 78, pp. 83–113. [[CrossRef](#)]
55. Guo, Z.; Du, S.; Zhang, B. Temperature field of thick thermoset composite laminates during cure process. *Compos. Sci. Technol.* **2005**, *65*, 517–523. [[CrossRef](#)]
56. Maistros, G.M.; Partridge, I.K. Monitoring autoclave cure in commercial carbon fibre/epoxy composites. *Compos. Part B Eng.* **1998**, *29*, 245–250. [[CrossRef](#)]
57. Konstantopoulos, S.; Tonejc, M.; Maier, A.; Schledjewski, R. Exploiting temperature measurements for cure monitoring of FRP composites—Applications with thermocouples and infrared thermography. *J. Reinf. Plast. Compos.* **2015**, *34*, 1015–1026. [[CrossRef](#)]
58. Dollimore, D. *Thermal Characterization of Polymeric Materials*; Turi, E.A., Ed.; Academic Press: New York, NY, USA; London, UK, 1981; p. 972.
59. Sourour, S.; Kamal, M.R. Differential scanning calorimetry of epoxy cure: Isothermal cure kinetics. *Thermochim. Acta* **1976**, *14*, 41–59. [[CrossRef](#)]
60. Vyazovkin, S.; Sbirrazzuoli, N. Isoconversional kinetic analysis of thermally stimulated processes in polymers. *Macromol. Rapid Commun.* **2006**, *27*, 1515–1532. [[CrossRef](#)]
61. Pantelelis, N.; Vrouvakis, T.; Spentzas, K. Cure cycle design for composite materials using computer simulation and optimisation tools. *Forsch. Ing.* **2003**, *67*, 254–262. [[CrossRef](#)]
62. *Technical Data Sheet CYCOM(R) 5320-1 Prepreg*; Solvay Composite Materials; Solvay: Brussels, Belgium, 2017.
63. Bruk, D. Implementation Methodology, Validation, and Augmentation of a Cure Kinetic Model for Carbon Fiber/CYCOM 5320-1, FM309-1, and FM300-2. Ph.D. Thesis, Washington University in St. Louis, St. Louis, MO, USA, 2021.
64. Kim, I.L.G.; Lee, D.G. Dielectric cure monitoring for glass/polyester prepreg composites. *Compos. Struct.* **2002**, *57*, 91–99. [[CrossRef](#)]
65. Marin, E.; Robert, L.; Triollet, S.; Ouedane, Y. Liquid resin infusion process monitoring with superimposed fibre Bragg grating sensor. *Polym. Test.* **2012**, *31*, 1045–1052. [[CrossRef](#)]
66. Wang, P.; Molimard, J.; Drapier, S.; Vautrin, A.; Minni, J.C. Monitoring the resin infusion manufacturing process under industrial environment using distributed sensors. *J. Compos. Mater.* **2011**, *46*, 691–706. [[CrossRef](#)]
67. Shevtsov, S.; Zhilyaev, I.; Soloviev, A.; Parinov, I.; Dubrov, V. Optimization of the composite cure process on the basis of thermo-kinetic model. *Adv. Mater. Res.* **2012**, *569*, 185–192. [[CrossRef](#)]
68. Aleksendrić, D.; Carlone, P.; Ćirović, V. Optimization of the temperature-time curve for the curing process of thermoset matrix composites. *Appl. Compos. Mater.* **2016**, *23*, 1047–1063. [[CrossRef](#)]
69. Chaloupka, A. Development of a Dielectric Sensor for the Real-Time In-Mold Characterization of Carbon Fiber Reinforced Thermosets. Ph.D. Thesis, University of Augsburg, Augsburg, Germany, 2018.
70. Day, D.R.; Lewis, T.J.; Lee, I.L.; Senturia, S.D. The role of boundary layer capacitance at blocking electrodes in the interpretation of dielectric cure data in adhesives. *J. Adhes.* **1985**, *18*, 73–90. [[CrossRef](#)]
71. Mijović, J.; Yee, C.F.W. Use of Complex Impedance To Monitor the Progress of Reactions in Epoxy/Amine Model Systems. *Macromolecules* **1994**, *27*, 7287–7293. [[CrossRef](#)]
72. Kim, J.-S.; Lee, D.G. On-line cure monitoring and viscosity measurement of carbon fiber epoxy composite materials. *J. Mater. Process. Technol.* **1993**, *37*, 405–416. [[CrossRef](#)]
73. Fournier, J.; Williams, G.; Duch, C.; Aldridge, G.A. Changes in molecular dynamics during bulk polymerization of an epoxide-amine system as studied by dielectric relaxation spectroscopy. *Macromolecules* **1996**, *29*, 7097–7107. [[CrossRef](#)]
74. Chaloupka, A.; Pflöck, T.; Horny, R.; Rudolph, N.; Horn, S.R. Dielectric and rheological study of the molecular dynamics during the cure of an epoxy resin. *J. Polym. Sci. Part B Polym. Phys.* **2018**, *56*, 907–913. [[CrossRef](#)]
75. Hardis, R.; Jessop, J.L.P.; Peters, F.E.; Kessler, M.R. Cure kinetics characterization and monitoring of an epoxy resin using DSC, Raman spectroscopy, and DEA. *Compos. Part A Appl. Sci. Manuf.* **2013**, *49*, 100–108. [[CrossRef](#)]
76. Mijović, J.; Anđelić, S.; Fitz, B.; Zurawsky, W.; Mondragon, L.; Bellucci, F.; Nicolais, L. Impedance spectroscopy of reactive polymers. 3. Correlations between dielectric, spectroscopic, and rheological properties during cure of a trifunctional epoxy resin. *J. Polym. Sci. Part B Polym. Phys.* **1996**, *34*, 379–388. [[CrossRef](#)]
77. Tifkitis, K.I.; Skordos, A.A. A novel dielectric sensor for process monitoring of carbon fibre composites manufacture. *Compos. Part A Appl. Sci. Manuf.* **2019**, *123*, 180–189. [[CrossRef](#)]
78. Mesogitis, T.S.; Maistros, G.M.; Asareh, M.; Lira, C.; Skordos, A.A. Optimisation of an in-process lineal dielectric sensor for liquid moulding of carbon fibre composites. *Compos. Part A Appl. Sci. Manuf.* **2021**, *140*, 106190. [[CrossRef](#)]
79. Kazilas, M.C.; Partridge, I.K. Exploring equivalence of information from dielectric and calorimetric measurements of thermoset cure—a model for the relationship between curing temperature, degree of cure and electrical impedance. *Polymer* **2005**, *46*, 5868–5878. [[CrossRef](#)]

80. Abraham, D.; McIlhagger, R. Glass fibre epoxy composite cure monitoring using parallel plate dielectric analysis in comparison with thermal and mechanical testing techniques. *Compos. Part A* **1998**, *29*, 811–819. [[CrossRef](#)]
81. O'Dwyer, M.J.; Maistros, G.M.; James, S.W.; Tatam, R.P.; Partridge, I.K. Relating the state of cure to the real-time internal strain development in a curing composite using in-fibre Bragg gratings and dielectric sensors. *Meas. Sci. Technol.* **1998**, *9*, 1153–1158. [[CrossRef](#)]
82. Kim, D.; Centea, T.; Nutt, S.R. In-situ cure monitoring of an out-of-autoclave prepreg: Effects of out-time on viscosity, gelation and vitrification. *Compos. Sci. Technol.* **2014**, *102*, 132–138. [[CrossRef](#)]
83. Yang, Y.; Plovie, B.; Chiesura, G.; Vervust, T.; Daelemans, L.; Mogosanu, D.-E.; Wuytens, P.; De Clerck, K.; Vanfleteren, J. Fully integrated flexible dielectric monitoring sensor system for real-time in situ prediction of the degree of cure and glass transition temperature of an epoxy resin. *IEEE Trans. Instrum. Meas.* **2021**, *70*, 6004809. [[CrossRef](#)]
84. Boll, D.; Schubert, K.; Brauner, C.; Lang, W. Miniaturized flexible interdigital sensor for in situ dielectric cure monitoring of composite materials. *IEEE Sens. J.* **2014**, *14*, 2193–2197. [[CrossRef](#)]
85. Kahali Moghaddam, M.; Breede, A.; Chaloupka, A.; Bödecker, A.; Habben, C.; Meyer, E.-M.; Brauner, C.; Lang, W. Design, fabrication and embedding of microscale interdigital sensors for real-time cure monitoring during composite manufacturing. *Sens. Actuators A Phys.* **2016**, *243*, 123–133. [[CrossRef](#)]
86. Park, H. Dielectric cure determination of a thermosetting epoxy composite prepreg. *J. Appl. Polym. Sci.* **2017**, *134*. [[CrossRef](#)]
87. Franieck, E.; Fleischmann, M.; Ilöck, O.; Kutuzova, L.; Kandelbauer, A. Cure kinetics modeling of a high glass transition temperature epoxy molding compound (EMC) based on inline dielectric analysis. *Polymers* **2021**, *13*, 1734. [[CrossRef](#)]
88. Lee, D.G.; Kim, H.G. Non-isothermal in situ dielectric cure monitoring for thermosetting matrix composites. *J. Compos. Mater.* **2007**, *38*, 977–993. [[CrossRef](#)]
89. Kim, S.S.; Murayama, H.; Kageyama, K.; Uzawa, K.; Kanai, M. Study on the curing process for carbon/epoxy composites to reduce thermal residual stress. *Compos. Part A Appl. Sci. Manuf.* **2012**, *43*, 1197–1202. [[CrossRef](#)]
90. Skordos, A.A.; Partridge, I.K. Effects of tool-embedded dielectric sensors on heat transfer phenomena during composite cure. *Polym. Compos.* **2007**, *28*, 139–152. [[CrossRef](#)]
91. Breede, A.; Moghaddam, M.K.; Brauner, C.; Herrmann, A.S.; Lang, W. Online process monitoring and control by dielectric sensors for a composite main spar for wind turbine blades. In Proceedings of the 20th International Conference on Composite Materials, Copenhagen, Denmark, 19–24 July 2015.
92. Lionetto, F.; Maffezzoli, A. Monitoring the cure state of thermosetting resins by ultrasound. *Materials* **2013**, *6*, 3783–3804. [[CrossRef](#)]
93. Tuloup, C.; Harizi, W.; Aboura, Z.; Meyer, Y.; Khellil, K.; Lachat, R. On the use of in-situ piezoelectric sensors for the manufacturing and structural health monitoring of polymer-matrix composites: A literature review. *Compos. Struct.* **2019**, *215*, 127–149. [[CrossRef](#)]
94. Challis, R.E.; Blarel, F.; Unwin, M.E.; Paul, J.; Guo, X. Models of ultrasonic wave propagation in epoxy materials. *IEEE Trans. Ultrason. Ferroelectr. Freq. Control* **2009**, *56*, 1225–1237. [[CrossRef](#)] [[PubMed](#)]
95. Perepechko, I. *Acoustic Methods Of Investigating Polymers*; Mir Publishers: Moscow, Russia, 1975.
96. Maffezzoli, A.; Quarta, E.; Luprano, V.A.M.; Montagna, G.; Nicolais, L. Cure monitoring of epoxy matrices for composites by ultrasonic wave propagation. *J. Appl. Polym. Sci.* **1999**, *73*, 1969–1977. [[CrossRef](#)]
97. Lionetto, F.; Montagna, G.; Maffezzoli, A. Ultrasonic dynamic mechanical analysis of polymers. *Appl. Rheol.* **2005**, *15*, 326–335. [[CrossRef](#)]
98. Lionetto, F.; Tarzia, A.; Coluccia, M.; Maffezzoli, A. Air-coupled ultrasonic cure monitoring of unsaturated polyester resins. *Macromol. Symp.* **2007**, *247*, 50–58. [[CrossRef](#)]
99. Lionetto, F.; Tarzia, A.; Maffezzoli, A. Air-coupled ultrasound: A novel technique for monitoring the curing of thermosetting matrices. *IEEE Trans. Ultrason. Ferroelectr. Freq. Control* **2007**, *54*, 1437–1444. [[CrossRef](#)] [[PubMed](#)]
100. Dorigi, J.; Krishnaswamy, S.; Achenbach, J.D. A fiber optic ultrasound sensor for monitoring the cure of epoxy. In *Review of Progress in Quantitative Nondestructive Evaluation*; Springer: Boston, MA, USA, 1998; pp. 657–664.
101. Ghodhbani, N.; Maréchal, P.; Duflo, H. Ultrasonic monitoring of the cure kinetics of an epoxy resin: Identification, frequency and temperature dependence. *Polym. Test.* **2016**, *56*, 156–166. [[CrossRef](#)]
102. Schmachtenberg, E.; Schulte zur Heide, J.; Töpker, J. Application of ultrasonics for the process control of Resin Transfer Moulding (RTM). *Polym. Test.* **2005**, *24*, 330–338. [[CrossRef](#)]
103. Hudson, T.B.; Yuan, F.G. Automated in-process cure monitoring of composite laminates using a guided wave-based system with high-temperature piezoelectric transducers. *J. Nondestruct. Eval. Diagn. Progn. Eng. Syst.* **2018**, *1*, 021008. [[CrossRef](#)]
104. Samet, N.; Maréchal, P.; Duflo, H. Ultrasonic characterization of a fluid layer using a broadband transducer. *Ultrasonics* **2012**, *52*, 427–434. [[CrossRef](#)]
105. Pindinelli, C.; Montagna, G.; Luprano, V.A.M.; Maffezzoli, A. Network development during epoxy curing: Experimental ultrasonic data and theoretical predictions. *Macromol. Symp.* **2002**, *180*, 73–88. [[CrossRef](#)]
106. Lionetto, F.; Rizzo, R.; Luprano, V.A.M.; Maffezzoli, A. Phase transformations during the cure of unsaturated polyester resins. *Mater. Sci. Eng. A* **2004**, *370*, 284–287. [[CrossRef](#)]
107. Challis, R.E.; Unwin, M.E.; Chadwick, D.L.; Freemantle, R.J.; Partridge, I.K.; Dare, D.J.; Karkanis, P.I. Following network formation in an epoxy/amine system by ultrasound, dielectric, and nuclear magnetic resonance measurements: A comparative study. *J. Appl. Polym. Sci.* **2003**, *88*, 1665–1675. [[CrossRef](#)]

108. Scholle, P.; Sinapius, M. Pulse ultrasonic cure monitoring of the pultrusion process. *Sensors* **2018**, *18*, 3332. [[CrossRef](#)] [[PubMed](#)]
109. Tuloup, C.; Harizi, W.; Aboura, Z.; Meyer, Y.; Ade, B.; Khellil, K. Detection of the key steps during Liquid Resin Infusion manufacturing of a polymer-matrix composite using an in-situ piezoelectric sensor. *Mater. Today Commun.* **2020**, *24*, 101077. [[CrossRef](#)]
110. Liebers, N.; Buggisch, M.; Kleineberg, M.; Wiedemann, M. Autoclave infusion of aerospace ribs based on process monitoring and control by ultrasound sensors. In Proceedings of the 20th International Conference on Composite Materials, Copenhagen, Denmark, 20–24 July 2015.
111. Liebers, N.; Bertling, D. Ultrasonic resin flow and cure monitoring. In Proceedings of the Conference on Flow Processing in Composite Materials, Luleå, Sweden, 30 May–1 June 2018.
112. Liebers, N.; Raddatz, F.; Schadow, F. Effective and flexible ultrasound sensors for cure monitoring for industrial composite production. In Proceedings of the Deutscher Luft- und Raumfahrtkongress, Berlin, Germany, 10–12 September 2012.
113. Lin, M.; Chang, F.-K. The manufacture of composite structures with a built-in network of piezoceramics. *Compos. Sci. Technol.* **2002**, *62*, 919–939. [[CrossRef](#)]
114. Khoun, L.; de Oliveira, R.; Michaud, V.; Hubert, P. Investigation of process-induced strains development by fibre Bragg grating sensors in resin transfer moulded composites. *Compos. Part A Appl. Sci. Manuf.* **2011**, *42*, 274–282. [[CrossRef](#)]
115. Murawski, L.; Opoka, S.; Majewska, K.; Mieloszyk, M.; Ostachowicz, W.; Weintrit, A. Investigations of marine safety improvements by structural health monitoring systems. *Int. J. Mar. Navig. Saf. Sea Transp.* **2012**, *6*, 223–229.
116. Min, R.; Liu, Z.; Pereira, L.; Yang, C.; Sui, Q.; Marques, C. Optical fiber sensing for marine environment and marine structural health monitoring: A review. *Opt. Laser Technol.* **2021**, *140*, 107082. [[CrossRef](#)]
117. Schubel, P.J.; Crossley, R.J.; Boateng, E.K.G.; Hutchinson, J.R. Review of structural health and cure monitoring techniques for large wind turbine blades. *Renew. Energy* **2013**, *51*, 113–123. [[CrossRef](#)]
118. Rao, Y.-J. In-fibre Bragg grating sensors. *Meas. Sci. Technol.* **1997**, *8*, 355–375. [[CrossRef](#)]
119. Li, C.; Cao, M.; Wang, R.; Wang, Z.; Qiao, Y.; Wan, L.; Tian, Q.; Liu, H.; Zhang, D.; Liang, T.; et al. Fiber-optic composite cure sensor: Monitoring the curing process of composite material based on intensity modulation. *Compos. Sci. Technol.* **2003**, *63*, 1749–1758. [[CrossRef](#)]
120. Buggy, S.J.; Chehura, E.; James, S.W.; Tatam, R.P. Optical fibre grating refractometers for resin cure monitoring. *J. Opt. A Pure Appl. Opt.* **2007**, *9*, S60–S65. [[CrossRef](#)]
121. Lekakou, C.; Cook, S.; Deng, Y.; Ang, T.W.; Reed, G.T. Optical fibre sensor for monitoring flow and resin curing in composites manufacturing. *Compos. Part A Appl. Sci. Manuf.* **2006**, *37*, 934–938. [[CrossRef](#)]
122. Tsai, L.; Cheng, T.-C.; Lin, C.-L.; Chiang, C.-C. Application of the embedded optical fiber Bragg grating sensors in curing monitoring of Gr/epoxy laminated composites. In *Smart Sensor Phenomena, Technology, Networks, and Systems 2009*; SPIE: Washington, DC, USA, 2009; pp. 57–64.
123. Leng, J.S.; Asundi, A. Real-time cure monitoring of smart composite materials using extrinsic Fabry-Perot interferometer and fiber Bragg grating sensors. *Smart Mater. Struct.* **2002**, *11*, 249–255. [[CrossRef](#)]
124. Jung, K.; Kang, T.J. Cure monitoring and internal strain measurement of 3-D hybrid braided composites using fiber bragg grating sensor. *J. Compos. Mater.* **2007**, *41*, 1499–1519. [[CrossRef](#)]
125. Sampath, U.; Kim, H.; Kim, D.G.; Kim, Y.C.; Song, M. In-Situ cure monitoring of wind turbine blades by using fiber Bragg grating sensors and fresnel reflection measurement. *Sensors* **2015**, *15*, 18229–18238. [[CrossRef](#)]
126. Yeager, M.; Todd, M.; Gregory, W.; Key, C. Assessment of embedded fiber Bragg gratings for structural health monitoring of composites. *Struct. Health Monit.* **2016**, *16*, 262–275. [[CrossRef](#)]
127. Gupta, N.; Sundaram, R. Fiber optic sensors for monitoring flow in vacuum enhanced resin infusion technology (VERITY) process. *Compos. Part A Appl. Sci. Manuf.* **2009**, *40*, 1065–1070. [[CrossRef](#)]
128. Kuang, K.S.C.; Zhang, L.; Cantwell, W.J.; Bennion, I. Process monitoring of aluminum-foam sandwich structures based on thermoplastic fibre-metal laminates using fibre Bragg gratings. *Compos. Sci. Technol.* **2005**, *65*, 669–676. [[CrossRef](#)]

CHAPTER 3: (PAPER 1) DIELECTRIC PARAMETER INDEPENDENT CURING ANALYSIS OF OUT-OF- AUTOCLAVE CARBON FIBRE/EPOXY COMPOSITES

3.1 Introduction

This chapter provides a systematic comparison of existing dielectric analysis methods with a set of newly proposed techniques. This builds on the review of existing dielectric analysis techniques, which were detailed in the Chapter 1 literature review. More than a dozen cure correlation methods have been proposed in literature to date, each focusing on a specific dielectric parameter and employing different definitions for how the methods should be implemented. This study collects dielectric signal data (dissipation factor, impedance, ionic conductivity/viscosity, loss factor, and permittivity) during cure of an out-of-autoclave thermoset prepreg and evaluates the results using analytical testing and numerical simulations. This systematic evaluation presented in this study prove that the parameters can be used interchangeably and, in some cases, can deliver complementary information. The major outcome of this study is a master list of dielectric analysis correlation techniques which can measure the thermoset degree of cure or T_g in addition to identify the timing of key cure events.

3.2 Links and implications

The comprehensive list of analysis techniques proposed in this study have significant implications for all future dielectric analysis studies, such as those presented in Chapter 4 (Paper 2). These methods have improved accuracy and repeatability in comparison to the existing analysis techniques, which are commonly proposed from a single data set. The use of five replicates in this study suggests the repeatability and accuracy of the proposed cure analysis methods. The repeatability of these methods for alternate sensor configurations is explored in Chapter 4, in which the methods are applied to a novel tool-mounted sensor which evaluates cure through the thickness of a composite laminate. Additionally, the newly discovered parameter-independence allows for more analysis flexibility than has previously been demonstrated. This has significant implications for live process monitoring of thermoset cure and could enable active control systems.

3.3 Published paper



Dielectric parameter independent curing analysis of out-of-autoclave carbon fibre/epoxy composites

Molly Hall^{a,*}, Xuesen Zeng^a, Tristan Shelley^a, Peter Schubel^a

^a Centre for Future Materials, University of Southern Queensland, Toowoomba, QLD 4350, Australia

ARTICLE INFO

Keywords:

A. Thermosetting resin
B. Cure behaviour
B. Electrical properties
Dielectric sensors

ABSTRACT

Due to their capability to evaluate the microscopic mobility of polymers, dielectric sensors are increasingly used for in-situ cure monitoring of thermoset composites. More than a dozen cure correlation methods have been proposed in literature to date, each of which focuses on a specific dielectric parameter. However, the wide variety of techniques have not been compared nor robustly evaluated for accuracy and repeatability. This study collects dielectric signal data (dissipation factor, impedance, ionic conductivity/viscosity, loss factor, and permittivity) during cure of an out-of-autoclave thermoset prepreg and conducts a systematic evaluation of the five dielectric parameters to prove that the parameters can be used interchangeably and, in some cases, can deliver complementary information. By correlating features of dielectric graphs to both experimentally measured and numerically simulated cure state events, a master list of correlation techniques is presented. The proposed techniques have improved accuracy and repeatability in comparison to the existing analysis techniques.

1. Introduction

Advanced thermoset polymer composites have been implemented by a range of industries due to their combination of excellent properties and wide variety of manufacturing techniques [1–14]. Fibre reinforced polymer (FRP) composites research is currently focused on enabling high quality and high complexity parts [15,16], with much emphasis on optimising the processing conditions for fabrication [17–19]. Composite parts are susceptible to a variety of quality issues due to high levels of manufacturing uncertainty stemming from variation in the raw materials and processing conditions [20,21]. A major challenge in optimising composites processing techniques is accounting for the impact of system variability on the final product output. Quality control requirements commonly dictate that components must achieve a specified state of resin cure, as the completion of the polymer conversion process is directly linked to the mechanical performance of the final product [22]. As the complexity and scale of composite parts increases it becomes more challenging to meet this threshold. Much research is being conducted on using different types of sensors for in-situ cure monitoring as a method of demonstrating compliance to quality requirements. In-situ sensor networks are also an appealing technology for enabling active control of the manufacturing process. By having direct knowledge of the material state, processes parameters can be updated live which allows

for process optimisation.

A range of sensor types have been investigated for their ability to monitor this thermoset cure state including thermocouples, ultrasonic sensors [23–25], fibre optic sensors [26–28], and dielectric sensors [29–31]. The capabilities and limitations of these sensors have been extensively reviewed [32,33]. A recent review on these four common in-situ cure monitoring sensors has explored the different methods for correlating monitored parameters to cure state information [34]. Thermocouples monitor the change in temperature, which can then be used as an input to a kinetic model for a given resin system to understand cure state. Ultrasonic sensors monitor the change in attenuation of ultrasonic waves as they propagate through the material, showing clear phase transformations as the matrix crosslinks and changes in density. Fibre optic sensors, depending on the type, will monitor how light refraction or strain changes in response to a cross-linking matrix. Dielectric sensors, however, are one of the most promising methods of in-situ cure monitoring as they have identified not just phase transitions, but degree of cure (DoC) and glass transition temperature (T_g) progression. The reader is encouraged to use this review as a supplement for the brief summary of analysis techniques provided here, and in particular for the current state of the art for dielectric analysis.

The dielectric sensor operates by generating a time varying electric field which fluctuates at a set frequency or range of frequencies.

* Corresponding author.

E-mail address: molly.hall@usq.edu.au (M. Hall).

<https://doi.org/10.1016/j.compositesa.2023.107755>

Received 1 June 2023; Received in revised form 2 August 2023; Accepted 24 August 2023

Available online 25 August 2023

1359-835X/© 2023 The Authors. Published by Elsevier Ltd. This is an open access article under the CC BY-NC-ND license (<http://creativecommons.org/licenses/by-nc-nd/4.0/>).

Dielectric analysis (DEA) is then conducted by monitoring changes in the electrical behaviour of the polymer during cure and relating these events in the electrical behaviour to physical material changes. A current is generated in response to the sensor's applied excitation voltage, which results in a total electrical impedance of the material. This measurement is composed of resistive and capacitive components, which originates from ion movement and dipole rotation within the material under test. As the material cures and the polymer chains crosslink, the ion and dipole movements are restricted. By monitoring these changes as the cure time progresses, it is possible to identify major curing events such as the onset of the cure reaction, point of minimum resin viscosity, and end of the cure reaction.

Many researchers have investigated methods of conducting DEA, however each have used different parameters and methods to correlate dielectric information with material cure state information. Commonly, analysis is completed by evaluating signal change as time progresses (time-spectrum) or signal change across a range of frequencies (frequency-domain) [35–37]. A summary of key time-spectrum analysis techniques is presented in Table 1. This material presented in this study displays frequency-independent behaviour at the investigated frequencies due to the impact of ion migration dominating the dielectric signal [38]. For this reason, this paper will focus on time-spectrum analyses and their correlations with thermodynamic transitions and reactions of the material under test. To date, the existing methods have not

been compared side by side to evaluate their accuracy and repeatability. This paper presents a systematic approach to correlating dielectric signals to material cure state information for the cure of Solvay CYCOM® 5320-1 carbon fibre/epoxy prepreg. Cure characterisation for 5320-1 has been completed by [39] and further refined by [40]. The kinetic model used here, via Convergent RAVEN, is based on the Kratz model [39]. A thorough evaluation is presented for multiple cures, with consideration of all dielectric parameters and their correlations to simulated and analytical test results. As all five dielectric parameters are calculated based on the materials' dielectric behaviour, specifically capacitive and resistive response, this paper hypothesises that the dielectric parameters can be used interchangeably for the monitoring of thermoset cure reactions. Based on this, a final set of correlation techniques is proposed, including validation and verification of existing techniques and proposed modifications and updates for future implementation.

2. Methodology

2.1. Materials and sample preparation

This study used Solvay CYCOM® 5320-1 carbon fibre/epoxy prepreg, for which the material definition is stated in Table 2. Prepreg squares measuring 80 mm by 80 mm were laid up in a [0,90]_s configuration, with a NETZSCH IDEX 115/60T interdigitated dielectric sensor and a K-type thermocouple embedded at the midplane as shown in Fig. 1. The four-ply configuration was chosen to ensure good contact between the sensor and the epoxy. It should be noted that the sensor has a penetration depth of 115 µm, which is within the first ply placed above the electrodes. Additional thermocouples collected thermal data on the top of the vacuum bag, under the tool, and in the air approximately 100 mm above the top of the bag. A secondary panel, also 80 mm by 80 mm, with layup scheme [0/90]_{4s} was manufactured without any embedded sensors to produce Dynamic Mechanical Analysis (DMA) test specimens. This layup sequence was chosen in accordance with the ASTM standard for DMA testing of composites [41]. Both laminates were fabricated on a 15 mm thick steel tool and vacuum bagged in accordance with the manufacturers recommended vacuum bagging schematic [42]. Five replicates of this assembly, designated IDEX1 through IDEX5, were cured in an oven under vacuum using a modified version of the manufacturers recommended cure cycle. The cure profile started from ambient conditions and increased at 2–2.5 °C/min to 180 °C, followed by a 2-hour dwell at 180 °C, and subsequent cooling back to ambient temperatures. The data collected from these panels follows the data flow indicated in Fig. 2. The following sections detail the methods used to complete the dielectric analysis, cure simulation, and analytical testing.

2.2. RAVEN simulation

Convergent RAVEN software was used to simulate the cure of the prepreg based on the temperature profile collected from the mid-plane thermocouple. This thermocouple was selected for simulation as it corresponds to the location of the embedded IDEX sensor. A 0D cure profile was run using the built-in material card for the CYCOM® 5320-1/IM7-12K Tape based on the Kratz cure kinetics model [39] and using the thermocouple data taken from the midplane of the laminate. Cure

Table 1

Overview of existing dielectric correlation methods, including the method used and the cure feature that is output from the method. Methods are indicated by the dielectric parameter with DISP indicating the dissipation factor (D), IMP indicating the Impedance (Z), COND indicating the ion conductivity (σ), LOSS indicating the loss factor (ε''), and VISC indicating the ion viscosity (ρ).

Name	Method	Cure Feature	Sources
DISP-1	First local maximum of $\frac{dD}{dt}$	Cure start	[47]
DISP-2	Plateau onset ($\frac{dD}{dt} = 0$)	Cure completion	[47]
DISP-3	$\tan\delta = 1$ defined as the crossover point between loss and permittivity	Gel point	[49]
IMP-1	Onset of the first plateau after the minimum value of impedance at 1 kHz	Gel point	[30,45]
IMP-2	Onset of the second plateau after the minimum value of impedance at 1 kHz	Vitrification	[30,45]
IMP-3	Linear regression to determine relationship between log(impedance) and degree of cure over the isothermal range	Degree of cure progression	[52]
COND-1	Global maximum of the conductivity	Minimum viscosity	[31,53]
COND-2	Inflection after the peak of the conductivity	First indication of gelled material	[31,53]
COND-3	Plateau onset ($\frac{d\sigma}{dt} = 0$)	Vitrification	[31,53]
COND-4	$T_g = \frac{\log\sigma_0 - \log\sigma_t}{\log\sigma_0 - \log\sigma_\infty} T_{g0}$ With the conductivity at the start (σ_0) and end (σ_∞) of the isothermal region, conductivity at time t (σ_t), and the measured glass transition temperature (T_{g0})	T_g progression	[46]
LOSS-1	$\alpha = \frac{\log\epsilon''_0 - \log\epsilon''_t}{\log\epsilon''_0 - \log\epsilon''_\infty}$ With the loss factor at the start (ϵ''_0) and end (ϵ''_∞) of the isothermal region, and the loss factor at time t (ϵ''_t).	Cure index	[54]
VISC-1	Plateau onset ($\frac{d\rho}{dt} = 0$)	Cure completion	[48,55]
VISC-2	$\alpha = \frac{\log\rho_t - \log\rho_{min}}{\log\rho_{max} - \log\rho_{min}}$ With the viscosity at time t (ρ_t), minimum viscosity (ρ_{min}), maximum viscosity (ρ_{max}), and the measured degree of cure (α_m)	Degree of cure progression	[30]

Table 2
Solvay CYCOM® 5320-1 prepreg definition and properties [42].

Property	Value
Resin	CYCOM® 5320-1
Fibre	IHexcel IM7 12 K
Prepreg Areal Weight (gsm)	145
Resin Content (%)	33
Form	Unidirectional Tape

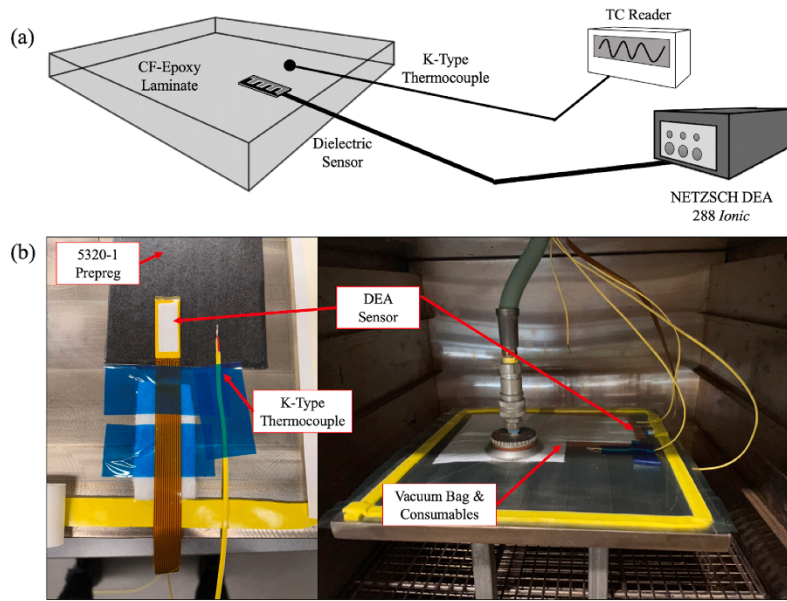


Fig. 1. Cure setup including (a) schematic of sensor placement within the midplane of the laminate and (b) image of sensor placement within the laminate and laminate placement within the oven. Note that placement of TC Reader and DEA Reader shown in (a) are located outside of the oven.

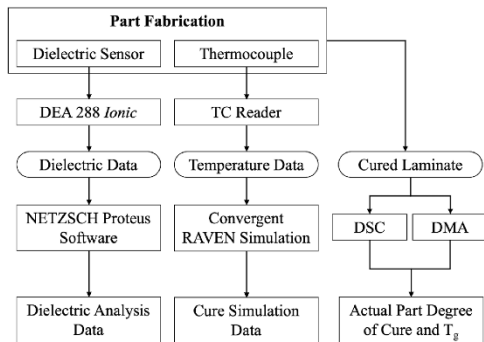


Fig. 2. Schematic of data flow from data collection to analysis.

features were identified for each IDEX panel in accordance with Fig. 3. The final degree of cure shown in (a) is identified as the end value of the degree of cure curve. The vitrification point shown in (b) is identified as the crossover point between the T_g and temperature, and the final T_g also shown in (b) is identified as the end value of the T_g curve. The start of cure and end of cure both found in (c) is indicated by the start and ending of the cure reaction rate. The time at minimum viscosity shown in (d) is indicated by the global minimum, and the gel point also shown in (d) is indicated by the inflection of the viscosity curve. The logarithmic scale for (d) should be noted.

2.3. DSC measurements

Differential Scanning Calorimetry (DSC) was conducted using a TA

DSC25. Approximately 5–10 mg of material cut from each IDEX panel was tested under a dynamic ramp rate of 5 °C/min from 25 to 280 °C. The actual laminate degree of cure was calculated by integrating under the heat flow-time curve and dividing by the total heat of reaction for 5320-1, which is indicated as 561.8 J/g per Convergent RAVEN.

2.4. DMA measurements

Dynamic Mechanical Analysis (DMA) was conducted using a TA HR-2 Hybrid Rheometer. Test coupons were cut by waterjet from the 10/90I₄₅ panel to dimensions of 8 mm wide by 45 mm long with a tolerance of ±0.2 mm. They were dried in an air circulated oven at 120 °C for a minimum of 16 h, and then held in a sealed container with desiccant prior to testing. They were tested by a dynamic ramp rate of 5 °C/min from 25 to 280 °C with a displacement of 50 μm oscillating at 1 Hz frequency. The T_g was calculated in accordance with ASTM D 7028 [41] by the storage modulus (E') onset, and the degree of cure was calculated using this value and the DiBenedetto equation.

2.5. Dielectric analysis

2.5.1. Data collection

Dielectric data was collected using NETZSCH IDEX 115/60T interdigitated sensors and the NETZSCH DEA 288 Ionic data analyser. The sensor collected parameter data for frequencies between 1 Hz and 10 kHz with 4 frequencies set logarithmically per decade. The resistive (R) and capacitive (C) responses of the material under the time varying electric field were used to calculate the five dielectric parameters.

The complex permittivity (ϵ^*) is a measure of the polarizability of a material under a time-varying electric field. It is composed of a relative permittivity (ϵ') calculated via Equation (1) and a loss component (ϵ'') calculated by Equation (2) [43].

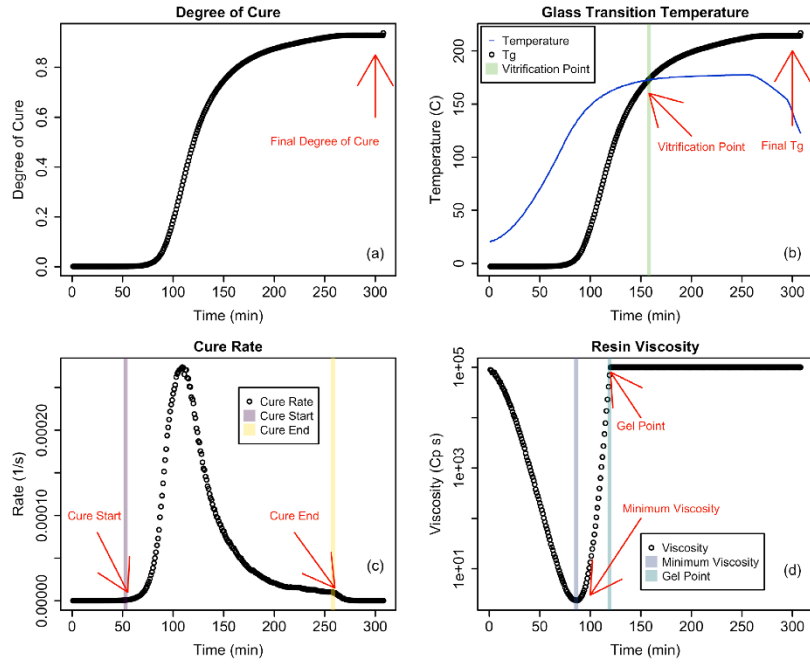


Fig. 3. Method of determining cure states using Convergent RAVEN, indicated with red arrows. (For interpretation of the references to colour in this figure legend, the reader is referred to the web version of this article.)

$$\epsilon' = \frac{Cd}{\epsilon_0 A} \quad (1)$$

$$\epsilon'' = \frac{d}{R\omega A \epsilon_0} \quad (2)$$

The dissipation factor (D), also known as $\tan\delta$, can be calculated in Equation (3) as the ratio of the dielectric loss (loss component) and permittivity (storage component) [44]:

$$D = \tan\delta = \frac{\epsilon''}{\epsilon'} = \frac{1}{\omega RC} \quad (3)$$

The ionic conductivity (σ) is a material property related to the bulk dielectric conductance (G), which is the inverse of the resistance (R). It is also related to the ion viscosity (ρ) by an inverse relationship demonstrated in Equation (4) [37]. It should be noted that the ion viscosity is a term which is used to represent the frequency independent resistivity (ρ_{DC}), which here will be represented as ρ for simplicity. Within dielectric analysis it is common to represent the log of the ionic conductivity, which is referred to as the LIC.

$$\rho = \frac{1}{\sigma} = \frac{RA}{d} \quad (4)$$

Impedance (Z) is calculated in Equation (5) with i representing the complex number [37].

$$Z = \frac{1}{\frac{1}{R} + i\omega C} \quad (5)$$

Equations (1)–(5) utilise the shape factor (A/d) driven by the electrode spacing and sensing area, permittivity of free space ($\epsilon_0 = 8.854 \times 10^{-12} \text{ F m}^{-1}$), and electrical excitation frequency (ω). It should be noted that the shape factor is commonly applied to a parallel plate

configuration, however it has been documented to be a relevant scaling factor for other configurations such as interdigitated electrodes, as are used in this paper.

Logarithmic scaling is commonly used for all dielectric parameters to isolate the effects of ion mobility and dipole rotation. For example, the permittivity represented in log scale takes the format of Equation (6). This allows for the separation of the capacitance from the constant variables which do not impact the curing: the electrode $\frac{A}{d}$ ratio and the permittivity of free space. By evaluating the logarithm of the dielectric parameters, the direct impact of curing on the capacitance and resistivity can be isolated.

$$\log \epsilon' = \log \frac{Cd}{\epsilon_0 A} = \log C - \log \frac{d}{\epsilon_0 A} \quad (6)$$

Data was processed using NETZSCH Proteus® software. Signals were smoothed up to software setting 6–8 to minimise signal noise. Data collected at a frequency of 1 Hz was used for all correlations, excepting all dissipation factor methods and IMP-1 and -2, as it most appropriately fits the timescale of the cure reaction for this out-of-autoclave epoxy. It should be noted that resin systems which cure more quickly, in the manner of minutes or seconds, may benefit from higher frequency measurements in order to accurately capture the cure events. Higher frequencies showed significant signal noise, and sufficient smoothing of these curves reduced the accuracy of the measurement. 1 Hz measurements generally had the best resolution and required minimal smoothing of the signal. As this material system displays a strong, frequency-independent conductive behaviour it is acceptable to perform the analyses on a single frequency. Cure state correlations on IDEX3 were repeated for 10 Hz, 100 Hz, and 1 kHz frequencies to verify that the results are aligned with 1 Hz measurements. It was confirmed that the choice of frequency for these methods does not impact the results. The 1

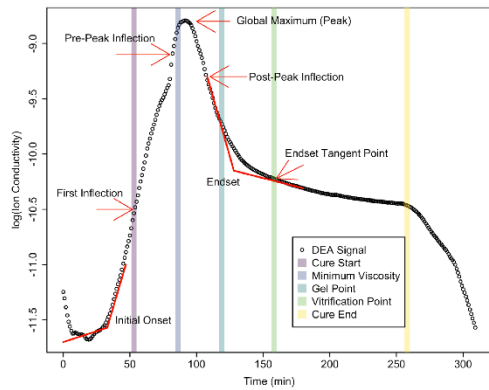


Fig. 4. Identifications of graph features and their placement relative to the RAVEN identified cure events.

Hz frequency was deemed inappropriate for the dissipation factor as it did not have reliable behaviour at low frequencies. Below 100 Hz the signal produced a double peak shape, which distorted the application of the analysis methods. Thus the 100 Hz frequency was selected for the dissipation factor to ensure that the methods can be applied as defined. Finally, the definition of IMP-1 and -2 provided by [30,45] specified the use of 1 kHz measurements, in which it is speculated that the high frequency allows for detection of molecular phenomena. In this study, frequencies between 1 and 3.16 kHz were selected in order to identify the double-shoulder behaviour most clearly.

Data analysis was conducted in accordance with the following sections. A comparison was conducted between the newly proposed correlations, existing correlations, and expansion of the existing correlations to include all dielectric parameters.

2.5.2. Proposed cure state identification methods

A cure point analysis was conducted to correlate graph features for each dielectric parameter with cure events defined by the RAVEN simulation. The change in the electrical signals indicates changes in polymer crosslinking, which can therefore be used to indicate the distinct “cure events” which occur during processing: start of cure, minimum resin viscosity, gel point, vitrification point, and the end of cure.

For this analysis, the timing of these cure events was identified from the RAVEN simulation in accordance with the criteria specified in Fig. 3. Similarly, the time at which key dielectric signal changes occurred was identified. These points are known as graph features, and includes inflections, global and local minima and maxima, onsets, endsets, and the point at which the endset intersects the curve (known as the endset tangent). An example of how these graph features are identified is shown in Fig. 4. It should be noted that the impedance follows a concave up graphical trend, whereas all other parameters are concave down. For this reason, the impedance will be referred to using minima where the other parameters will indicate a maximum. The minimum absolute value point of the derivative was used to compare with the end of cure. This point was found by identifying the time at which the minimum absolute value of the derivative curve occurs after the global maximum.

Next, the RAVEN cure events were compared with the dielectric graph features to identify which features correlated most strongly. A preliminary visual comparison, Fig. 5, was conducted to identify which graph features should be considered for comparison. This comparison

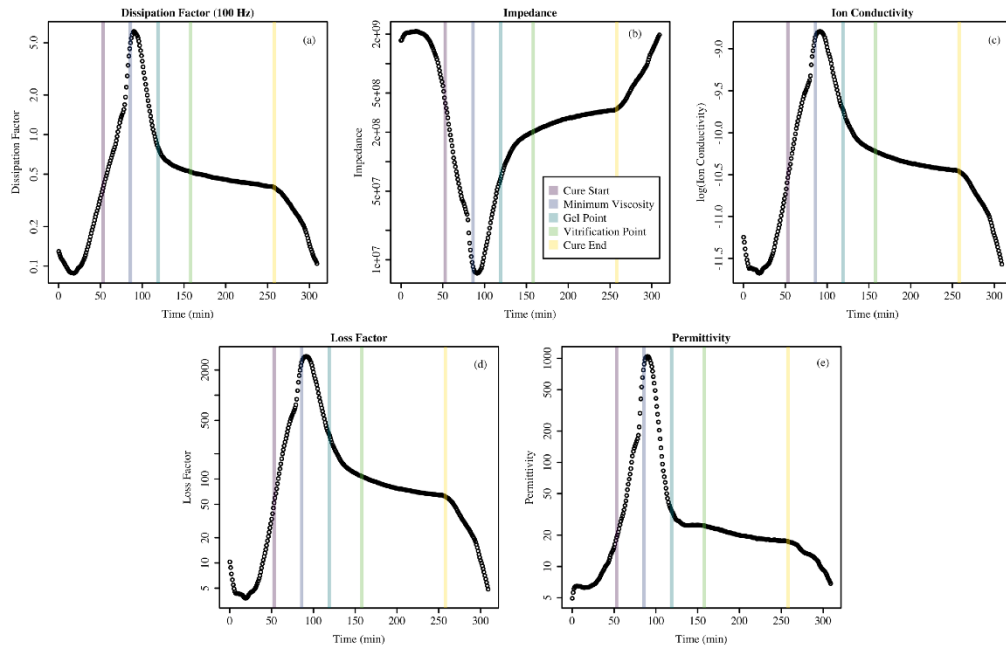


Fig. 5. Comparison of RAVEN cure events (coloured lines) to dielectric signals for (a) Dissipation Factor at 100 Hz frequency, (b) Impedance, (c) Log of the Ionic Conductivity, (d) Loss Factor and (e) Permittivity. Graphs (b-c) represent 1 Hz frequency measurements.

allowed for a down-selection of cure event-graph feature pairs. For some cure events there are multiple graph features which have a potentially strong correlation. For example, the minimum viscosity is located near both the inflection prior to the global maximum, and to the global maximum itself. Both graph feature pairs were identified for the cure point analysis to identify which of them has the strongest correlation amongst all five test replicates. It should be noted that the 100 Hz measurement for the dissipation factor was used for this analysis as it displays a single peak behaviour which most similarly aligns with the behaviour of the other parameters.

The measure of discrepancy strength for each pair was calculated as a percentage of how close the graph feature is to the cure event using Equation (7).

$$\Delta\% = \left| 100 * \frac{(t_{RAVEN} - t_{DEA})}{t_{TOTAL}} \right| \quad (7)$$

The strength ($\Delta\%$) was calculated using the time differential between when the RAVEN cure event occurs (t_{RAVEN}) and when the dielectric graph feature occurs (t_{DEA}). It is then normalised by the overall cure time (t_{TOTAL}), which in this case refers to the RAVEN estimated cure end time, in order to scale the results with the duration of the cure. The values and average values are reported as absolute values. This discrepancy rating was calculated for each dielectric parameter, for each pair, for each test replicate (IDEX1-5).

2.5.3. Further development of published cure state identification methods

Many existing DEA correlations have been proposed in literature, however each method specifically identifies a single dielectric variable. These correlations, which are listed in Table 1 are named for the parameter which was originally evaluated. For example, COND-4 proposed by Yang et al. [46] uses the log of the ionic conductivity (LIC) to calculate the progression of the glass transition temperature. Similarly, DISP-1 and DISP-2 which were proposed by Kim et al. [47] identify the start and end of cure by identifying features of the graph of the dissipation factor. This paper evaluates all of the methods proposed in Table 1 for a single material and compares their results across five test replicates. Further, each method was applied across all five dielectric parameters to identify if the method is parameter-dependent.

Developments have been made to some of the existing methods to account for differences in the data structure or as a proposed clarification of the original method. Redefinition or clarifications are detailed below and are summarised for conciseness in Table 3.

- **DISP-2 Redefinition:** DISP-2 identifies the completion of cure as the time where the dissipation factor derivative reaches zero. However, in this study, the derivatives approach zero but never reach it, as cure is stopped prior to the degree of cure reaching 100%. Instead the correlation will define the end of cure, meaning the point where the cure reaction stops, as the minimum of the absolute value of the derivative.
- **DISP-3 Clarification:** DISP-3 was only analysed for the dissipation factor and not implemented for the remaining dielectric parameters as the dissipation factor is specifically a ratio of the loss factor and the permittivity.
- **IMP-1 and IMP-2 Frequency Redefinition:** IMP-1 and IMP-2 were originally identified as the start of two plateau regions identified for the impedance at 1 kHz frequencies. In this study, the double plateau phenomena was only observed at 1 kHz frequencies for IDEX 1 and IDEX5. IDEX3 was most clearly identified at 1.78 kHz, and IDEX2 and 4 at 3.16 kHz. These methods were not applied to other parameters as the double plateau phenomena was not clearly present for the remaining parameters.
- **IMP-3 Boundary Redefinition:** IMP-3 utilises the linear correlation between the impedance (represented on a log scale) and the degree of cure for the isothermal region of cure. As the cure cycles utilised in

Table 3 Summary of improvements to the DEA analysis techniques specified in Table 1.

Name	Original Method	Improved Method
DISP-1	First local maximum of $\frac{dD}{dt}$	No change
DISP-2	Plateau onset ($\frac{dD}{dt} = 0$)	Minimum abs(dD/dt)
DISP-3	$\tan\delta = 1$ defined as the crossover point between loss and permittivity	No change
IMP-1	Onset of the first plateau after the minimum value of impedance at 1 kHz	Onset of the first plateau after the minimum value of the impedance, at the frequency it can be most clearly identified (1 kHz or higher)
IMP-2	Onset of the second plateau after the minimum value of impedance at 1 kHz	Onset of the second plateau after the minimum value of the impedance, at the frequency it can be most clearly identified (1 kHz or higher)
IMP-3	Linear regression to determine relationship between log (Impedance) and degree of cure over the isothermal range	Linear regression to determine relationship between log (Impedance) and degree of cure between the global minimum and the end of the isothermal hold
COND-1	Global maximum of the conductivity	No change
COND-2	Inflection after the peak of the conductivity	No change
COND-3	Plateau onset ($\frac{d\sigma}{dt} = 0$)	Plateau onset defined as the tangent point of the onset after the global maximum
COND-4	$T_g = \frac{\log\sigma_0 - \log\sigma_\infty}{\log\sigma_0 - \log\sigma_\infty} T_{gs}$ With the conductivity at the start (σ_0) and end (σ_∞) of the isothermal region, conductivity at time t (σ_t), and the measured glass transition temperature (T_{gs})	$\alpha = \frac{\log\sigma_0 - \log\sigma_t}{\log\sigma_0 - \log\sigma_\infty}$ With the conductivity at the maximum (σ_0), the conductivity at the end of the isothermal region (σ_∞), the conductivity at time t (σ_t), and the measured degree of cure (α_{DSC})
LOSS-1	$\alpha = \frac{\log\epsilon''_0 - \log\epsilon''_\infty}{\log\epsilon''_0 - \log\epsilon''_\infty}$ With the loss factor at the start (ϵ''_0) and end (ϵ''_∞) of the isothermal region, and the loss factor at time t (ϵ''_t).	$\alpha = \frac{\log\epsilon''_0 - \log\epsilon''_t}{\log\epsilon''_0 - \log\epsilon''_\infty}$ With the loss factor at the maximum (ϵ''_0), the loss factor at the end of the isothermal region (ϵ''_∞), the loss factor at time t (ϵ''_t), and the measured degree of cure (α_{DSC})
VISC-1	Plateau onset ($\frac{d\rho}{dt} = 0$)	Minimum abs(dρ/dt)
VISC-2	$\alpha = \frac{\log\rho_t - \log\rho_{min}}{\log\rho_{max} - \log\rho_{min}}$ With the viscosity at time t (ρ_t), minimum viscosity (ρ_{min}), maximum viscosity (ρ_{max}), and the measured degree of cure (α_m)	See COND-4

this study were not perfectly isothermal, instead the region was bounded from the global maximum or minimum to the end of the isothermal hold.

- **COND-3 Definition Clarification:** COND-3 originally defined the vitrification point as the start of the plateau region, without providing a clear definition of how to identify the start of the plateau region. Based on the results of the proposed correlations, this point was defined specifically as the tangent point of the onset after the global maximum.
- **COND-4 Boundary Redefinition:** Similar to the redefinition for IMP-3 the boundaries of the equation used in this study were not defined as the isothermal period. Rather, σ_0 was defined as the point of maximum conductivity and σ_∞ was defined as the end of the isothermal temperature region. Further, as the T_g and degree of cure are directly related by the DiBenedetto equation, COND-4 in this study was used to determine the degree of cure progression in accordance with Equation (8) in which the equation is normalised by the actual degree of cure calculated by DSC (α_{DSC}). The rationale for this decision is that the simulated progression of both the T_g and degree of cure made in RAVEN are defined by their DiBenedetto

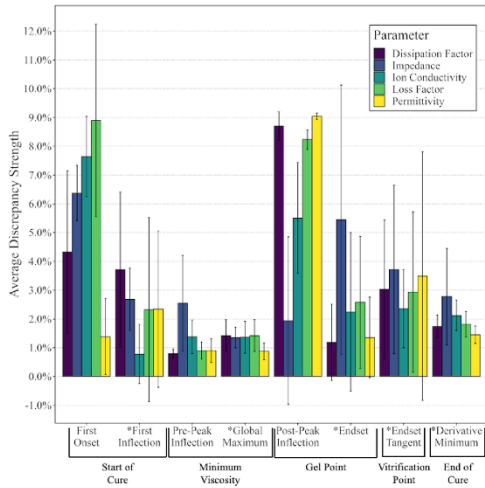


Fig. 6. Results of the cure state identification assessment indicating the average discrepancy strength and standard deviation for each graph feature-cure event pair across all five IDEX replicates.

relationship so the comparison of COND-4 to the simulated degree of cure progression is representative of the relationship and allows for a direct comparison to the other methods which calculate degree of cure (IMP-3, LOSS-1, and VISC-2).

Table 4a
Results comparison for the start of cure.

Time at Cure Start (min)				
Method		Average Value	Std. Dev	Δ%
DISP-1 (1 Hz)	first $\frac{dD}{dt}$ maximum	56.3	5.0	1.4%
	first $\frac{dD}{dt}$ maximum	61.3	5.9	3.4%
Dissipation (100 Hz)	first $\frac{dD}{dt}$ maximum	61.3	5.9	3.4%
	first $\frac{dZ}{dt}$ minimum	45.4	2.0	2.8%
Impedance	first $\frac{dZ}{dt}$ minimum	45.4	2.0	2.8%
	first $\frac{d\sigma}{dt}$ maximum	51.9	2.7	0.9%
Ion Conductivity	first $\frac{d\sigma}{dt}$ maximum	51.9	2.7	0.9%
	first $\frac{d\sigma}{dt}$ maximum	56.7	9.2	2.9%
Loss	first $\frac{d\sigma}{dt}$ maximum	56.7	9.2	2.9%
	first $\frac{d\sigma}{dt}$ maximum	58.8	7.9	2.9%
Permittivity	first $\frac{d\sigma}{dt}$ maximum	58.8	7.9	2.9%
	Time at start of cure rate increase (min)	52.7	0.5	-
RAVEN Predictions				

Table 4b
Results comparison for the time at minimum viscosity.

Time at Minimum Viscosity (min)				
Method		Average Value	Std. Dev	Δ%
COND-1	Global maximum	88.9	1.8	1.2%
	Global maximum	88.7	1.4	1.1%
Dissipation (100 Hz)	Global maximum	88.7	1.4	1.1%
	Global minimum	88.8	1.8	1.1%
Impedance	Global minimum	88.8	1.8	1.1%
	Global maximum	88.9	1.8	1.2%
Loss	Global maximum	88.9	1.8	1.2%
	Global maximum	87.7	1.3	0.7%
Permittivity	Global maximum	87.7	1.3	0.7%
	Time at minimum viscosity (min)	85.6	0.9	-
RAVEN Predictions				

Table 4c
Results comparison for the gel point.

Gel Point (min)				
Method		Average Value	Std. Dev	Δ%
COND-2	Post-peak inflection	104.0	4.4	5.4%
DISP-3 (100 Hz)	$\tan \delta$ 1	110.5	5.1	2.8%
IMP-1 (1 kHz)	First endset	105.0	1.3	5.0%
Dissipation (100 Hz)	Endset	119.6	3.4	1.0%
	Endset	130.5	10.8	4.9%
Impedance	Endset	130.5	10.8	4.9%
Ion Conductivity	Endset	122.4	6.7	2.3%
Loss	Endset	124.9	6.0	2.8%
Permittivity	Endset	116.0	5.5	1.4%
RAVEN Predictions	Time at inflection of viscosity (min)	117.7	1.0	-

$$\alpha = \frac{\log \sigma_0 - \log \sigma_t}{\log \sigma_0 - \log \sigma_{ss}} \alpha_{DSC} \quad (8)$$

- **LOSS-1 Boundary Redefinition:** The calculation for degree of cure defined by LOSS-1 is redefined with the same rationale as COND-4 due to the cure for this study not being truly isothermal. Instead of bounding the start and end of the isothermal region, e_0^r is defined as the value at the global maximum. Further, the LOSS-1 equation calculates a cure index, which is a relative representation of the degree of cure between values of 0 and 1. This paper normalises the value by the actual degree of cure measured from DSC testing, in the manner of methods COND-2 and VISC-2.

Table 4d
Results comparison for the vitrification point.

Vitrification Point (min)				
Method		Average Value	Std. Dev	Δ%
IMP-2 (1 kHz)	Second endset	143.7	5.6	4.6%
COND-3	Flattening of the curve	161.3	2.1	2.2%
Dissipation (100 Hz)	Endset tangent point	162.2	4.3	2.8%
	Endset tangent point	165.0	5.6	3.6%
Impedance	Endset tangent point	165.0	5.6	3.6%
Loss	Endset tangent point	161.3	5.3	3.1%
Permittivity	Endset tangent point	148.9	8.6	3.5%
RAVEN Predictions	Time at Tg-T crossover (min)	155.6	1.4	-

Table 4e
Results comparison for the end of cure.

Time at Cure End (min)				
Method		Average Value	Std. Dev	Δ%
DISP-2 (1 Hz)	$\frac{dD}{dt} = 0$	N/A	N/A	N/A
VISC-1	$\frac{dD}{dt} = 0$	N/A	N/A	N/A
Dissipation (100 Hz)	Minimum $\left \frac{dD}{dt} \right $	250.6	1.8	2.9%
	Minimum $\left \frac{dZ}{dt} \right $	245.9	6.4	4.7%
Impedance	Minimum $\left \frac{dZ}{dt} \right $	245.9	6.4	4.7%
	Minimum $\left \frac{d\sigma}{dt} \right $	248.0	3.3	3.9%
Ion Conductivity	Minimum $\left \frac{d\sigma}{dt} \right $	248.0	3.3	3.9%
	Minimum $\left \frac{d\sigma}{dt} \right $	250.4	1.7	2.9%
Loss	Minimum $\left \frac{d\sigma}{dt} \right $	250.4	1.7	2.9%
	Minimum $\left \frac{d\sigma}{dt} \right $	252.2	1.3	2.2%
Permittivity	Minimum $\left \frac{d\sigma}{dt} \right $	252.2	1.3	2.2%
	Time at end of cure rate (min)	257.9	0.6	-
RAVEN Predictions				

- **VISC-1 Redefinition:** VISC-1 identifies the completion of cure as the time where the viscosity derivative reaches zero. However, in this study, the derivatives approach zero but never reach it, as cure is stopped prior to the degree of cure reaching 100%. Instead the correlation will define the end of cure, meaning the point where the cure reaction stops, as the minimum of the absolute value of the derivative.
- **VISC-2 Redefinition:** As the ion conductivity is the inverse of the ion viscosity, COND-4 will be used in place of VISC-2 in order to eliminate redundancy.

3. Results

3.1. Newly proposed cure state identification assessments

The results of the cure point analysis are displayed in Fig. 6. The individual cure events are paired with their proposed graph features in

accordance with the x-axis labels. Within each pair grouping, the average discrepancy strength across the replicates of IDEX1-5 as calculated by Equation (7) is displayed for each dielectric parameter. The error bar represents the standard deviation across the part replicates. Note that while the average value is calculated as an absolute value per Equation (7), the standard deviation is calculated based on the true values in order to accurately convey the variance of where t_{DEA} lies relative to t_{RAVEN} .

The pairs with the best consistency and accuracy (indicated in Fig. 6 by asterisks*) are proposed as new correlations: the initial inflection indicating the start of the cure reaction, peak value (global maxima or minima) indicating the point of minimum viscosity, the endset after the global peak indicating the gel point, and the onset tangent point correlating to the vitrification point. These correlations were then compared quantitatively to the existing correlations, shown in Table 4a-c. The existing correlations in Table 4 are indicated in italics.

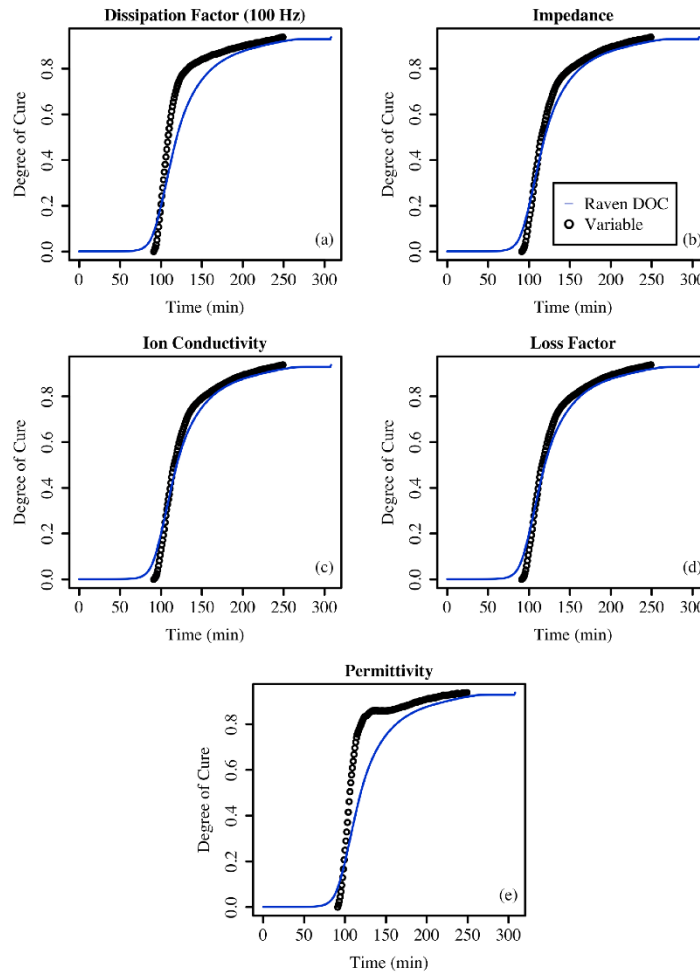


Fig. 7. Calculation of degree of cure for IDEX1 using the (a) dissipation factor at 100 Hz, (b) impedance, (c) ion conductivity, (d) loss factor, and (e) permittivity with all calculations shown in comparison to the RAVEN simulation. Graphs (b-e) represent 1 Hz frequency measurements.

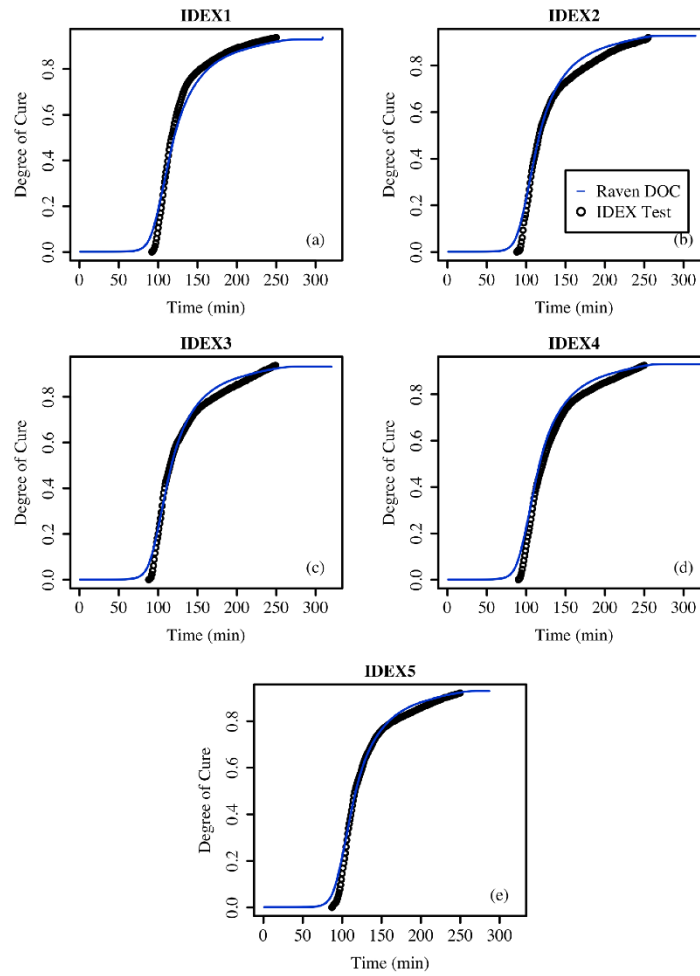


Fig. 8. Comparison of degree of cure calculations via COND-4 (1 Hz) for IDEX tests 1 through 5.

3.2. Accuracy comparisons of different cure state identifications

The results of all proposed and existing correlations which identify discrete cure points are shown in Table 4a-e. For each specified method an average value, standard deviation, and percentage of how closely the value deviates from the RAVEN prediction are presented. The percent discrepancy ($\Delta\%$) is calculated in accordance with Equation (7). Note that existing correlations in accordance with Table 3 are indicated in italics.

3.3. Graphical methods

Fig. 7 demonstrates the methods of COND-4 and LOSS-4 applied to all five dielectric parameters for IDEX1. Dielectric correlations are compared to the RAVEN simulated degree of cure. As previously noted, COND-4 is not utilised to calculate the T_g as the T_g and degree of cure are

directly related via the DiBenedetto equation. All these correlations were normalised by the actual degree of cure measured by DSC. Further, Fig. 8 displays the part-to-part consistency of COND-4 across the five cure replicates.

The methodology proposed by IMP-3 was applied to all parameters, with the results for IDEX2 shown in Fig. 9 correlations between the RAVEN degree of cure and the parameters are shown in (a-e), including the R^2 value. The linear region was determined from the global maxima or minima to the end of the isothermal dwell, and the correlation function was determined per Equation (9) in which X represents the dielectric parameter, a_{RAVEN} representing the RAVEN calculated degree of cure, and c and b as fitting parameters. The linear equations for each parameter and replicate are given in Table 5.

$$\log X = c a_{RAVEN} + b \tag{9}$$

This equation was then used to calculate a predicted degree of cure

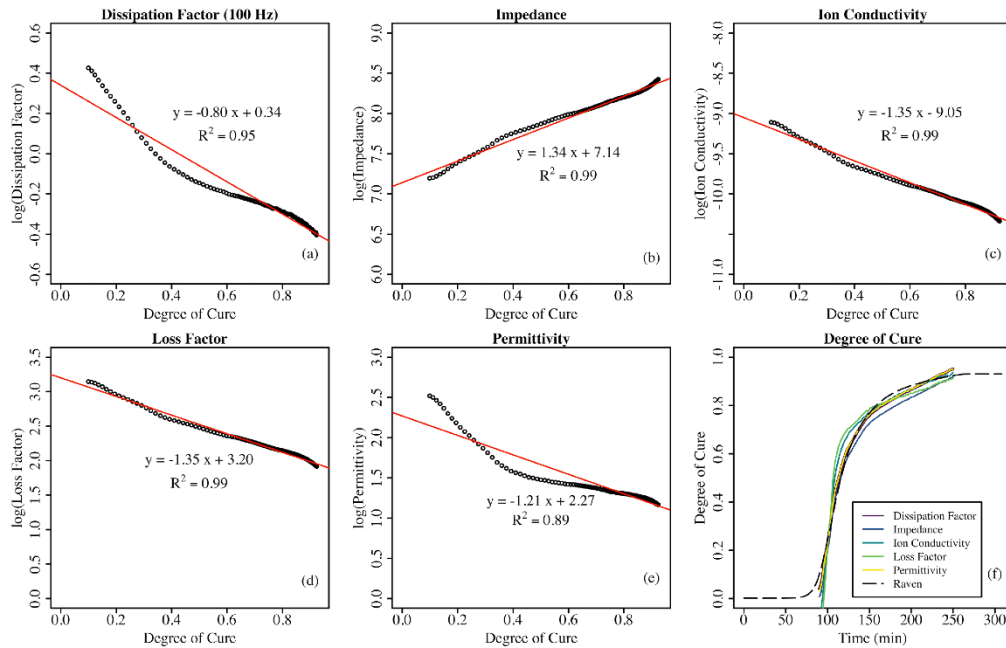


Fig. 9. Linear regression in accordance with IMP-3 for each parameter of IDEX3 indicating the linear relationship between degree of cure and the logarithm of (a) dissipation factor at 100 Hz, (b) impedance, (c) ion conductivity, (d) loss factor, and (e) permittivity. Degree of cure predictions for each parameter compared to the RAVEN simulation are shown in (f). Graphs (b-e) represent 1 Hz frequency measurements.

Table 5

Linear relationships for each dielectric parameter following the method of IMP-3. Note that the 100 Hz correlation for the dissipation factor was used for the degree of cure calculation, and the 1 Hz relationship is only included for the purposes of analysing the slopes.

	IDEX1	IDEX2	IDEX3	IDEX4	IDEX5
Dissipation (100 Hz)	-1.44D + 0.89	-0.82D + 0.33	-0.80D + 0.34	-0.79D - 0.39	-1.26D + 0.81
Dissipation (1 Hz)	-0.33D - 0.91	-0.39D + 1.12	-0.14D + 0.93	-0.30D - 0.94	-0.22D + 0.86
Impedance	2.31Z + 6.43	1.46Z + 7.12	1.34Z + 7.14	1.42Z + 7.05	1.94Z + 6.66
Ion Conductivity	-2.33σ - 8.34	-1.47σ - 9.03	-1.35σ - 9.05	-1.44σ - 8.96	-1.95σ - 8.57
Loss Factor	-2.33ε + 3.92	-1.47ε + 3.23	-1.35ε + 3.20	-1.44ε + 3.30	-1.95ε - 3.68
Permittivity	-2.00ε'' + 3.00	-1.08ε'' + 2.10	-1.21ε'' - 2.27	-1.14ε'' + 2.36	-1.73ε'' - 2.82

using the actual log values and the fitting parameters. Degree of cure curves for each parameter in IDEX3 are shown in Fig. 9(f) in comparison to the RAVEN predicted degree of cure. The final values of this calculation indicate the final degree of cure for each test. These values are compared with actual degree of cure measurements in Table 6.

4. Discussion

4.1. Cure event correlations

Looking first at the cure event correlations determined from Fig. 6 it is apparent the proposed correlations (specified by the asterisks*) are as

Table 6

Predicted degree of cure values as calculated from IMP-3 correlations. Values are compared to analytical results from DSC and DMA and to simulated results from RAVEN.

		IDEX1	IDEX2	IDEX3	IDEX4	IDEX5
Analytical and Simulated Results	DSC	93.8%	92.0%	92.8%	92.5%	92.0%
	DMA ^a	93.5%	93.6%	93.2%	93.7%	93.0%
	RAVEN	92.9%	92.8%	93.1%	93.0%	92.9%
DEA Correlations	Dissipation Factor	90.4%	90.1%	93.6%	92.7%	89.9%
	Impedance	92.2%	95.0%	95.1%	94.8%	92.2%
	Ion Conductivity	93.3%	95.4%	91.7%	91.2%	92.8%
	Loss Factor	91.0%	91.7%	95.1%	94.3%	92.5%
	Permittivity	87.7%	87.7%	91.3%	94.1%	90.0%

^a As calculated using the DiBenedetto equation.

good as or better than the existing methods for CYCOM® 5320-1, as demonstrated in the Table 4 comparisons for each cure event. The discrepancy strengths for the proposed correlations are all within 5%, indicating strong alignment with the RAVEN predictions.

Firstly, there is a weak correlation between the first inflection (also known as the first local $\frac{dX}{dt}$ maximum, in which X represents the relevant dielectric parameter) and the start of cure as proposed in DISP-1 and displayed in Table 4a. At the start of cure the resin has started to soften and lower in mechanical viscosity. This results in a rapid change of the ionic viscosity, which manifests as a rapid increase in the signal. However, the rapid change of temperature during this region has a significant impact on ion viscosity and reduces the accuracy of this correlation. It is proposed that this point may generally indicate that the reaction has started, however the variability should be considered. The ion conductivity measurement, and thus the ion viscosity measurement, have the strongest and most consistent correlations for identifying cure start.

The point of minimum mechanical viscosity, shown in Table 4b, is a key parameter for many manufacturing processes including out of autoclave prepreg processing and resin infusion processing. This time event is very strongly identified as the global maxima or minima of each dielectric parameter, with strong correlations for all tests. COND-1 proposed that the peak value of the ionic conductivity curve has been well identified as the point of maximum ion viscosity. This directly correlates to the point of minimum mechanical viscosity (η) through Equation (10) which is calculated using the ion radius (r), charge (q), and concentration (n) [48]:

$$\rho = \frac{6\pi\eta r}{q^2 n} \quad (10)$$

This study demonstrates that this correlation is valid for all five dielectric parameters as well.

The gel point is challenging to identify, as mechanical gelation occurs over time. There are multiple definitions of gel from the onset of crosslinking to the point of rapid mechanical viscosity increase. Existing correlations such as COND-2 and IMP-1 likely correlate well with the onset of gel, results of which are shown in Table 4c. However, they are less accurate in estimating gel per the definition used by this paper, which is the time at inflection of the mechanical viscosity. DISP-3 correlates well to the gel point and has been shown to relate directly to the crossover point of the storage and loss modulus as calculated in rheology testing [49]. Rather than the inflection point, which was proposed by COND-2, the endset after the global peak correlates strongly to the gel point across all dielectric parameters. At the gel point the resin experiences a rapid increase in the mechanical viscosity, which significantly reduces both ion mobility and dipole movement as the polymer chains rapidly crosslink. As the viscosity curve in Fig. 3(b) shows, the inflection point occurs very close in time to the resin achieving maximum viscosity. The endset of the dielectric parameters indicates that the change in electrical signal has rapidly slowed down and suggests a strong alignment to this physical event.

The vitrification point, as defined by the time that the T_g surpasses the processing temperature, is also an arbitrary physical event that is challenging to model with electrical phenomena. As indicated in Table 4d, IMP-2 correlates moderately well for cures of 5320-1, however it is challenging to identify this point at a consistent electrical field excitation frequency. COND-3 was not demonstrated to correlate well for this resin system, and instead applies best to the end of cure, as will be discussed later. The newly proposed endset tangent point aligns strongly for all dielectric parameters. This point is proposed as a clarified definition of the “onset of the plateau region” which has previously been suggested to indicate vitrification. Physically, vitrification indicates the rapid slowing of the cure reaction as the reaction rate becomes diffusion controlled. At this plateau onset, the electrical signal begins a slow leveling out into a linear region. After this point there is no major change to the electrical signal until the cure ends and the lowered processing

temperature causes the signal to decline. Thus, we can see that the onset of this plateau region correlates to the onset of the diffusive region of cure during which the crosslinking process is far more subtle.

Finally, by modifying the definitions of DISP-2 and VISC-1 it is possible to identify the end of cure for both curing types across all parameters as shown in Table 4e. As stated previously, the derivative of each signal did not achieve a value of 0. However, all parameters are shown to trend towards 0, until the signal drifts at the end of the cure due to the reduction in temperature. This final point, defined as the minimum of the absolute value of the derivative function ($\left|\frac{dX}{dt}\right|_{\min}$), has a strong correlation to the end of the cure reaction rate. It should be noted here that literature has previously referred to this as the completion of the cure reaction. This paper will clarify this definition as the stopping of the cure reaction, which is distinct from the cure reaction proceeding to 100% complete. In a typical composite cure, it is unnecessary to achieve 100% conversion, and instead the cure is considered complete once it has reached a specific threshold, for example, at 88.2% for 5320-1 [50]. As none of the cures in this study were progressed to 100% conversion, it is only possible to correlate this point to the end of the cure reaction rate, which occurs when temperature is removed from the system and the reaction rate lacks sufficient energy to proceed. Taking these definitions, the end of the reaction is very reliably identified across the dielectric parameters.

4.2. Graphical methods

The graphical methods of performing dielectric analysis were also demonstrated to be applicable across all parameters. The results of Fig. 7 and indicate that the methods proposed by COND-4, LOSS-1, and VISC-2 apply to the other dielectric parameters. Fig. 8 demonstrates that this method is also consistent from part to part and can thus be used reliably to evaluate the degree of cure and T_g progression. While the permittivity measurement deviated from the RAVEN prediction during the middle portion of the cure, the end stages of cure aligned well.

4.3. Linear analysis (IMP-3) correlation

The linear regression process proposed by IMP-3 carries much promise for predictive cure modelling. For the example presented in Fig. 9 for IDEX 3, showed very strong linear relationships as indicated by high R^2 values. This resulted in the degree of cure trends for the parameters which aligned very closely with the simulated curve. The linear trends for each IDEX replicate, which are displayed in Table 5, also indicate possible patterns which could be used for predictive cure modelling.

Within each test replicate the impedance, conductivity, and loss factor follow a trend of having very closely matching slopes. As all three of these parameters are dependent on the conductance of the material (G) we can determine that this slope may be associated with the conductive behaviour. Similarly, the permittivity is dependent on the capacitive behaviour of the sample. The dissipation factor can be calculated as the ratio of the permittivity to the loss, and written in logarithmic terms Equation (3) can be rewritten using the inverse relationship of resistivity to conductance as follows:

$$\log D = \log\left(\frac{1}{\omega RC}\right) = \log\left(\frac{G}{\omega C}\right) = \log G - \log C - \log \omega \quad (11)$$

From Equation (11) we can observe that the log of the dissipation factor is defined by the differences in the log of the conductance and capacitance. This pattern is demonstrated by the slopes of the 1 Hz dissipation factor equations, which are almost exactly the difference between the three conductance-based equations (impedance, conductivity, and loss factor) and the capacitive-based equation (permittivity).

It can also be observed that IDEX tests 2, 3, and 4 displayed very consistent slopes within each parameter. Results for IDEX1 and 5

display, however, different trends, which suggest that linear analysis may be sensitive to the natural manufacturing variability from material and process inconsistencies.

In addition to closely aligning to the degree of cure trend, the IMP-3 correlation has also predicted the final degree of cure by identifying the final value predicted by the model. The values indicated in Table 6 show a high degree of accuracy and are on average within 2.5% of the RAVEN predictions.

4.4. Summary of new methods

Based on the results and discussion presented in the previous sections, Table 7 provides a final list of suggested dielectric analysis techniques. The techniques are identified by the cure state feature that they identify, the previously existing techniques that contributed to the methodology, and notes on how the original technique has been modified or improved. Details of the methods are specified in Table 3.

These methods have potential repercussions to live process monitoring techniques and active control systems. The cure event techniques to identify the start of cure, point of minimum viscosity, gel point, and vitrification point can potentially be identified live as the cure progresses. The cure end identification technique is a response to the change in temperature as the process ends and thus cannot be identified until the final dwell temperature has been completed. It is, however, a good point of redundancy against sensors which monitor the processing temperatures and would reinforce that the process step has completed. DoC(2) has the potential for live prediction of cure if a master equation is determined to capture the linear correlation. Such an equation may be material and process-cycle dependent and may need to account for factors which influence signal and cure variation such as materials and temperature uncertainty. DoC(1) must be calculated after the cure has completed, as the equation is dependent on the final value of the signal at the end of the isothermal plateau. For this reason, it is unlikely to provide live monitoring, however it can provide valuable information after the process has completed.

The use of such dielectric analysis methods also has significant implications on quality control systems for high performance applications. Process requirements are commonly validated using indirect methods such as temperature monitoring. Temperature-based methods rely on knowledge of the material cure kinetics and what permissible temperature windows will produce components which meet quality standards.

Table 7
Final list of parameter-independent correlations, including modifications or clarifications of existing correlations.

Analysis Feature	Method	Incorporated Techniques	Notes
DoC (1)	Calculation per VISC-2	COND-4, LOSS-1, VISC-2	Updated to include all parameters
DoC (2)	Linear analysis per IMP-3	IMP-3	Updated to include all parameters
Cure Start	First local maximum of dX/dt	DISP-1	Updated to include all parameters
Viscosity	Global maximum or minimum	COND-1	Updated to include all parameters
Gel Point	Endset after global max/min	COND-2	Modified - applies to all parameters, updated definition due to stronger correlation to endset rather than inflection
Vitrification	Tangent point after endset	COND-3	Modified - applies to all parameters, updated definition of "plateau onset"
Cure End	Minimum of absolute value of dX/dt	DISP-2, VISC-1	Modified - applies to all parameters, updated definition

However, uncertainty in cure kinetics and processing conditions can produce a range of unexpected outcomes [19,51]. By directly monitoring the material state during cure it is possible to objectively identify how the cure progresses for that specific part at that specific time. Dielectric analysis is unique in its ability to directly produce information related to both the stage of cure and final degree of cure, without the required assumptions which predicated temperature monitoring methods.

5. Conclusion

The consistency and accuracy of dielectric analysis has been demonstrated through analysis of multiple part cures. Test results are consistent from part to part and from parameter to parameter, indicating that DEA is capable of reliably identifying material changes throughout the cure process. A comprehensive evaluation of existing and proposed DEA techniques across all dielectric parameters has resulted in the final list of analysis techniques summarised in Table 7. These techniques have been demonstrated to be parameter-independent and to have high degrees of accuracy when compared to analytical and simulated results. Further, correlation methods DISP-3, IMP-1, and IMP-2 have been confirmed to apply to the tests conducted here, however they are parameter-dependent.

The methods evaluated here have implications for live process monitoring and active control, as some methods are capable of providing material state information during the progression of the cure. Further, dielectric analysis has been shown to directly monitor cure state and degree of cure, in contrast to other methods which make assumptions of the material state based on temperature monitoring. This direct monitoring can be used to certify that process conditions are met without concern for process uncertainty or variability.

CRedit authorship contribution statement

Molly Hall: Conceptualization, Methodology, Formal analysis, Investigation, Writing – original draft, Visualization. **Xuesen Zeng:** Writing – review & editing, Supervision, Funding acquisition. **Tristan Shelley:** Writing – review & editing, Supervision. **Peter Schubel:** Writing – review & editing, Supervision, Funding acquisition.

Declaration of Competing Interest

The authors declare that they have no known competing financial interests or personal relationships that could have appeared to influence the work reported in this paper.

Data availability

Data will be made available on request.

References

- [1] Alajarmeh O, Zeng X, Aravinthan T, Shelley T, Alhawandeh M, Mohammed A, et al. Compressive behaviour of hollow box pultruded FRP columns with continuous-wound fibres. *Thin-Walled Struct* 2021;168:108300.
- [2] Alhawandeh M, Alajarmeh O, Aravinthan T, Shelley T, Schubel P, Mohammed A, et al. Review on local buckling of hollow box FRP profiles in civil structural applications. *Polymers (Basel)* 2021;13(23):4159.
- [3] Brøndsted P, Lilholt H, Lystrup A. Composite materials for wind power turbine blades. *Annu Rev Mat Res* 2005;35(1):505–38.
- [4] Mishnevsky L, Branner K, Petersen HN, Beauson J, McGugan M, Sørensen BF. Materials for wind turbine blades: an overview. *Materials (Basel)* 2017;10(11).
- [5] Weaver A. Composites drive VT diversification. *Reinf Plast* 1997;41(1):28–31.
- [6] Kim S-Y, Shim CS, Sturtevant C, Kim D, Song HC. Mechanical properties and production quality of hand-layup and vacuum infusion processed hybrid composite materials for CFRP marine structures. *Int J Nav Archit Ocean Eng* 2014;6(3):723–36.
- [7] Mouritz AP, Cellert E, Burchill P, Challis K. Review of advanced composite structures for naval ships and submarines. *Compos Struct* 2001;53(1):21–42.

- [8] Hayman B, Echtermeyer A, McGeorge D. Use of fibre composites in naval ships. 2001.
- [9] Kim D-D-W, Hennigan DJ, Beuvers KD. Effect of fabrication processes on mechanical properties of glass fiber reinforced polymer composites for 49 meter (160 foot) recreational yachts. *Int J Naval Architect Ocean Eng* 2010;2(1):45–56.
- [10] Feraboli P, Masini A. Development of carbon/epoxy structural components for a high performance vehicle. *Compos B Eng* 2004;35(4):323–30.
- [11] Barile C, Casavola C. Mechanical characterization of carbon fiber reinforced plastics specimens for aerospace applications. *Polym Compos* 2018;40(2):716–22.
- [12] Rocha II, Semprinoschnig C, Nunes JP. Sensors for process and structural health monitoring of aerospace composites: a review. *Eng Struct* 2021;237:112231.
- [13] Mouton S, Telsandier D, Sébastien P, Nadeau JP. Manufacturing requirements in design: The RTM process in aeronautics. *Compos A Appl Sci Manuf* 2010;41(1):125–30.
- [14] Marsh G. Composites - Prime enabler for wind energy. *Reinf Plast* 2003.
- [15] Summerscales J, Searle T. Low-pressure (vacuum infusion) techniques for moulding large composite structures. In: *Seminar on Advanced Processes and Manufacture of Composite Structure*. Bristol 2005.
- [16] Michaud DJ, Beris AN, Dhurjati PS. Thick-sectioned RTM composite manufacturing: Part I – In situ cure model parameter identification and sensing. *J Compos Mater* 2016;36(10):1175–200.
- [17] Tifititsis KI, Skordos AA. Stochastic multi-objective optimisation of composites manufacturing process. In: *Thematic Conference on Uncertainty Quantification in Computational Sciences and Engineering*. Rhodes, Island, Greece, 2017. p.690-705.
- [18] Michaud DJ, Beris AN, Dhurjati PS. Thick-sectioned RTM composite manufacturing, Part II. Robust cure cycle optimization and control. *J Compos Mater* 2016;36(10):1201–31.
- [19] Mesogitis TS, Skordos AA, Long AC. Stochastic simulation of the influence of cure kinetics uncertainty on composites cure. *Compos Sci Technol* 2015;110:145–51.
- [20] Mesogitis TS, Skordos AA, Long AC. Uncertainty in the manufacturing of fibrous thermosetting composites: a review. *Compos A Appl Sci Manuf* 2014;57:67–75.
- [21] Konstantopoulos S, Hueber C, Antoniadis I, Summerscales J, Schledjewski R. Liquid composite molding reproducibility in real-world production of fiber reinforced polymeric composites: a review of challenges and solutions. *Adv Manuf Polym Compos Sci* 2019;5(3):85–99.
- [22] Ersoy N, Garfika T, Potter K, Wisnom MR, Porter D, Clegg M, et al. Development of the properties of a carbon fiber reinforced thermosetting composite through cure. *Compos A Appl Sci Manuf* 2010;41(3):401–9.
- [23] Pindinelli C, Montagna G, Luprano VAM, Maffezzoli A. Network development during epoxy curing: experimental ultrasonic data and theoretical predictions. *Macromol Symp* 2002;180(1):73–88.
- [24] Lionetto F, Montagna F, Maffezzoli A. Ultrasonic dynamic mechanical analysis of polymers. *Appl Rheol* 2005;15(5):326–35.
- [25] Brummer C, Sinapius M. A Novel approach to monitoring the curing of epoxy in closed tools by use of ultrasonic spectroscopy. *Sensors (Basel)* 2017;18(1):96.
- [26] Rao Y-J. In-fibre Bragg grating sensors. *Meas Sci Technol* 1997;8(4):355–75.
- [27] Lekakou C, Cook S, Deng Y, Ang TW, Reed GT. Optical fibre sensor for monitoring flow and resin curing in composites manufacturing. *Compos A Appl Sci Manuf* 2006;37(6):934–8.
- [28] Grande AM, Di Landro L, Bettini P, Baldi A, Sala G. RTM process monitoring and strain acquisition by fibre optics. *Procedia Eng* 2011;10:3497–502.
- [29] Senturia SI, Sheppard Jr NF. Dielectric Analysis of Thermoset Cure 1985.
- [30] Mijovic J, Sa A, Fitz B, Zurawsky W, Mondragon I, Bellucci F, et al. Impedance spectroscopy of reactive polymers. 3. Correlations between dielectric, spectroscopic, and rheological properties during cure of a trifunctional epoxy resin. *J Polym Sci B* 1996;34(2):379–88.
- [31] Maistros GM, Partridge IK. Monitoring autoclave cure in commercial carbon fibre/epoxy composites. *Compos B Eng* 1998;29(3):245–50.
- [32] Konstantopoulos S, Fauster E, Schledjewski R. Monitoring the production of FRP composites: a review of in-line sensing methods. *Express Polym Lett* 2014;8(11):823–40.
- [33] Torres M. Parameters' monitoring and in-situ instrumentation for resin transfer moulding: a review. *Compos A Appl Sci Manuf* 2019;124:105500.
- [34] Hall M, Zeng X, Shelley T, Schubel P. In situ thermoset cure sensing: a review of correlation methods. *Polymers (Basel)* 2022;14(15):2978.
- [35] Fournier J, Williams G, Duch C, Aldridge GA. Changes in molecular dynamics during bulk polymerization of an epoxide-amine system as studied by dielectric relaxation spectroscopy. *Macromolecules* 1996;29(22):7097–107.
- [36] Tifititsis KI, Skordos AA. A novel dielectric sensor for process monitoring of carbon fibre composites manufacture. *Compos A Appl Sci Manuf* 2019;123:180–9.
- [37] Mijovic J, Yee CFW. Use of complex impedance to monitor the progress of reactions in epoxy/amine model systems. *Macromolecules* 1994;27(25):7287–93.
- [38] Steeman PAM, van 'tHurnhout J. A numerical Kramer-Kronig transfer for the calculation of dielectric relaxation losses free from Ohmic conduction losses. *Colloid Polym Sci* 1997;275(2):106–15.
- [39] Kratz J, Hsiao K, Fernlund G, Hubert P. Thermal models for MTM45-1 and Cycom 5320 out-of-autoclave prepreg resins. *J Compos Mater* 2012;47(3):341–52.
- [40] Kim D, Centea T, Nutt SR. Out-time effects on cure kinetics and viscosity for an out-of-autoclave (OOA) prepreg: modelling and monitoring. *Compos Sci Technol* 2014;100:63–9.
- [41] ASTM D7028-07(2015). Standard Test Method for Glass Transition Temperature (DMA T_g) of Polymer Matrix Composites by Dynamic Mechanical Analysis (DMA). West Conshohocken, PA: ASTM International; 2015.
- [42] Technical Data Sheet CYCOM(R) 5320-1 Prepreg. Solvay Composite Materials.
- [43] Day DR, Lewis TJ, Lee HI, Senturia SI. The role of boundary layer capacitance at blocking electrodes in the interpretation of dielectric cure data in adhesives. *J Adhes* 2006;18(1):73–90.
- [44] Kim J-S, Lee DG. On-line cure monitoring and viscosity measurement of carbon fiber epoxy composite materials. *J Mater Process Technol* 1993;37(1–4):405–16.
- [45] Mijovic J, Yee CFW. Use of complex impedance to monitor the progress of reactions in epoxy/amine model systems. *Macromolecules* 2002;27(25):7287–93.
- [46] Yang Y, Plovie B, Chiesura G, Verma T, Daelemans L, Mogsosanu D-E, et al. Fully integrated flexible dielectric monitoring sensor system for real-time in situ prediction of the degree of cure and glass transition temperature of an epoxy resin. *IEEE Trans Instrum Meas* 2021;70:1–9.
- [47] Kim SS, Murayama H, Kageyama K, Uzawa K, Kanai M. Study on the curing process for carbon/epoxy composites to reduce thermal residual stress. *Compos A Appl Sci Manuf* 2012;43(8):1197–202.
- [48] Boll D, Schubert K, Brauner C, Lang W. Miniaturized flexible interdigital sensor for in situ dielectric cure monitoring of composite materials. *IEEE Sens J* 2014;14(7):2193–7.
- [49] Chaloupka A, Pfock T, Horny R, Rudolph N, Horn SR. Dielectric and rheological study of the molecular dynamics during the cure of an epoxy resin. *J Polym Sci B* 2018;56(12):907–13.
- [50] Bruk D. Implementation Methodology, Validation, and Augmentation of a Cure Kinetic Model for Carbon Fiber/CYCOM 5320-1, FM309-1, and FM300-2 [Doctoral thesis]. Washington University in St. Louis; 2021.
- [51] Mesogitis TS, Skordos AA, Long AC. Stochastic heat transfer simulation of the cure of advanced composites. *J Compos Mater* 2016;50(21):2971–86.
- [52] Kazilas MC, Partridge IK. Exploring equivalence of information from dielectric and calorimetric measurements of thermoset cure – a model for the relationship between curing temperature, degree of cure and electrical impedance. *Polymer* 2005;46(16):5868–78.
- [53] O'Dwyer MJ, Maistros GM, James SW, Tatam RP, Partridge IK. Relating the state of cure to the real-time internal strain development in a curing composite using in-fibre Bragg gratings and dielectric sensors. *Meas Sci Technol* 1998;9(8):1153–8.
- [54] Hardis R, Jessop JLP, Peters EL, Kessler MR. Cure kinetics characterization and monitoring of an epoxy resin using DSC, Raman spectroscopy, and DEA. *Compos A Appl Sci Manuf* 2013;49:100–8.
- [55] Kahali Moghaddam M, Breede A, Chaloupka A, Bödecker A, Habben C, Meyer E-M, et al. Design, fabrication and embedding of microscale interdigital sensors for real-time cure monitoring during composite manufacturing. *Sens Actuat. A* 2016;243:123–33.

CHAPTER 4: (PAPER 2) IMPACT OF THROUGH-THICKNESS DIELECTRIC SENSOR EFFECTS ON CARBON FIBRE/EPOXY CURE MONITORING

4.1 Introduction

This chapter builds on the methodologies established in Paper 1 by implementing the newly proposed correlation methods for a prototype through-thickness dielectric sensor. A novel tool-mounted monotrode sensor with theoretical capabilities for sensing depths up to 20 mm was developed by NETZSCH and assessed in this study. Repetitions of thick parts, ranging 2 to 20 mm, were cured to determine the consistency of the methods from part to part, which were validated using off-line analytical techniques and numerical modelling. It was determined that the prototype sensor is insensitive to the influence of temperature or presence of conductive fibres and does not demonstrate undesirable polarisation effects. Further, once a correction factor is applied to account for the sensor components, the dielectric signals showed high accuracy and repeatability when evaluated according to the methods determined in Paper 1.

4.2 Links and implications

There are two main implications from this study: understanding of the influence of sensor design on the dielectric signal, and confirmation that the dielectric methods presented in Paper 1 are applicable across different sensor configurations. While it was known that this prototype sensor includes a polyether ether ketone (PEEK) spacer ring between the electrodes, it was identified that this caused an unintended dual material reading of the PEEK and the epoxy. To compensate for this, a correction factor was applied to the dielectric signals to correct for the impact of temperature and part thickness on the dielectric response. This discovery provides a strong suggestion for future sensor design to include materials which do not exhibit such an influence. However, once the correction factor was applied, the dielectric analysis methods were conducted successfully. The analysis of the corrected signal had good accuracy and part-to-part repeatability across all the laminate thicknesses tested. This suggests that the analysis methods are applicable to through-thickness cure monitoring and may enable a high fidelity yet non-invasive cure monitoring system which has not been available to date.

4.3 Paper manuscript

Impact of through-thickness dielectric sensor effects on carbon fibre/epoxy cure monitoring

Molly Hall ^{a*}, Xuesen Zeng ^a, Tristan Shelley ^a, Peter Schubel ^a

- a. Centre for Future Materials, University of Southern Queensland, Toowoomba, QLD
4350, Australia

Corresponding Author*: Molly Hall (molly.hall@usq.edu.au)

Abstract

Dielectric sensors are an appealing solution for in-situ cure monitoring of thermoset polymers and thermoset composites. Analysis techniques have been shown to produce highly accurate and repeatable insight into cure state metrics both during and after cure. However, most dielectric sensors only report data on the surface of the material the sensor is in direct contact with, neglecting the remainder of the thickness of the component. This study evaluates a novel dielectric sensor which is designed with a 20 mm penetration depth to monitor through the thickness of the composite part. While the prototype sensor design was shown to interfere with the raw data signal, a correction factor was successfully applied, and signals were analysed in accordance with the standard set of methods. The corrected signal had good accuracy and repeatability across laminates from 2 to 20 mm thick, demonstrating a non-invasive, through-thickness monitoring for a range of part designs.

Keywords: Thermosetting resin, Cure behaviour, Electrical properties, Dielectric sensors

1 Introduction

Dielectric analysis is an increasingly attractive method for process monitoring of polymer and composite systems. Recently there has been considerable research on dielectric analysis for monitoring thermoset polymers and thermoset composites during both isothermal and dynamic cure cycles [58-61], such as for epoxies [42, 62-65] and polyesters [60, 64]. Dielectrics have also been used for crystallisation monitoring in thermoplastics processing [66-68], composite damage detection [69, 70], evaluation of adhesive bonds [71], resin infusion flow [72-74], and prediction of resin state prior to infusion [75]. One of their most attractive capabilities is for in-line sensing of thermoset cure processes. Traditional temperature monitoring techniques use the time/temperature relationship for a thermoset polymer, which is dictated by cure kinetics reactions [76, 77]. A major advantage of dielectric sensors is they can capture the molecular movement during cure, leading to identification of major curing events such as gel and vitrification [78, 79]. Dielectric sensor cure monitoring capabilities and limitations have been well documented [32, 33]. The sensing methodologies have been compared with known off-line analysis techniques [80, 81] and other in-line monitoring sensors including ultrasonics and fibre optics [36, 82, 83].

Current trends towards live-monitoring and active control of the manufacturing process [84-87] rely on accurate, repeatable sensing methods which capture cure progression through the entire part. Many techniques rely on sensor networks to monitor various locations throughout the part. Cure monitoring for very thick parts has additional challenges, as surface or contact measurements are unlikely to be representative of the cure gradient existent through the part [57, 88]. Use of invasive techniques such as embedded sensors [89] can capture through-thickness cure data, however the presence of the sensor in the cured part can compromise the mechanical performance of the final component. Dielectric cure monitoring can be comprised of different sensor configurations such as interdigitated electrodes, tool mounted monotrodes, or parallel plate electrodes. Interdigitated sensors and traditional monotrode sensors cast a narrow fringe field to take a contact measurement. Through-thickness dielectric monitoring is historically achieved using parallel plate electrodes [42, 80]. However, this configuration is sensitive to part thickness changes during cure and results rely on correct alignment of the electrodes. To date, there are no commercially available sensors which can monitor through the thickness of large cross-sections without embedded sensors or a parallel plate configuration. This paper investigates a prototype monotrode sensor design, in which the electrode configuration creates a bulk field which is theoretically capable of measurements up to 20 mm.

Dielectric sensors apply an electric field which alternates in response to a set frequency or frequencies. The applied electric field causes a response from the charged particles within the material. For a reactive polymer, such as a thermoset, the electrical response of the material changes throughout the curing process [90]. The electrical response of mobile ions and dipoles becomes restricted as the material crosslinks and these charged particles become fixed in place. Within a given material there is a given concentration of ions, which are mobile charge carriers such as from impurities and unreacted monomer, and of dipoles. Dipoles can be induced from charge separation within the polymer chain, or permanent dipoles which exist most commonly as mobile branches along the chain [91]. Ion mobility results in an electric current and strongly contributes to the conductive behaviour of the material. Dipole rotation and relaxation, or the storage and release of energy due to dipole alignment, causes capacitive behaviour.

Dielectric behaviour in thermosets polymers can be modelled by an electric circuit [43]. When the electric field is applied, the resulting excitation voltage (V) causes the material to respond with an applied current (I). This response comes after a delay called the phase shift (ϕ), which indicates how rapidly the material responds to the applied electric field. Based on this shift, the material responds with a capacitive (C) or conductive (G) response, which then drives the values of the measured dielectric signals [92]. This phenomenon, shown as the material admittance (Y) represented on the complex plane, is conveyed in Figure 1. This is most represented as the material impedance (Z), as defined in Equation (1). The real component of the material admittance is the bulk conductive response, which is represented in dielectric analysis as the ionic conductivity (σ). The imaginary component of the admittance gives the capacitive response, which provides the material permittivity (ϵ^*). The complex permittivity is comprised of a storage component (ϵ') and a loss component (ϵ''). It can also be represented as a ratio called the dissipation factor (D), or $\tan\delta$, for which delta (δ) is the complementary angle to the phase shift. The calculations for these parameters can be found in Equations (2) for the ion conductivity, (3) for the permittivity (ϵ'), (4) for the loss factor, and (5) for the dissipation factor. It is worth noting that the ionic conductivity can be represented as the inverse of the resistivity or ion viscosity (ρ). These equations use the scaling factor or shape factor (A/d), permittivity of free space ($\epsilon_0 = 8.854 \times 10^{-12} \text{ F m}^{-1}$), and electrical excitation frequency (ω).

$$Z = \frac{1}{Y} = \frac{1}{G + i\omega C} \quad (1)$$

$$\sigma = \frac{1}{\rho} = \frac{G}{\left(\frac{A}{d}\right)} \quad (2)$$

$$\varepsilon' = \frac{C}{\varepsilon_0 \left(\frac{A}{d}\right)} \quad (3)$$

$$\varepsilon'' = \frac{G}{\omega \left(\frac{A}{d}\right) \varepsilon_0} \quad (4)$$

$$D = \tan \delta = \frac{\varepsilon''}{\varepsilon'} = \frac{G}{\omega C} \quad (5)$$

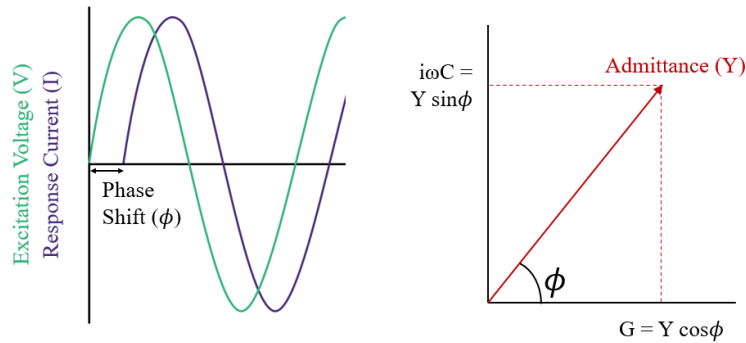


Figure 1 – Demonstration of how phase shift is derived and the impact that it has on the dielectric capacitance (C) and conductance (G).

Thermoset cure is a time-dependent dielectric process, meaning the dielectric behaviour changes throughout the physical cure process. This is commonly represented in dielectric analysis by monitoring the signal across a timescale for a set frequency or across a frequency-domain at set times. Dielectric spectroscopy, achieved by frequency analysis, can provide information on the molecular dynamics and their changes throughout cure [78, 79]. This is a common technique used when molecular motion, such as from dipole relaxation, is the dominating force which contributes to the material cure. Time-spectrum analysis monitors the thermodynamic phase transitions as they occur over time. It is more appropriate to use this type of analysis when ion mobility dominates the signal, producing a frequency-independent result. An analysis of a given material over a range of frequencies can indicate the frequency-dependence of the signal and can assist the user in deciding which analysis methodology is optimal. Choosing a reasonable frequency for measurement is still important for time-spectrum analysis. The relevant time scale for out-of-autoclave thermoset curing is on the magnitude of

minutes, so a 1 Hz frequency may be sufficient. However, faster curing thermosets which cure on the scale of seconds to minutes [93] may benefit from higher frequency measurements.

The dielectric signal can be influenced by several factors which distract from the direct material response. Parasitic effects such as electrode polarisation and internal surface charge build-up can occur due to ion movement during processing. Electrode polarisation occurs when mobile ions accumulate on the electrode surface. The build-up of surface charges on internal surfaces, such as along reinforcing fibre interfaces or other impurities, is called Maxwell/Wagner/Sillar (MWS) polarisation. Polarisation effects are identified by a distortion in the loss factor at low frequencies. Both types of polarisations must commonly be accounted for to ensure the effects do not distort the actual material response, typically with a correction factor or improved design. New sensors may also be influenced by the sensor and cable design itself [43], the processing temperature [94-96], and the presence of conductive fibres [97, 98]. Calibrations of the temperature signal may be necessary to ensure accurate corrections are applied [99].

This paper evaluates a novel tool-mounted monotrode dielectric sensor which is capable of monitoring through the thickness of a 20 mm component due to the circumferential electrode design. In this study a popular out-of-autoclave carbon fibre/epoxy prepreg was cured in thickness ranging from 2 mm to 20 mm, with repetitions of each thickness included to determine the consistency of the results. The results of the dielectric analysis were used to evaluate the sensor behaviour and capabilities. Firstly, the sensor characteristics are evaluated, including investigations on the influence of temperature, conductive carbon fibres, polarisation, and sensor configuration and design effects. Next, a correction factor is provided which accounts for the influence of part thickness and temperature on the dielectric response. Finally, a comprehensive evaluation of dielectric analysis methods is conducted on the corrected signal. Special attention is paid to the accuracy and repeatability of the signal in predicting the cure properties through the entirety of the component thickness.

2 Methods

2.1 Materials and Sample Preparation

This study used Solvay CYCOM® 5320-1/IM7 carbon fibre/epoxy prepreg [100] which was stacked to thicknesses of 2 to 20 mm. Five replicates of 20 mm laminates were fabricated, in addition to two replicates of each thickness 2-, 5-, 10-, and 15-mm. Laminates are designated by their thickness and replicate number, for example TMM20-3 is the third replicate of the 20 mm thickness. One half of each laminate measuring approximately 80 mm by 80 mm was

dedicated to the dielectric sensor reading. The second half of each laminate, also measuring 80 mm by 80 mm, was dedicated to analytical testing. Due to the large thicknesses of some of the panels, the analytical half of the laminate was separated into sub laminates using a release film. The film was used to separate each laminate into five segments: three testing panels located at the bottom, middle, and top of the laminate and two filler segments which are used to space out the testing panels to the appropriate thicknesses. A schematic of this is shown in Figure 2. The testing panels each had the layup definition of $[0/90]_{4s}$ and the filler panels had the layup definition of $[0/90]_x$ where x is determined by the layup sequence. A ply of dry fibreglass was placed under the DEA half of the laminate to isolate the sensor from the conductive carbon fibres. Layup sequences and analytical sub laminate nomenclature is given in Table 1.

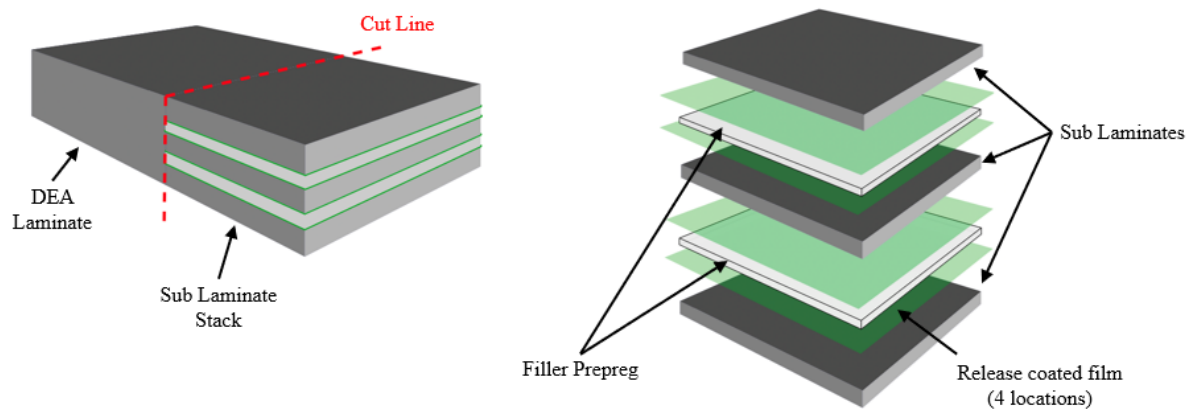


Figure 2 – Laminate schematic showing the configuration of (left) the DEA laminate and analytical sub laminates and (right) and exploded view showing the sequence of the sub laminates, filler prepreg, and release film placement.

Table 1 – Laminate definitions including ply count, layup sequence, and sub laminate terminology in which X indicates the part replicate. Sub laminates are indicated by the bottom (B), middle (M), and top (T) location. Fibreglass plies are designated by “FG” and release film locations are designated by “RF”.

Laminate	Ply Count	Layup Sequence	Test Panels
TMM20-1,2,3,4,5	144	FG, [0/90] _{4s} , RF, [0,90] ₂₄ , RF, [0/90] _{4s} , RF, [90,0] ₂₄ , RF, [0/90] _{4s}	TMM20-XB, TMM20-XM, TMM20-XT
TMM15-1,2	100	FG, [0/90] _{4s} , RF, [0,90] ₁₃ , RF, [0/90] _{4s} , RF, [90,0] ₁₃ , RF, [0/90] _{4s}	TMM15-XB, TMM15-XM, TMM15-XT
TMM10-1,2	66	FG, [0/90] _{4s} , RF, [0,90] ₄ , 0, RF, [0/90] _{4s} , RF, 0, [90,0] ₄ , RF, [0/90] _{4s}	TMM10-XB, TMM10-XM, TMM10-XT
TMM5-1,2	34	FG, [0/90] _{4s} , RF, [90,90], RF, [0/90] _{4s}	TMM5-XB, TMM5-XT
TMM2-1,2	16	[0/90] _{4s} ,	TMM2-XB

The parts were laid up on a 15 mm thick steel tool in which the NETZSCH through-thickness sensor was mounted. The sensor location relative to the tool and laminate is shown in Figure 3 (a) and (c). The laminate was then vacuum bagged in accordance with the manufacturers recommended vacuum bagging schematic [100], also replicated in Figure 3 (a). The parts were cured in an air circulating oven starting from ambient conditions. Figure 3 (b) shows the bagged laminate in the oven. The temperature was increased at a rate of 2 °C/min to 180 °C, followed by a 2-hour dwell at 180 °C as determined by the lagging thermocouple (bottom TC), before cooling to ambient temperatures. This modified version of the manufacturers recommended cure cycle was used for simplicity, as the single dwell temperature allows thermal effects on the sensor to be accounted for.

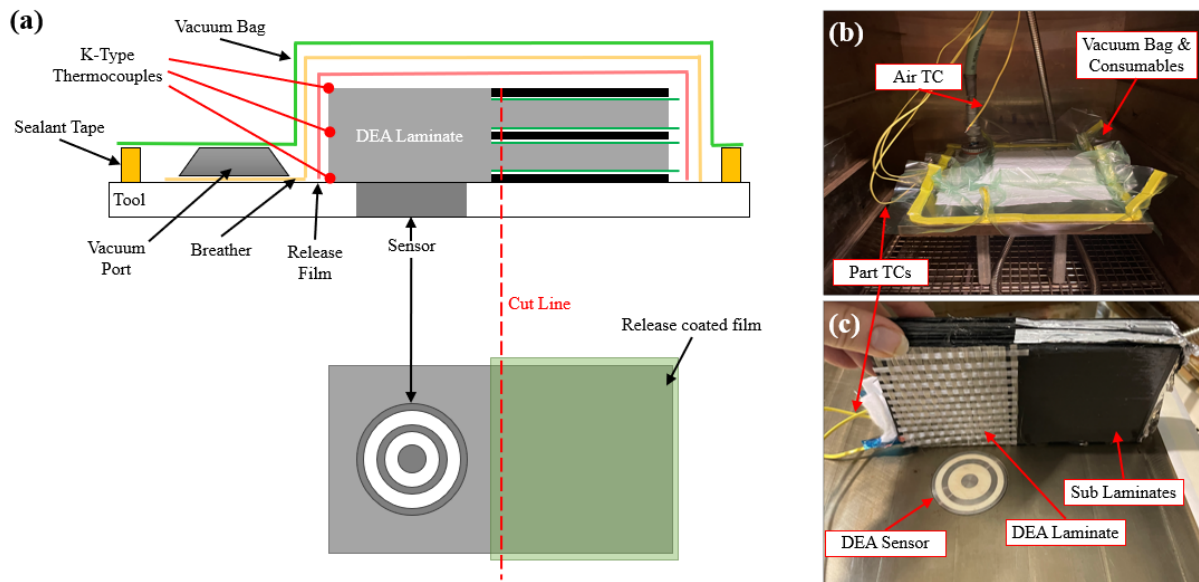


Figure 3 – Layup configuration showing (a) the bagging schematic and orientation of the laminate on the tool, (b) the vacuum bagged laminate in the oven including the air thermocouple placement, and (c) the location of the sensor in the tool relative to the laminate sections.

Data was collected by the dielectric sensor, which is mounted flush with the surface of the tool, and with embedded K-type thermocouples. Thermocouples (TC) were embedded within the DEA half of the laminate, with care taken to ensure that the thermocouples did not lie directly over top of the sensor location. They were embedded on top of the first ply (bottom TC), in the middle of the laminate (middle TC), and below the final ply (top TC). An additional thermocouple was placed approximately 100 mm above the surface of the laminate to measure the air temperature (air TC). The data collected from these panels follows the data flow in [101]. The following sections detail the methods used to complete the dielectric analysis, cure simulation, and analytical testing.

2.2 Dielectric Analysis

2.2.1 Data Collection

Dielectric data was collected using a prototype NETZSCH Tool Mounted Monotrode (TMM) sensor and the NETZSCH DEA 288 *Ionic* data analyser. The sensor is a prototype monotrode design with a circumferential electrode configuration, in which the electrodes were spaced by polyetheretherketone (PEEK) rings. The electrode design is based on the TMM10 sensor and is adapted to allow for both fringe electrical fields and bulk fields which arc up to 20 mm into the component. The choice of PEEK as the spacer material was selected due to limited material

availability due to the COVID-19 pandemic and is not the material of choice for this sensor design.

The sensor collected parameter data for frequencies between 1 Hz and 10 kHz with 4 frequencies set logarithmically per decade. The dielectric parameters under investigation in this paper are the dissipation factor (D , also known as $\tan\delta$), impedance (Z), ion conductivity (σ), loss factor (ϵ''), and permittivity (ϵ'). In accordance with the authors previous study [101], logarithmic scaling was used for each parameter to isolate the impact of curing on the dielectric signal. Data was processed using NETZSCH Proteus® software, with the signals smoothed up to software setting 6-10 to minimise signal noise. The phase angle (φ) for each test was also recorded and used to evaluate the sensor functionality.

2.2.2 Sensor Characterisation

Firstly, the performance of the prototype monotrode sensor used in this study was assessed. Dielectric sensors can be subject to a number of influences such as temperature [94, 99], electrode and interfacial polarisation effects [58, 102], and cable and sensor design [43]. Such effects can distort the signal and compromise measurements. As this sensor is a prototype these influences must be investigated.

Signal quality was evaluated using the phase angle and loss factor. The phase angle measurements were represented as a surface plot to evaluate the change of phase angle with time and across the frequency spectrum. The phase angle is expected to start at approximately 90 degrees at the beginning of cure, with a drop towards lower values due to the increase of material conductivity with the increased temperature. From the minimum phase angle, which roughly correlates to the point of minimum viscosity of the material, the phase angle increases back towards higher values as the curing reaction increases the material capacitance. The evaluation of this behaviour was used to validate the selected analysis frequencies and to verify the credibility of the measurement.

Polarisation effects due to electrode polarisation or interfacial polarisation were evaluated by reviewing the frequency spectra of the loss factor throughout the cure. The logarithm of the loss factor was plotted against the logarithm of the monitored frequencies for intervals of 10 minutes, and the slope was measured. A slope in the low-frequency region of -1 indicates a dominant Ohmic conductivity [91, 103], and slopes which deviate from this indicate electrode polarisation. This analysis is presented for a selection of representative parts to identify if results are consistent across part thicknesses.

The impact of conductive carbon fibres, which may cause interfacial polarisation, was also tested. A previously cured sample, TMM20-2, was post-cured for 2 hours at 200 °C to ensure completion of the cure reaction. The fully cured sample was then placed over the sensor, and vacuum bagged to maintain contact and location with the surface of the sensor and the tool. It was then processed through a standard cure cycle, and the dielectric signal analysed for drift. These results were compared with an empty test of the sensor in the tool, which was processed to the same temperature conditions but with no material present.

The sensor design, specifically the impact of the PEEK spacer rings, was also evaluated using an empty cure cycle. A dynamic cycle was run from 20 to 190 °C at a rate of 1 °C/minute, and dielectric spectra was evaluated to determine how the PEEK spacers may influence the sensor measurements. This temperature range was selected as it encompasses the T_g of PEEK, which is around 140 °C, and the maximum processing temperature for this study, approximately 180 °C. The loss factor was evaluated across the temperature domain for each frequency, and across the frequency domain at temperatures spaced at 10 °C increments. The relationship of loss factor to temperature demonstrated how the PEEK T_g impacts the dielectric signal, with the alpha relaxation event confirmed with the frequency domain evaluation.

2.2.3 Correction Factor

As a result of the sensor characterisation, it was determined that a correction factor may be necessary to account for signal impacts due to the presence of the PEEK spacers. As a result of the PEEK in the design, the sensor is performing simultaneous readings of the PEEK and the curing epoxy. The PEEK causes a distortion of the signal which must be accounted for. However, the exact ratio of monitored responses is unknown, as it is dependent on the volume of material being tested and the electric field strength in that direction. As methods to evaluate field strength and direction were not available for this study, a correction factor was developed to account for the impact of the sensor design.

The primary assumption for the correction factor is that dielectric analysis has been proven to reliably and repeatably detect cure events for the material system under investigation [101]. To this end, a correction factor was determined by establishing a correlation between the DEA- and RAVEN-detected cure events, which are known to be reliably consistent with one another. The cure events were determined in accordance with Table 2 for each individual dielectric parameter. The cure end, as determined by the minimum of absolute value of dX/dt , was excluded from this analysis as the value is a direct response to the change in temperature experienced by the sensor. This value indicates the stopping of the cure reaction due to

reduction in temperature and does not have an identifiable dielectric event associated with it and is therefore not necessary to correct for.

Table 2 – Methods of identifying cure events through dielectric analysis (DEA) and RAVEN simulation. Adapted from [101].

Cure Event	DEA Identification Method	RAVEN Identification Method
Cure start	First local maximum of dX/dt	Onset of reaction rate increase
Minimum viscosity	Global maximum or minimum	Minimum of viscosity curve
Gel point	Endset after global max/min	Inflection of viscosity curve
Vitrification point	Tangent point after endset	Crossover of $T-T_g$

Individual Arrhenius plots were created for each part thickness to determine the impact of part thickness on the signal reading. The difference (Δ) between the time prediction from DEA and the time prediction from RAVEN was taken as $\Delta = t_{DEA} - t_{RAVEN}$. The natural logarithm of Δ was then plotted with the inverse of the temperature at the sensor, and a linear fit was applied according to Equation (6). The fit parameters m and b for each part thickness were plotted against the part thickness to determine if there is a thickness dependence. The final parameters, with the incorporated thickness (x) dependences, were compiled into Equation (7) to identify the correction factor which must be applied to the dielectric signal. In this equation the coefficient (A) is derived from the thickness dependence of b , and the exponential factor (B) is derived from the thickness dependence of m . The correction factor was subtracted from the time measurement for each dielectric function to produce a new, corrected time scale in accordance with Equation (8).

$$\ln \Delta = m \left(\frac{1}{T} \right) + b \quad (6)$$

$$\Delta_{\text{correction}} = A(x) \exp \left(-\frac{B(x)}{T} \right) \text{ where } A(x) = \exp(b(x)) \text{ and } B(x) = \quad (7)$$

$$m(x)$$

$$t_{\text{corrected}} = t_{\text{DEA}} - \Delta_{\text{correction}} \quad (8)$$

2.2.4 Cure Analysis Methods

The corrected dielectric signals are evaluated in accordance with the methods provided in Table 3, which is adapted from the methods evaluated in [101]. The degree of cure (DoC) methods utilise graphical techniques to plot the degree of cure progression. The remaining methods identify discrete cure events. All methods are compared for accuracy and repeatability against the RAVEN simulation data and the analytical results from DSC and DMA testing.

Table 3 – Dielectric analysis methodology. Adapted from [101].

Name	Method	Relevant Publications
	$\alpha = \frac{\log X_0 - \log X}{\log X_0 - \log X_\infty} \alpha_{RAVEN}$	
DoC (1)	In which the X_0 is the maxima of the signal X , and X_∞ is the end of the isothermal region of the signal.	[40, 59, 80, 104]
DoC (2)	Linear regression of the log of the signal against the degree of cure calculated from the time of global maxima to the end of the isothermal hold.	[61]
Cure Start	First local maximum of dX/dt	[105]
Viscosity	Global maximum or minimum	[36, 41, 106]
Gel Point	Endset after global max/min	[36, 41]
Vitrification	Tangent point after endset	[36, 41]
Cure End	Minimum of absolute value of dX/dt	[105, 107, 108]

To ensure consistency with the methods reported in [101] the 1 Hz frequency is used for all correlations excepting for the dissipation factor, which used a 100 Hz frequency. The

dissipation factor at lower frequencies exhibited a double-peak behaviour which prohibited the definitions of Table 3 from being applied as described. The 100 Hz frequency demonstrated a shape which was reliably consistent with the remaining parameters. Rationale for this is presented in the sensor characterisation discussion regarding the phase angle.

2.3 Validation of the Dielectric Analysis

2.3.1 RAVEN Simulation

Convergent RAVEN software was used to simulate the cure of the prepreg based on the temperature profile collected through the thickness of the laminates. The simulation results were used to validate the result of the dielectric analysis. The bottom ply, mid ply and top ply thermocouple readings were input into a 0D temperature profile using the material card for CYCOM® 5320-1/IM7-12K, which is based on the Kratz cure kinetics model [109]. Cure features were identified in accordance with the methodology from [101]:

- The final degree of cure is identified as the end value of the degree of cure curve.
- The vitrification point is identified as the crossover point between the T_g and temperature.
- The final T_g is identified as the end value of the T_g curve.
- The start of cure and end of cure is indicated by the start and ending of the cure reaction rate.
- The time at minimum viscosity is indicated by the global minimum.
- The gel point is indicated by the inflection of the viscosity curve.

As the dielectric signal collects a single measurement representing the full part thickness, the average of the three RAVEN measurements was considered. The analysis in this paper assumes that the sensor takes an equal reading through the entirety of the thickness, rather than a signal which is weighted towards or away from the surface of the sensor.

2.3.2 DSC and DMA

Prior to conducting analytical tests, the laminates were separated into the assigned sub laminates. The analytical half of the panel was cut from the DEA half of the panel, and the release coated film was used to separate the vertical stack of panels. From each part thickness sub laminates were extracted from the bottom, middle, and top of the laminate (designated B, M and T), and the filler sections were discarded. It should be noted that due to part thickness

limitations the 5 mm laminate was only comprised of a bottom and a top sub laminate, and the 2 mm laminate was only comprised of a bottom sub laminate.

Differential Scanning Calorimetry (DSC) was conducted using a TA DSC25. Approximately 5-10 mg of material cut from each sub laminate, and was tested under a dynamic ramp rate of 5 °C/min from 25-280 °C. The actual laminate degree of cure was calculated by integrating under the heat flow-time curve and dividing by the total heat of reaction for 5320-1, which is indicated as 561.8 J/g per Convergent RAVEN.

Dynamic Mechanical Analysis (DMA) was conducted using a TA HR-2 Hybrid Rheometer. Test coupons were cut by waterjet from each sub laminate to dimensions of 8 mm wide by 45 mm long with a tolerance of ± 2 mm. They were dried in an air circulated oven at 120 °C for a minimum of 16 hours, and then held in a sealed container with desiccant prior to testing. Coupons were tested by a dynamic ramp rate of 5 °C/min from 25-280 °C with a displacement of 50 μ m oscillating at 1 Hz frequency. The T_g was calculated in accordance with ASTM D 7028 [31] by the storage modulus (E') onset, and the degree of cure was calculated using this value and the DiBenedetto equation.

3 Processed TMM Sensor Results

3.1 Sensor Characterisation

3.1.1 Phase Angle

The phase angle response provides information on the ratio of the conductive and capacitive behaviour of the material. This can be used to evaluate the credibility of the signal measurement and to identify potential erroneous signal responses. Phase angle measurements over time and across the frequency spectrum was compared for TMM20-2 and TMM15-2, which are representative of the two responses seen in this study. A surface plot of the entire frequency spectra is shown in Figure 4 for these two tests.

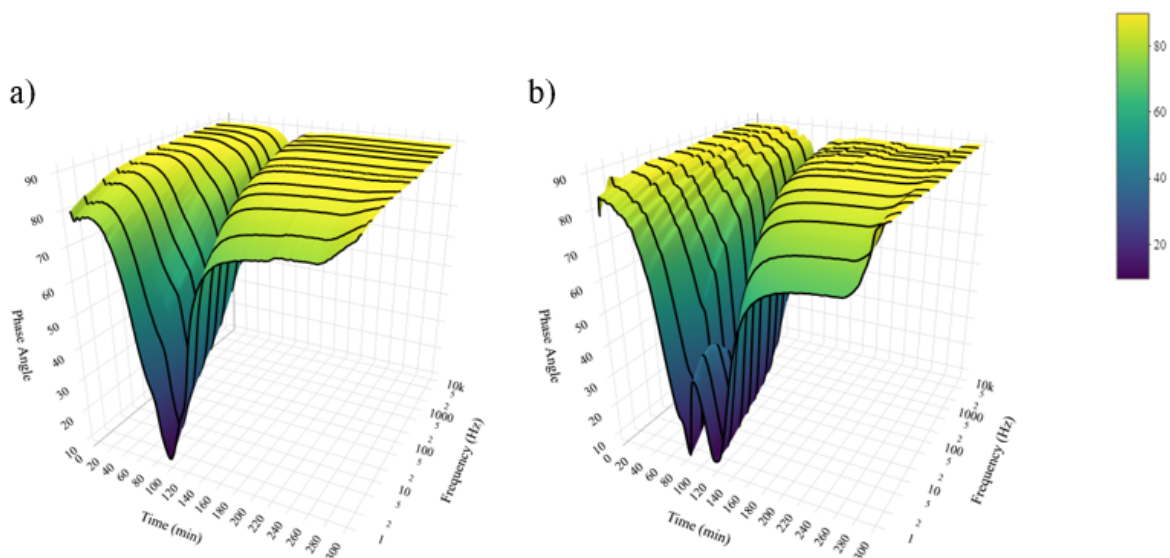


Figure 4 – Phase angle in response to temperature and frequency for TMM20-2 (left) and TMM15-2 (right).

In general, the phase angle measurements from all part replicates display the expected behaviour, which validates the measurements taken for this study. Both signals drop initially, indicating an increase in conductive behaviour, which is the expected response due to the increase in temperature allowing for an increase in mobility of conductive ions. TMM20-2 shows an increasing phase angle after the point of maximum conductivity, which occurs at 99 minutes for the 1 Hz measurement. This corresponds to the increasing capacitive behaviour due to the progression of the cure reaction which restricts ion and dipole mobility. However, TMM15-2 shows a double peak behaviour around the minimum phase angle for low frequency measurements. This is due to a very high magnitude of loss factor for this measurement. The double peak behaviour disappears in frequencies higher than 100 Hz, with Figure 5 showing the individual measurements at 1 Hz and 100 Hz for these two parts. Qualitatively, the 1 Hz and 100 Hz signals for TMM20-2 show similar responses, just of differing magnitude. Due to the double peak behaviour for some parts at low frequencies, the 100 Hz measurement was selected for the dissipation factor analyses, as the dissipation factor is directly calculated from the phase angle. Using the 100 Hz measurement ensures that the definitions used in the analysis methodologies can be applied. However, the 1 Hz measurement is applicable to the remaining parameters, as they are not impacted by the inversion of the phase angle.

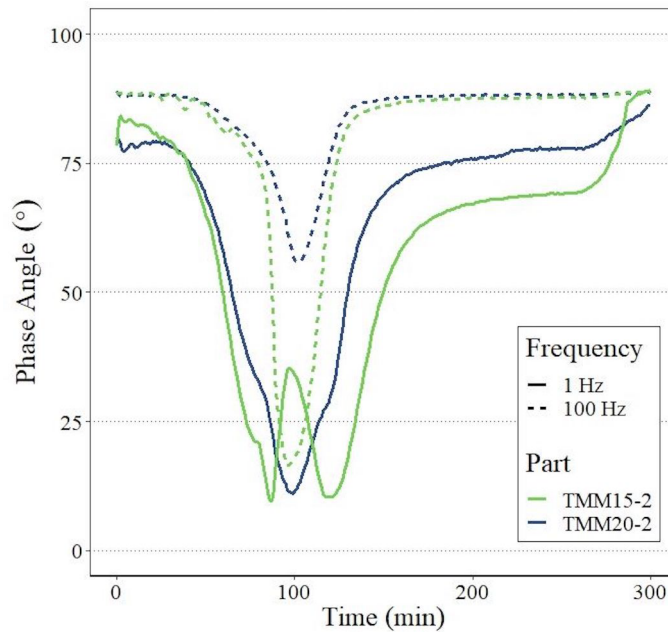


Figure 5 - Phase angle comparisons for 1 Hz and 100 Hz for TMM20-2 and TMM15-2.

3.1.2 Polarisation Effects

Electrode polarisation due to build-up of charges on the electrode surface is a known concern for dielectric sensors. Polarisation due to interfacial charge build-up, called Maxwell/Wagner/Sillar (MWS) polarisation, is also common in dielectric monitoring of multi-phase materials. In the case of a carbon fibre reinforced epoxy, the interface between the carbon fibres and the epoxy is where the charges are likely to build up. Three representative tests were evaluated through the frequency spectrum to further understand potential polarisation effects. TMM20-2, 10-1 and 2-1 were selected as representative tests to evaluate polarisation for the range of part thicknesses. The choice of these samples was to demonstrate the consistency of behaviour across all part thicknesses, as all part replicates followed these trends. The samples were plotted against the measurement frequencies to evaluate the slope on a log-log plot. Measurements with a slope of -1 are known to follow Ohm's law and indicate the measurement is conductivity-driven and free from polarisation effects. The three sets of curves, shown in Figure 6, show that the samples are free of obvious polarisation effects. All measurements display a slope of approximately -1 at lower frequencies and display no notable deviations or erratic behaviour which would indicate polarisation. A deeper investigation into frequency effects and relaxation events will be provided in the following section.

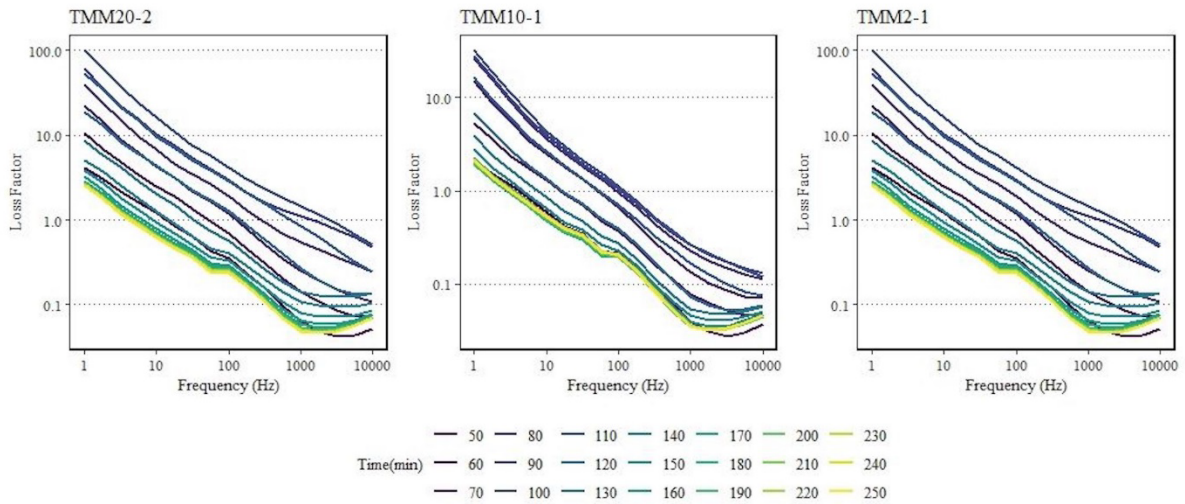


Figure 6 – Frequency spectra of the loss factor for TMM20-2, TMM10-1, and TMM2-1 to investigate the presence of electrode polarisation.

It is also possible that the presence of the conductive carbon fibres can influence the signal. Dielectric measurements were collected for tests with no curing reaction present to isolate the influence of the carbon fibres. The sensor was tested with an empty set up, without the presence of any prepreg material, to determine the impact of temperature on the sensor reading. It was then tested with a fully cured sample (TMM20-2) which was post-cured to 100% conversion, to identify the impact of the presence of conductive fibres. The ion conductivity of the empty test and the fully cured tests are given in Figure 7 and compared with the original dielectric signal for the TMM20-2 cure for reference. It is apparent that there is a slight sensor drift over time as the temperature increases, which will be discussed further in the following section. The conductivity measurement of the fully cured sample is very slightly higher than the empty test. This can be attributed to the lingering conductivity in the cured sample, for example intrinsic conductivity from electron shifts in atomic bonds. Overall, the response of the fully cured signal aligns with the response of the sensor itself to temperature effects which will be explored in more detail in the next section. There are no notable effects from the presence of the carbon fibre which need to be accounted for in these tests.

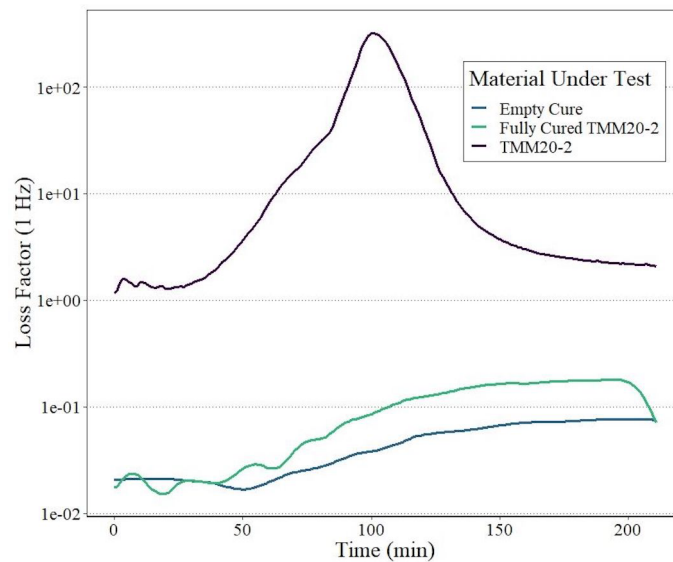


Figure 7 – Results of the sensor drift test (labelled Empty Cure) and the conductive fibre test (labelled Fully Cured) in comparison with TMM20-2 cure test.

3.1.3 Impact of PEEK

As can be seen from the comparison Figure 7 the sensor itself displays a response with temperature. This is attributed to the simultaneous measurement of the epoxy-based prepreg which is being cured, and the measurement of the PEEK rings which are spaced between the electrodes. The melting and softening temperature of PEEK is dependent on the specific composition and relates to the molecular weight and crystalline content. In general, PEEK has a melting point between 330-340 °C, depending on the content of the crystalline and amorphous phases [110, 111]. The rubbery region, again depending on the polymer blend, can begin in the region of 240 °C [112]. As temperatures in this study do not exceed 180 °C, it can be concluded that the PEEK does not approach its melting range or softening point. Instead, the critical transition is the glass transition which for PEEK exists around 140 °C [113, 114]. There have been several dielectric spectroscopy evaluations of PEEK relating to the alpha relaxation events, which are representative of the glass transition. Studies have shown that alpha relaxation is sensitive to the crystalline content of the polymer [115], with the amorphous material mobilising at temperatures above the glass transition [116]. The presence of the crystalline region can cause a broader relaxation range compared with the amorphous material [117], with previous studies showing a sharp increase in the dielectric loss for the amorphous phase at a range of frequencies [116]. In the time-domain, the amorphous and crystalline phases cause an increase in the dielectric loss and permittivity in response to the glass transition [118].

The results of the loss factor for the dynamic temperature test of the sensor are given in Figure 8. The results display the same trends documented in the literature: notably the visible increase in loss factor is clear once the temperature exceeds 140 °C. The increase in loss is less prevalent for higher frequency measurements, however the molecular mobility is visible across the frequency spectrum. Also clear are molecular relaxation events at 31.6 Hz and 100 Hz. The presence of two relaxation peaks may be a result of the limited frequencies evaluated in this range for this test, or it may be indicative of individual relaxation peaks for the amorphous component of PEEK and crystalline component of PEEK. Regardless of the original processing conditions of the PEEK during the manufacture of the sensor, it is likely that the material has fully crystallised, which is at a maximum 40% crystalline [113], during the heating and cooling during the sensor trials. Therefore, the 31.6 Hz peak may be attributed to the mobile amorphous phase, as this peak becomes clearly visible only once the glass transition has been reached. The 100 Hz peak is visible through the entirety of the temperature range and may be attributed to the more restricted crystalline phase.

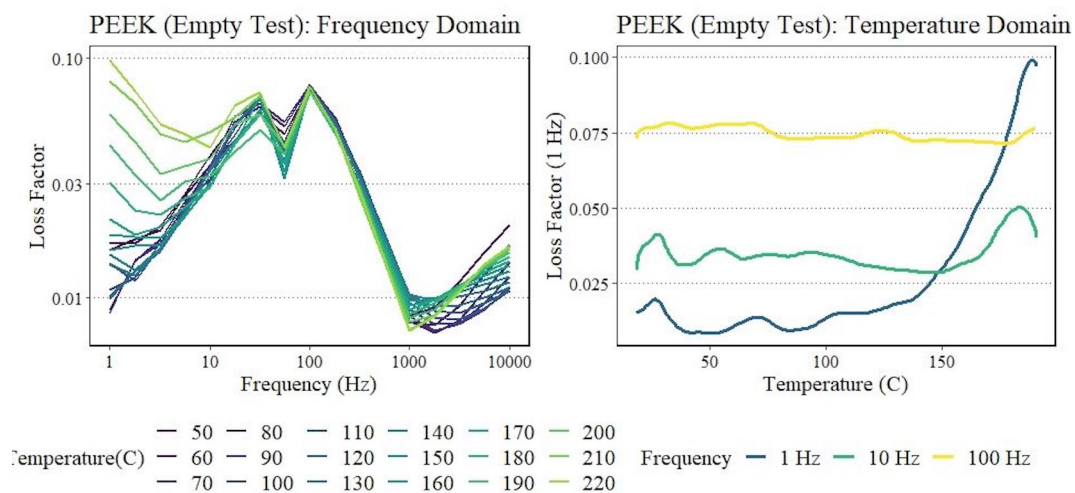


Figure 8 - Loss factor measurements for PEEK integrated into the sensor showing (left) frequency domain response and (right) temperature domain response.

This response is also clear in the epoxy measurements for this test, during which a simultaneous epoxy-PEEK measurement is taken. Figure 9 compares PEEK and epoxy-PEEK measurements, showing similar relaxation events at 31.6 Hz and 100 Hz. The presence of these peaks in later durations of the cure indicates that in the early stages, when the epoxy has the highest mobility, the epoxy response dominates the dielectric signal. The magnitude of the values for the PEEK are lower than those as measured in the epoxy tests, however, this is not necessarily indicative of the measurement ratio.

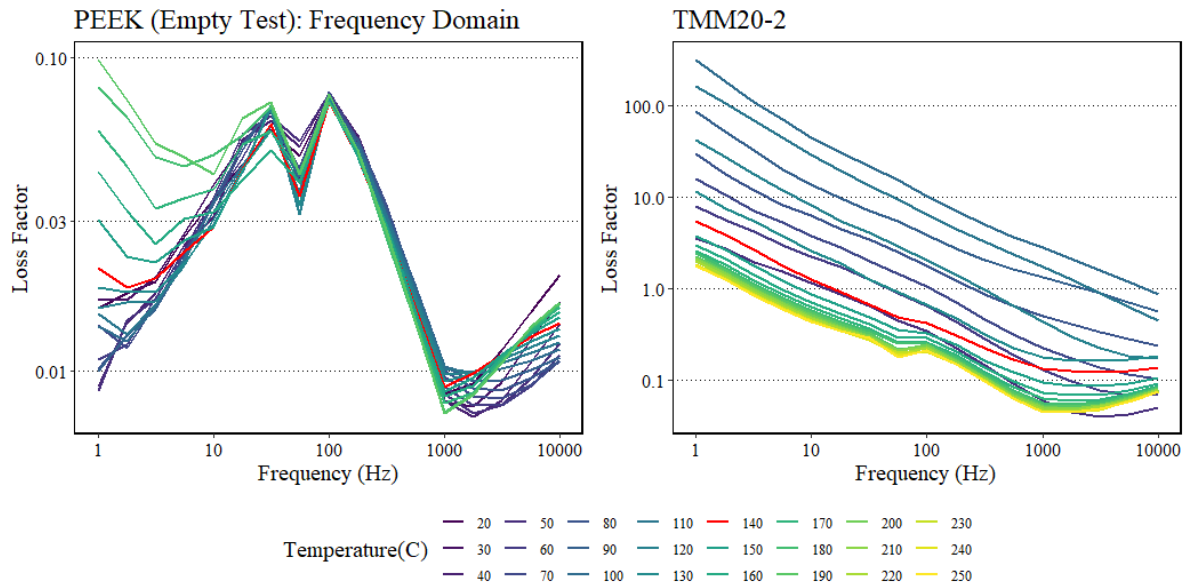


Figure 9 - Loss factor measurements for (left) PEEK compared with (right) TMM20-2 measurement including PEEK and epoxy components. Note that the T_g of PEEK (140 °C) is indicated in red to clearly display the response of the signal from frequency independent, uninfluenced response (before 140 °C) to a noticeable shifting relaxation peak.

Dielectric measurements of multi-phase materials have been represented by the simple mixture bounds demonstrated by Equation (9) [117]. However, these are thought to be overly simplistic, considering only the volume fraction of each material. An array of assumptions regarding morphology, isotropy, and geometry have allowed for development of complex permittivity bounds for a material with three or more components [119]. However, both calculations are based on the chief assumption of homogeneity of the material in which both materials are exposed to the same electric field, which is not applicable here. The schematic shown in Figure 10 conveys these assumptions. In (a) is a multi-phase material with known volume fractions of each component, and a known electric field (E) applied to a region of the material defined by a circle of radius r . For this case, regardless of the value of r the ratio of the material volumes remains the same. However, in (b) which is representative of the configuration in this study, we see that the two separate materials under test are impacted by separate electric fields of differing strengths. Further, while the PEEK rings (impacted by E_2 radial fields) occupy a known volume, the quantity of the epoxy (impacted by E_1 bulk and fringe fields) is unknown. The material thickness, which is varied in this study, is quantifiable, however the radius of the impacted region is unknown. For this reason, it is impractical to assume the correct ratio of signal measurements for these tests.

$$\frac{1}{\frac{V_1}{\epsilon_1} + \frac{V_2}{\epsilon_2}} \leq \epsilon^* \leq V_1\epsilon_1 + V_2\epsilon_2 \quad (9)$$

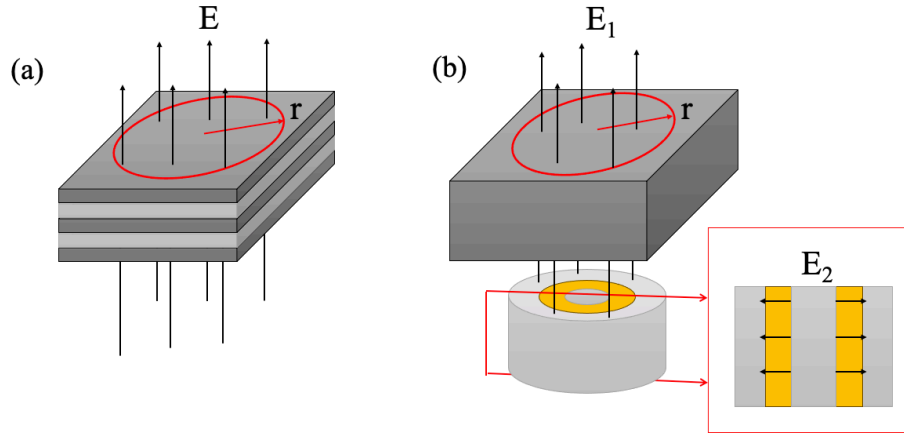


Figure 10 - Application of (a) an electric field (E) to a multi-phase material and (b) two individual measurements by two individual electric fields for which $E = E_1 + E_2$ onto two individual materials, as is applicable in this study.

3.2 Temperature Correction Factor

A temperature correction factor was determined to account for the impact of the PEEK on the signal measurement of the epoxy. The correction factor was established by identifying the time shift between the sensor reading and the known material state, which was defined by RAVEN.

Firstly, the cure events were determined from both the dielectric signals and the RAVEN simulation in accordance with Table 2. The discrepancy strength ($\Delta\%$) for each pair was calculated in accordance with Equation (10) and the average values for each part thickness and for individual parameters is represented in Figure 11, The discrepancy strength is calculated from time differential between when the RAVEN cure event occurs (t_{RAVEN}) and when the dielectric graph feature occurs (t_{DEA}) and then normalised by the overall cure time (t_{TOTAL}).

$$\Delta\% = \left| 100 * \frac{(t_{RAVEN} - t_{DEA})}{t_{TOTAL}} \right| \quad (10)$$

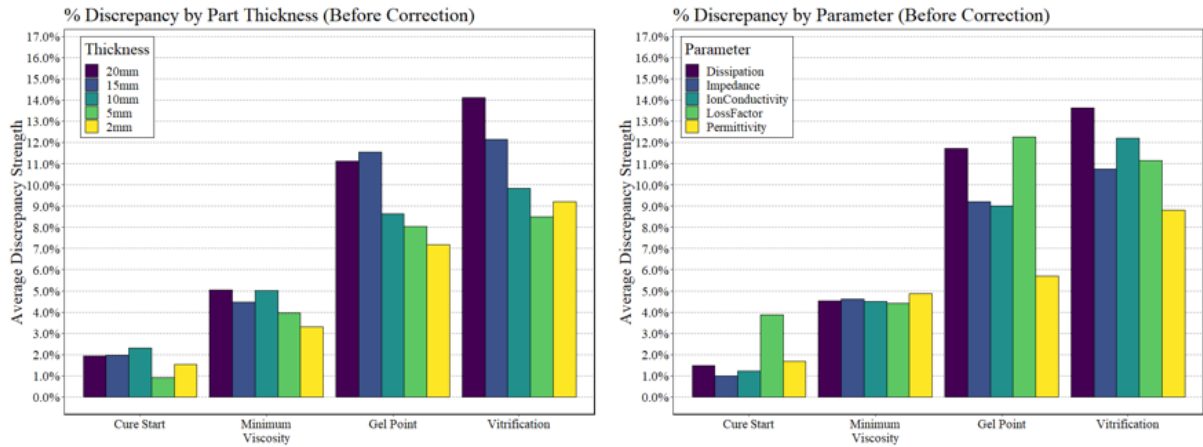


Figure 11 – Discrepancy strength showing the initial difference between the dielectric signal and the simulated values for varying cure events. Shown as a function of the (left) part thickness and (right) dielectric parameter.

From Figure 11 we can determine that there are two consistent trends of the discrepancy strength: the strength weakens (meaning the discrepancy value is higher) as the part thickness increases, and the strength weakens as the duration in cure progresses. As the temperature increases throughout the duration of the cure, it is indicated that there is a temperature dependence component to the discrepancy strength. These trends are consistent with the impact of PEEK on the signal reading: the signal is influenced by the temperature relative to the PEEK T_g , and by the part thickness and therefore volumetric ratio of epoxy to PEEK. The other item of note is that within each dielectric parameter there is no identifiable trend, and thus we can conclude that the parameters are reasonably interchangeable. Based on this rationale, the next stages of the analysis make use of an averaged value across all parameters.

Molecular relaxation events in PEEK are known to follow Arrhenius trends [114, 118], so this approach was used here. The temperature correlation plots are shown in Figure 12, including the preliminary fitting equations and the R^2 indicating the goodness of fit for each function. From these equations, a master equation was derived to describe the behaviour of the entire system. The master equation fits the form of Equation (7) with the thickness dependent functions indicated in Equations (11) and (12). It is worth noting the consistent trends with thickness for both the coefficient of the linear fit and the y-intercept. This indicates that the signal correction must incorporate a thickness dependence, which is supported by the visible trend in the left figure of Figure 11. Further, the correction factor corrects for the influence of PEEK on the dielectric signal and must account for the difference in material volume ratios between the sensor and the differing part thicknesses. The relationships derived in Equations (11) and (12) are the best function fit to account for this thickness dependence.

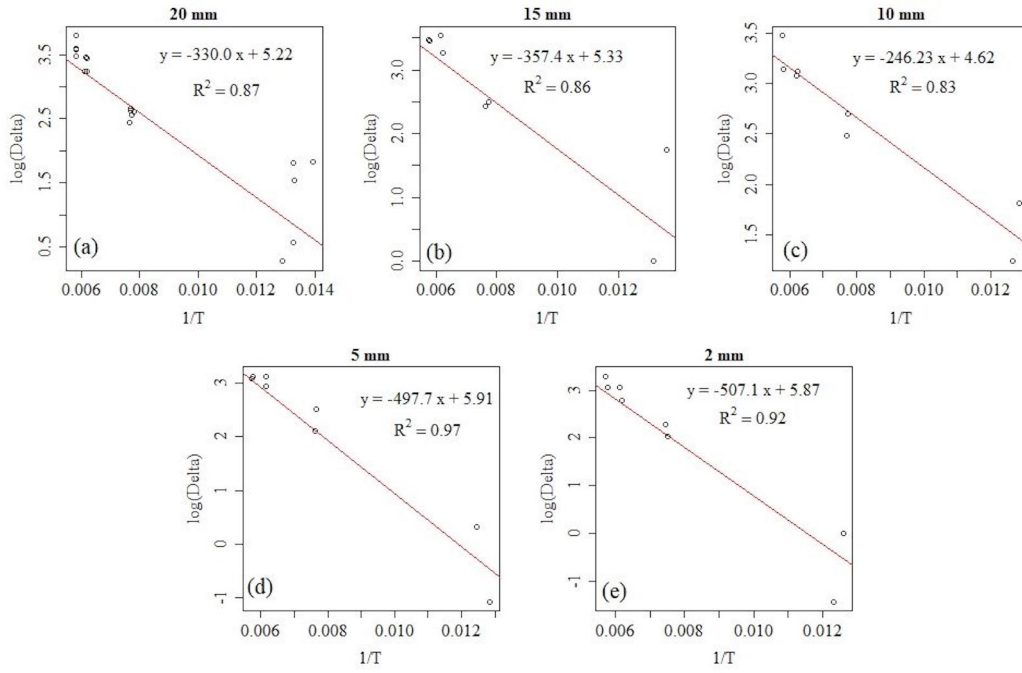


Figure 12 - Temperature correlations for each part thickness, indicating the fitting equation and R^2 for each part thickness.

Recalculations of the dielectric signal for all the tested thicknesses validates the goodness of fit of this set of correction functions and allow a simple correction of the signal.

$$A(x) = -224 \ln(x) + 783 \quad (11)$$

$$B(x) = 135 \ln(x) - 674 \quad (12)$$

The correction factor, Equation (8), was applied to the signals and the cure event timing was recalculated. The new discrepancy strengths for the corrected signals are shown in Figure 13. The corrected signals produce an extremely good fit to the predicted values of the different cure events. Compared with the initial discrepancy strengths, which reach as high as 10-14%, the cure predictions in Figure 13 are now all within 5%. This is consistent with the accuracy seen in the IDEX sensors [101]. Further, the application of the correction factor appears to significantly reduce the impact of part thickness. The corrected values also lack a strong preference for the dielectric parameter; thus, all parameters can continue to be used interchangeably. The point of minimum viscosity, which occurs around 145 °C, displays the closest fit. As this is the closest event to the onset of the PEEK T_g , which indicates the correction factor successfully accounts for the influence of the PEEK on the signal.

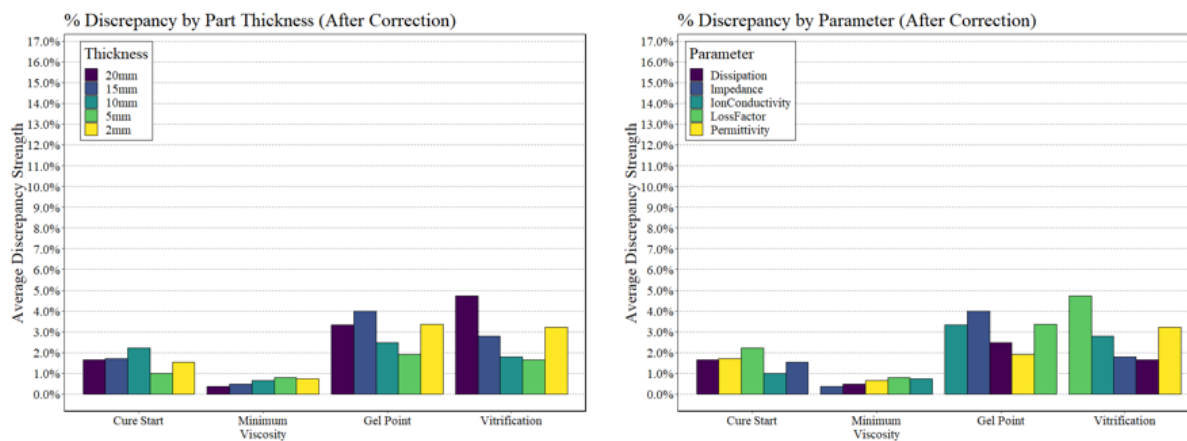


Figure 13 – Discrepancy strengths for the corrected dielectric signal shown as a function of the part thickness (left) and dielectric parameter (right). Note that the y-axis scale is consistent with the scale reported in Figure 11.

4 Dielectric Cure Analysis Results and Discussion

4.1 Graphical Methods

Each part replicate and each parameter were evaluated for DoC(1) in accordance with the equation provided in Table 3. The curves were normalised by the average degree of cure determined by RAVEN and then compared with the average of the RAVEN degree of cure simulation curves. Firstly, the results of DoC(1) analysis on a corrected and uncorrected ion conductivity signal are given in Figure 14. This comparison confirms the use of the corrected signal for this analysis, as the onset of the degree of cure increase is far more comparable to the RAVEN simulation. The uncorrected signal has an approximated 20-minute delay for the onset of the degree of cure increase. While the correct signal has a quicker rise to the full cure value compared to RAVEN, the general progression of the cure is aligned. The discrepancy can be attributed to the influence of PEEK on the signal magnitude. The results of DoC(1) for each parameter in each part thickness are given in Figure 15. The remaining parameters and part thicknesses display a similar trend to Figure 14: the onset of the cure reaction is accurate, and the general shape of the cure progression is aligned to that of the simulation. DoC(1) is shown to have good repeatability regardless of the part thickness or dielectric parameter used.

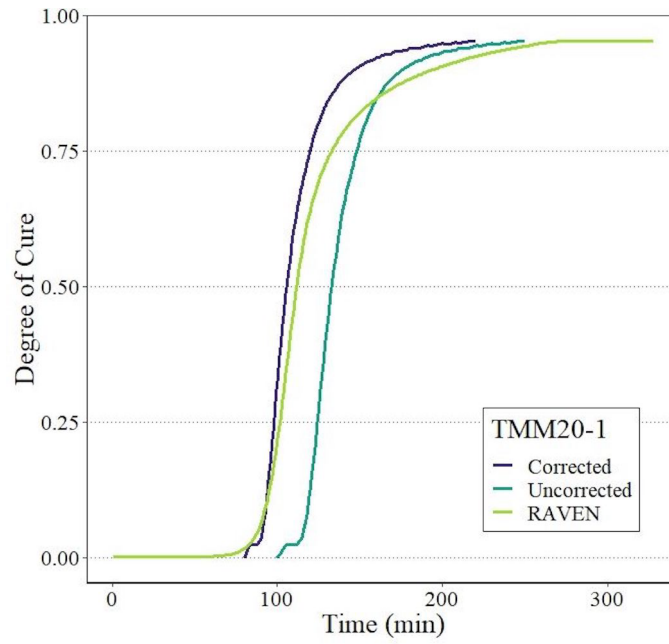


Figure 14 - Comparison of DoC(1) for the corrected and uncorrected ion conductivity signal for part replicate TMM20-1

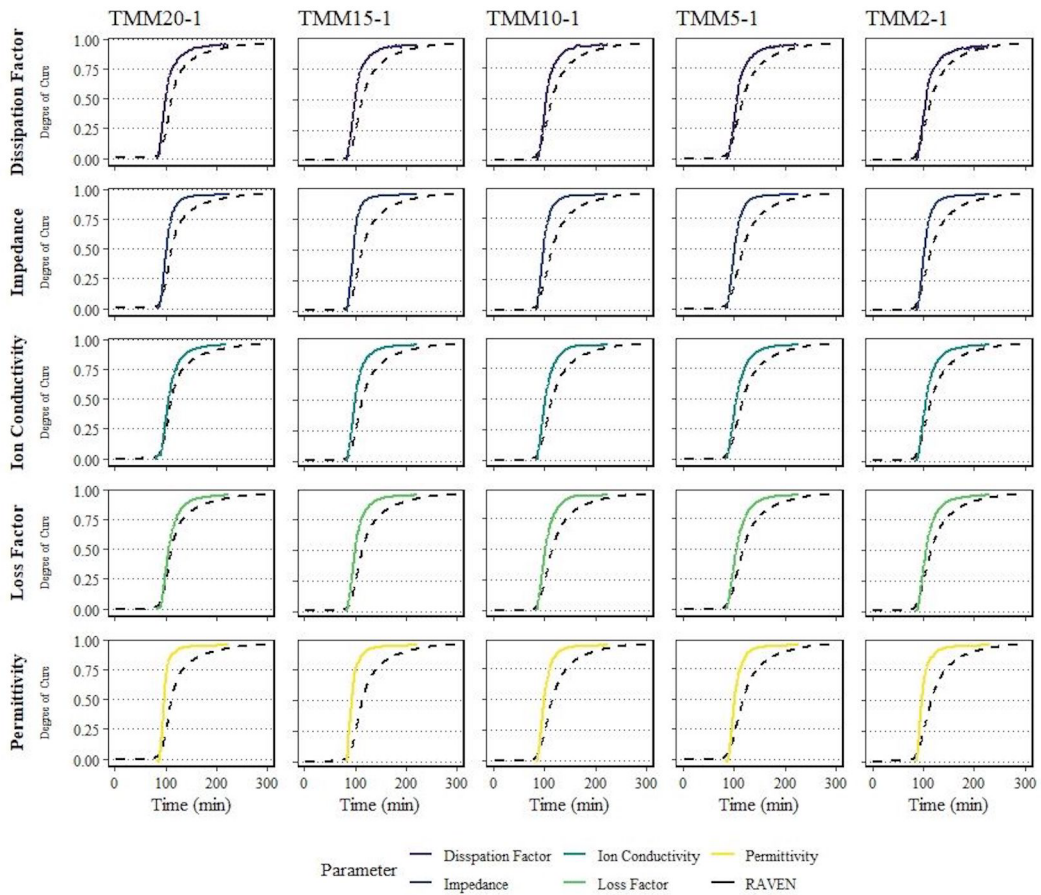


Figure 15 - DoC(1) method applied to each dielectric parameter for each part thickness. Measurements are at 1 Hz excepting the dissipation factor which was measured at 100 Hz.

The results of DoC(2) for a representative part of each thickness, and for each dielectric parameter, are given in Figure 16. The predicted final values of degree of cure for this method are given in Table 4. In general, the dielectric parameters estimate the degree of cure progression with reasonable accuracy, and the parameters can be used interchangeably. The applied correction factor successfully shifts the time scale of the dielectric parameters, and the result aligns extremely well with the onset of degree of cure predicted by RAVEN. The general shape of the degree of cure curves matches well with that provided by RAVEN, with the conductivity-driven parameters, the ionic conductivity and loss factor, fitting slightly better to the degree of cure progression for cures between 50-80%. In accordance with the methods in Table 3, the predictions stop at the end of the isothermal temperature region, which occurs at 250 minutes. However, the actual predicted degree of cure progression continues until approximately 270 minutes. Due to this, the estimates do not capture the final stages of the degree of cure progression, and the final predicted values in Table 4 are slightly lower than the actual expected degree of cure. As with DoC(1) this method had reasonable accuracy for the corrected dielectric signal.

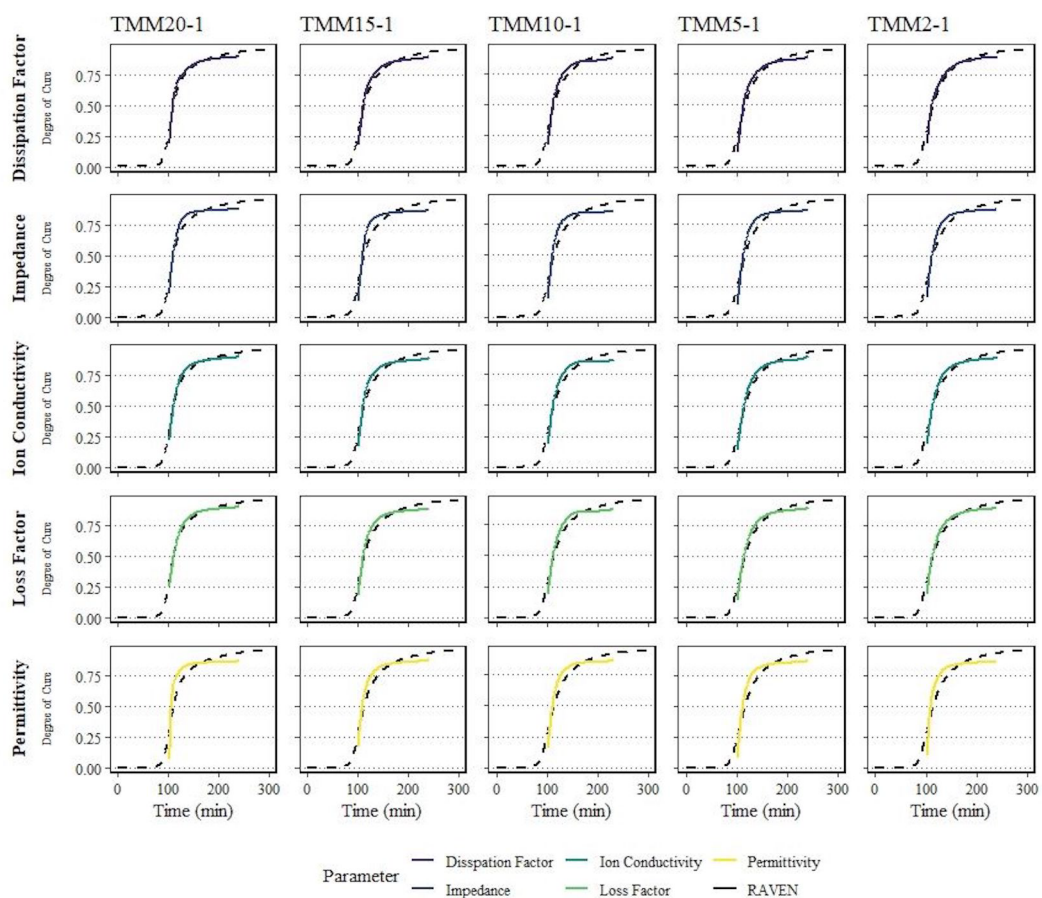


Figure 16 - DoC(2) method applied to each dielectric parameter for each part thickness. Measurements are at 1 Hz excepting the dissipation factor which was measured at 100 Hz.

Table 4 – Predicted degree of cure values from DoC(2). Results are compared with analytical results from DSC and DMA and simulated results from RAVEN. DoC(2) value is averaged over all dielectric parameters. Analytical and simulated results are averaged over all replicates and part thicknesses.

Part	DoC(2)	DSC	DMA*	RAVEN
TMM20-1	90.0%	94.9%	95.5%	95.2%
TMM20-2	90.6%	94.8%	95.4%	95.1%
TMM20-3	89.4%	94.6%	95.5%	94.7%
TMM20-4	89.8%	94.6%	95.4%	94.9%
TMM20-5	90.7%	94.4%	95.0%	94.4%
TMM15-1	88.7%	94.7%	95.3%	94.8%
TMM15-2	88.9%	94.5%	95.4%	94.9%
TMM10-3	87.1%	95.0%	95.3%	93.9%
TMM10-4	77.1%	94.6%	95.6%	94.0%
TMM5-1	88.4%	94.5%	95.3%	94.3%
TMM5-2	89.0%	94.7%	95.1%	93.9%
TMM2-1	88.7%	94.6%	94.0%	94.9%
TMM2-2	87.8%	93.6%	93.8%	93.9%

* As calculated using the DiBenedetto equation.

4.2 Cure Point Methods

In addition to the comparison provided in Figure 13, comparing of cure point identification for the corrected dielectric signal with the RAVEN simulation is provided in Table 5. Included are the average value and standard deviation across all dielectric parameters and part replicates for each part thickness. Also shown is the average percent discrepancy calculated from Equation (10).

Table 5 – Results of the cure point analysis methods conveying the average time at each cure event for each part thickness, the standard deviation, and the percent discrepancy compared with the RAVEN simulation.

Cure Event	Part Thickness (mm)	Average Value (min)	Std. Dev (min)	Δ%
Cure Start	20	57.6	6.0	1.7%
	15	57.1	5.0	1.7%
	10	59.5	7.7	2.4%
	5	55.5	3.4	1.0%
	2	53.9	5.4	1.6%
Minimum	20	86.8	1.1	0.4%
Viscosity	15	85.6	0.2	0.5%
	10	86.9	0.5	0.7%
	5	86.1	0.5	0.8%
	2	86.4	0.8	0.6%
Gel Point	20	120.1	7.9	3.3%
	15	122.2	8.2	4.0%
	10	115.1	5.6	1.8%
	5	119.9	5.5	1.9%
	2	120.6	8.4	3.2%
Vitrification Point	20	154.7	7.1	4.7%
	15	153.7	5.4	2.8%
	10	152.0	2.8	1.9%
	5	154.2	5.6	1.6%
	2	159.0	6.0	3.0%
Cure End	20	251.6	4.0	3.0%
	15	250.5	3.7	4.2%
	10	247.9	6.3	3.0%
	5	248.8	3.8	2.6%
	2	251.5	2.4	2.9%

5 Conclusion

A prototype dielectric sensor was evaluated in this paper for sensor quality, applicability of analysis methods to through-thickness sensing, and part-to-part consistency. It was demonstrated that:

- Phase angle measurements and dielectric signals are reliable and as expected for the 5320-1 carbon fibre/epoxy material system.
- The sensor is free of polarisation effects, temperature effects, and is not impacted by conductive carbon fibres.
- The presence of PEEK spacer rings in the sensor distorts the signal due to the simultaneous epoxy-PEEK reading and necessitated a correction factor. The correction factor assumes that the sensor identifies cure events in the same manner as the IDEX sensor, and accounts for temperature and thickness variation.

The application of the correction factor allowed for successful application of parameter-independent dielectric analysis methods. The corrected signal is very accurate and resulted in identifying cure point times within 5% compared with averaged RAVEN results, including predicting the point of minimum viscosity within 1% and the gel point within 4%. Graphical methods were also applied with good accuracy, including degree of cure predictions from DoC(2) within 6% compared to simulated and analytical methods. The progression of cure was successfully monitored throughout the entire part thickness and applicable to parts from 2 to 20 mm thick. Finally, the results were repeatable for each part thickness across the manufactured replicates, indicating robustness of the sensor design.

6 References

- [1] Nass KA, Seferis JC. Analysis of the Dielectric Response of Thermosets During Isothermal and Nonisothermal Cure. *Polymer Engineering & Science*. 1989;29(5):315-24.
- [2] Day DR. Dielectric determination of cure state during non-isothermal cure. *Polym Eng Sci*. 1989;29(5):334-8.
- [3] Lee DG, Kim HG. Non-Isothermal in Situ Dielectric Cure Monitoring for Thermosetting Matrix Composites. *Journal of Composite Materials*. 2004;38(12):977-93.
- [4] Kazilas MC, Partridge IK. Exploring equivalence of information from dielectric and calorimetric measurements of thermoset cure—a model for the relationship between curing temperature, degree of cure and electrical impedance. *Polymer*. 2005;46(16):5868-78.
- [5] Kim J-S, Lee DG. On-line cure monitoring and viscosity measurement of carbon fiber epoxy composite materials. *Journal of Materials Processing Technology*. 1993;37(1-4):405-16.
- [6] Abraham D, McIlhagger R. Glass fibre epoxy composite cure monitoring using parallel plate dielectric analysis in comparison with thermal and mechanical testing techniques. *Composites Part A*. 1998;29:811-9.
- [7] Bang KG, Kwon JW, Lee DG, Lee JW. Measurement of the degree of cure of glass fiber–epoxy composites using dielectrometry. *Journal of Materials Processing Technology*. 2001;113(1-3):209-14.
- [8] Kim HG, Lee DG. Dielectric cure monitoring for glass/polyester prepreg composites. *Compos Struct*. 2002;57(1-4):91-9.
- [9] Maffezzoli A, Trivisano A, Opalicki M, Mijovic J, Kenny JM. Correlation between dielectric and chemorheological properties during cure of epoxy-based composites. *Journal of Materials Science*. 2004;29(3):800-8.
- [10] Hubner M, Klatt A, Koerd M, Lang W. Online monitoring of thermoplastic crystallization with miniaturized interdigital sensors. *IEEE*. p. 1-4.
- [11] Gonnet JM, Guillet J, Sirakov I, Fulchiron R, Seytre G. ?In-situ? monitoring of the non-isothermal crystallization of polymers by dielectric spectroscopy. *Polym Eng Sci*. 2002;42(6):1159-70.
- [12] Chaloupka A, Grund D, Wedel A, Rudolph NM, Drechsler K. In-Situ Detection Of Phase Transitions Of Semi- Crystalline Carbon Fiber Reinforced Thermoplastics Using Dielectric

Analysis And Its Correlation To Dma And Dsc. European Conference on Composite Materials. Munich, Germany2016.

[13] Vadlamudi V, Shaik R, Raihan R, Reifsnider K, Iarve E. Identification of current material state in composites using a dielectric state variable. *Compos Part a-Appl S.* 2019;124:105494.

[14] Raihan R, Reifsnider K, Cacuci D, Liu Q. Dielectric signatures and interpretive analysis for changes of state in composite materials. *ZAMM - Journal of Applied Mathematics and Mechanics / Zeitschrift für Angewandte Mathematik und Mechanik.* 2015;95(10):1037-45.

[15] Boinard P, Pethrick RA, Banks WM, Crane RL. Non destructive evaluation of adhesively bonded composite structures using high frequency dielectric spectroscopy. *Journal of Materials Science.* 2000;35(6):1331-7.

[16] Breede A, Moghaddam MK, Brauner C, Herrmann AS, Lang W. Online Process Monitoring And Control By Dielectric Sensors For A Composite Main Spar For Wind Turbine B^la des. 20th International Conference on Composite Materials. Copenhagen2011.

[17] Tifkitsis KI, Skordos AA. A novel dielectric sensor for process monitoring of carbon fibre composites manufacture. *Compos Part a-Appl S.* 2019;123:180-9.

[18] Mesogitis TS, Maistros GM, Asareh M, Lira C, Skordos AA. Optimisation of an in-process lineal dielectric sensor for liquid moulding of carbon fibre composites. *Compos Part a-Appl S.* 2021;140.

[19] Shin JH, Nutt S. In situ resin age assessment using dielectric analysis and resin cure map for efficient vacuum infusion. *Advanced Manufacturing: Polymer & Composites Science.* 2020;6(4):212-25.

[20] Wang P, Molimard J, Drapier S, Vautrin A, Minni JC. Monitoring the resin infusion manufacturing process under industrial environment using distributed sensors. *Journal of Composite Materials.* 2011;46(6):691-706.

[21] Michaud DJ, Beris AN, Dhurjati PS. Thick-Sectioned RTM Composite Manufacturing: Part I – In Situ Cure Model Parameter Identification and Sensing. *Journal of Composite Materials.* 2016;36(10):1175-200.

[22] Pethrick RA, Hayward D. Real time dielectric relaxation studies of dynamic polymeric systems. *Progress in Polymer Science.* 2002;27(9):1983-2017.

- [23] Kyriazis A, Charif S, Rager K, Dietzel A, Sinapius M. A Parametric Model for the Analysis of the Impedance Spectra of Dielectric Sensors in Curing Epoxy Resins. *Sensors*. 2023;23(4):1825.
- [24] Konstantopoulos S, Fauster E, Schledjewski R. Monitoring the production of FRP composites: A review of in-line sensing methods. *Express Polym Lett*. 2014;8(11):823-40.
- [25] Torres M. Parameters' monitoring and in-situ instrumentation for resin transfer T moulding: A review. *Composites Part A*. 2019;124.
- [26] Hardis R, Jessop JLP, Peters FE, Kessler MR. Cure kinetics characterization and monitoring of an epoxy resin using DSC, Raman spectroscopy, and DEA. *Compos Part a-Appl S*. 2013;49:100-8.
- [27] Chaloupka A, Pflock T, Horny R, Rudolph N, Horn SR. Dielectric and rheological study of the molecular dynamics during the cure of an epoxy resin. *J Polym Sci Pol Phys*. 2018;56(12):907-13.
- [28] Hall M, Zeng X, Shelley T, Schubel P. In Situ Thermoset Cure Sensing: A Review of Correlation Methods. *Polymers (Basel)*. 2022;14(15):2978.
- [29] Kyriazis A, Pommer C, Lohuis D, Rager K, Dietzel A, Sinapius M. Comparison of Different Cure Monitoring Techniques. *Sensors*. 2022;22(19):7301.
- [30] O'Dwyer MJ, Maistros GM, James SW, Tatam RP, Partridge IK. Relating the state of cure to the real-time internal strain development in a curing composite using in-fibre Bragg gratings and dielectric sensors. *Measurement Science and Technology*. 1998;9(8):1153-8.
- [31] Tifkitsis KI, Winistoerfer A, Skordos AA. Online optimisation and active control of the cure process of thick composite laminates. *Journal of Manufacturing Processes*. 2023;87:221-30.
- [32] Lawrence JM, Hsiao K-T, Don RC, Simacek P, Estrada G, Sozer EM, et al. An approach to couple mold design and on-line control to manufacture complex composite parts by resin transfer molding. *Composites Part A: Applied Science and Manufacturing*. 2002;33(7):981-90.
- [33] Modi D, Correia N, Johnson M, Long A, Rudd C, Robitaille F. Active control of the vacuum infusion process. *Compos Part a-Appl S*. 2007;38(5):1271-87.
- [34] Alms JB, Advani SG, Glancey JL. Liquid Composite Molding control methodologies using Vacuum Induced Preform Relaxation. *Compos Part a-Appl S*. 2011;42(1):57-65.

- [35] Anandan S, Dhaliwal GS, Huo Z, Chandrashekhara K, Apetre N, Iyyer N. Curing of Thick Thermoset Composite Laminates: Multiphysics Modeling and Experiments. *Appl Compos Mater*. 2018;25(5):1155-68.
- [36] Skordos AA, Partridge IK. Effects of tool-embedded dielectric sensors on heat transfer phenomena during composite cure. *Polym Composite*. 2007;28(2):139-52.
- [37] Stephan F, Duteurtre X, Fit A. In-process control of epoxy composite by microdielectrometric analysis. Part II: On-line real-time dielectric measurements during a compression molding process. *Polym Eng Sci*. 1998;38(9):1566-71.
- [38] Senturia SD, Sheppard NF, Jr. *Dielectric Analysis of Thermoset Cure*. 1985.
- [39] Kremer F, Schönhals A. *Broadband Dielectric Spectroscopy* 2003.
- [40] Chaloupka A. *Development of a dielectric sensor for the real-time in-mold characterization of carbon fiber reinforced thermosets*: University of Augsburg; 2018.
- [41] Nass KA. *Dielectric thermal analysis of polymeric matrices*: ProQuest Dissertations Publishing; 1989.
- [42] Stadler H, Kiss P, Stadlbauer W, Plank B, Burgstaller C. Influence of consolidating process on the properties of composites from thermosetting carbon fiber reinforced tapes. *Polym Composite*. 2022;43(7):4268-79.
- [43] Yan S, Zeizinger H, Merten C, Schmauder S. In-situ investigation of dielectric properties and reaction kinetics of a glass-fiber-reinforced epoxy composite material using dielectric analysis. *Polym Eng Sci*. 2021;61(6):1673-84.
- [44] Irvani MA, Deparis J, Davarzani H, Colombano S, Guérin R, Mainault A. The influence of temperature on the dielectric permittivity and complex electrical resistivity of porous media saturated with DNAPLs: A laboratory study. *Journal of Applied Geophysics*. 2020;172:103921.
- [45] Kapilaratne RG CJ, Lu M. Automated general temperature correction method for dielectric soil moisture sensors. *Journal of Hydrology*. 2017;551:203-16.
- [46] Ravindran AR, Ladani RB, Wu S, Kinloch AJ, Wang CH, Mouritz AP. The electric field alignment of short carbon fibres to enhance the toughness of epoxy composites. *Compos Part a-Appl S*. 2018;106:11-23.
- [47] Chao H-W, Hsu H-C, Chen Y-R, Chang T-H. Characterizing the dielectric properties of carbon fiber at different processing stages. *Scientific Reports*. 2021;11(1):17475.

- [48] Mano JF, Lanceros-Méndez S, Nunes AM, Dionísio M. Temperature Calibration in Dielectric Measurements. *J Therm Anal Calorim.* 2001;65(1):37-49.
- [49] Technical Data Sheet CYCOM(R) 5320-1 Prepreg. Solvay Composite Materials.
- [50] Hall M, Zeng X, Shelley T, Schubel P. Dielectric Parameter Independent Curing Analysis of Out-Of-Autoclave Carbon Fibre/Epoxy Composites. *Compos Part a-Appl S.* 2023:107755.
- [51] Day DR, Lewis TJ, Lee HL, Senturia SD. The Role of Boundary Layer Capacitance at Blocking Electrodes in the Interpretation of Dielectric Cure Data in Adhesives. *The Journal of Adhesion.* 2006;18(1):73-90.
- [52] van Turnhout J, Wubbenhorst M. Conduction-free dielectric loss $\delta\epsilon''/\delta\epsilon''_{\text{ion}}$ - a powerful tool for the analysis of strong (ion) conducting dielectric materials. *Dielectric Newsletter.* 2000.
- [53] Kratz J, Hsiao K, Fernlund G, Hubert P. Thermal models for MTM45-1 and Cycom 5320 out-of-autoclave prepreg resins. *Journal of Composite Materials.* 2012;47(3):341-52.
- [54] ASTM D7028-07(2015), Standard Test Method for Glass Transition Temperature (DMA T_g) of Polymer Matrix Composites by Dynamic Mechanical Analysis (DMA). West Conshohocken, PA: ASTM International; 2015.
- [55] Lattimer MP, Hobbs JK, Hill MJ, Barham PJ. On the origin of the multiple endotherms in PEEK. *Polymer.* 1992;33(18):3971-3.
- [56] Takahashi T, Serizawa M, Okino T, Kaneko T. A round-robin test of the softening temperature of plastics by thermomechanical analysis. *Thermochimica Acta.* 1989;147(2):387-99.
- [57] Barba D, Arias A, Garcia-Gonzalez D. Temperature and strain rate dependences on hardening and softening behaviours in semi-crystalline polymers: Application to PEEK. *International Journal of Solids and Structures.* 2020;182-183:205-17.
- [58] Jonas A, Legras R. Relation between PEEK semicrystalline morphology and its subglass relaxations and glass transition. *Macromolecules.* 1993;26(4):813-24.
- [59] Mourgues-Martin M, Bernés A, Lacabanne C. Dielectric relaxation phenomena in PEEK. *Thermochimica Acta.* 1993;226:7-14.
- [60] Kalika DS, Krishnaswamy RK. Influence of crystallinity on the dielectric relaxation behavior of poly(ether ether ketone). *Macromolecules.* 1993;26(16):4252-61.

- [61] Huo P, Cebe P. Temperature-dependent relaxation of the crystal-amorphous interphase in poly(ether ether ketone). *Macromolecules*. 1992;25(2):902-9.
- [62] Boyd RH. Relaxation processes in crystalline polymers: molecular interpretation — a review. *Polymer*. 1985;26:1123-33.
- [63] Arous M, Amor IB, Kallel A, Fakhfakh Z, Perrier G. Crystallinity and dielectric relaxations in semi-crystalline poly(ether ether ketone). *The Journal of physics and chemistry of solids*. 2007;68(7):1405-14.
- [64] Golden K. Bounds on the complex permittivity of a multicomponent material. *Journal of the Mechanics and Physics of Solids*. 1986;34(4):333-58.
- [65] Yang Y, Plovie B, Chiesura G, Vervust T, Daelemans L, Mogosanu D-E, et al. Fully Integrated Flexible Dielectric Monitoring Sensor System for Real-Time In Situ Prediction of the Degree of Cure and Glass Transition Temperature of an Epoxy Resin. *IEEE Transactions on Instrumentation and Measurement*. 2021;70:1-9.
- [66] Mijović J, Andjelic Sa, Fitz B, Zurawsky W, Mondragon I, Bellucci F, et al. Impedance spectroscopy of reactive polymers. 3. Correlations between dielectric, spectroscopic, and rheological properties during cure of a trifunctional epoxy resin. *J Polym Sci Pol Phys*. 1996;34(2):379-88.
- [67] Kim SS, Murayama H, Kageyama K, Uzawa K, Kanai M. Study on the curing process for carbon/epoxy composites to reduce thermal residual stress. *Compos Part a-Appl S*. 2012;43(8):1197-202.
- [68] Maistros GM, Partridge IK. Monitoring autoclave cure in commercial carbon fibre/epoxy composites. *Compos Part B-Eng*. 1998;29(3):245-50.
- [69] Shepard DD, Twombly B. Simultaneous dynamic mechanical analysis and dielectric analysis of polymers. *Thermochimica Acta*. 1996;272:125-9.
- [70] Boll D, Schubert K, Brauner C, Lang W. Miniaturized Flexible Interdigital Sensor for In Situ Dielectric Cure Monitoring of Composite Materials. *IEEE Sensors Journal*. 2014;14(7):2193-7.
- [71] Kahali Moghaddam M, Breede A, Chaloupka A, Bödecker A, Habben C, Meyer E-M, et al. Design, fabrication and embedding of microscale interdigital sensors for real-time cure monitoring during composite manufacturing. *Sensors and Actuators A: Physical*. 2016;243:123-33.

CHAPTER 5: (PAPER 3) STOCHASTIC MODELLING OF OUT-OF-AUTOCLAVE EPOXY COMPOSITE CURE CYCLES UNDER UNCERTAINTY

5.1 Introduction

The final study in this thesis explores the variability of epoxy cure properties when exposed to sources of processing uncertainty. The objective was to quantify how variable the cure process is, and to validate the predictions using experimental data. In this study, a stochastic cure model using Monte Carlo methods was developed for CYCOM® 5320-1 carbon fibre/epoxy to account for cure kinetics modelling and process temperature variability. A new method for quantifying cure kinetic parameter uncertainty is proposed, which is based on knowledge of equipment, process, and analysis method error tolerances. The stochastically modelled cure and viscosity of the resin system produced a distribution of output parameters, and an analysis was done on the extent of their variability. Experimental data collected during the laminate cures from the Paper 1 study was used to validate the convergence analysis, proving that the final cure properties vary according to the predictions.

5.2 Links and implications

The implication of the results presented in this paper are threefold. Firstly, it was determined that the proposed method for characterising uncertainty is comparable with existing methods which require extensive analytical testing. This new low-effort technique could be applied to any material system with a known cure kinetics model without the need for cumbersome analytical testing and difficult analysis. Secondly, recommendations for process requirements due to expected variability are provided for the 5320-1 material system. In particular, the high range of time to completed cure reactions indicates that the cure process should be optimised with caution. Lastly, the findings from this paper strongly support the need for process monitoring technologies, such as those presented in Chapters 3 and 4. The unique capabilities of dielectric sensing technologies for evaluating cure progressions are an excellent method for ensuring that the actual part properties are accurately captured during processing, eliminating the need for guesswork and assumptions.

5.3 Paper manuscript

Stochastic modelling of out-of-autoclave epoxy composite cure cycles under uncertainty

Molly Hall ^{a*}, Xuesen Zeng ^a, Tristan Shelley ^a, Peter Schubel ^a

a. Centre for Future Materials, University of Southern Queensland, Toowoomba, QLD 4350,
Australia

Corresponding Author*: Molly Hall (molly.hall@usq.edu.au)

Abstract

Thermoset polymers and composites are subject to several sources of uncertainty which can produce a range of cure outcomes. Recent research into stochastically modelled thermoset cure has indicated that accounting for raw material and process uncertainty can model this range of expected output parameters. However, the uncertainty quantification methods are highly test-intensive, and the results of the simulations haven't been validated with experimental data. This study proposes a simple approach to cure kinetics uncertainty quantification that can be applied to any cure kinetics model without the need for additional testing. Stochastic cure kinetics and temperature conditions for a popular out-of-autoclave carbon fibre/epoxy prepreg were used to produce output distribution functions for key cure events, and the results were validated using data from ten cure replicates. The quantified variation expected from the cure of this prepreg resulted in processing recommendations to ensure quality metrics are met during processing.

Keywords: Thermosetting resin, Cure behaviour, Process simulation, Stochastic cure simulation

1 Introduction

Thermoset composites are an attractive option for high-performance components in a variety of industries. Performance is strictly tied to quality parameters such as the degree of cure and the glass transition temperature (T_g) at the end of the cure cycle, which are directly related to the processing conditions [17]. A current trend in composites research is to accelerate and optimise the processing conditions, while still producing parts of a sufficient quality. Optimisation techniques include exhaustive test matrices [44] or numerical methods [45, 46] including gradient based techniques [47], genetic algorithms [48], and the Evolutionary Strategy [22]. Optimisation techniques typically target minimising a specific feature such as the total process time [22], temperature gradient [49], or the exotherm temperature [50] or maximising the part quality [20] or performance [51]. Studies have also investigated the balance of multiple objective functions which can potentially have conflicting solutions [50-52]. The success of the optimisation activities is dependent on the accuracy of the numerical modelling tool which is used to produce the optimised parameters.

Cure simulation tools can predict cure behaviour over a range of complexities and scales. A 0-dimensional (0D) simulation provides the most fundamental view of how a thermoset polymer reacts to a given cure profile. A 1-dimensional (1D) or 2-dimensional (2D) simulation will provide insight to how the depth or spatial area of a resin responds, which encompasses heat transfer behaviour from the surrounding polymer reaction [27, 120]. Finally, a 3-dimensional (3D) view provides the highest complexity with the capability of modelling specific part geometries [23, 28, 121]. However, thermoset composites display a large amount of final part property variation due to uncertainty which impacts the accuracy of these practices. Typically these systems do not account for process uncertainty, instead they rely on a deterministic cure kinetics model which has limited accuracy [121, 122]. By not considering this uncertainty there is an increased risk of an optimised process resulting in a part not meeting the quality requirements.

Uncertainty in composites originates from several sources including fibre architecture, resin formulation and mixing, environmental conditions, and from the processing steps [10, 53]. It is also shown that variation in resin formulations and mixing can strongly impact the viscosity and cure behaviour [56]. Varying parameter values to illustrate this uncertainty can produce a significant impact on the final part outcome [54]. The multiple origins and sources of uncertainty may also interact with one another, making it necessary to understand their impacts both independently and together. For example, an epoxy vinyl ester resin system [77] produced

equivalent responses for varying cure kinetics parameters and for varying heat transfer model parameters by one standard deviation [123]. Another epoxy system, however, had a far stronger influence of temperature and heat transfer coefficient boundary conditions compared with the impact of cure kinetics [124]. As each polymer is unique, it is necessary to identify the influence of uncertainty sources for each system.

Uncertainty in cure cycle designs can be modelled using stochastic methods [125-127], multiperiod formulations [128], and parametric methods [129]. Stochastic methods have characterised a number of composites aspects which display high levels of uncertainty including flow during resin infusion [130, 131], wrinkling effects in woven composites [132], residual stress build-up [133], delamination onset time [134], tow impregnation [135], structural properties [127], and resin curing [52, 126, 136]. Stochastic methods are based on uncertainty quantification, sampling of parameters from the resultant distribution, inputting the parameters into a deterministic model, and extracting output parameters over a series of iterations to establish a converging value. A variety of rationales have been provided for quantifying uncertainty in composites processes, with a summary of the methods and their use in stochastic modelling given in Table 1.

Table 1 – A summary of studies implementing stochastic modelling to capture composites processing uncertainty including details on uncertainty quantification method, sampling method, and input and output parameters.

Source	Stochastic Parameters	Uncertainty Quantification	Sampling Method	Material	Output Parameters
[126]	Temperature, cure kinetics parameters	Assigned 1.5%, 3%, 5% variance with normalised deviations	Latin hypercube	Epoxy, polyester	Cure time
[54]	Temperature, cure kinetics parameters	Assigned 2%, 3.5%, 5%, 10% variance	Latin hypercube	Polyester	Cure time, maximum temperature, maximum temperature difference, degree of cure
[124, 130]	Temperature, heat transfer coefficient, cure kinetics parameters	Experimentally determined	Monte Carlo, Probabilistic Collocation	Carbon fibre/epoxy	Cure time
[54, 130]	Preform permeability, resin viscosity, and cure kinetics parameters	Assigned 1% probability distributions	Latin hypercube	Generalised resin transfer moulding materials	Fill time, degree of cure
[131]	Woven fabric preform permeability	1D and 2D flow measurements to quantify variance	Monte Carlo	Woven fabric	Flow ending location
[132]	Fibre tow direction and dimensions	Image analysis to quantify probability distributions for parameters	Monte Carlo	Carbon fibre/epoxy	Wrinkling strain
[135]	Initial degree of prepreg impregnation	Analysis of CT scans to quantify stochastic distributions	Probabilistic collocation	Out-of-autoclave prepreg	Void content
[136]	Cure kinetics parameters	Experimentally determined	Monte Carlo, Probabilistic Collocation	Carbon fibre/epoxy	Maximum temperature, time at maximum temperature

A popular out-of-autoclave carbon fibre/epoxy prepreg, CYCOM® 5320-1 [100, 137] has been evaluated in many studies. Areas of interest have included modelling of cure kinetics [25, 109,

138, 139], viscosity [25, 138, 139], thermal expansion coefficient [140], residual stress development [141], and cure cycle evaluation and optimisation [57, 142]. While there have been numerous cure kinetics models proposed for this resin system, it is unknown how the models respond to sources of uncertainty. This paper characterises the stochastic behaviour of 5320-1 under two sources of uncertainty: cure kinetics modelling and processing temperature. A new methodology for assessing cure kinetics parameter variance for complex cure models is proposed and compared with existing methodologies. Stochastic cure simulations for a standard ramp and dwell cure cycle are provided, with assessments on how the cure kinetics and viscosity models react to uncertainty in the temperature and kinetics. The resulting distribution of output parameters is then compared with experimental data to assess the accuracy of the simulation. Finally, suggestions are made for cure cycle considerations to ensure conforming products.

2 Methodologies

2.1 Cure Kinetics and Viscosity Models

2.1.1 CYCOM® 5320-1

The original model for CYCOM® 5320 epoxy was developed by Kratz et al [109]. The updated 5320-1 version was later developed to improve the material out-life [143], which has resulted in multiple kinetic models that apply to this system of materials. These models include a two-step kinetic equation similar to that of 5320 [139], a two-step equation with parameters designated by a lookup table based on degree of cure change [144], and a neural network model [138]. The model used in this paper was developed by Kim et al [25], which is comprised of four distinct reactions and weighted parameters to account for the impact of material out-time on the reaction rates. This model has been validated in multiple publications including to evaluate the effect of cure cycles on degree of cure [57, 142]. Other available models were evaluated; however, the Kim model was determined to be the most accurate for the purposes of this study and is shown in Equations (1) and (2):

$$\frac{d\alpha}{dt} = \sum_{i=1,3} w_i K_i \alpha^{m_i} (1 - \alpha)^{n_i} \quad (1)$$

$$+ \sum_{j=2,4} \frac{w_j K_j \alpha^{m_j} (1 - \alpha)^{n_j}}{1 + \exp\left(D_j \left(\alpha - (\alpha_{c0,j} + \alpha_{CT,j} T)\right)\right)}$$

$$K_n = A_n \exp\left(-\frac{E_{A,n}}{RT}\right) \quad \text{where } n = i, j \quad (2)$$

where the reaction rate $\left(\frac{d\alpha}{dt}\right)$ is calculated as functions of the degree of cure (α) and the temperature (T). In these equations A_n and E_n are respectively the Arrhenius coefficient and activation energies, R is the gas constant, m and n are reaction orders. The impact of diffusion is taken into account using the Chern and Poehlein model [145], modified by [146] for which D is the diffusion constant, α_{C0} and α_{CT} are the critical degree of cure at absolute zero and its increase at the instantaneous temperature. Parameter values can be found in [25]. The weight factors (w) originally represented the impact of out-time on the curing kinetics, but as the out time for the prepreg used here is not precisely known the values used were $w_1 = 0.8$, $w_2 = 0.35$, $w_3 = 1.1$, $w_4 = 1.2$, as these values provided the best fit for the model against a known cure simulation tool, as can be seen in Figure 1.

The model was compiled in MATLAB, which was used to generate the cure behaviour and output parameters. This model and the reported weight factors were validated using Convergent RAVEN simulation software, with the results provided in Figure 1. A set of 0D cure profiles were evaluated using the CYCOM® 5320-1/IM7-12K material card which is available in RAVEN. This material card makes use of a lookup table to assign kinetic parameters [138]. Isothermal cure cycles were run at 170 °C, 180 °C, 190 °C, and 200 °C. Dynamic cure cycles were run from 20 °C to 300 °C at rates of 2.0, 5.0, 7.5, and 10.0 °C per minute. The degree of cure progression during each cure cycle was exported for comparison with the MATLAB degree of cure for the same cycle. The degree of cure progression compares well for these models. The key areas of interest, the time at 88% cured and the final degree of cure, show close fitting.

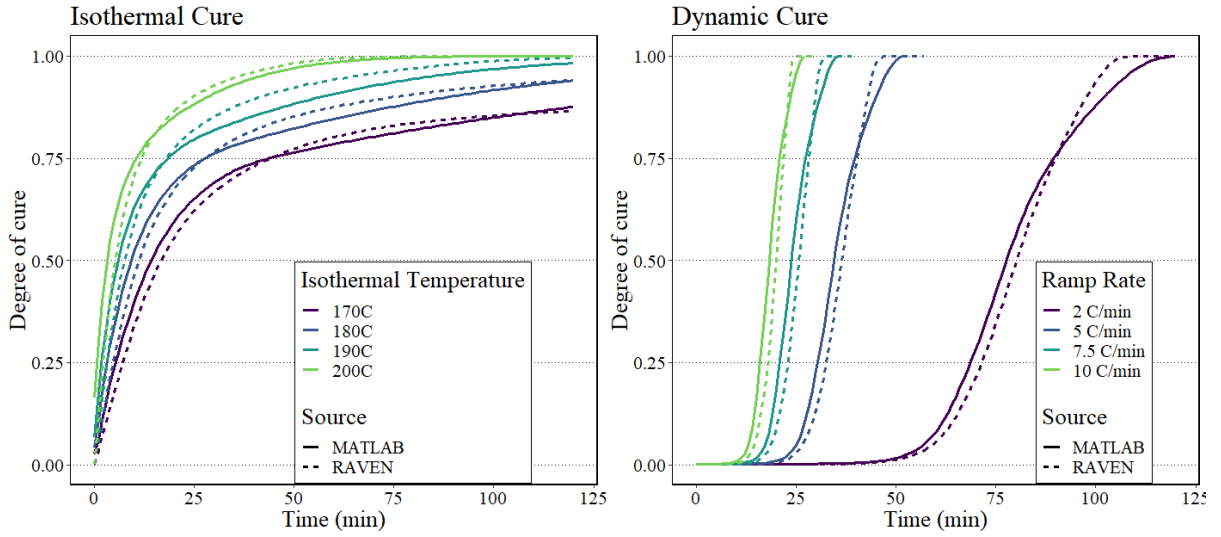


Figure 1 - Comparison of MATLAB generated kinetic model from [25] for a (left) isothermal cure and (right) dynamic cure rate, demonstrating a good model fitting compared with RAVEN.

The viscosity model for 5320-1 used for this study is also published in [25], where the parameter values can be found. The model takes the form shown in Equation (3). In this model the viscosity (η) is calculated using two terms. The first term is solved by the Arrhenius viscosity component (η_i) given in Equation (4), which contains the viscosity activation energy (E_{η}), the gas constant, and the temperature. The second term of this equation is from the Castro-Macosko model [147], which relates viscosity with the degree of cure and the gel conversion point (α_{gel}), and uses fitting constants A , B , C , d , and e . As the weight factors (w) are derived from the out-time, which is unknown, fitting parameters $w_1 = 1, w_2 = 2$, were chosen to ensure the best fit compared with RAVEN. Parameter values are published in [25].

$$\eta = w_1\eta_1 + w_2\eta_2 \left(\frac{\alpha_{gel}}{\alpha_{gel} - \alpha} \right)^{A+B\alpha^d+C\alpha^e} \quad (3)$$

$$\eta_i = A_{\eta_i} \exp\left(\frac{E_{\eta_i}}{RT}\right) \quad \text{where } i = 1,2 \quad (4)$$

The MATLAB viscosity model was written and included the cure kinetics model as detailed above. This model was also validated using Convergent RAVEN simulation software. A set of 0D cure profiles were evaluated using the CYCOM® 5320-1/IM7-12K material card, and the viscosity curve was extracted. Isothermal cure cycles were run at 180 °C, 190 °C, and 200 °C, and dynamic cure cycles were run from 20 °C to 300 °C at rates of 2.0, 5.0, 7.5, and 10.0 °C per minute. A comparison of the RAVEN output with the MATLAB output is given in Figure

2, showing good comparison between the models. Of note is the minimum viscosity is slightly lower in the MATLAB model for both isothermal and dynamic cures. However, this study will evaluate only the time at which the minimum viscosity occurs, which is comparable for both models.

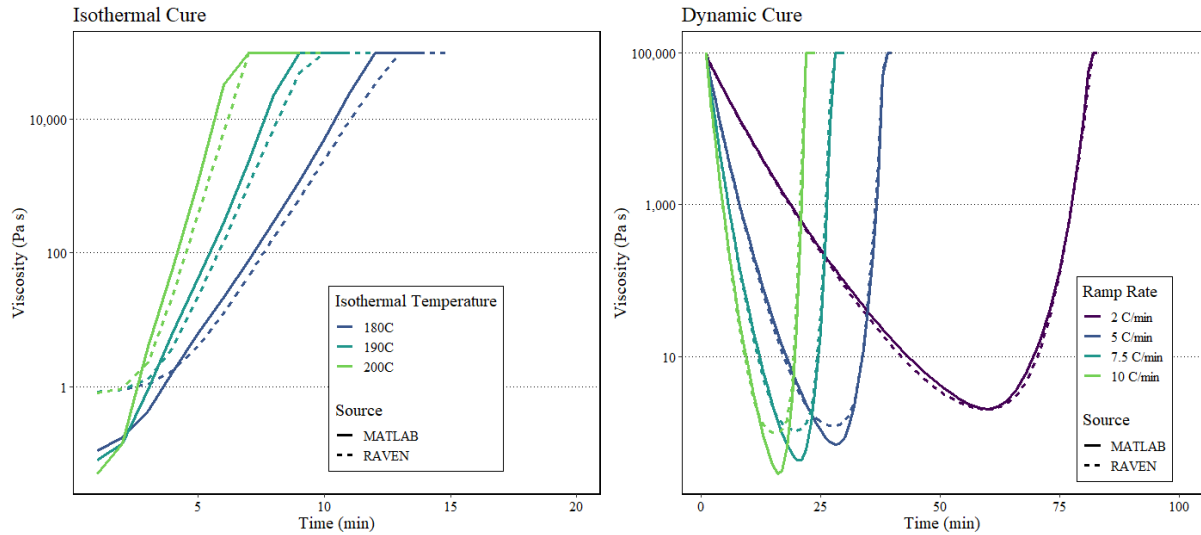


Figure 2 - Comparison of MATLAB generated viscosity model from [25] for a (left) isothermal cure and (right) dynamic cure rate, demonstrating a good model fitting compared with RAVEN.

2.1.2 Hexcel RTM6

Kinetic modelling of Hexcel RTM6 was also completed using MATLAB for the purposes of validating the uncertainty quantification method presented in this paper. The kinetic model was originally developed in [26, 148] and is given in Equation (5), with the comprehensive set of parameter values reported in [50]:

$$\frac{d\alpha}{dt} = K_1(1 - \alpha)^{n_1} + K_2\alpha^m(1 - \alpha)^{n_2} \quad (5)$$

$$\frac{1}{K_i} = \frac{1}{K_d} + \frac{1}{K_c} \quad \text{where } i = 1,2 \quad (6)$$

$$K_d = A_d \exp\left(-\frac{E_{A,d}}{RT}\right) \exp\left(-\frac{b}{0.00048(T-T_g)+0.025}\right) \quad (7)$$

where K_1 and K_2 are modified by the Rabinowitch model [149] in Equation (6), which accounts for either the control mechanism being chemical (c) or diffusion (d) driven. For this, K_c is given by Equation (2) and K_d represents the diffusion rate constant given by the Macedo and Litovitz expression [150] in Equation (7). In this equation, A_d and E_d represent the coefficient and activation energy for diffusion, b is a fitting constant, and T_g represents the instantaneous glass

transition temperature. There are multiple diffusion models which may account for the rates balance between the chemical reaction and diffusion step [145, 146, 151-154]. While RTM6 has been modelled using both the Macedo and Litovitz model [50, 148] and the Chern and Poehlein model [84], this paper will use the Macedo/Litovitz expression for simplicity. RTM6 was unavailable for this study, so the validation of this model will be assumed from the subsequent publications from the research group given in [50, 84, 124, 155].

2.1.3 Cure Cycles

The cure cycle used in this study is based on actual measurements taken during a part cure. The cure cycle is a modified version of the manufacturers recommended cure cycle [100] which has a 2 °C per minute dynamic ramp to 180 °C, followed by a 180 minute isothermal dwell. The cure kinetics model used in this paper is a 0D model, meaning that it reports the cure progression of a dimensionless point in space. As the 0D kinetic model does not account for heat transfer influence on the actual temperature experienced by the laminate, the cure cycle used is a representative temperature cycle taken from the mid-plane of the IDEX2 cure from [101]. In this laminate cure, the oven temperature was set to the defined cure cycle, and the temperature profile was measured by an embedded thermocouple in the centre of the laminate. The laminate was verified to meet the manufacturers recommended cure cycle, which requires a minimum of 120 minutes above 171 °C [100]. This laminate achieved exactly 120 minutes at the cure temperature, and thus represents the threshold for complete cure.

2.2 Stochastic Methodology

2.2.1 Uncertainty Quantification

Accounting for sources of uncertainty is the foundation of the stochastic approach, as the resultant variation in the manufacturing system has a very real impact on the actual process conditions that the part experiences. This study focuses on uncertainty in the cure kinetics and viscosity models and due to the applied temperature cycle. Both cure kinetics and viscosity modelling uncertainty originate from variation in raw material composition (for example, monomer content) and model fitting variation (for example, from baseline selection, equipment measurement, data reduction and fitting [152]). The main source of temperature uncertainty is due to equipment variability which can originate from the temperature control mechanism [156], temperature tolerance [157], and part location within the oven or autoclave [158].

Kinetic Model

Previous methods have attempted to capture the actual variation of the cure kinetics values, as measured from batch-to-batch DSC testing [136]. However, as the 5320-1 model has 22 parameters this method was deemed impractical. Instead, a new approach for estimating parameter variance is proposed here, in which a coefficient of variation (COV) of 3% was assumed for all stochastic variables based on the expected model fitting of within 3% error [152]. This assumption of a 3% COV is consistent with previous works [54, 126] and supported by standard error expected by DSC measurements [159]. A sensitivity analysis was conducted to verify that 3% is applicable to all parameters without distorting the cure kinetics outside of reasonable bounds. Each parameter was varied by +/- 3% and the resulting maximum reaction rate was compared to the deterministic solution. Previous works have indicated that variation in model fitting practices can produce mode 10% variability of the result [152]. Thus, values which yielded a greater than 10% deviance from the maximum reaction rate were rejected, as such values would have likely changed the fitting of the original model. Any values with deviations of over 10% were examined at reduced COVs until a value was found which kept it within the 10% boundaries. To evaluate if the 3% assumption allows for excessive variation, a second set of analyses were conducted using half the COV. The baseline variation was set to 1.5%, and any parameters which required a reduced variation were also reduced by half.

To validate this approach, a comparison was made on the well-studied epoxy, RTM6, which has been evaluated for stochastic cure kinetics by Mesogitis et al. [136]. In the reported study, the cure kinetic parameter variation was determined experimentally by fitting multiple DSC curves and examining the variance of each parameter amongst the different fittings. Using the kinetic model for RTM6 indicated in Equation (5) the three stochastic parameters indicated by Mesogitis (α_0 , E_2 , m) were varied according to their calculated COV. A stochastic simulation and convergence analysis was run for both a dynamic cure rate from 20 °C to 250 °C at a rate of 2 °C per minute, and for the standard cure cycle used in this study. The time to reach 88% cured was reported as the output variable. The results of this convergence analysis were then compared to the method proposed here, of a standard 3% variance of parameters, and a simulation using the actual COV of all parameters reported by Mesogitis. The half-variance method was also included.

Viscosity Models

The viscoelastic behaviour of a thermoset polymer is primarily influenced by the temperature and cross-linking of the polymer [160] and can be modelled with reasonable accuracy [161]. For this reason, the viscosity model absorbs the temperature and cure kinetics modelling

uncertainty. While viscosity modelling may have additional sources of uncertainty due to measurement or fitting error, this will not be the focus of this paper. The viscosity modelling uncertainty will focus only on the temperature and cure kinetics modelling variance, with the aim to demonstrate the range of properties that these sources impact.

Temperature Profile

Temperature profile uncertainty was determined based on a series of oven measurements. The oven used for this study is a fan forced convection oven with internal dimensions of 500 mm (width) by 500 mm (depth) by 550 mm (height). Thermal measurements were made using a thermocouple in air, approximately 100 mm above the part, and a thermocouple embedded in the centre of the part. The tool was placed with the rack in the middle shelving position in the oven, which places the part at approximately 150 mm below the top of the oven. The standard cure profile used in this study was measured from [101] test measurement labelled IDEX2. Ten cure profiles represented in this paper were compared to determine the actual expected variance of mid-part temperature for cures in this oven. The stochastically generated standard cure profile was varied by this percentage from the original IDEX2 temperature curve. As the small oven used for this study demonstrated a very reliable temperature profile, an additional set of analyses were done with a higher temperature variation of 5%. This limit was chosen to account for the maximum temperature tolerance limit of 5% which is commonly imposed on composites processing ovens and autoclaves [157].

2.2.2 Output Parameters

The output parameters which will be evaluated in this study are given in Table 2, including their definitions for this paper.

Table 2 – Test plan for comparing different methods of stochastic parameter assignment.

Model	Output Parameters	Definition
Cure Kinetics	Vitrification point (min)	$T = T_g$
	Time at fully cured (min)	Time at degree of cure of
	Final degree of cure (%)	88% Final value of the degree of cure
Viscosity	Time at minimum viscosity (min)	Time at minimum viscosity
	Gel point (min)	Time at viscosity = 10,000 cP

2.2.3 Stochastic Methods and Convergence Analysis

The stochastic method involves identification and quantification of the parameters under uncertainty, sampling of the parameters, incorporating these parameters into a deterministic numerical model, and extraction of the output parameters. All of this occurs repetitively over several iterations until the output parameters converge to a resultant value. The approached used in this study is summarised in Figure 3.

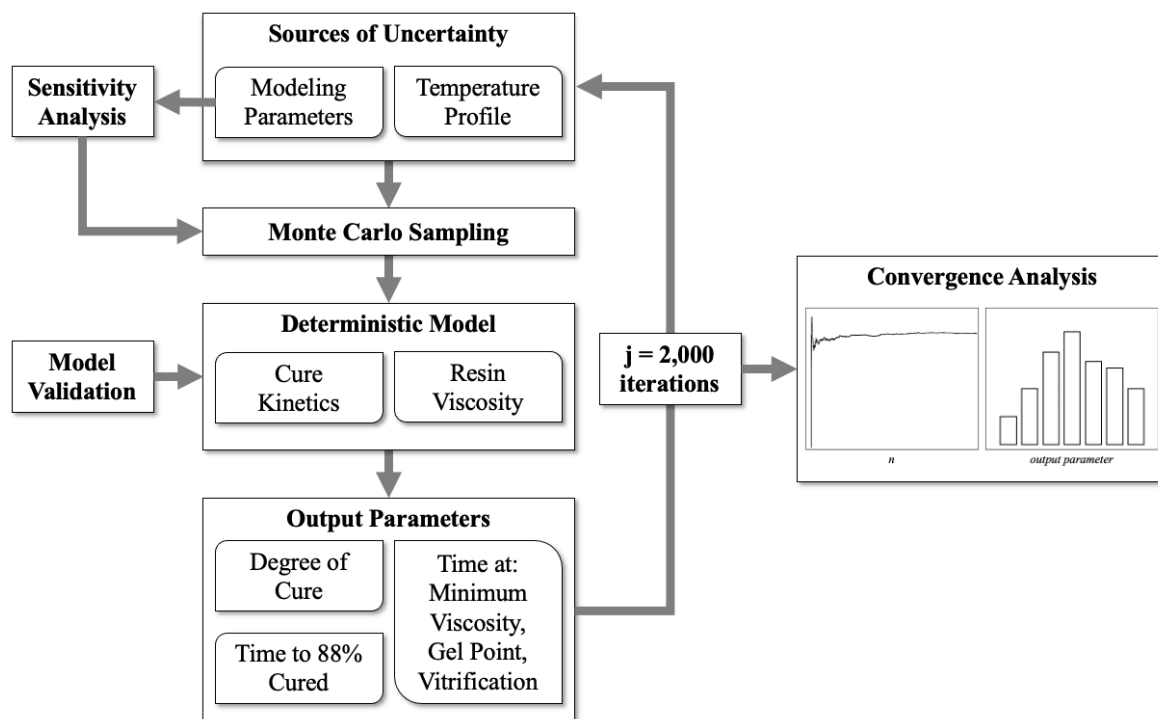


Figure 3 - Schematic depicting the stochastic methodology.

The combination of sources of uncertainty to be examined are defined in Table 3. As previously stated, the kinetic parameters are assumed to have a 3% variance (CK-3) due to natural batch-to-batch fluctuations in resin composition and due to kinetic modelling error. The temperature variance is calculated based on actual measured temperature variation from oven cures (T and All). To evaluate the impact of these, cure kinetics with a half-COV (CK-Half) and a standard 5% of temperature (T-5) were also evaluated. The parameters were randomly sampled using a Monte Carlo distribution method. The sampled parameters are then input to the deterministic models, Equations (1) and (3). The output parameters were extracted in accordance with Table 2 and added to an iterative list. The output parameters are iterated for 2,000 cycles to ensure that the standard deviation converges to within 5%. The stochastic outputs are compared with the deterministic solution, for which the MATLAB code was run with a variance of 0% for all variables.

Table 3 – Set of stochastic analyses to be evaluated in this paper detailing the sources of variation and their limits.

Analysis Name	Cure Kinetics Variance	Temperature Variance
CK-3	3%*	None
CK-Half	1.5%*	None
T	None	Actual measurement (1.5%)
T-5	None	5%
All	3%	Actual measurement (1.5%)

* Excepting parameters with reduced variances.

2.3 Experimental Validation

The results of the convergence analysis are compared with actual measurements from 5320-1 cures meeting the requirements of the standard cure cycle definition. The cure methods and data collection techniques for the experimental tests can be found in [101]. The temperature profile data from the laminate mid-point for each part was then run through the code used for this paper, and the relevant outputs were determined in accordance with Table 2 for the standard cure.

3 Results and Discussion

3.1 Uncertainty Quantification

3.1.1 Cure Kinetics

The methods employed in [136] were compared to the new method proposed in this paper, which uses a standard 3% variance of kinetic parameters. The kinetic parameters for RTM6 were varied by $\pm 3\%$ to evaluate the impact to the reaction rate maxima. The results shown in Table 4 demonstrate that all parameters excepting E_1 and E_2 provide a satisfactory outcome when varied by 3%. E_1 and E_2 both exceeded 10% deviation to the maximum reaction rate, indicating that the parameters are unlikely to be varied as high as 3% while still providing a good fitting to the actual reaction rate. This is supported by the actual measured variation of each parameter being 1% as reported by [136]. Subsequently, the COV of each parameter was reduced until the fit falls within 10% with new COV values for E_1 being 2% and E_2 being 1.5%. The half-COV measurements for these were 1% and 0.75% respectively.

Table 4 – Results of varying RTM6 kinetic parameters by $\pm 3\%$ on the maximum reaction rate. Also indicated are the parameters reported actual COV and an * identifying the stochastic variables from [136].

Parameter	Reported COV	Reaction Rate Deviation, -3%	Reaction Rate Deviation, +3%	Notes
α_0 *	19%	-0.1%	0.1%	
A_1	3.5%	-0.9%	1.0%	
E_1	1%	13.5%	-15.1%	Rejected, > 10%
		9.0%	-9.4%	Updated COV = $\pm 2\%$
n_1	9%	0.0%	0.0%	
A_2	2.6%	1.1%	-0.6%	
E_2 *	1%	-20.0%	16.4%	Rejected, > 10%
		-9.5%	8.6%	Updated COV = $\pm 1.5\%$
m *	7%	1.5%	-1.0%	
n_2	6%	-2.7%	2.6%	
A_d	4%	0.0%	0.0%	
E_d	2%	0.0%	0.0%	
b	11%	0.0%	0.0%	

Parameter	Reported COV	Reaction Rate Deviation, -3%	Reaction Rate Deviation, +3%	Notes
<i>w</i>	9%	0.0%	0.0%	
<i>g</i>	19%	0.0%	0.0%	

Using the determined COV values, the three parameter uncertainty methods were compared, with the results in Table 5. All stochastic simulations converged to the deterministic solution, which confirms that the parameters variance doesn't distort the simulation results. The method from [136] resulted in a variance approximately halfway between the 3% COV and half-COV evaluations shown here. This indicates that the method from [136] may align best to a variation of near 2.25%. While the variance for the 3% method is slightly higher than the method reported by [136], it still produces a satisfactory result.

Table 5 – Comparison of three methods of determining parameters variance on predicting the average value and variance of the time for RTM6 to reach 88% cured.

Cure Cycle	Method	Average (min)	Standard Deviation (min)	COV (%)
Dynamic	Deterministic solution	94	--	--
	COV from [136], 3 stochastic parameters	93.85	1.26	1.34
	COV from [136], all parameters are stochastic	93.85	1.40	1.49
	3% COV	93.87	1.69	1.80
	Half COV (1.5%)	93.84	0.90	0.96
Standard Cure Cycle	Deterministic solution	156	--	--
	COV from [136], 3 stochastic parameters	156.07	4.74	3.03
	COV from [136], all parameters are stochastic	156.08	5.27	3.38
	3% COV	156.38	6.48	4.14
	Half COV (1.5%)	155.98	3.27	2.09

As the 3% variance method has been shown to be comparable to previous methods for the RTM6 resin, the same sensitivity analysis was performed on 5320-1. The results of this are in Table 6. Of note are the results for E_1 , E_3 , and E_4 , which all produced variances which exceeded the 10% threshold. As noted in the table, these parameter variances have been reduced to 2.5%, 0.8%, and 2% respectively, with the half variances at 1.25%, 0.4%, and 1%.

Table 6 - Results of varying 5320-1 kinetic parameters by $\pm 3\%$ on the maximum reaction rate.

Parameter	Reaction Rate Deviation, -3%	Reaction Rate Deviation, +3%	Notes
A_1	-0.6%	0.7%	
	-16.6%	10.3%	Rejected, > 10%
E_1			Updated COV =
	-4.8%	6.0%	$\pm 2.5\%$
m_1	1.0%	-0.9%	
n_1	-0.9%	0.8%	
A_2	0.1%	-0.1%	
E_2	-2.2%	1.3%	
m_2	-0.1%	0.1%	
n_2	0.0%	0.0%	
D_2	0.0%	0.0%	
$\alpha_{C0,2}$	0.0%	0.0%	
$\alpha_{CT,2}$	0.0%	0.0%	
A_3	1.8%	-1.8%	
	-45.9%	26.3%	Rejected, > 10%
E_3			Updated COV =
	-9.9%	8.5%	$\pm 0.8\%$
m_3	-6.8%	6.2%	
n_3	-3.9%	3.6%	
A_4	0.7%	-0.7%	
	-12.7%	8.1%	Rejected, > 10%
E_4			Updated COV =
	-7.8%	5.8%	$\pm 2\%$
m_4	-2.6%	2.3%	
n_4	-0.3%	0.3%	
D_4	0.0%	0.0%	
$\alpha_{C0,4}$	0.0%	0.0%	
$\alpha_{CT,4}$	0.0%	0.0%	

3.1.2 Temperature

Firstly, the range of temperatures measured during a standard cure profile for 5320-1 are shown in Figure 4. The average variation between the runs was 1.5%, which will be used as the temperature COV for this study. While this variation is representative of the small oven used in this study, a 5% variation will also be used to demonstrate the variation which is possible in larger ovens. IDEX8 demonstrates a slightly different temperature profile compared with the other tests and shows more fluctuation throughout the cure. At the completion of the cure, it was identified the laminate had shifted, and the part was cured under only one layer of breather material, in contrast with the other laminates which were cured under two layers. This variation resulted in a large impact on the heat transfer through the laminate and demonstrates another source of uncertainty which can impact composite cures.

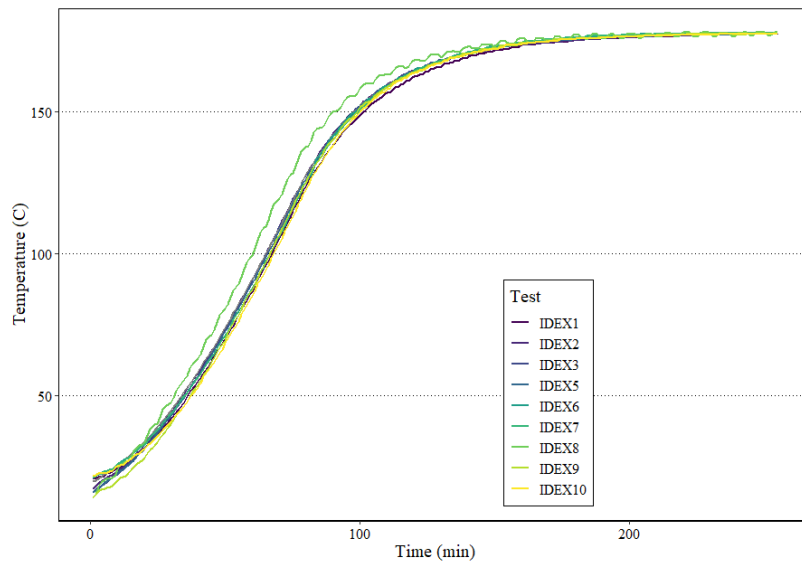


Figure 4 – Actual measured temperature profiles at the mid-plane of the 5320-1 IDEX panels.

3.2 Convergence Analyses

The impact of cure kinetics and temperature uncertainty on the viscosity modelling outcomes is given explicitly in Table 7 and portrayed graphically in Figure 5. All stochastic evaluations converge approximately to the deterministic solution, which confirms that the parameter variance is not drastically impacting the simulation.

The variance for all scenarios is low, indicating that the viscosity of this material system has a low sensitivity to cure kinetics and temperature variation. The highest variance is for the 5% temperature COV on the gel point. For this case, the standard deviation of less than 4 minutes shows that the gel point of 5320-1 is very stable. It is also evident that the cure kinetics variation has a stronger impact on the output variance compared to the temperature. The 3% variance in

cure kinetics results in 2.63% variance in gel point, where the 1.5% variance in temperature only results in 1.00% variance in gel point. When these two scenarios are combined (All) the variance is 2.84%, which is largely dominated by the influence of cure kinetics uncertainty rather than the influence being additive. The magnitude of temperature variation influences the results, with the T-5 resulting in a 3.4% variation on the gel point time, indicating that a higher temperature variation would likely contribute a proportionally stronger influence if coupled with the cure kinetics variation.

Table 7 – Results of the 5320-1 convergence analysis of viscosity modelling outputs, reflecting the impact of stochastic parameters.

Stochastic Parameter	Time at Minimum Viscosity			Time at Gel Point		
	Avg	Std Dev	COV (%)	Avg	Std Dev	COV (%)
Deterministic Solution	85	--	--	110	--	--
CK-3	82.40	1.95	2.37	110.00	2.89	2.63
CK-Half	82.83	1.47	1.77	110.07	1.42	1.29
T	82.83	1.46	1.76	109.98	1.10	1.00
T-5	82.40	1.97	2.38	110.19	3.76	3.42
All	82.40	1.99	2.42	109.98	3.12	2.84

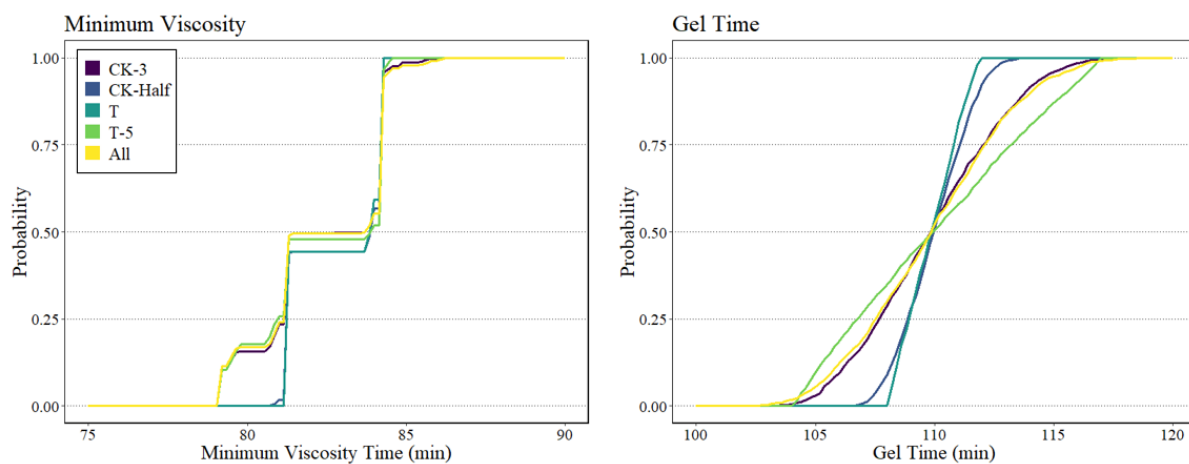


Figure 5 – Probability distributions for the stochastic cases for 5320-1 Gel Time (left) and minimum viscosity (right).

The results of the cure kinetics stochastic simulation are given in Table 8, with the probability distributions shown in Figure 6. These output parameters follow similar trends to that of the viscosity outputs: cure kinetics and high temperature variations have a strong influence, low

temperature variation has minimal influence, and cure kinetics influence dominates when combined with a low temperature variance. However, beyond this there are several items of note.

Firstly, the final degree of cure for all scenarios showed a low variance, indicating that the final degree of cure is stable for 5320-1. However, for CK-3, T-5, and All there are a number of parts which do not achieve the necessary degree of cure. Visually, the 88% threshold is shown in Figure 6 for the number of parts which are below 88% in the probability distribution. The number of under cured parts is also detailed in Table 9, including the percentage of the total parts for this set. The most extreme scenario, which includes both cure kinetics and temperature variance, results in 5.8% of parts being under cured.

Secondly, the variation of the time to fully cured is quite high for CK-3, T-5, and All, with variances of more than 10%. While most parts met the minimum cure threshold for this study, the high COV indicates that there is a strong likelihood of under cure if an aggressive cure cycle were to be used. It should be noted that the output parameter of Time to Fully Cured only includes the parts which have achieved 88% cured. This is reflected in the probability distribution in Figure 6, which shows a final probability of less than 1 for several of the cases. The gap here is due to the under cured parts, which are quantified in Table 9.

The results of the probability distributions support the following recommendations for processing considerations for 5320-1:

1. Determination of temperature variation for any given manufacturing conditions should be accurately determined and minimised where possible. Common equipment requirements allow for a 5% variation of temperature within the oven or autoclave, with larger heating chambers and parts potentially having larger variations. If this translates to a 5% variation of temperature within the part itself, a potentially large variation of final cure properties can result. As can be seen in Table 8, the final degree of cure for T-5 only varies by 3%, however, the time to fully cured varies by over 10%. While a longer cure may guarantee a satisfactory part, a shorter or optimised cure may be at risk of not meeting quality requirements.
2. The point of minimum viscosity and the gel point have low output variation, indicating that the material system is a robust choice for out of autoclave processing. In the worst-case scenario, there is a 15-minute window between the minimum viscosity and the gel. During this time the prepreg can achieve satisfactory volatile release, resin flow, and ply compaction prior to the gel event. However, if the early stages of cure are

accelerated too quickly, this window may shorten and the resin may achieve gel prior to achieving sufficient consolidation, resulting in a part with high porosity which must be rejected. It is thus recommended that the compaction stage of the composite cure be accelerated with caution.

3. The time to fully cured displays a high amount of variation, and the process times should be treated conservatively. Shortening of process times may result in parts which are under cured, unless a direct cure monitoring method is used to evaluate the degree of cure progression [101]. Without directly monitoring the degree of cure it is possible that under cured parts are fabricated, despite complying with an approved cure cycle.

Table 8 - Results of the convergence analysis of 5320-1 kinetic modelling outputs, reflecting the impact of stochastic parameters.

Stochastic Parameter	Vitrification Point			Time to Fully Cured			Final DOC		
	Avg	Std Dev	COV (%)	Avg	Std Dev	COV (%)	Avg	Std Dev	COV (%)
Deterministic									
Solution	163	--	--	218	--	--	93.3	--	--
CK-3	164.7	11.9	6.67	221.5	24.3	10.97	93.0	2.7	2.95
CK-Half	164.2	5.5	3.33	220.1	12.7	5.75	93.2	1.5	1.57
T	164.0	1.5	0.93	220.0	7.2	3.25	93.2	0.9	0.96
T-5	164.1	5.1	3.12	221.4	23.3	10.53	93.1	2.9	3.12
All	164.4	11.3	6.84	219.6	23.6	10.75	93.1	2.9	3.13

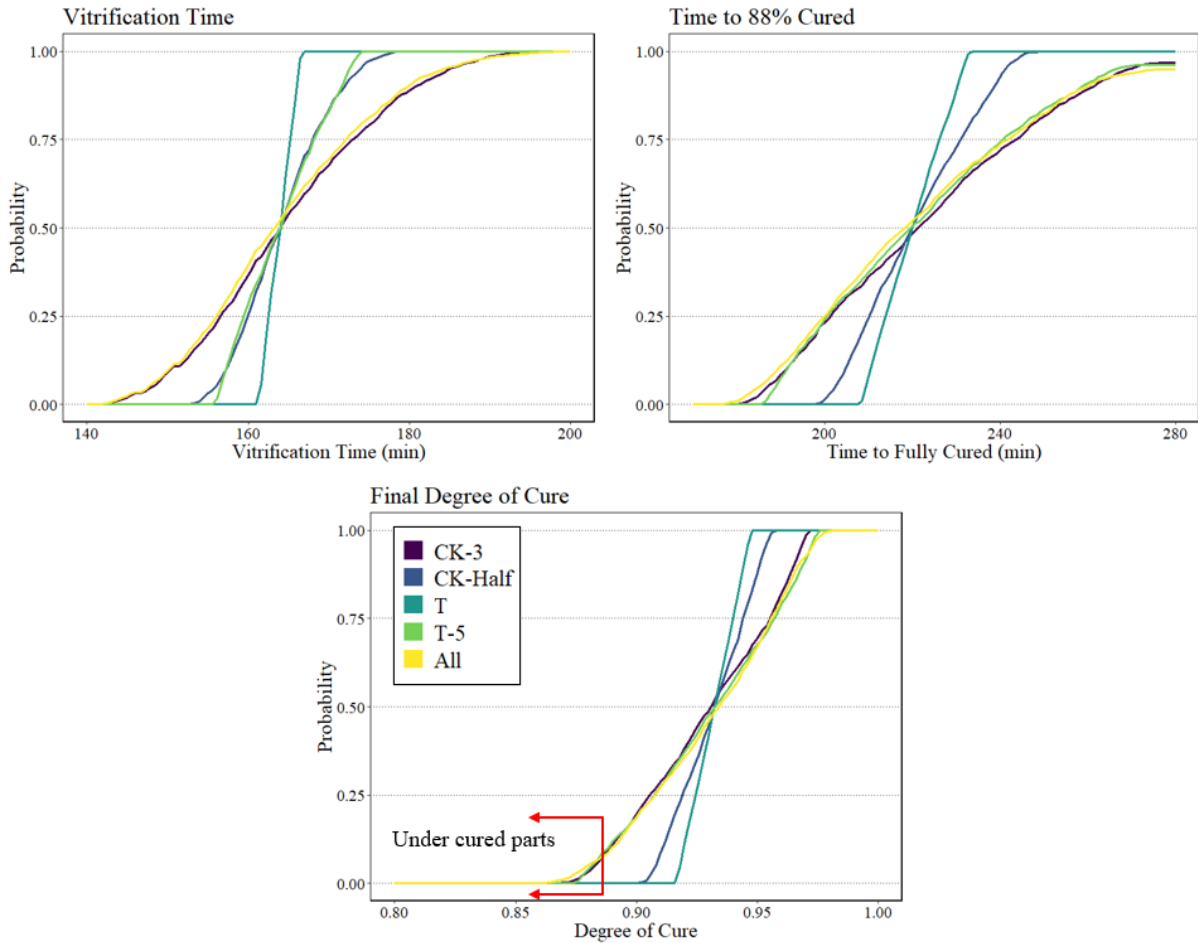


Figure 6 - Probability distributions for the stochastic cases for 5320-1 Vitrification Time (top left), time to fully cured (top right), and final degree of cure (bottom).

Table 9 – Under cured parts (below 88% final degree of cure) for each stochastic scenario of 5320-1.

Stochastic Parameters	# Parts Under cured (of 2000)	Percent Parts Under cured (%)
CK-3	55	2.75
CK-Half	0	0
T	0	0
T-5	70	3.50
All	116	5.80

3.3 Experimental validation

The results from the cure tests of the $[0,90]_s$ laminates are given in Table 10, with the values being calculated in the same manner as the deterministic values provided in this paper.

Table 10 – Results of the 5320-1 IDEX test temperature profiles, as calculated using the MATLAB code methodology in this paper.

Part	Minimum Viscosity (min)	Gel Point (min)	Vitrification Point (min)	Time at Fully Cured (min)	Final Degree of Cure (%)
IDEX1	86.2	113.2	168.6	223.2	93.3
IDEX2	84.0	110.0	164.0	219.8	93.2
IDEX3	82.2	110.2	165.0	217.8	93.6
IDEX4	83.2	110.2	164.8	218.6	93.5
IDEX5	84.2	110.6	165.2	218.6	93.3
IDEX6	83.4	110.8	165.0	217.8	93.5
IDEX7	83.2	111.4	165.2	217.2	93.7
IDEX8	77.2	103.4	158.8	210.4	93.9
IDEX9	82.2	111.4	165.4	219.0	93.5
IDEX10	86.2	112.8	166.6	220.2	93.3

As only one batch of prepreg was tested for this study, the cure kinetics variation will be disregarded. The source of variation which will be investigated here is oven temperature variance. The 1.5% COV value will be used as this is representative of the actual variance measured for this oven. The results of the temperature convergence analysis compared with the experimental results is shown in Figure 7.

All the values measured in Table 10 are consistent with the probability distribution predicted by this study. The minimum viscosity, gel time, and vitrification time values span the probability distribution ranges generated by the stochastic simulation. The final degree of cure and the time to cure are also aligned with the predicted values, however the actual range appears to follow a slightly tighter distribution than predicted. This indicates that the results of the stochastic model maybe slightly more conservative than the experimental results. Additionally, the convergence analyses were conducted as a 0D simulation of the epoxy cure only, not in the presence of carbon fibres. The experimental validation was completed with 5320-1 prepreg, which has a fibre volume content of approximately 67% [100]. The presence of the carbon fibres can influence the heat transfer in the epoxy and is a potential source of deviation between the experimental results and the convergence analyses. Additionally, IDEX8 appeared to be a slight outlier for some metrics, however it is noted in Figure 4 that the temperature profile

appears to be deviated from the rest of the test replicates. This has been attributed to the shift of the breather material during vacuum bagging and cure. This further demonstrates how slight variations in the cure configuration can impact the final part properties for identical oven programs.

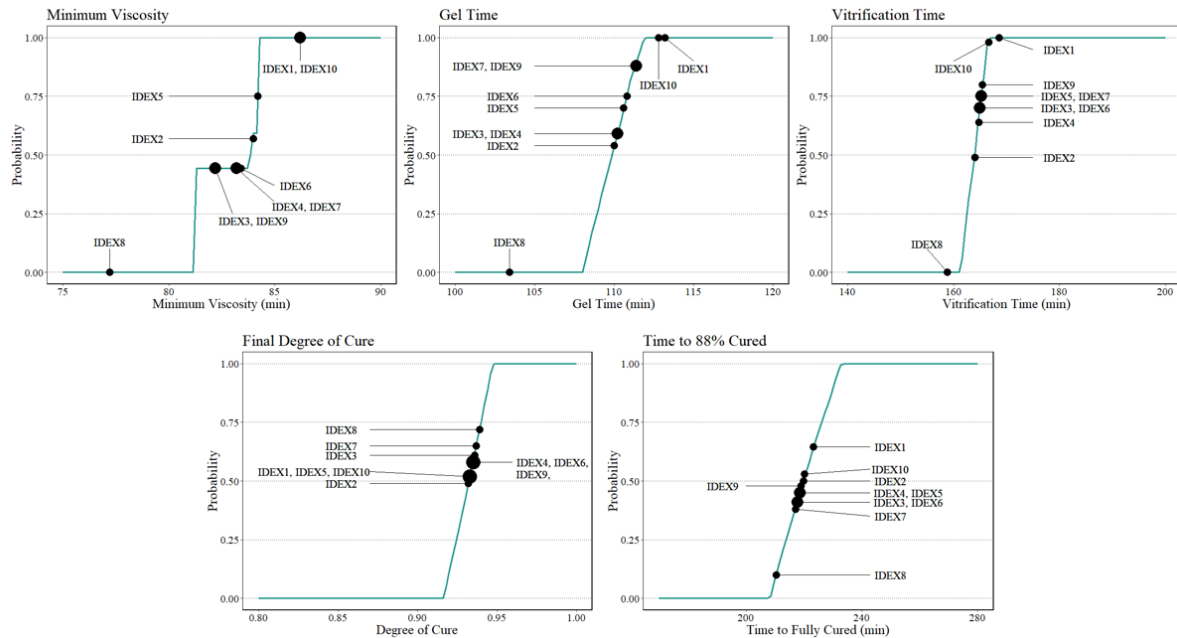


Figure 7 – A comparison of the distribution functions of the output parameters with actual measured values from 5320-1 IDEX panels from the results detailed in Table 10.

4 Conclusion

CYCOM® 5320-1 epoxy/carbon fibre prepreg was evaluated using stochastic methodologies to capture the resulting variance due to cure kinetics and temperature uncertainty. A new proposed method for estimating parameters uncertainty provided a satisfactory result compared with methods which require extensive testing. This method is applicable to any known cure kinetics model, regardless of the model type or complexity.

The impact of uncertainty on the resin viscosity and cure kinetics were demonstrated by a series of convergence analyses. For this material system, the impact of strongly varied cure kinetics or temperature conditions resulted in the highest amount of output variation. When compounded with a consistently low-variation oven the cure kinetics effect dominated, with the temperature effect only contributing slightly. Thus, it is important to capture the actual temperature variation expected for a given manufacturing scenario. The convergence analysis was compared with results from 10 cure cycles and confirmed that 1.5% temperature uncertainty accurately represented the distribution of the given output parameters.

Cure cycle limitations for 5320-1 have been proposed, including recommendations on utilising direct-cure monitoring methods to ensure compliant parts are produced. Overall, 5320-1 displays robust viscosity behaviour which is suitable for an out-of-autoclave prepreg. However, optimisation of the cure process should be viewed with caution to minimise the chance for poorly compacted or under cured parts. Further, equipment temperature control should be well characterised so that large temperature variations are avoided, thus avoiding unintended product variability.

5 References

- [1] Centea T, Grunenfelder LK, Nutt SR. A review of out-of-autoclave prepregs – Material properties, process phenomena, and manufacturing considerations. *Compos Part a-Appl S*. 2015;70:132-54.
- [2] Sharma S, Wetzel KK. Process Development Issues of Glass—Carbon Hybrid-reinforced Polymer Composite Wind Turbine Blades. *Journal of Composite Materials*. 2009;44(4):437-56.
- [3] Struzziero G, Teuwen JJE, Skordos AA. Numerical optimisation of thermoset composites manufacturing processes: A review. *Compos Part a-Appl S*. 2019;124:105499.
- [4] Rai N, Pitchumani R. Optimal cure cycles for the fabrication of thermosetting-matrix composites. *Polym Composite*. 1997;18(4):566-81.
- [5] Li M, Tucker CL. Optimal curing for thermoset matrix composites: Thermochemical and consolidation considerations. *Polym Composite*. 2002;23(5):739-57.
- [6] Vafayan M, Abedini H, Ghoreishy MHR, Beheshty MH. Effect of cure kinetic simulation model on optimized thermal cure cycle for thin-sectioned composite parts. *Polym Composite*. 2013;34(7):1172-9.
- [7] Pantelelis N, Vrouvakis T, Spentzas K. Cure cycle design for composite materials using computer simulation and optimisation tools. *Forsch Ingenieurwes*. 2003;67(6):254-62.
- [8] Shevtsov S, Zhilyaev I, Soloviev A, Parinov I, Dubrov V. Optimization Of The Composite Cure Process On The Basis Of Thermo-Kinetic Model. 18th International Conference On Composite Materials.
- [9] Struzziero G, Skordos AA. Multi-objective optimisation of the cure of thick components. *Compos Part a-Appl S*. 2017;93:126-36.
- [10] Polowick C. Optimizing Vacuum Assisted Resin Transfer Moulding (VARTM) Processing Parameters to Improve Part Quality: Carleton University; 2013.
- [11] Seretis G, Kouzilos G, Manolakos D, Provatidis C. Multi-Objective Curing Cycle Optimization for Glass Fabric/Epoxy Composites Using Poisson Regression and Genetic Algorithm. *Mater Res-Ibero-Am J*. 2018;21(2).
- [12] Tifkitsis KI, Mesogitis TS, Struzziero G, Skordos AA. Stochastic multi-objective optimisation of the cure process of thick laminates. *Compos Part a-Appl S*. 2018;112:383-94.
- [13] Bogetti TA, Gillespie JW. Two-Dimensional Cure Simulation of Thick Thermosetting Composites. *Journal of Composite Materials*. 1991;25(3):239-73.
- [14] Hojjati M, Hoa SV. Curing simulation of thick thermosetting composites. *Compos Manuf*. 1994;5(3):159-69.
- [15] Park HC, Lee SW. Cure Simulation of Thick Composite Structures Using the Finite Element Method. *Journal of Composite Materials*. 2001;35(3):188-201.
- [16] Capehart TW, Kia HG, Abujoudeh T. Cure Simulation of Thermoset Composite Panels. *Journal of Composite Materials*. 2007;41(11):1339-60.
- [17] Yi S, Hilton HH, Ahmad MF. A finite element approach for cure simulation of thermosetting matrix composites. *Computers & Structures*. 1997;64(1):383-8.
- [18] Johnston A, Hubert P, Poursartip A, Nelson K. Cure Kinetics and Viscosity Model of 8552 Epoxy Resin - FULL PAPER. 2023.
- [19] Mesogitis TS, Skordos AA, Long AC. Uncertainty in the manufacturing of fibrous thermosetting composites: A review. *Compos Part a-Appl S*. 2014;57:67-75.
- [20] Konstantopoulos S, Hueber C, Antoniadis I, Summerscales J, Schledjewski R. Liquid composite molding reproducibility in real-world production of fiber reinforced polymeric composites: a review of challenges and solutions. *Advanced Manufacturing: Polymer & Composites Science*. 2019;5(3):85-99.

- [21] Kim D, Nutt SR. Processability of DDS isomers-cured epoxy resin: Effects of amine/epoxy ratio, humidity, and out-time. *Polymer engineering and science*. 2018;58(9):1530-8.
- [22] Mawardi A, Pitchumani R. Cure Cycle Design for Thermosetting-Matrix Composites Fabrication under Uncertainty. *Annals of Operations Research*. 2004;132(1-4):19-45.
- [23] Michaud DJ, Beris AN, Dhurjati PS. Thick-Sectioned RTM Composite Manufacturing: Part I – In Situ Cure Model Parameter Identification and Sensing. *Journal of Composite Materials*. 2016;36(10):1175-200.
- [24] Michaud DJ, Beris AN, Dhurjati PS. Thick-Sectioned RTM Composite Manufacturing, Part II. Robust Cure Cycle Optimization and Control. *Journal of Composite Materials*. 2016;36(10):1201-31.
- [25] Mesogitis TS, Skordos AA, Long AC. Stochastic heat transfer simulation of the cure of advanced composites. *Journal of Composite Materials*. 2016;50(21):2971-86.
- [26] Mesogitis T. Stochastic simulation of the cure of advanced composites: Cranfield University; 2015.
- [27] Padmanabhan SK, Pitchumani R. Stochastic analysis of isothermal cure of resin systems. *Polym Composite*. 1999;20(1):72-85.
- [28] Zhou X-Y, Qian S-Y, Wang N-W, Xiong W, Wu W-Q. A review on stochastic multiscale analysis for FRP composite structures. *Compos Struct*. 2022;284:115132.
- [29] Acquah C, Datskov I, Mawardi A, Zhang F, Achenie LEK, Pitchumani R, et al. Optimization under uncertainty of a composite fabrication process using a deterministic one-stage approach. *Comput Chem Eng*. 2006;30(6):947-60.
- [30] Acevedo J, Pistikopoulos EN. A Parametric MINLP Algorithm for Process Synthesis Problems under Uncertainty. *Industrial & engineering chemistry research*. 1996;35(1):147-58.
- [31] Padmanabhan SK, Pitchumani R. Stochastic modeling of nonisothermal flow during resin transfer molding. *International journal of heat and mass transfer*. 1999;42(16):3057-70.
- [32] Li J, Zhang C, Liang Z, Wang B. Stochastic simulation based approach for statistical analysis and characterization of composites manufacturing processes. *J Manuf Syst*. 2006;25(2):108-21.
- [33] Skordos AA, Sutcliffe MPF. Stochastic simulation of woven composites forming. *Compos Sci Technol*. 2008;68(1):283-96.
- [34] Blanco S, You H, Kerekes TW, Yun GJ. Cure-induced residual stress buildup and distortions of CFRP laminates with stochastic thermo-chemical and viscoelastic models: Experimental verifications. *Mechanics of advanced materials and structures*. 2022;29(19):2740-56.
- [35] Yi S, Hilton HH, Fouad Ahmad M. Cure-Cycle Simulations Of Composites With Temperature- And Cure-Dependent Anisotropic Viscoelastic Properties And Stochastic Delaminations. *Mechanics of advanced materials and structures*. 1998;5(1):81-101.
- [36] Helmus R, Hinterhölzl R, Hubert P. A stochastic approach to model material variation determining tow impregnation in out-of-autoclave prepreg consolidation. *Compos Part a-Appl S*. 2015;77:293-300.
- [37] Mesogitis TS, Skordos AA, Long AC. Stochastic simulation of the influence of cure kinetics uncertainty on composites cure. *Compos Sci Technol*. 2015;110:145-51.
- [38] Technical Ia Sheet CYCOM(R) 5320-1 Prepreg. Solvay Composite Materials.
- [39] Man M, Ng Y, Tomblin J. Low Initial Temperature Vacuum-Bag-Only Cure, Medium Toughness Epoxy Prepregs (Cytec Cycom 5320-1). NMS 532 Rev A ed: National Center for Advanced Materials Performance; 2015.
- [40] Lee C, Gibson T, Tienda K, Storage T. Reaction rate and viscosity model development for Cytec's Cycom 5320 family of resins. Proc 42nd int SAMPE tech conf. Salt Lake City, UT2010.

- [41] Kratz J, Hsiao K, Fernlund G, Hubert P. Thermal models for MTM45-1 and Cycom 5320 out-of-autoclave prepreg resins. *Journal of Composite Materials*. 2012;47(3):341-52.
- [42] Hwang S-S, Park SY, Kwon G-C, Choi WJ. Cure kinetics and viscosity modeling for the optimization of cure cycles in a vacuum-bag-only prepreg process. *International journal of advanced manufacturing technology*. 2018;99(9-12):2743-53.
- [43] Kim D, Centea T, Nutt SR. Out-time effects on cure kinetics and viscosity for an out-of-autoclave (OOA) prepreg: Modelling and monitoring. *Compos Sci Technol*. 2014;100:63-9.
- [44] Lee C, Tienda K, Storage T. Experimental methods and material model development for a toughened epoxy. *International SAMPE Technical Conference 2014*.
- [45] Brockman R, Storage T, Lee C, Coomer R, Volk B. Characterizing, Modeling, And Validating The Processing Of Out-Of-Autoclave Organic Matrix Composites As A Function Of Cure Cycle. *20th International Conference on Composite Materials*. Copenhagen2015.
- [46] Hyun D-K, Kim D, Hwan Shin J, Lee B-E, Shin D-H, Hoon Kim J. Cure cycle modification for efficient vacuum bag only prepreg process. *Journal of Composite Materials*. 2021;55(8):1039-51.
- [47] Anandan S, Dhaliwal GS, Huo Z, Chandrashekhara K, Apetre N, Iyyer N. Curing of Thick Thermoset Composite Laminates: Multiphysics Modeling and Experiments. *Appl Compos Mater*. 2018;25(5):1155-68.
- [48] Lucas S, Howard S, Senger J. Vacuum Bag Only Processing; Improving Prepreg Out-Time and Porosity for Large Composite Structure. *Society for the Advancement of Material and Process Engineering*. Seattle, WA2010.
- [49] CCA Material Constitutive Model Documentation. *Convergent Manufacturing Technologies, Inc.*; 2019.
- [50] Chern C-S, Poehlein GW. A kinetic model for curing reactions of epoxides with amines. *Polym Eng Sci*. 1987;27(11):788-95.
- [51] Cole KC, Hechler JJ, Noel D. A new approach to modeling the cure kinetics of epoxy/amine thermosetting resins. 2. Application to a typical system based on bis[4-(diglycidylamino)phenyl]methane and bis(4-aminophenyl) sulfone. *Macromolecules*. 1991;24(11):3098-110.
- [52] Castro JM, Macosko CW. Studies of mold filling and curing in the reaction injection molding process. *AIChE Journal*. 1982;28(2):250-60.
- [53] Karkanias PI, Partridge IK. Cure modeling and monitoring of epoxy/amine resin systems. I. Cure kinetics modeling. *J Appl Polym Sci*. 2000;77(7):1419-31.
- [54] Karkanias PI, Partridge IK, Attwood D. Modelling the cure of a commercial epoxy resin for applications in resin transfer moulding. *Polymer international*. 1996;41(2):183-91.
- [55] Rabinowitch E. Collision, co-ordination, diffusion and reaction velocity in condensed systems. *Transactions of the Faraday Society*. 1937;33(0):1225-33.
- [56] Macedo PB, Litovitz TA. On the Relative Roles of Free Volume and Activation Energy in the Viscosity of Liquids. *The Journal of Chemical Physics*. 2004;42(1):245-56.
- [57] Wise CW, Cook WD, Goodwin AA. Chemico-diffusion kinetics of model epoxy-amine resins. *Polymer (Guilford)*. 1997;38(13):3251-61.
- [58] Dykeman D. *Minimizing Uncertainty in Cure Modeling for Composites Manufacturing*: University of British Columbia; 2008.
- [59] Williams ML, Landel RF, Ferry JD. The Temperature Dependence of Relaxation Mechanisms in Amorphous Polymers and Other Glass-forming Liquids. *Journal of the American Chemical Society*. 1955;77(14):3701-7.
- [60] Wisanrakkit G, Gillham J. The glass transition temperature (T_g) as an index of chemical conversion for a high-T_g amine/epoxy system: Chemical and diffusion-controlled reaction kinetics. *J Appl Polym Sci*. 1990;41:2885-929.

- [61] Tifkitsis KI, Winistoerfer A, Skordos AA. Online optimisation and active control of the cure process of thick composite laminates. *Journal of Manufacturing Processes*. 2023;87:221-30.
- [62] Skordos AA, Partridge IK. Cure kinetics modeling of epoxy resins using a non-parametric numerical procedure. *Polym Eng Sci*. 2001;41(5):793-805.
- [63] Hall M, Zeng X, Shelley T, Schubel P. Dielectric Parameter Independent Curing Analysis of Out-Of-Autoclave Carbon Fibre/Epoxy Composites. *Compos Part a-Appl S*. 2023:107755.
- [64] Ryckaert VG, Claes JE, Van Impe JF. Model-based temperature control in ovens. *Journal of Food Engineering*. 1999;39(1):47-58.
- [65] Pyrometry. SAE AMS2750G: SAE; 2022.
- [66] Kluge NEJ, Lundström TS, Ljung AL, Westerberg LG, Nyman T. An experimental study of temperature distribution in an autoclave. *Journal of Reinforced Plastics and Composites*. 2016;35(7):566-78.
- [67] Mulligan D, Gnaniyah S, Sims G. Thermal analysis techniques for composites^{es} and adhesives. 2nd ed.: National Physical Laboratory; 2000.
- [68] Halley PJ, Mackay ME. Chemorheology of thermosets—an overview. *Polym Eng Sci*. 1996;36(5):593-609.
- [69] González UF, Shen SF, Cohen C. Rheological characterization of fast-reacting thermosets through spiral flow experiments. *Polym Eng Sci*. 1992;32(3):172-81.

CHAPTER 6: DISCUSSION AND CONCLUSION

6.1 Conclusions

While process monitoring for thermosets and thermoset composites is an actively researched topic, there are still notable gaps in the literature to date. Across the range of sensor types and analysis methods, there is a lack of clarity as to how and when methods should be used, and to what extent can they provide material cure information. This PhD research aimed to close this gap with regards to dielectrics, by identifying the capabilities of dielectric sensors for use in cure monitoring. The work presented in this thesis demonstrates the accuracy and repeatability for multiple types of dielectric sensors. Further, through the work on stochastic cure modelling, this thesis asserts that direct cure monitoring such as with dielectric sensors is critical for capturing process variation due to sources of uncertainty.

Paper 1, which is presented in Chapter 3, evaluated existing and newly proposed dielectric analysis methodologies, and resulted in a new set of comprehensive and parameter-independent methods. The key findings from this study support Research Objective 1 and include:

- Many dielectric analysis techniques are parameter independent. This finding enables blanket use of the proposed methods across all dielectric parameters and includes clear and consistent definitions for implementation.
- Critical cure events including the start and end of the cure reaction rate, the point of minimum resin viscosity, the gel point, and the vitrification point can be determined via dielectric analysis with a high degree of accuracy.
- Dielectric analysis methods can calculate the degree of cure or T_g progression with a high degree of accuracy. This includes a method which has potential for predicting live properties as the cure is actively progressing.
- Dielectric sensors have high part-to-part repeatability and produce consistent results across multiple part replicates.

Paper 2, which is presented in Chapter 4, evaluated a novel through-thickness dielectric sensor for cure monitoring of thick parts. Key findings and outcomes of this study include:

- The prototype through-thickness tool mounted dielectric sensor is capable of monitoring cure for thermoset laminates between 2 and 20 mm in thickness, with good part-to-part repeatability. By implementing a correction factor to account for sensor

design, the sensor can successfully implement the dielectric analysis methods from Paper 1 for through-thickness cure monitoring with results consistent to those for the off-the-shelf IDEX sensor. This addresses Research Objective 2 item a.

- The prototype sensor is free of polarisation effects, temperature effects, and is capable of monitoring cure in the presence of conductive fibres without interference. This addresses Research Objective 2 items b, c, and d.

Paper 3, which is presented in Chapter 5, proposed a new approach to stochastic cure modelling of an out-of-autoclave epoxy, and included an assessment of expected output property variation. Key findings and outcomes of this study include:

- A new method for quantifying uncertainty in composite cure, which involves no additional analytical testing, was demonstrated to produce comparable results with existing methods which require extensive testing and replication. The method is based on knowledge of sources of error in cure kinetics modelling and is capable of quantifying uncertainty for any resin for which there is a known cure kinetics model. It is particularly appropriate to resin systems, such as CYCOM® 5320-1, which have complex kinetic equations. This addresses Research Objective 3.
- The resin system under investigation, 5320-1, was evaluated for multiple combinations and magnitudes of cure kinetics and temperature uncertainty, which addresses Research Objective 4. It was demonstrated to be sensitive to uncertainty in cure kinetics modelling and high amounts of temperature influence, with the time to full cure varying by 11% and 10.5% respectively for the cycle studied here. The viscosity is less sensitive to variation in cure kinetics and temperature, with the time at minimum viscosity and gel varying by less than 3.5% for all cases studied.
- Recommendations for cure cycle design for 5320-1, satisfying Research Objective 5, include the following:
 - The viscosity behaviour has low variation for the cure cycle presented, indicating this prepreg system is appropriate for out-of-autoclave processing.
 - The final degree of cure, for a 120-minute cure cycle, shows low variability. This indicates that the current cure cycle requirements are likely to reliably produce compliant parts.

- The time to fully cured, defined here as 88% cured, has the highest variation. This indicates that efforts to optimise the cure process by shortening it could potentially risk a high percentage of parts being under cured.
- Temperature variation has a strong influence on the cure outcome range and should be considered with caution. Equipment tolerances of 5 °C which result in part temperature variances of 5 °C could result in parts being under cured or cured to an unknown degree.

The cumulative findings of this study assert that a direct monitoring technique such as with dielectrics are necessary to guarantee the quality of cured parts. The stochastic modelling study sheds light on the extent of natural variation that a cure cycle can produce, potentially resulting in parts of unknown quality. Using a technique which directly monitors the cure progress would enable explicit confirmation that each individual cure is meeting the necessary requirements. The works presented in this thesis demonstrate that dielectric sensing can produce high quality, highly repeatable information about the cure progression for thermoset cure. Such sensors can be integrated into a production environment to confirm the cure state of composite parts and satisfy the quality assurance requirements for certifying composite components.

6.2 Suggestions for future work

The research conducted in support of this thesis investigated dielectric technologies for directly monitoring the thermoset cure reaction to quantify the exact cure outcomes for a process which is impacted by uncertainty. While the contributions of this work provide a deeper understanding of dielectric cure monitoring and its applications in thermoset processing, there is further research which can enable more widespread use of these technologies. Suggestions for future work are as follows:

1. **Validation of dielectric methods with other resin systems.** The methods proposed by Paper 1 were only applied to the CYCOM® 5320-1 carbon fibre/epoxy prepreg system. Validating these methods for other epoxies and other thermoset systems would demonstrate the robustness of dielectric technologies. Additionally, noting that 5320-1 is a toughened epoxy, it would be valuable to evaluate an untoughened version to assess how the toughening potentially influences the signal.
2. **Implementation of dielectric techniques for thermoplastics.** Current literature suggests that dielectric analysis and dielectric spectroscopy have applications in thermoplastic processing relating to melt, crystallisation, and degradation monitoring.

An understanding of how process monitoring techniques could be applied to this class of materials would broaden the potential applications for dielectric analysis.

3. **Commercialisation of the through-thickness dielectric sensor.** The major limitation of the through-thickness sensor used in this study was due to the presence of the PEEK spacer rings. Production of a commercialised sensor with a traditional monotrode design would allow for directly monitoring only the thermoset cure reaction and provide clarity on how accurate the through-thickness sensor is. If such as sensor were available, a more specific evaluation of through-thickness monitoring capabilities could be accomplished. Additionally, a thorough evaluation of sensor repeatability and uncertainty would be of value. In particular, determination of the statistical significance of the signal would enable a successful implementation of this sensor.
4. **Integration of dielectric sensing into an actively controlled cure system.** The results of these studies demonstrate a high fidelity of data collection during the monitoring of thermoset cure. Such as sensor could integrate into a system which provides live cure monitoring which then enables live updating of process conditions depending on the information collected. For example, if a cure reaction is completed earlier than planned the process could automatically shut down, which would result in time and cost savings.
5. **Stochastic modelling and validation for alternate resin systems.** The 5320-1 material system is a very robust out-of-autoclave epoxy. Applying the stochastic methods used in this to a more volatile resin system could provide further insight to the accuracy of the model for a material which has a higher range of output values. Further, the stochastic methods used here could be applied to uncertainty in thermosets melting, degradation, and crystallisation as well.
6. **Stochastic modelling and validation for 2D and 3D architectures.** The stochastic model presented in this thesis is focused on the fundamental methods and stochastic approach, as applied to a 0D resin system. Integration within a finite element model incorporating heat transfer mechanisms would enable further information on how resin exotherms and heat transfer variability impacts the viscosity and cure kinetics.

REFERENCES

- [1] Grant RG, Museum DIW, Institution S. Flight: 100 Years of Aviation: Dorling Kindersley; 2010.
- [2] Gardiner G. Hypersonix receives CMC scramjet manufacturing demonstrator. *CompositesWorld*2023.
- [3] Zhang X, Chen Y, Hu J. Recent advances in the development of aerospace materials. *Progress in Aerospace Sciences*. 2018;97:22-34.
- [4] Padture NP. Advanced structural ceramics in aerospace propulsion. *Nature Materials*. 2016;15(8):804-9.
- [5] Blakey-Milner B, Gradl P, Snedden G, Brooks M, Pitot J, Lopez E, et al. Metal additive manufacturing in aerospace: A review. *Materials & Design*. 2021;209:110008.
- [6] Laurvick CAC, Singaraju B. Nanotechnology in aerospace systems. *IEEE Aerospace and Electronic Systems Magazine*. 2003;18(9):18-22.
- [7] Parveez B, Kittur MI, Badruddin IA, Kamangar S, Hussien M, Umarfarooq MA. Scientific Advancements in Composite Materials for Aircraft Applications: A Review. *Polymers*. 2022;14(22):5007.
- [8] Bhatt AT, Gohil PP, Chaudhary V. Primary Manufacturing Processes for Fiber Reinforced Composites: History, Development & Future Research Trends. *IOP Conference Series: Materials Science and Engineering*. 2018;330(1):012107.
- [9] Mason H. Boeing 777X achieves first successful flight. *CompositeWorld*2020.
- [10] Konstantopoulos S, Hueber C, Antoniadis I, Summerscales J, Schledjewski R. Liquid composite molding reproducibility in real-world production of fiber reinforced polymeric composites: a review of challenges and solutions. *Advanced Manufacturing: Polymer & Composites Science*. 2019;5(3):85-99.
- [11] Composite materials handbook CMH-17-3G. Warrendale, Pa: SAE International on behalf of CMH-17; 2017.
- [12] Fernandez JA. Contextual Role of TRLs and MRLs in Technology Management. In: *Laboratories SN*, editor.2010.
- [13] Tew D, Wallace K. An Analysis of Technology Transition Within the Department of Defense: Naval Postgraduate School; 2010.
- [14] Brown KR, McCleskey CM. Paper Session II-B-National Spaceport Testbed. 2000.
- [15] Straub J. In search of technology readiness level (TRL) 10. *Aerospace Science and Technology*. 2015;46:312-20.
- [16] Feraboli P. Composite Materials Strength Determination Within the Current Certification Methodology for Aircraft Structures. *Journal of Aircraft - J AIRCRAFT*. 2009;46:1365-74.
- [17] Centea T, Grunenfelder LK, Nutt SR. A review of out-of-autoclave prepregs – Material properties, process phenomena, and manufacturing considerations. *Compos Part a-Appl S*. 2015;70:132-54.
- [18] Ersoy N, Garstka T, Potter K, Wisnom MR, Porter D, Clegg M, et al. Development of the properties of a carbon fibre reinforced thermosetting composite through cure. *Compos Part a-Appl S*. 2010;41(3):401-9.
- [19] Zade A, Kuppasamy RRP. A review on numerical optimization in liquid composite moulding processes. *Mater Today-Proc*. 2019;19:329-32.
- [20] Polowick C. Optimizing Vacuum Assisted Resin Transfer Moulding (VARTM) Processing Parameters to Improve Part Quality: Carleton University; 2013.
- [21] Swery EE, Meier R, Lomov SV, Drechsler K, Kelly P. Predicting permeability based on flow simulations and textile modelling techniques: Comparison with experimental values and

- verification of FlowTex solver using Ansys CFX. *Journal of Composite Materials*. 2015;50:601.
- [22] Pantelidis N, Vrovvakis T, Spentzas K. Cure cycle design for composite materials using computer simulation and optimisation tools. *Forsch Ingenieurwes*. 2003;67(6):254-62.
- [23] Yi S, Hilton HH, Ahmad MF. A finite element approach for cure simulation of thermosetting matrix composites. *Computers & Structures*. 1997;64(1):383-8.
- [24] Bruk D. Implementation Methodology, Validation, and Augmentation of a Cure Kinetic Model for Carbon Fiber/CYCOM 5320-1, FM309-1, and FM300-2 [Doctoral thesis]: Washington University in St. Louis; 2021.
- [25] Kim D, Centea T, Nutt SR. Out-time effects on cure kinetics and viscosity for an out-of-autoclave (OOA) prepreg: Modelling and monitoring. *Compos Sci Technol*. 2014;100:63-9.
- [26] Karkanis PI, Partridge IK. Cure modeling and monitoring of epoxy/amine resin systems. I. Cure kinetics modeling. *J Appl Polym Sci*. 2000;77(7):1419-31.
- [27] Bogetti TA, Gillespie JW. Two-Dimensional Cure Simulation of Thick Thermosetting Composites. *Journal of Composite Materials*. 1991;25(3):239-73.
- [28] Park HC, Lee SW. Cure Simulation of Thick Composite Structures Using the Finite Element Method. *Journal of Composite Materials*. 2001;35(3):188-201.
- [29] Committee G-AAQS. Quality Management Systems - Requirements for Aviation, Space, and Defense Organizations. SAE International; 2016.
- [30] ASTM E2070-13(2018), Standard Test Methods for Kinetic Parameters by Differential Scanning Calorimetry Using Isothermal Methods. West Conshohocken, PA: ASTM International; 2018.
- [31] ASTM D7028-07(2015), Standard Test Method for Glass Transition Temperature (DMA Tg) of Polymer Matrix Composites by Dynamic Mechanical Analysis (DMA). West Conshohocken, PA: ASTM International; 2015.
- [32] Konstantopoulos S, Fauster E, Schledjewski R. Monitoring the production of FRP composites: A review of in-line sensing methods. *Express Polym Lett*. 2014;8(11):823-40.
- [33] Torres M. Parameters' monitoring and in-situ instrumentation for resin transfer T moulding: A review. *Compos Part a-Appl S*. 2019;124.
- [34] Konstantopoulos S, Tonejc M, Maier A, Schledjewski R. Exploiting temperature measurements for cure monitoring of FRP composites—Applications with thermocouples and infrared thermography. *Journal of Reinforced Plastics and Composites*. 2015;34(12):1015-26.
- [35] Lekakou C, Cook S, Deng Y, Ang TW, Reed GT. Optical fibre sensor for monitoring flow and resin curing in composites manufacturing. *Compos Part a-Appl S*. 2006;37(6):934-8.
- [36] O'Dwyer MJ, Maistros GM, James SW, Tatam RP, Partridge IK. Relating the state of cure to the real-time internal strain development in a curing composite using in-fibre Bragg gratings and dielectric sensors. *Measurement Science and Technology*. 1998;9(8):1153-8.
- [37] Liebers N, Bertling D. Ultrasonic resin flow and cure monitoring. *Conference On Flow Processing In Composite Materials2018*.
- [38] Lionetto F, Maffezzoli A. Monitoring the Cure State of Thermosetting Resins by Ultrasound. *Materials (Basel)*. 2013;6(9):3783-804.
- [39] Maffezzoli A, Quarta E, Luprano VAM, Montagna G, Nicolais L. Cure monitoring of epoxy matrices for composites by ultrasonic wave propagation. *J Appl Polym Sci*. 1999;73(10):1969-77.
- [40] Mijović J, Andjelic Sa, Fitz B, Zurawsky W, Mondragon I, Bellucci F, et al. Impedance spectroscopy of reactive polymers. 3. Correlations between dielectric, spectroscopic, and rheological properties during cure of a trifunctional epoxy resin. *J Polym Sci Pol Phys*. 1996;34(2):379-88.
- [41] Maistros GM, Partridge IK. Monitoring autoclave cure in commercial carbon fibre/epoxy composites. *Compos Part B-Eng*. 1998;29(3):245-50.

- [42] Abraham D, McIlhagger R. Glass fibre epoxy composite cure monitoring using parallel plate dielectric analysis in comparison with thermal and mechanical testing techniques. *Compos Part a-Appl S.* 1998;29:811-9.
- [43] Chaloupka A. Development of a dielectric sensor for the real-time in-mold characterization of carbon fiber reinforced thermosets: University of Augsburg; 2018.
- [44] Sharma S, Wetzel KK. Process Development Issues of Glass—Carbon Hybrid-reinforced Polymer Composite Wind Turbine Blades. *Journal of Composite Materials.* 2009;44(4):437-56.
- [45] Struzziero G, Teuwen JJE, Skordos AA. Numerical optimisation of thermoset composites manufacturing processes: A review. *Compos Part a-Appl S.* 2019;124:105499.
- [46] Rai N, Pitchumani R. Optimal cure cycles for the fabrication of thermosetting-matrix composites. *Polym Composite.* 1997;18(4):566-81.
- [47] Li M, Tucker CL. Optimal curing for thermoset matrix composites: Thermochemical and consolidation considerations. *Polym Composite.* 2002;23(5):739-57.
- [48] Vafayan M, Abedini H, Ghoreishy MHR, Beheshty MH. Effect of cure kinetic simulation model on optimized thermal cure cycle for thin-sectioned composite parts. *Polym Composite.* 2013;34(7):1172-9.
- [49] Shevtsov S, Zhilyaev I, Soloviev A, Parinov I, Dubrov V. Optimization Of The Composite Cure Process On The Basis Of Thermo-Kinetic Model. 18th International Conference On Composite Materials.
- [50] Struzziero G, Skordos AA. Multi-objective optimisation of the cure of thick components. *Compos Part a-Appl S.* 2017;93:126-36.
- [51] Seretis G, Kouzilos G, Manolakos D, Provatidis C. Multi-Objective Curing Cycle Optimization for Glass Fabric/Epoxy Composites Using Poisson Regression and Genetic Algorithm. *Mater Res-Ibero-Am J.* 2018;21(2).
- [52] Tifkitsis KI, Mesogitis TS, Struzziero G, Skordos AA. Stochastic multi-objective optimisation of the cure process of thick laminates. *Compos Part a-Appl S.* 2018;112:383-94.
- [53] Mesogitis TS, Skordos AA, Long AC. Uncertainty in the manufacturing of fibrous thermosetting composites: A review. *Compos Part a-Appl S.* 2014;57:67-75.
- [54] Mawardi A, Pitchumani R. Cure Cycle Design for Thermosetting-Matrix Composites Fabrication under Uncertainty. *Annals of Operations Research.* 2004;132(1-4):19-45.
- [55] Michaud DJ, Beris AN, Dhurjati PS. Thick-Sectioned RTM Composite Manufacturing, Part II. Robust Cure Cycle Optimization and Control. *Journal of Composite Materials.* 2002;36(10):1201-31.
- [56] Kim D, Nutt SR. Processability of DDS isomers-cured epoxy resin: Effects of amine/epoxy ratio, humidity, and out-time. *Polymer engineering and science.* 2018;58(9):1530-8.
- [57] Anandan S, Dhaliwal GS, Huo Z, Chandrashekhara K, Apetre N, Iyyer N. Curing of Thick Thermoset Composite Laminates: Multiphysics Modeling and Experiments. *Appl Compos Mater.* 2018;25(5):1155-68.
- [58] Nass KA, Seferis JC. Analysis of the Dielectric Response of Thermosets During Isothermal and Nonisothermal Cure. *Polym Eng Sci.* 1989;29(5):315-24.
- [59] Day DR. Dielectric determination of cure state during non-isothermal cure. *Polym Eng Sci.* 1989;29(5):334-8.
- [60] Lee DG, Kim HG. Non-Isothermal in Situ Dielectric Cure Monitoring for Thermosetting Matrix Composites. *Journal of Composite Materials.* 2004;38(12):977-93.
- [61] Kazilas MC, Partridge IK. Exploring equivalence of information from dielectric and calorimetric measurements of thermoset cure—a model for the relationship between curing temperature, degree of cure and electrical impedance. *Polymer.* 2005;46(16):5868-78.
- [62] Kim J-S, Lee DG. On-line cure monitoring and viscosity measurement of carbon fiber epoxy composite materials. *Journal of Materials Processing Technology.* 1993;37(1-4):405-16.

- [63] Bang KG, Kwon JW, Lee DG, Lee JW. Measurement of the degree of cure of glass fiber–epoxy composites using dielectrometry. *Journal of Materials Processing Technology*. 2001;113(1-3):209-14.
- [64] Kim HG, Lee DG. Dielectric cure monitoring for glass/polyester prepreg composites. *Compos Struct*. 2002;57(1-4):91-9.
- [65] Maffezzoli A, Trivisano A, Opalicki M, Mijovic J, Kenny JM. Correlation between dielectric and chemorheological properties during cure of epoxy-based composites. *Journal of Materials Science*. 2004;29(3):800-8.
- [66] Hubner M, Klatt A, Koerdt M, Lang W. Online monitoring of thermoplastic crystallization with miniaturized interdigital sensors. *IEEE*. p. 1-4.
- [67] Gonnet JM, Guillet J, Sirakov I, Fulchiron R, Seytre G. ?In-situ? monitoring of the non-isothermal crystallization of polymers by dielectric spectroscopy. *Polym Eng Sci*. 2002;42(6):1159-70.
- [68] Chaloupka A, Grund D, Wedel A, Rudolph NM, Drechsler K. In-Situ Detection Of Phase Transitions Of Semi- Crystalline Carbon Fiber Reinforced Thermoplastics Using Dielectric Analysis And Its Correlation To Dma And Dsc. *European Conference on Composite Materials*. Munich, Germany2016.
- [69] Vadlamudi V, Shaik R, Raihan R, Reifsnider K, Iarve E. Identification of current material state in composites using a dielectric state variable. *Compos Part a-Appl S*. 2019;124:105494.
- [70] Raihan R, Reifsnider K, Cacuci D, Liu Q. Dielectric signatures and interpretive analysis for changes of state in composite materials. *ZAMM - Journal of Applied Mathematics and Mechanics / Zeitschrift für Angewandte Mathematik und Mechanik*. 2015;95(10):1037-45.
- [71] Boinard P, Pethrick RA, Banks WM, Crane RL. Non destructive evaluation of adhesively bonded composite structures using high frequency dielectric spectroscopy. *Journal of Materials Science*. 2000;35(6):1331-7.
- [72] Breede A, Moghaddam MK, Brauner C, Herrmann AS, Lang W. Online Process Monitoring And Control By Dielectric Sensors For A Composite Main Spar For Wind Turbine Blades. *20th International Conference on Composite Materials*. Copenhagen2011.
- [73] Tifkitsis KI, Skordos AA. A novel dielectric sensor for process monitoring of carbon fibre composites manufacture. *Compos Part a-Appl S*. 2019;123:180-9.
- [74] Mesogitis TS, Maistros GM, Asareh M, Lira C, Skordos AA. Optimisation of an in-process lineal dielectric sensor for liquid moulding of carbon fibre composites. *Compos Part a-Appl S*. 2021;140.
- [75] Shin JH, Nutt S. In situ resin age assessment using dielectric analysis and resin cure map for efficient vacuum infusion. *Advanced Manufacturing: Polymer & Composites Science*. 2020;6(4):212-25.
- [76] Wang P, Molimard J, Drapier S, Vautrin A, Minni JC. Monitoring the resin infusion manufacturing process under industrial environment using distributed sensors. *Journal of Composite Materials*. 2011;46(6):691-706.
- [77] Michaud DJ, Beris AN, Dhurjati PS. Thick-Sectioned RTM Composite Manufacturing: Part I – In Situ Cure Model Parameter Identification and Sensing. *Journal of Composite Materials*. 2016;36(10):1175-200.
- [78] Pethrick RA, Hayward D. Real time dielectric relaxation studies of dynamic polymeric systems. *Progress in Polymer Science*. 2002;27(9):1983-2017.
- [79] Kyriazis A, Charif S, Rager K, Dietzel A, Sinapius M. A Parametric Model for the Analysis of the Impedance Spectra of Dielectric Sensors in Curing Epoxy Resins. *Sensors*. 2023;23(4):1825.
- [80] Hardis R, Jessop JLP, Peters FE, Kessler MR. Cure kinetics characterization and monitoring of an epoxy resin using DSC, Raman spectroscopy, and DEA. *Compos Part a-Appl S*. 2013;49:100-8.

- [81] Chaloupka A, Pflock T, Horny R, Rudolph N, Horn SR. Dielectric and rheological study of the molecular dynamics during the cure of an epoxy resin. *J Polym Sci Pol Phys*. 2018;56(12):907-13.
- [82] Hall M, Zeng X, Shelley T, Schubel P. In Situ Thermoset Cure Sensing: A Review of Correlation Methods. *Polymers (Basel)*. 2022;14(15):2978.
- [83] Kyriazis A, Pommer C, Lohuis D, Rager K, Dietzel A, Sinapius M. Comparison of Different Cure Monitoring Techniques. *Sensors*. 2022;22(19):7301.
- [84] Tifkitsis KI, Winistoerfer A, Skordos AA. Online optimisation and active control of the cure process of thick composite laminates. *Journal of Manufacturing Processes*. 2023;87:221-30.
- [85] Lawrence JM, Hsiao K-T, Don RC, Simacek P, Estrada G, Sozer EM, et al. An approach to couple mold design and on-line control to manufacture complex composite parts by resin transfer molding. *Composites Part A: Applied Science and Manufacturing*. 2002;33(7):981-90.
- [86] Modi D, Correia N, Johnson M, Long A, Rudd C, Robitaille F. Active control of the vacuum infusion process. *Compos Part a-Appl S*. 2007;38(5):1271-87.
- [87] Alms JB, Advani SG, Glancey JL. Liquid Composite Molding control methodologies using Vacuum Induced Preform Relaxation. *Compos Part a-Appl S*. 2011;42(1):57-65.
- [88] Skordos AA, Partridge IK. Effects of tool-embedded dielectric sensors on heat transfer phenomena during composite cure. *Polym Composite*. 2007;28(2):139-52.
- [89] Stephan F, Duteurtre X, Fit A. In-process control of epoxy composite by microdielectrometric analysis. Part II: On-line real-time dielectric measurements during a compression molding process. *Polym Eng Sci*. 1998;38(9):1566-71.
- [90] Senturia SD, Sheppard NF, Jr. *Dielectric Analysis of Thermoset Cure*. 1985.
- [91] Kremer F, Schönhals A. *Broadband Dielectric Spectroscopy* 2003.
- [92] Nass KA. *Dielectric thermal analysis of polymeric matrices: ProQuest Dissertations Publishing*; 1989.
- [93] Stadler H, Kiss P, Stadlbauer W, Plank B, Burgstaller C. Influence of consolidating process on the properties of composites from thermosetting carbon fiber reinforced tapes. *Polym Composite*. 2022;43(7):4268-79.
- [94] Yan S, Zeizinger H, Merten C, Schmauder S. In-situ investigation of dielectric properties and reaction kinetics of a glass-fiber-reinforced epoxy composite material using dielectric analysis. *Polym Eng Sci*. 2021;61(6):1673-84.
- [95] Irvani MA, Deparis J, Davarzani H, Colombano S, Guérin R, Mainault A. The influence of temperature on the dielectric permittivity and complex electrical resistivity of porous media saturated with DNAPLs: A laboratory study. *Journal of Applied Geophysics*. 2020;172:103921.
- [96] Kapilaratne RG CJ, Lu M. Automated general temperature correction method for dielectric soil moisture sensors. *Journal of Hydrology*. 2017;551:203-16.
- [97] Ravindran AR, Ladani RB, Wu S, Kinloch AJ, Wang CH, Mouritz AP. The electric field alignment of short carbon fibres to enhance the toughness of epoxy composites. *Compos Part a-Appl S*. 2018;106:11-23.
- [98] Chao H-W, Hsu H-C, Chen Y-R, Chang T-H. Characterizing the dielectric properties of carbon fiber at different processing stages. *Scientific Reports*. 2021;11(1):17475.
- [99] Mano JF, Lanceros-Méndez S, Nunes AM, Dionísio M. Temperature Calibration in Dielectric Measurements. *J Therm Anal Calorim*. 2001;65(1):37-49.
- [100] Technical Data Sheet CYCOM(R) 5320-1 Prepreg. Solvay Composite Materials.
- [101] Hall M, Zeng XS, Shelley T, Schubel P. Dielectric parameter independent curing analysis of out-of-autoclave carbon fibre/epoxy composites. *Composites Part a-Applied Science and Manufacturing*. 2023;175:107755.

- [102] Day DR, Lewis TJ, Lee HL, Senturia SD. The Role of Boundary Layer Capacitance at Blocking Electrodes in the Interpretation of Dielectric Cure Data in Adhesives. *The Journal of Adhesion*. 2006;18(1):73-90.
- [103] van Turnhout J, Wubbenhorst M. Conduction-free dielectric loss $\Delta\epsilon/\Delta T$ - a powerful tool for the analysis of strong (ion) conducting dielectric materials. *Dielectric Newsletter*. 2000.
- [104] Yang Y, Plovie B, Chiesura G, Vervust T, Daelemans L, Mogosanu D-E, et al. Fully Integrated Flexible Dielectric Monitoring Sensor System for Real-Time In Situ Prediction of the Degree of Cure and Glass Transition Temperature of an Epoxy Resin. *IEEE Transactions on Instrumentation and Measurement*. 2021;70:1-9.
- [105] Kim SS, Murayama H, Kageyama K, Uzawa K, Kanai M. Study on the curing process for carbon/epoxy composites to reduce thermal residual stress. *Compos Part a-Appl S*. 2012;43(8):1197-202.
- [106] Shepard DD, Twombly B. Simultaneous dynamic mechanical analysis and dielectric analysis of polymers. *Thermochimica Acta*. 1996;272:125-9.
- [107] Boll D, Schubert K, Brauner C, Lang W. Miniaturized Flexible Interdigital Sensor for In Situ Dielectric Cure Monitoring of Composite Materials. *IEEE Sensors Journal*. 2014;14(7):2193-7.
- [108] Kahali Moghaddam M, Breede A, Chaloupka A, Bödecker A, Habben C, Meyer E-M, et al. Design, fabrication and embedding of microscale interdigital sensors for real-time cure monitoring during composite manufacturing. *Sensors and Actuators A: Physical*. 2016;243:123-33.
- [109] Kratz J, Hsiao K, Fernlund G, Hubert P. Thermal models for MTM45-1 and Cycom 5320 out-of-autoclave prepreg resins. *Journal of Composite Materials*. 2012;47(3):341-52.
- [110] Lattimer MP, Hobbs JK, Hill MJ, Barham PJ. On the origin of the multiple endotherms in PEEK. *Polymer*. 1992;33(18):3971-3.
- [111] Takahashi T, Serizawa M, Okino T, Kaneko T. A round-robin test of the softening temperature of plastics by thermomechanical analysis. *Thermochimica Acta*. 1989;147(2):387-99.
- [112] Barba D, Arias A, Garcia-Gonzalez D. Temperature and strain rate dependences on hardening and softening behaviours in semi-crystalline polymers: Application to PEEK. *International Journal of Solids and Structures*. 2020;182-183:205-17.
- [113] Jonas A, Legras R. Relation between PEEK semicrystalline morphology and its subglass relaxations and glass transition. *Macromolecules*. 1993;26(4):813-24.
- [114] Mourgues-Martin M, Bernés A, Lacabanne C. Dielectric relaxation phenomena in PEEK. *Thermochimica Acta*. 1993;226:7-14.
- [115] Kalika DS, Krishnaswamy RK. Influence of crystallinity on the dielectric relaxation behavior of poly(ether ether ketone). *Macromolecules*. 1993;26(16):4252-61.
- [116] Huo P, Cebe P. Temperature-dependent relaxation of the crystal-amorphous interphase in poly(ether ether ketone). *Macromolecules*. 1992;25(2):902-9.
- [117] Boyd RH. Relaxation processes in crystalline polymers: molecular interpretation — a review. *Polymer*. 1985;26:1123-33.
- [118] Arous M, Amor IB, Kallel A, Fakhfakh Z, Perrier G. Crystallinity and dielectric relaxations in semi-crystalline poly(ether ether ketone). *The Journal of physics and chemistry of solids*. 2007;68(7):1405-14.
- [119] Golden K. Bounds on the complex permittivity of a multicomponent material. *Journal of the Mechanics and Physics of Solids*. 1986;34(4):333-58.
- [120] Hojjati M, Hoa SV. Curing simulation of thick thermosetting composites. *Compos Manuf*. 1994;5(3):159-69.
- [121] Capehart TW, Kia HG, Abujoudeh T. Cure Simulation of Thermoset Composite Panels. *Journal of Composite Materials*. 2007;41(11):1339-60.

- [122] Johnston A, Hubert P, Poursartip A, Nelson K. Cure Kinetics and Viscosity Model of 8552 Epoxy Resin - FULL PAPER. 2023.
- [123] Michaud DJ, Beris AN, Dhurjati PS. Thick-Sectioned RTM Composite Manufacturing, Part II. Robust Cure Cycle Optimization and Control. *Journal of Composite Materials*. 2016;36(10):1201-31.
- [124] Mesogitis TS, Skordos AA, Long AC. Stochastic heat transfer simulation of the cure of advanced composites. *Journal of Composite Materials*. 2016;50(21):2971-86.
- [125] Mesogitis T. Stochastic simulation of the cure of advanced composites: Cranfield University; 2015.
- [126] Padmanabhan SK, Pitchumani R. Stochastic analysis of isothermal cure of resin systems. *Polym Composite*. 1999;20(1):72-85.
- [127] Zhou X-Y, Qian S-Y, Wang N-W, Xiong W, Wu W-Q. A review on stochastic multiscale analysis for FRP composite structures. *Compos Struct*. 2022;284:115132.
- [128] Acquah C, Datskov I, Mawardi A, Zhang F, Achenie LEK, Pitchumani R, et al. Optimization under uncertainty of a composite fabrication process using a deterministic one-stage approach. *Comput Chem Eng*. 2006;30(6):947-60.
- [129] Acevedo J, Pistikopoulos EN. A Parametric MINLP Algorithm for Process Synthesis Problems under Uncertainty. *Industrial & engineering chemistry research*. 1996;35(1):147-58.
- [130] Padmanabhan SK, Pitchumani R. Stochastic modeling of nonisothermal flow during resin transfer molding. *International journal of heat and mass transfer*. 1999;42(16):3057-70.
- [131] Li J, Zhang C, Liang Z, Wang B. Stochastic simulation based approach for statistical analysis and characterization of composites manufacturing processes. *J Manuf Syst*. 2006;25(2):108-21.
- [132] Skordos AA, Sutcliffe MPF. Stochastic simulation of woven composites forming. *Compos Sci Technol*. 2008;68(1):283-96.
- [133] Blanco S, You H, Kerekes TW, Yun GJ. Cure-induced residual stress buildup and distortions of CFRP laminates with stochastic thermo-chemical and viscoelastic models: Experimental verifications. *Mechanics of advanced materials and structures*. 2022;29(19):2740-56.
- [134] Yi S, Hilton HH, Fouad Ahmad M. Cure-Cycle Simulations Of Composites With Temperature- And Cure-Dependent Anisotropic Viscoelastic Properties And Stochastic Delaminations. *Mechanics of advanced materials and structures*. 1998;5(1):81-101.
- [135] Helmus R, Hinterhölzl R, Hubert P. A stochastic approach to model material variation determining tow impregnation in out-of-autoclave prepreg consolidation. *Compos Part a- Appl S*. 2015;77:293-300.
- [136] Mesogitis TS, Skordos AA, Long AC. Stochastic simulation of the influence of cure kinetics uncertainty on composites cure. *Compos Sci Technol*. 2015;110:145-51.
- [137] Man M, Ng Y, Tomblin J. Low Initial Temperature Vacuum-Bag-Only Cure, Medium Toughness Epoxy Prepregs (Cytec Cycom 5320-1). NMS 532 Rev A ed: National Center for Advanced Materials Performance; 2015.
- [138] Lee C, Gibson T, Tienda K, Storage T. Reaction rate and viscosity model development for Cytec's Cycom 5320 family of resins. *Proc 42nd int SAMPE tech conf*. Salt Lake City, UT2010.
- [139] Hwang S-S, Park SY, Kwon G-C, Choi WJ. Cure kinetics and viscosity modeling for the optimization of cure cycles in a vacuum-bag-only prepreg process. *International journal of advanced manufacturing technology*. 2018;99(9-12):2743-53.
- [140] Lee C, Tienda K, Storage T. Experimental methods and material model development for a toughened epoxy. *International SAMPE Technical Conference* 2014.
- [141] Brockman R, Storage T, Lee C, Coomer R, Volk B. Characterizing, Modeling, And Validating The Processing Of Out-Of-Autoclave Organic Matrix Composites As A Function Of Cure Cycle. *20th International Conference on Composite Materials*. Copenhagen2015.

- [142] Hyun D-K, Kim D, Hwan Shin J, Lee B-E, Shin D-H, Hoon Kim J. Cure cycle modification for efficient vacuum bag only prepreg process. *Journal of Composite Materials*. 2021;55(8):1039-51.
- [143] Lucas S, Howard S, Senger J. *Vacuum Bag Only Processing; Improving Prepreg Out-Time and Porosity for Large Composite Structure*. Society for the Advancement of Material and Process Engineering. Seattle, WA2010.
- [144] CCA Material Constitutive Model Documentation. Convergent Manufacturing Technologies, Inc.; 2019.
- [145] Chern C-S, Poehlein GW. A kinetic model for curing reactions of epoxides with amines. *Polym Eng Sci*. 1987;27(11):788-95.
- [146] Cole KC, Hechler JJ, Noel D. A new approach to modeling the cure kinetics of epoxy/amine thermosetting resins. 2. Application to a typical system based on bis[4-(diglycidylamino)phenyl]methane and bis(4-aminophenyl) sulfone. *Macromolecules*. 1991;24(11):3098-110.
- [147] Castro JM, Macosko CW. Studies of mold filling and curing in the reaction injection molding process. *AIChE Journal*. 1982;28(2):250-60.
- [148] Karkanis PI, Partridge IK, Attwood D. Modelling the cure of a commercial epoxy resin for applications in resin transfer moulding. *Polymer international*. 1996;41(2):183-91.
- [149] Rabinowitch E. Collision, co-ordination, diffusion and reaction velocity in condensed systems. *Transactions of the Faraday Society*. 1937;33(0):1225-33.
- [150] Macedo PB, Litovitz TA. On the Relative Roles of Free Volume and Activation Energy in the Viscosity of Liquids. *The Journal of Chemical Physics*. 2004;42(1):245-56.
- [151] Wise CW, Cook WD, Goodwin AA. Chemico-diffusion kinetics of model epoxy-amine resins. *Polymer (Guilford)*. 1997;38(13):3251-61.
- [152] Dykeman D. *Minimizing Uncertainty in Cure Modeling for Composites Manufacturing*: University of British Columbia; 2008.
- [153] Williams ML, Landel RF, Ferry JD. The Temperature Dependence of Relaxation Mechanisms in Amorphous Polymers and Other Glass-forming Liquids. *Journal of the American Chemical Society*. 1955;77(14):3701-7.
- [154] Wisanrakkit G, Gillham J. The glass transition temperature (T_g) as an index of chemical conversion for a high- T_g amine/epoxy system: Chemical and diffusion-controlled reaction kinetics. *J Appl Polym Sci*. 1990;41:2885-929.
- [155] Skordos AA, Partridge IK. Cure kinetics modeling of epoxy resins using a non-parametric numerical procedure. *Polym Eng Sci*. 2001;41(5):793-805.
- [156] Ryckaert VG, Claes JE, Van Impe JF. Model-based temperature control in ovens. *Journal of Food Engineering*. 1999;39(1):47-58.
- [157] Pyrometry. SAE AMS2750G: SAE; 2022.
- [158] Kluge NEJ, Lundström TS, Ljung AL, Westerberg LG, Nyman T. An experimental study of temperature distribution in an autoclave. *Journal of Reinforced Plastics and Composites*. 2016;35(7):566-78.
- [159] Mulligan D, Gnaniyah S, Sims G. *Thermal analysis techniques for composites and adhesives*. 2nd ed.: National Physical Laboratory; 2000.
- [160] Halley PJ, Mackay ME. Chemorheology of thermosets—an overview. *Polym Eng Sci*. 1996;36(5):593-609.
- [161] González UF, Shen SF, Cohen C. Rheological characterization of fast-reacting thermosets through spiral flow experiments. *Polym Eng Sci*. 1992;32(3):172-81.
- [162] DEA 288 Ionic – Dielectric Cure Monitoring: Method, Technique, Applications. NETZSCH-Gerätebau GmbH.
- [163] Direct T. PFA Insulated Flat Twin (250°C). https://www.tcdirect.net.au/Default.aspx?level=2&department_id=540/1#540/1/02.

[164] Direct T. Miniature Thermocouple Connectors (rated to 220°C).
https://www.tcdirect.net.au/Default.aspx?level=2&department_id=280/1.

APPENDIX A: MANUFACTURING PROCEDURE

This appendix is suggested to be used a supplement for the methods provided in Chapters 3 and 4.

A1. IDEX Sensor Definition

Technical details of the IDEX sensor and the NETZSCH DEA 288 Ionic are given in Figure 2 and Figure 3 [162]. The sensor used in this study is the filtered IDEX with a 115 μm electrode spacing.

Specifications for Available Sensor Types

Sensor Type	Sensing Area	Max. Temperature	Electrode Spacing	Main Application	
Micron Sensor (MS)	2.5 mm ² , 26 mm ² , 70 mm ²	200°C or 350°C*	1, 5 or 25 μm	Paints, inks, adhesives	
Mini-IDEX (Interdigitated Electrode)	33 mm ²	275°C	100 μm	All resins (small cavities)	
IDEX (Interdigitated Electrode)	233 mm ²	200°C or 275°C*	115 μm	All resins (epoxy, polyester PES, polyurethane PUR, etc.)	
IDEX, filtered	233 mm ²	200°C or 275°C*	115 μm	Carbon fiber-reinforced polymers (CFRP)	
Tool Mountable Monotrode (TMM)	13 mm ² , 79 mm ² , 707mm ²	220°C	–	Especially for SMC/BMC, PUR foams	
Tool Mountable Comb Electrode (TMC)	214 mm ²	220°C	500 μm	All resins (EP, PES, PUR, etc.)	
Coated Tool Mountable Comb Electrode (TMCC)	254 mm ²	220°C	500 μm	All resins, composites and other polymers with electrically conductive fillers	

* depending on the wiring of the sensor head

Figure 2 - Description of NETZSCH dielectric sensors, from NETZSCH brochure [162]. The IDEX sensors used in this study are the IDEX filtered type.

A2. NETZSCH DEA 288 Ionic

Key Technical Specifications

DEA 288 Ionic	
Frequency range	1 mHz to 1 MHz, freely selectable values
Data acquisition	Multiple DEA modules; true simultaneous operation of all channels
Minimum data acquisition time	< 5 ms
Sensor connection	Shielded 4-wire technique (compensation of resistivity and capacity of the wire as a prerequisite for precise measurements)
DEA modules	<ul style="list-style-type: none">▪ Portable version: All-purpose version, up to 7 channels▪ Industrial Rack version: up to 8 channels (extension possible for up to 16 channels)
I/O ports	Input and output of measuring signals or signals from peripheral devices such as pressure or temperature sensors. DEA allows for triggering by manufacturing machines.



Adaptor box – fast, easy and reliable connection of all disposable sensors, thermocouples or RTD sensors

Figure 3 - Description of the NETZSCH DEA 288 Ionic, from NETZSCH brochure [162].

A3. Thermocouples

The thermocouples used for this research were PFA insulated flat twin Type K – 7/0.2 mm thermocouples (Figure 4) purchased from TC Direct. They are rated to 250 °C. The thermocouples were purchased as a spool, cut to approximately 1 meter in length, wired to miniature K type thermocouple connector plugs (Figure 5), and welded at the tip.

PFA Insulated Flat Twin (250°C)



[view larger image](#)

We supply 7/0.2mm, 13/0.2mm dia stranded or 1/0.5mm dia solid cable in 25, 50, 100 or 200 metre lengths in thermocouple types KX, TX, JX, NX or RCA/SCA. Each conductor is insulated in PFA, the cores are laid flat and then overall sheathed in PFA. All conductors used (except for compensating cable) are made from the relevant thermocouple material and meets IEC 60584-1: Class 2 up to 250°C. The insulation material is colour coded to ANSI MC96.1 as shown below.

- 7/0.2mm, 13/0.2mm dia stranded or 1/0.5mm dia solid conductors, laid flat and overall sheathed construction
- Insulation: PFA, rated to 250°C
- Colour coded:-
 - Type KX: yellow outer sheath, yellow positive wire and red negative wire
 - Type TX: blue outer sheath, blue positive wire and red negative wire
 - Type JX: black outer sheath, white positive wire and red negative wire
 - Type NX: orange outer sheath, orange positive wire and red negative wire
 - Type RX/SX: green outer sheath, black positive wire and red negative wire
- Available in a variety of lengths
- Easy connection to our range of sensors via our range of connector systems or the rear terminals on our range of indicators, controllers and programmers

The following types are available:

- ▶ Type KX - 7/0.2mm PFA Insulated Flat Twin Thermocouple Extension Cable
- ▶ Type KX - 13/0.2mm PFA Insulated Flat Twin Thermocouple Extension Cable
- ▶ Type KX - 1/0.5mm PFA Insulated Flat Twin Thermocouple Extension Cable
- ▶ Type TX - 7/0.2mm PFA Insulated Flat Twin Thermocouple Extension Cable
- ▶ Type TX - 13/0.2mm PFA Insulated Flat Twin Thermocouple Extension Cable
- ▶ Type TX - 1/0.5mm PFA Insulated Flat Twin Thermocouple Extension Cable
- ▶ Type JX - 7/0.2mm PFA Insulated Flat Twin Thermocouple Extension Cable
- ▶ Type JX - 13/0.2mm PFA Insulated Flat Twin Thermocouple Extension Cable
- ▶ Type JX - 1/0.5mm PFA Insulated Flat Twin Thermocouple Extension Cable
- ▶ Type NX - 7/0.2mm PFA Insulated Flat Twin Thermocouple Extension Cable
- ▶ Type NX - 13/0.2mm PFA Insulated Flat Twin Thermocouple Extension Cable
- ▶ Type NX - 1/0.5mm PFA Insulated Flat Twin Thermocouple Extension Cable
- ▶ Type RCA/SCA - 7/0.2mm PFA Insulated Flat Twin Thermocouple Compensating Cable
- ▶ Type RCA/SCA - 13/0.2mm PFA Insulated Flat Twin Thermocouple Compensating Cable

Figure 4 - Thermocouple definition, with type K 7/0.2 mm dimensions being used for this research [163].

Miniature Thermocouple Connectors (rated to 220°C)



[view larger image](#)

These flat pin miniature connectors are ideal for connecting thermocouple sensors and extension or compensating cable to each other. The pins are polarised to avoid an incorrect connection and the connector body is additionally marked for polarity. They are rated for use between -50°C and +220°C. In addition to offering a plug and socket, panel sockets and panel blanking sockets are also available. Panel blanking sockets are useful for when using a panel with less connectors than cut-outs, to avoid having an empty slot. Matching anodised aluminium connector panels can also be found in this section. Weatherproof silicone rubber boots for added protection in moist environments and cable clamps are also available.

- Body: Thermoplastic compound rated -50°C to +220°C
- Suitable for wire diameters up to 0.8mm
- Color coded to ANSI MC96.1-1982. Type K - Yellow, Type T - Blue, Type J - Black, Type N - Orange, Type RX/SX - Green and Copper - White
- Dimensions: Plug 19x16x8mm (LxWxD) with 12mm long pins Socket 26x16x8mm (LxWxD) Panel sockets are typically 19x16x8mm (LxWxD) and panel blanking sockets are 14.5x16x8mm (LxWxD) with front bezel 23.5x14mm supplied with bracket for attachment to panel
- Cable clamps and weatherproof silicone rubber boots offered as options but cannot be used at the same time
- Manufactured by the TC Group

Figure 5 - Thermocouple connector definition, with Type K plugs being used for this research [164].

APPENDIX B: DEA SIGNAL EVALUATION

This appendix is suggested to be used a supplement for the methods provided in Chapters 3 and 4.

B1. Dielectric Smoothing Procedure and Frequency Selection

As discussed in Chapter 3, there are several criteria for selecting an appropriate dielectric signal. This section will explore the best practices for identification of measurement frequency and signal smoothing. This section will use the loss factor curve for IDEX5, the details of which are provided in Chapter 3. As a key finding of the paper provided in Chapter 3 is that the dielectric signals can be used interchangeably, only the loss factor is provided for this example.

Firstly, it is recognised that there is noise present in the dielectric signal, and it is beneficial to use a smoothing operation to reduce this noise. The NETZSCH Proteus Analysis software has a built-in smoothing function, which was used in this study. Figure 7 shows a successful smoothing operation, in which the graph shape is retained but the signal appears more consistent. This figure shows the smoothing to a Level 8, which is the maximum used in this study. As a contrast, Figure 8 shows that smoothing this signal to a Level 9 causes a noticeable distortion in the signal shape. For this reason, a Level 8 was the maximum used to smooth the dielectric signals for this study. Each signal was smoothed independently to the minimum level necessary to make the signal more consistent, and each smoothing was verified to not distort the signal.

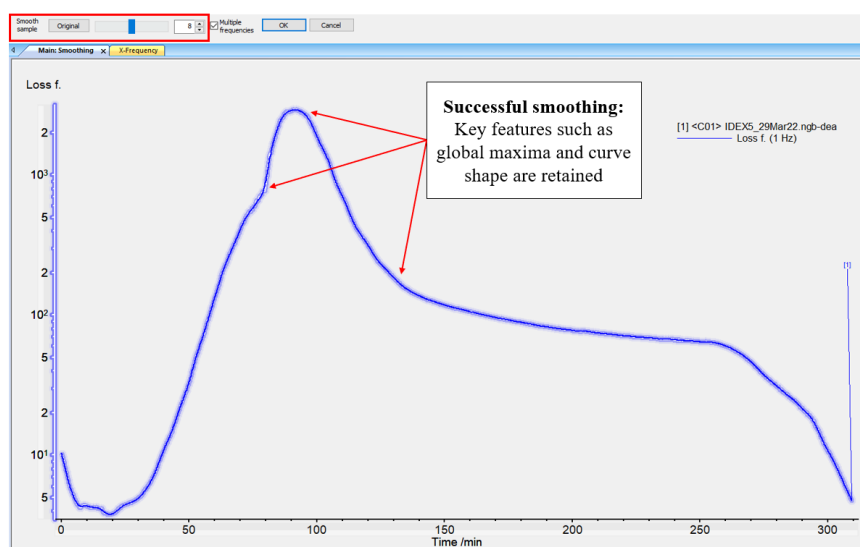


Figure 7 - Smoothing to a Level 8, which successfully retains the graph features while still simplifying the signal.

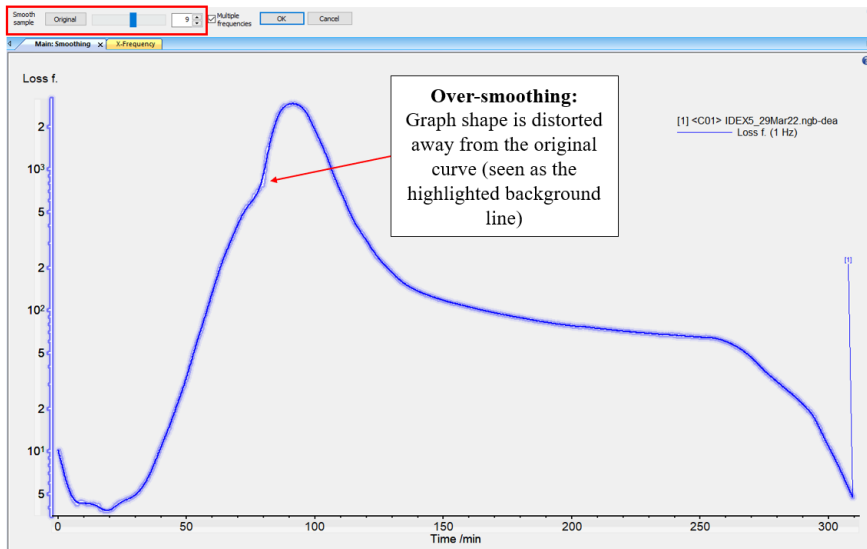


Figure 8 - An unsuccessful smoothing practice to Level 9, which is performed on the same signal as shown in Figure 7. Smoothing to a 9 in this case causes the graph to distort away from the original signal.

In both examples, the original signal displays minimal signal noise. However, the first derivative of the signal, shown in Figure 9 (left), does show noticeable noise. A smoothed signal, shown in Figure 9 (right), shows a significantly more consistent derivative which indicates an overall more consistent signal.

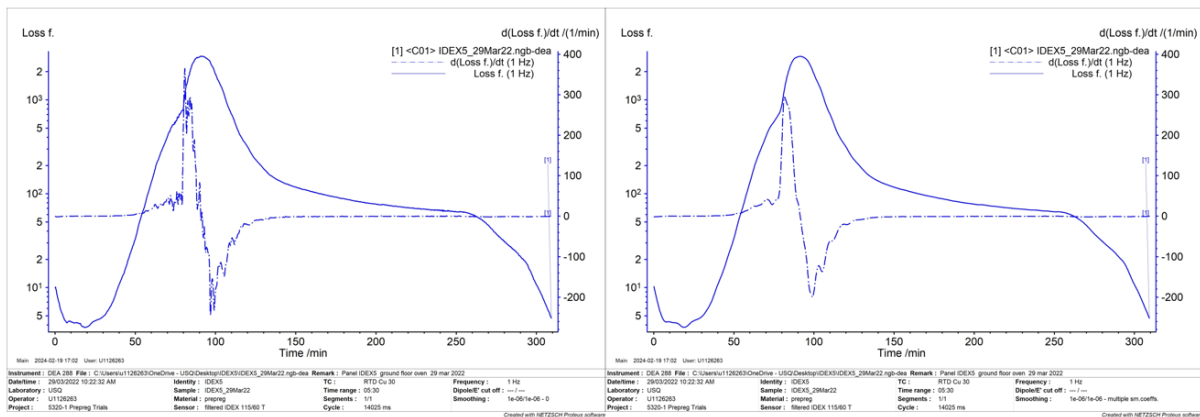


Figure 9 - Signal from Figure 7 shown with the first derivative of the signal (left) unsmoothed and (right) smoothed. In both cases the original signal (the loss factor) was smoothed, and the derivative was calculated from the smoothed signal.

Additionally, the higher frequency measurements contain more data points per time period, and thus contained more noise. Figure 10 displays the signal used in previous examples, with the addition of higher frequency measurements at 10 Hz, 100 Hz, and 1 kHz. The higher frequency measurements show more signal noise near the beginning and end of the cure but remain consistent in the remainder of the curve shape and time event. The smoothed signals, shown on the right, show that all frequencies remain consistent once smoothed. It should be

noted here that the examples show the loss factor, which is a frequency dependent value, and thus the difference in magnitude between frequencies is expected.

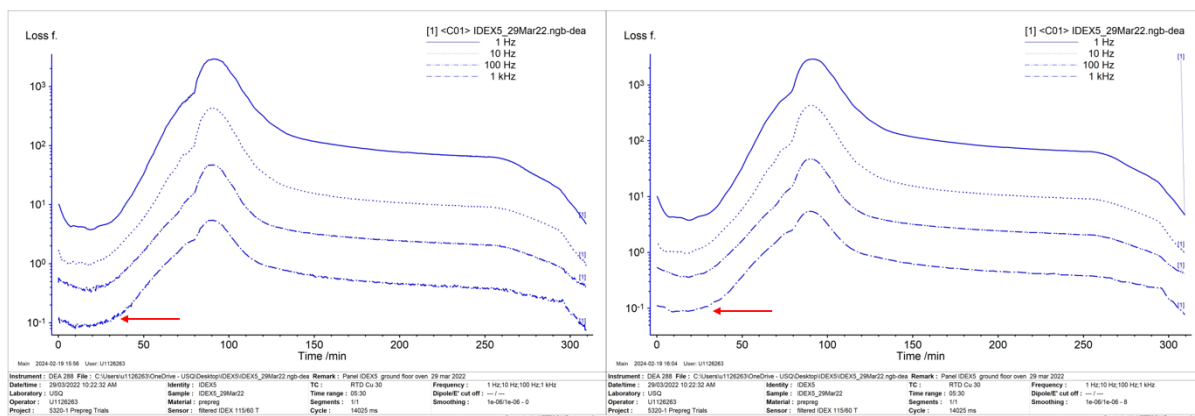


Figure 10 - Signal comparison for 1 Hz, 10 Hz, 100 Hz, and 1 kHz measurements which are (left) unsmoothed and (right) smoothed. The red arrow indicates the maximum area of noise on the 1 kHz measurement, and how the area is more consistent after smoothing.

From Figure 10 we can see that each indicated frequency from 1-1,000 Hz displays approximately the same graphical response. As stated previously the magnitude is disregarded, but the times at which the graph exhibits key features (i.e., global maxima, endset) appear consistent between all frequencies. This is further explored in Figure 11 which shows the total set of frequency measurements for IDEX5. On the left we see that the observation that the graphs display consistent behaviour across all measured frequencies. On the right we explore the frequency-domain response, which is explored more deeply in Chapter 4 in Section 3.1.2 of the manuscript. In this it is stated that within the frequency domain, signals which display a slope of -1, as this data set does in the low frequency range, display Ohmic conductivity. This means that the signal response in these ranges is driven by the conductive behaviour, which is frequency-independent. Due to the lower noise levels in the lower frequencies, and the frequency-independence in this range, the 1 Hz frequency was chosen for the signal analysis for the work provided in this thesis.

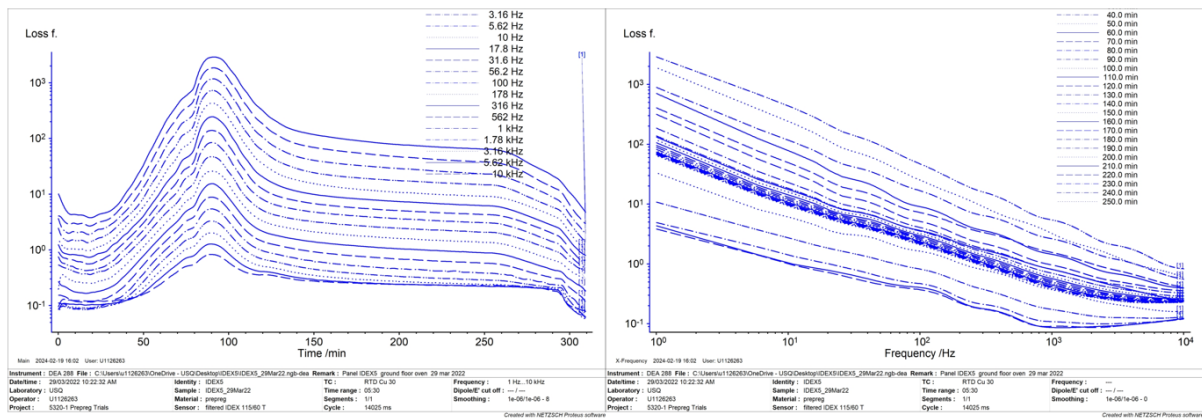


Figure 11 - Complete set of frequency measurements for the loss factor in IDEX5 showing (left) the time-dependent response for each frequency and (right) the frequency-dependent response for the duration of cure (40 minutes to 250 minutes).

The notable exception to the 1 Hz frequency choice, as stated in Chapter 2 Section 2.5.1 of the published paper, is the dissipation factor. As explained in Chapter 4 Section 3.1.1 of the manuscript, some signals display a double peak behaviour in the phase angle at low frequencies. As the dissipation factor is calculated from the phase angle response, this directly impacts the dissipation factor in a way that does not show up in the other dielectric parameters. For this reason, the 100 Hz frequency was selected for the dissipation factor analyses, to ensure that the analysis methods could be consistently implemented. As with the TMM tests, the IDEX tests all displayed consistent single-peak behaviour at 100 Hz, such as is visible in Figure 12. Due to the above rationale on frequency independence for the low frequencies, the 100 Hz frequency was selected for the dissipation factor correlations.

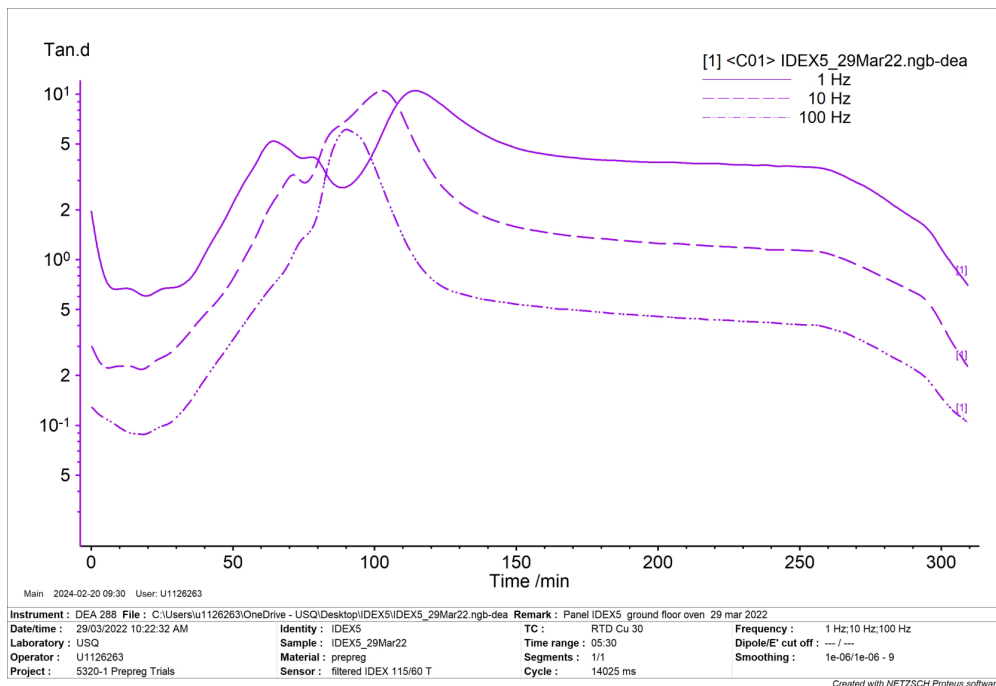


Figure 12 - Dissipation factor for IDEX5 at frequencies of 1 Hz, 10 Hz, and 100 Hz showing that the single peak behaviour is present in the 100 Hz signal.

To further validate the choice of 1 Hz frequencies, the full set of analysis methods proposed in Chapter 3 were performed on IDEX3 for multiple frequencies. The average time response for each frequency, and the standard deviation across all dielectric parameters, is provided in Figure 13. All signals are, on average, within 6% of the RAVEN estimate which indicates that any of the frequencies can be selected with reasonable accuracy. For this sample, the 1 Hz and 100 Hz frequencies were the most consistent, and the 1 Hz frequency was selected due to having the least signal noise.

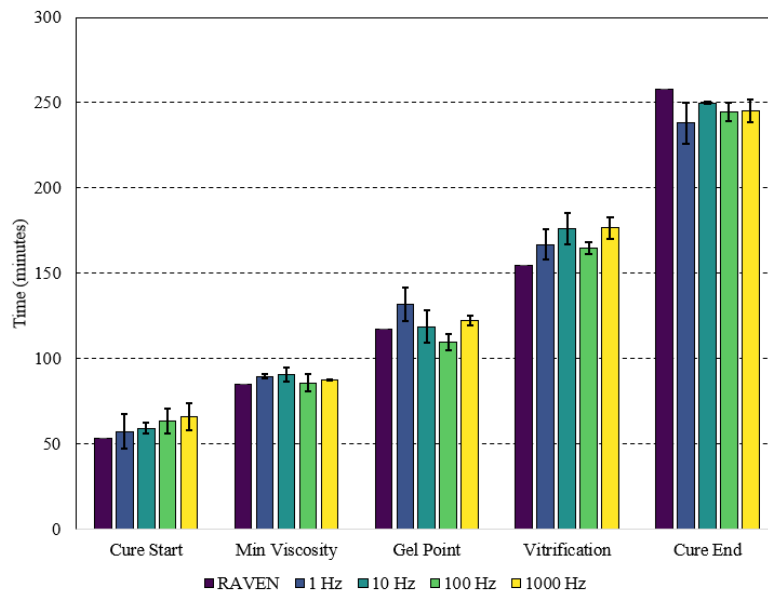


Figure 13 - Cure event correlations for IDEX3 performed on 1 Hz, 10 Hz, 100 Hz, and 1 kHz frequencies.

B2. TMM Sensor Correction Factor

It should be noted that the correction factor applied to the TMM sensor, discussed in Chapter 4, is specific to the prepreg system studied here. As stated in the chapter, the correction factor is due to the multi-phase material evaluation of the PEEK rings and the 5320-1 prepreg under test. For this case, the correction factor is specific to this material combination and to the range of thicknesses tested. This concept is discussed in Chapter 4, Section 3.1.3 (Equation 9), which explores how the mixed material response is driven by the ratio of the individual signal responses. For a different material system, it would be expected that the ratio of responses is different. As discussed in Chapter 4, the exact volume ratio between the PEEK rings and the material under test is unknown due to uncertainties of the electric field and the field strength in a given direction. Further, another material may have a different temperature response or cure time, which would further influence the correction factor.

B3. TMM Fully Cured Prepreg Test

Chapter 4 Section 3.1.2 of the manuscript describes a fully cured test in which a previous prepreg stack (TMM20-2) was post-cured to 100% conversion and then re-run with the TMM sensor to evaluate the influence of conductive carbon fibre *without* the epoxy curing reaction on the sensor. For this test, the TMM20-2 panel was post-cured for 2 hours at 200 °C, and the temperature profile was simulated in RAVEN to ensure that full conversion was achieved. The RAVEN simulation for the oven cycle is shown in Figure 14.

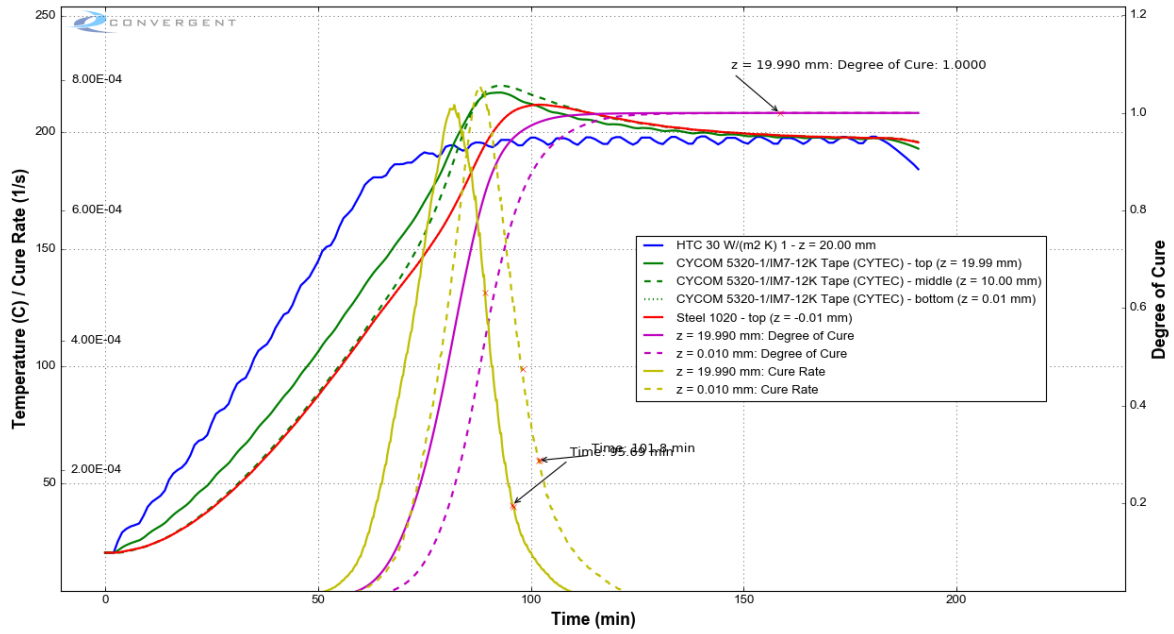


Figure 14 - RAVEN simulation of TMM20-2 post cure, demonstrating full conversion.

APPENDIX C: STOCHASTIC MODELLING CODE (MATLAB)

This appendix is suggested to be used as a supplement for the methods provided in Chapter 5.

An example of one of the MATLAB code sets is provided below. This code includes:

1. Cure kinetics equation for 5320-1.
2. 3% variation on all cure kinetics parameters (except where reductions are indicated per Chapter 5).
3. 5% variation in temperature profile.
4. Relevant convergence analyses.
5. An example output from this code compilation (Figure 15).

All other stochastic code is a variation on this, with the cure kinetics and temperature varied depending on the data set in question. The viscosity code is written the same way, with the inclusion of the viscosity model in addition to the cure model. The experimental validation code is compiled using the same code with no variation of any parameters ($s[x] = 0$). For each validation cure cycle, the desired file name is referenced in line 86.

```

1  % Defining a randomly assigned normal distribution between -1 and 1 across
2  % 2000 iterations for each varied parameter
3  s1 = -1 + (2).*rand(2000,1);
4  s2 = -1 + (2).*rand(2000,1);
5  s3 = -1 + (2).*rand(2000,1);
6  s4 = -1 + (2).*rand(2000,1);
7  s5 = -1 + (2).*rand(2000,1);
8  s6 = -1 + (2).*rand(2000,1);
9  s7 = -1 + (2).*rand(2000,1);
10 s8 = -1 + (2).*rand(2000,1);
11 s9 = -1 + (2).*rand(2000,1);
12 s10 = -1 + (2).*rand(2000,1);
13 s11 = -1 + (2).*rand(2000,1);
14 s12 = -1 + (2).*rand(2000,1);
15 s13 = -1 + (2).*rand(2000,1);
16 s14 = -1 + (2).*rand(2000,1);
17 s15 = -1 + (2).*rand(2000,1);
18 s16 = -1 + (2).*rand(2000,1);
19
20 num = 0;
21 uncured = 0;
22
23 for j = 1:1:2000          % loop 2000 times
24
25 % Define baseline kinetic parameters
26 t_g0 = -3;
27 t_ginf = 235;
28 lambda = 0.8;
29
30 A1 = 14800000;
31 E1_R = 10200;
32 m1 = 0.17;
33 n1 = 19.3;
34
35 A2 = 83000;
36 E2_R = 8540;
37 m2 = 0.70;
38 n2 = 0.87;
39 D2 = 97.4;
40 a_c02 = -1.6;
41 a_cT2 = 0.0057;
42
43 A3 = 63900000;
44 E3_R = 8940;
45 m3 = 1.65;
46 n3 = 16.6;
47
48 A4 = 98000;
49 E4_R = 7100;
50 m4 = 1.66;
51 n4 = 3.9;
52 D4 = 63.3;
53 a_c04 = -0.6;
54 a_cT4 = 0.003;
55
56
57 cureTime = 0;
58
59 % Assigning Stochastic Variables (3% COV)
60 COV = 0.03;
61 A1_S = A1 + (A1 * COV * s1(j,1));
62 E1_S = E1_R + (E1_R * 0.025 * s2(j,1));          % 2.5% COV
63 m1_S = m1 + (m1 * COV * s3(j,1));
64 n1_S = n1 + (n1 * COV * s4(j,1));
65 A2_S = A2 + (A2 * COV * s5(j,1));

```

```

66     E2_S = E2_R + (E2_R * COV * s6(j,1));
67     m2_S = m2 + (m2 * COV * s7(j,1));
68     n2_S = n2 + (n2 * COV * s8(j,1));
69     A3_S = A3 + (A3 * COV * s9(j,1));
70     E3_S = E3_R + (E3_R * 0.008 * s10(j,1));           % 0.8% COV
71     m3_S = m3 + (m3 * COV * s11(j,1));
72     n3_S = n3 + (n3 * COV * s12(j,1));
73     E4_S = E4_R + (E4_R * 0.02 * s16(j,1));           % 2% COV
74     A4_S = A4 + (A4 * COV * s13(j,1));
75     n4_S = n4 + (n4 * COV * s14(j,1));
76     m4_S = m4 + (m4 * COV * s15(j,1));
77
78     %-----DEFINE CURE PROFILE-----%
79     doc = 0.002 ;           % 0.2% initial DOC
80     deltaTime = 12;       % 1 min increments
81
82     i = 1;
83
84     st = (-1 + (2).*rand(1,1)); % Temperature: varied randomly by 5%
85
86     tempM = readmatrix('idex6L.xlsx'); % Read temperature profile file
87     tempM = tempM + (0.015 * tempM * st); % Modify temperature
88
89
90     for time = 0:0.2:309
91
92         %----- Identify Temperature -----%
93         T = tempM(i) + 273;
94
95         %----- Tg Calculation -----%
96         if doc > 0.999
97             t_g = t_ginf;
98             doc = 1;
99         else
100            t_g = t_g0 + (((t_ginf - t_g0) * lambda * doc)/(1 - ((1 - lambda) *
101                (doc))));
102        end
103
104        %----- 4 Rate functions -----%
105        k1 = A1_S * exp(-E1_S / T);
106        k2 = A2_S * exp(-E2_S / T);
107        k3 = A3_S * exp(-E3_S / T);
108        k4 = A4_S * exp(-E4_S / T);
109
110        r1 = k1 * (doc^m1_S) * ((1 - doc)^n1_S);
111        r2 = (k2 * (doc^m2_S) * ((1 - doc)^n2_S))/(1 + exp(D2 * (doc - (a_c02 + (a_cT2
112            * T)))));
113        r3 = k3 * (doc^m3_S) * ((1 - doc)^n3_S);
114        r4 = (k4 * (doc^m4_S) * ((1 - doc)^n4_S))/(1 + exp(D4 * (doc - (a_c04 + (a_cT4
115            * T)))));
116
117        %----- Calculate cure rate -----%
118        if doc > 0.999
119            cureRate = 0;
120        else
121            cureRate = 0.8*r1 + .35*r2 + 1.1*r3 + 1.2*r4;
122        end
123
124        doc = doc + (deltaTime * cureRate); % Calculate instantaneous degree of cure
125
126
127        %----- Calculate time to 88% cure -----%
128        if doc < 0.88
129            cureTime = time;
130        end

```

```

131
132 %----- Calculate Vitrification Time -----%
133 vitTemp = T - 273;
134 if t_g < vitTemp
135     vitTime = time;
136 end
137
138 %----- Fill Matrices -----%
139 doc_m(1,i) = doc; % DOC matrix
140 time_m(1,i) = time; % time matrix
141 rate(i,1) = cureRate; % Rate matrix
142 tg(i,1) = t_g; % Tg matrix
143 temp(i,1) = T-273; % Temp matrix
144
145 i = i + 1;
146
147 end
148 if doc < 0.88
149     uncured = uncured + 1;
150 end
151
152 doc_m(1,i) = doc; % DOC matrix
153 time_m(1,i) = time; % Time matrix
154 temp(i,1) = T-273; % Temp matrix
155 rate(i,1) = cureRate; % Rate matrix
156
157 %----- Time to 88% Cure: Convergence -----%
158 if doc > 0.88
159     timeToCure(j,1) = cureTime; % Cure Time Matrix
160 else
161     timeToCure(j,1) = nan;
162 end
163
164 aT = nanmean(timeToCure,'all'); % Avg time to cure
165 avgTime(j,1) = aT; % Avg time to cure Matrix - Convergence
166 sT = nanstd(timeToCure); % Std dev time to cure
167 devTime(j,1) = sT; % STD time to cure Matrix - Convergence
168
169 %----- Total Degree of Cure: Convergence -----%
170 totalDOC(j,1) = max(doc_m); % Final DOC Matrix
171 aDOC = mean(totalDOC); % Avg total DOC
172 avgDOC(j,1) = aDOC; % Avg total DOC - Convergence
173 sDOC = std(totalDOC); % Std dev total DOC
174 devDOC(j,1) = sDOC; % STD total DOC Matrix - Convergence
175
176 %----- Vitrification: Convergence -----%
177 vitM(j,1) = max(vitTime); % Final DOC Matrix
178 aVIT = mean(vitM); % Avg total DOC
179 avgVIT(j,1) = aVIT; % Avg total DOC - Convergence
180 sVIT = std(vitM); % Std dev total DOC
181 devVIT(j,1) = sVIT; % STD total DOC Matrix - Convergence
182
183 %----- Maximum Reaction Rate (value): Convergence -----%
184 mRate = max(rate);
185
186 maxRate(j,1) = mRate; % rate Matrix
187 aR = mean(maxRate); % Avg max rate
188 avgRate(j,1) = aR; % Avg max rate Matrix - Convergence
189 sR = std(maxRate); % Std dev max rate
190 devRate(j,1) = sR; % STD max rate Matrix - Convergence
191
192 count(j,1) = j;
193
194

```

```

195
196 end
197
198 format longg
199
200 aT;
201 sT;
202 covT = 100 * sT/aT;
203 disp(['Average time to 88% cured is ' num2str(aT) ' min'])
204 disp(['Deviation of time to 88% cured is ' num2str(sT) ' min'])
205 disp(['Time to cure COV is ' num2str(covT) '%'])
206
207 aDOC = aDOC*100;
208 sDOC = sDOC*100;
209 covDOC = 100 * sDOC/aDOC;
210 disp(['Average final DOC is ' num2str(aDOC) '%'])
211 disp(['Deviation of final DOC is ' num2str(sDOC) '%'])
212 disp(['Total DOC COV is ' num2str(covDOC) '%'])
213
214 aVIT;
215 sVIT;
216 covVIT = 100 * sVIT/aVIT;
217 disp(['Average Vitrification time is ' num2str(aVIT) ' min'])
218 disp(['Deviation of Vitrification time is ' num2str(sVIT) '%'])
219 disp(['Total Vit time COV is ' num2str(covVIT) '%'])
220
221 disp(['Total number of undercured parts is ' num2str(uncured)])
222
223 aR;
224 sR;
225 covR = 100 * sR/aR;
226 disp(['Average Maximum Reaction Rate is ' num2str(aR) ' 1/s'])
227 disp(['Deviation of Maximum Reaction Rate is ' num2str(sR) ' 1/s'])
228 disp(['Total Maximum Reaction Rate COV is ' num2str(covR) '%'])
229
230

```

```
Command Window
>> S_Cure_IDEX6_KineticsTemp
Average time to 88% cured is 220.6478 min
Deviation of time to 88% cured is 24.0229 min
Time to cure COV is 10.8875%
Average final DOC is 92.8842 %
Deviation of final DOC is 2.9343 %
Total DOC COV is 3.1591%
Average Vitrification time is 165.0767 min
Deviation of Vitrification time is 11.4365 %
Total Vit time COV is 6.928%
Total number of undercured parts is 110
Average Maximum Reaction Rate is 0.00029037 1/s
Deviation of Maximum Reaction Rate is 3.8212e-05 1/s
Total Maximum Reaction Rate COV is 13.1598%
fx >> |
```

Figure 15 - An example output from the above MATLAB code, which varies the cure kinetics by 3% and temperature by 5%.